# Delayed catalyst function enables direct enantioselective conversion of nitriles to $NH_2$-amines

Shaochen Zhang,*[,1] Juan del Pozo,*[1] Filippo Romiti,*[1,2] Yucheng Mu,[1] Sebastian Torker,[1,2] Amir H. Hoveyda[1,2,§]

[1]*Department of Chemistry, Merkert Chemistry Center, Boston College, Chestnut Hill, Massachusetts 02467, USA*

[2]*Supramolecular Science & Engineering Institute, University of Strasbourg, Strasbourg 67000, France*

e-mail: amir.hoveyda@bc.edu or ahoveyda@unistra.fr

# SUPPLEMENTARY MATERIAL

## *Table of Contents*

# 1 General information and Reagents

Infrared (IR) spectra were recorded on a Bruker FT-IR Alpha (ATR mode) spectrophotometer, $\lambda_{max}$ in $cm^{-1}$. Bands are characterized as broad (br), strong (s), medium (m), and weak (w). $^{1}H$ NMR spectra were recorded on a Varian Unity INOVA 400 (400 MHz), Varian Unity INOVA 500 (500 MHz), or Varian Unity INOVA 600 (600 MHz) spectrometer. Chemical shifts are reported in ppm from tetramethylsilane with the solvent resonance as the internal standard ($CDCl_3$: δ 7.26 ppm). Data are reported as follows: chemical shift, integration, multiplicity (s = singlet, d = doublet, t = triplet, q = quartet, br = broad, m = multiplet), and coupling constant (Hz). $^{13}C$ NMR spectra were recorded on a Varian Unity INOVA 400 (101 MHz), Varian Unity INOVA 500 (126 MHz) or Varian Unity INOVA 600 (151 MHz) spectrometer with complete proton decoupling. Chemical shifts are reported in ppm from tetramethylsilane with the solvent resonance as the internal standard ($CDCl_3$: δ 77.16 ppm). $^{11}B$ NMR spectra were recorded on a Varian Unity INOVA 400 (128 MHz), Varian Unity INOVA 500 (160 MHz) or Varian Unity INOVA 600 (192 MHz) spectrometer with complete proton decoupling. Chemical shifts are reported in ppm with $BF_3{\cdot}Et_2O$ as reference. High-resolution mass spectrometry was performed on a JEOL AccuTOF DART (positive mode) at the Mass Spectrometry Facility, Boston College. Enantiomeric ratios were determined by HPLC analysis (Chiral Technologies Chiralpak AZ–H (4.6 x 250 mm), Chiralcel OD–H (4.6 x250 mm), Chiralpak AD–H (4.6 x 250 mm), Chiralcel OZ–H (4.6 x250 mm) and Chiralpak IC (4.6 x 250 mm) in comparison with authentic racemic materials. Specific rotations were measured on an ATAGO® AP-300 Automatic Polarimeter or a Rudolph Research Analytical Autopol IV Polarimeter. Melting points were measured on a Thomas Hoover capillary melting point apparatus and are uncorrected.

Unless otherwise noted, reactions were carried out with distilled and degassed solvents under an atmosphere of dry $N_2$ in oven- (135 °C) or flame-dried glassware with standard dry box or vacuum-line techniques. Solvents were purified under a positive pressure of dry argon by a modified Innovative Technologies purification system: toluene, benzene and hexanes were purified through a copper oxide column and an alumina column; $CH_2Cl_2$ and $Et_2O$ were purged with Ar and purified by passage through two alumina columns. Tetrahydrofuran (thf; Aldrich Chemical Co.) was purified by distillation from sodium benzophenone ketyl immediately prior to use unless otherwise specified. All work-up and purification procedures were carried out with reagent grade solvents (purchased from Fisher Scientific, Inc.) in air.

**[1,3-Bis(cyclohexyl)imidazol-2-ylidene]CuO*t*-Bu (NHC–Cu-1)** was prepared according to a reported procedure (*42*).

**[1,3-Bis(2,6-diisopropylphenyl)imidazol-2-ylidene]CuO*t*-Bu (NHC–Cu-1)** was prepared according to a reported procedure (*43*).

**Acetonitrile** was purchased from Fisher Scientific and purified by passage through an alumina column.

**Acetyl chloride** was purchased from Sigma-Aldrich and used as received.

**Acrylonitrile** was purchased from Aldrich or Acros and purified by distillation from $CaH_2$ (Strem) prior to use.

**Allenes** were prepared according to previously reported procedures (*44,45*).

**Aluminum trifluoromethanesulfonate** was purchased from Aldrich and used as received.

**Azobisisobutyronitrile:** purchased from Aldrich Chemical Co. and used as received.

**Benzonitrile** (**anhydrous grade)** was purchased from Sigma-Aldrich and used as received.

**Benzoyl chloride** was purchased from Sigma-Aldrich and used as received.

**Bis(pinacolato)diboron [$B_2(pin)_2$]** was purchased from Frontier, recrystallized from hexanes and dried under vacuum prior to use.

**Chlorotrimethylsilane** was purchased from Oakwood Chemical and purified by distillation from $CaH_2$ (Strem) prior to use.

**(*E*)-1,4,5-Hexatrien-1-ylbenzene** was prepared according to previous reported procedures (*46,47,48*).

**Copper(I) chloride** was purchased from Strem and used as received.

**Copper(I) iodide** was purchased from Strem and used as received.

**Copper(I) *t*-butoxide** was prepared according to previous reported procedures (*49,50*).

**Dicyclohexylamine** was purchased from Aldrich and purified by distillation from $CaH_2$ (Strem) prior to use.

**2,6-Diisopropylphenylimidoneophylidene molybdenum(VI) bis(hexafluoro-*t*-butoxide) (Mo-1)** was purchased from Strem and used as received.

**2,6-di*t*-Butyl-4-methylpyridine** was purchased from Tokyo Chemical Industry Co. or Oakwood Chemical and used as received.

**Imidazole** was purchased from Oakwood Chemical and used as received.

**Imidazolium salts Imid-1 and Imid-2** were purchased from Sigma-Aldrich and used as received.

**Lithium borohydride (2.0 M in thf)** was purchased from Sigma-Aldrich and used as received.

**Mesitylcopper(I)** was prepared according to previously reported procedures (*51,52*).

**Methanol** was purchased from Fisher Scientific and dried over Mg turnings and distilled prior to use.

**3-Methyl-1,2-butadiene** was purchased from SynQuest and used as received.

**2-Methyl-2-propanol** was purchased from Aldrich and purified by distillation from $CaH_2$ (Strem) prior to use.

**Nitriles** were purchased from Sigma-Aldrich, Alfa Aesar or Acros Organics and used as received.

**Palladium(II) acetate** was purchased from Strem and used as received.

**Paraformaldehyde** was purchased from Aldrich and used as received.

**1-phenylpropan-1-imine:** Prepared according to a reported procedure.[33]

**Phosphines** were purchased from Strem and used as received.

**Polymethylhydrosiloxane** (**PMHS**) was purchased from Alfa Aesar and used as received.

**Potassium carbonate** was purchased from Aldrich and used as received.

**Potassium fluoride** was purchased from Acros Organics and used as received.

**Propan-2-ol** was purchased from Fisher Scientific and purified by distillation from $CaH_2$ (Strem) prior to use.

**Propargyl alcohol** was purchased from Aldrich and used as received.

**Sodium borohydride** was purchased from Oakwood Chemical and used as received.

**Sodium cyanoborohydride** was purchased from Oakwood Chemical and used as received.

**Sodium iodide** was purchased from Alfa Aesar and used as received.

**Sodium methoxide** was purchased from Strem and used as received.

**Sodium *t*-butoxide** was purchased from Strem and used as received.

***t*-Butyldimethylsilyl chloride** was purchased from Oakwood Chemical and used as received.

**Tributyltin hydride** was purchased from Oakwood Chemical and used as received.

**Trifluoromethanesulfonic anhydride ($Tf_2O$)** was purchased from Oakwood Chemical and purified by distillation from $CaH_2$ (Strem) prior to use.

# 2 Initial Studies Regarding Catalytic Addition to a Nitrile and Ketimine Reduction

## 2.1 Probing feasibility

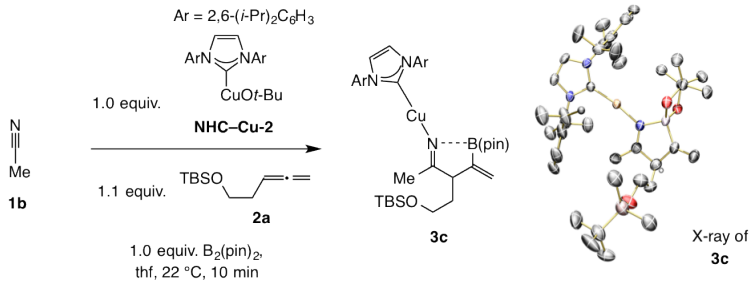


In an $N_2$-filled glove box, an oven-dried 2-dram vial was charged with [1,3-bis(2,6-diisopropylphenyl)imidazol-2-ylidene]CuO*t*-Bu (**NHC–Cu-2**) (20.0 mg, 0.038 mmol), $B_2(pin)_2$ (9.6 mg, 0.038 mmol) and monosubstituted allene **2a** (10 μL, 0.042 mmol). This mixture was then charged with thf (0.5 mL) and was allowed to stir for five min, resulting in a clear colorless solution. At this point acetonitrile (10 μL, 0.076 mmol) was added through syringe, and the resulting colorless solution was transferred to a J-young NMR tube; the original vial was then washed with thf (0.1 m). Reaction progress was monitored through $^1H$ NMR spectroscopy, by irradiation of the thf signals with a PRESAT pulse sequence. In less

than 10 min the transformation afforded Cu-ketimide **3c** quantitatively. The sample was brought back to the glove box and the solution was passed through a plug of Celite, washed with thf (1 mL in total) and the volatiles were removed in vacuo to leave behind colorless oil, which was re-dissolved in hexanes and kept in the freezer in a glove box for 12-16 h at –40 °C. Crystals suitable for x-ray diffraction were thus obtained. The remainder of the crystalline material was filtered and dried under vacuum, affording 22.0 mg of Cu-ketiminde **3c** (70% yield).

### 2.1.1 [3-(2-((*tert*-Butyldimethylsilyl)oxy)ethyl)-4-(4,4,5,5-tetramethyl-1,3,2-dioxaborolan-2-yl)pent-4-en-2-imido][1,3-bis(2,6-diisopropylphenyl)imidazol-2-ylidene]copper(I) (3c):

**$^1$H NMR (toluene-$d_8$, 500 MHz):** δ 7.35 (t, *J* = 7.8 Hz, 2H), 7.21 (d, *J* = 7.9 Hz, 2H), 7.16 (d, *J* = 7.9 Hz, 2H), 6.54 (s, 2H), 5.75 (d, *J* = 4.1 Hz, 1H), 5.41 (d, *J* = 4.4 Hz, 1H), 4.08 (q, *J* = 8.3 Hz, 1H), 3.75 (s, 1H), 3.06 (d, *J* = 8.0 Hz, 1H), 2.71 (hept, *J* = 7.3 Hz, 5H), 2.26 (s, 2H), 1.59 (s, 3H), 1.52 (s, 9H), 1.40 (d, *J* = 6.9 Hz, 6H), 1.22 (s, 13H), 1.15 (s, 11H), 1.02 (s, 2H), 0.26 (s, 6H). **$^{13}$C NMR (toluene-$d_8$, 126 MHz):** δ 185.6, 182.1, 145.7, 145.7, 135.4, 130.7, 124.8, 124.6, 123.3, 110.0, 78.2, 61.6, 55.3, 35.9, 29.1, 29.0, 28.1, 27.3, 27.2, 26.7, 26.4, 24.8, 24.6, 24.0, 23.6, –4.9, –5.0. The carbon bearing the boron atom could not be detected due to quadrupolar effects. **$^{11}$B NMR (toluene-$d_8$, 160 MHz):** δ 10.26. Attempts at obtaining an IR spectrum and mass spec data were unsuccessful due to rapid decomposition.

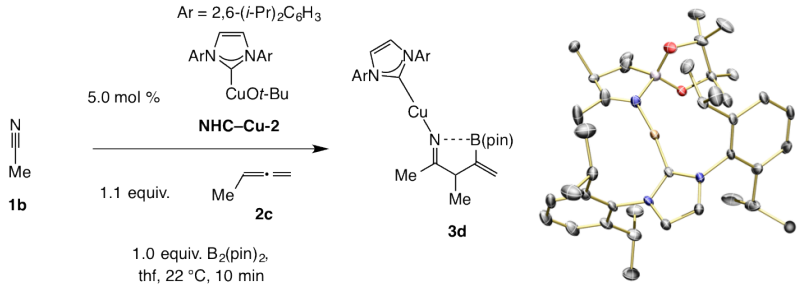


Based on a similar procedure as described above but with Me-substituted allene **2b** (dispensed as a stock solution in thf, 0.100 mmol) we synthesized 23.0 mg (0.034 mmol) of Cu-ketimide **3d** (90% yield). Single crystals suitable for X-ray diffraction were obtained by vapor diffusion of hexanes into a concentrated solution of **3d** in thf, which is present in the unit cell but has been omitted in the ORTEP figure for clarity.

### 2.1.2 [3-Methyl-4-(4,4,5,5-tetramethyl-1,3,2-dioxaborolan-2-yl)pent-4-en-2-imido][1,3-bis(2,6-diisopropylphenyl)imidazol-2-ylidene]copper(I) (3d)

**$^1$H NMR ($C_6D_6$, 600 MHz):** δ 7.21–7.14 (m, 2H), 7.02 (d, *J* = 7.8 Hz, 4H), 6.26 (s, 2H), 5.82 –5.75 (m, 1H), 5.46 – 5.38 (m, 1H), 2.99 (q, *J* = 7.4 Hz, 1H), 2.58–2.46 (m, *J* = 7.0 Hz, 4H), 1.54 (s, 3H), 1.29 (dd, *J* = 6.9, 5.2 Hz, 12H), 1.22 (d, *J* = 7.3 Hz, 3H), 1.07–0.98 (m, 22H). **$^{13}$C NMR ($C_6D_6$, 151 MHz):** δ 186.4, 181.9, 145.7, 135.4, 130.7, 128.3, 124.7, 123.2, 121.7, 108.8, 78.4, 78.2, 51.7, 29.0, 27.9, 27.8, 27.2, 27.1, 24.8, 24.8, 24.1, 24.0, 23.3, 17.6. The carbon directly attached to the boron atom could not be detected due to quadrupolar effects. **$^{11}$B NMR ($C_6D_6$, 160 MHz):** δ 10.16. Attempts at obtaining an IR spectrum and mass spec data were unsuccessful due to rapid decomposition.

## 2.2 Synthesis of an N-H Ketimine by Catalytic Addition to a Nitrile and Competitive Alkene Isomerization

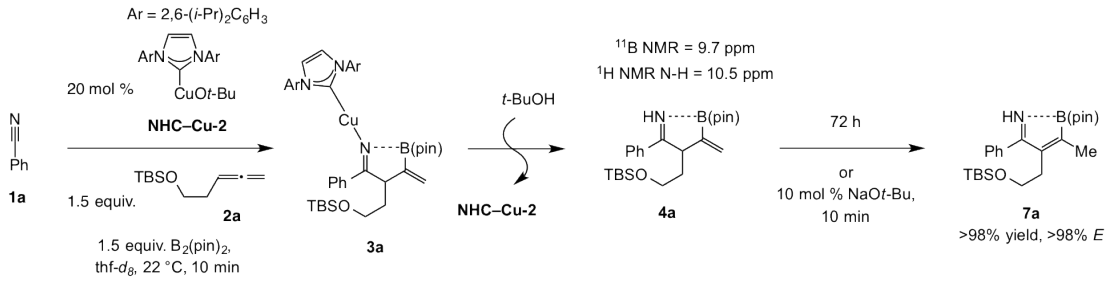


In an $N_2$-filled glove box, an oven-dried 2-dram vial was charged with [1,3-bis(2,6-diisopropylphenyl)imidazol-2-ylidene]CuO*t*-Bu (**NHC–Cu-2**) (6.0 mg, 0.011 mmol), $B_2(pin)_2$ (21.8 mg, 0.086 mmol), allene **2a** (20 μL, 0.084 mmol) and $PhCH_2Ph$ (9 μL, 0.057 mmol, internal standard). To this mixture was added thf-$d_8$ (0.5 mL) by syringe and the mixture was allowed to stir for five min. Then PhCN (5.9 μL, 0.057 mmol) was added by syringe and the resulting colorless solution was transferred to a J-young NMR tube and the original vial was washed with thf-$d_8$ (0.1 mL).

Reaction progress was monitored by $^1$H NMR spectroscopy (Fig. S1), allowing us to confirm the formation of Cu-ketimide **3a**. The most representative peaks, assigned by analogy to related complexes **3b** and **3c** (see above), are highlighted.

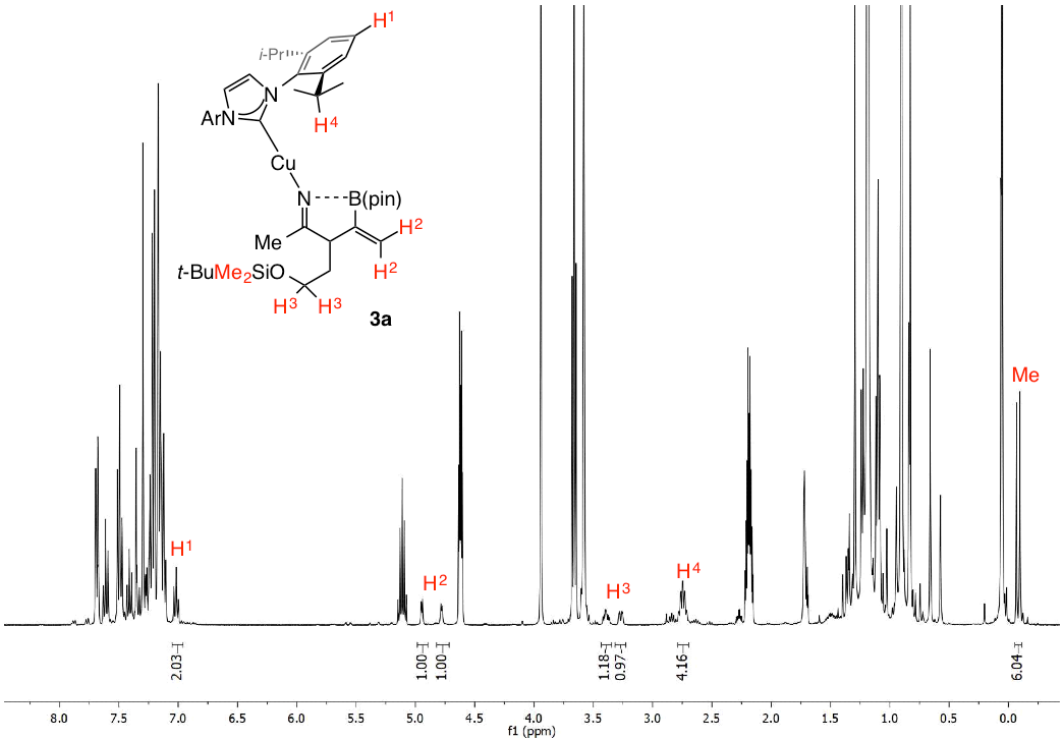


**Fig. S1.** The $^1$H NMR spectrum corresponding to the transformation leading to the formation of Cu-ketimide **3a**.

The sample was brought back to the glove box and the solution was charged *t*-BuOH (9 μL, 0.0914 mmol) by syringe and reaction progress was monitored by $^1$H NMR analysis after 10 min, allowing us to confirm that ketimine **4a** is formed (Fig. S2).

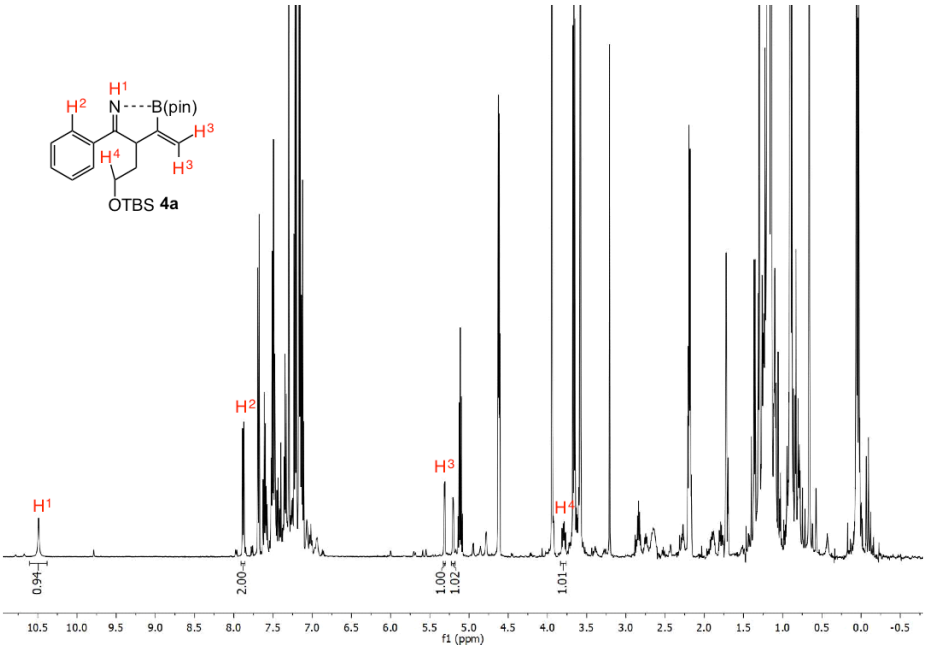


**Fig. S2.** $^{1}$H NMR spectrum corresponding to reaction of Cu-ketimide **3a** with *t*-BuOH to afford N–H ketimine **4a**.

Although the peaks corresponding to various unidentifiable byproducts were present in trace amount (Fig. S3a), none of α,β-unsaturated ketimine **7a** could be detected after 10 min in the $^{1}$H NMR spectrum. Accordingly, olefin isomerization was monitored spectroscopically, leading us to establish that isomerization of β,γ-unsaturated ketimine **4a** to α,β-unsaturated ketimine **7a** takes place relatively slowly. After 2 h at 22 °C (Fig. S3b), 40% isomerization was observed, and only 72 h conversion to **7a** was completed (>98%; Fig. S3e).

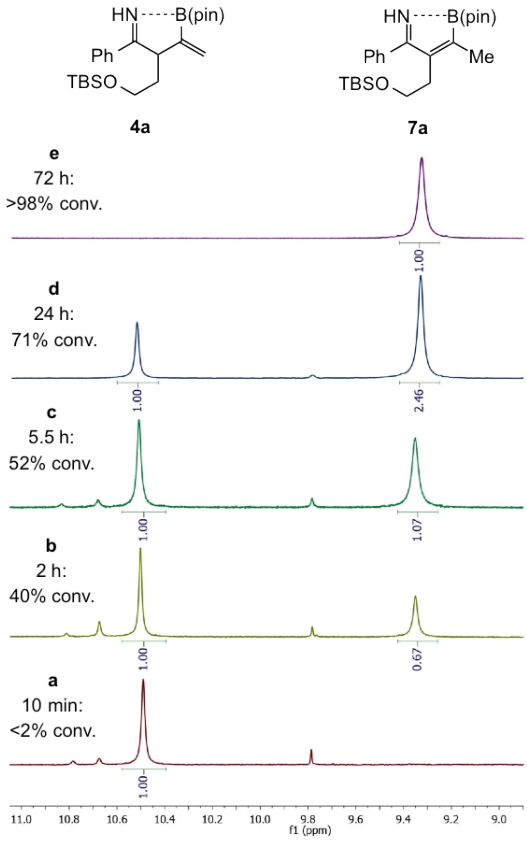


**Fig. S3.** Investigation of the facility of alkene isomerization in the absence of a metal alkoxide.

Control experiments showed that the alkene in β,γ-unsaturated ketimine **4a** readily isomerizes in the presence of 10 mol % NaO*t*-Bu (see Fig. S4).

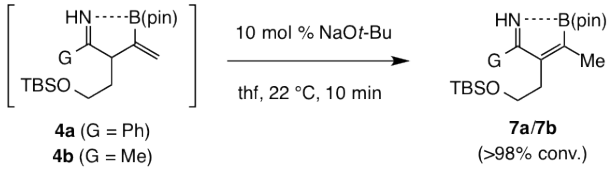


In an $N_2$-filled glove box, an oven-dried 2-dram vial was charged with [1,3-bis(2,6-diisopropylphenyl)imidazol-2-ylidene]CuO*t*-Bu (**NHC–Cu-2**) (2.6 mg, 0.0050 mmol), $B_2(pin)_2$ (38.1 mg, 0.150 mmol), allene **2a** (36 μL, 0.150 mmol). At this point, thf (0.5 mL) was added through syringe and the mixture was allowed to stir for five min (leading to clear solution). Subsequently, the mixture was charged with PhCN (10.0 μL, 0.100 mmol) and *t*-BuOH (16.3 μL, 0.170 mmol) through syringe. The resulting colorless solution was transferred to a J-young NMR tube and the original vial was washed with thf-$d_8$ (0.1 mL) and reaction progress was monitored by $^1$H NMR spectroscopy. Complete (>98%) conversion to α,β-unsaturated ketimine **7a** was observed after 72 h.

The sample was brought back to the glove box and the solution was transferred to a vial containing NaO*t*-Bu (1 mg, 0.0914 mmol, 0.010 mmol). Further spectroscopic analysis confirmed quantitative conversion to **7a** in <10 min.

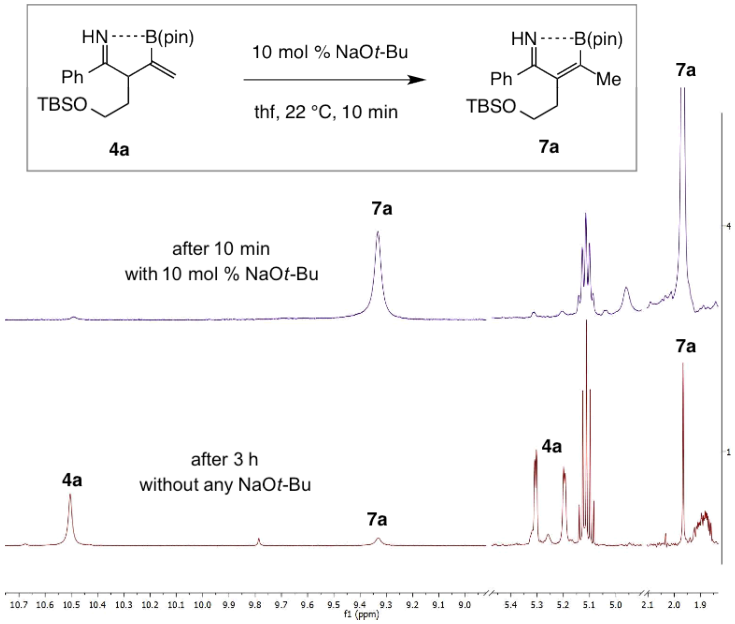


**Fig. S4.** Investigation of the facility of alkene isomerization in the presence of 10 mol % NaO*t*-Bu.

## 2.3 Isolation and Characterization of Two α,β-Unsaturated Ketimines

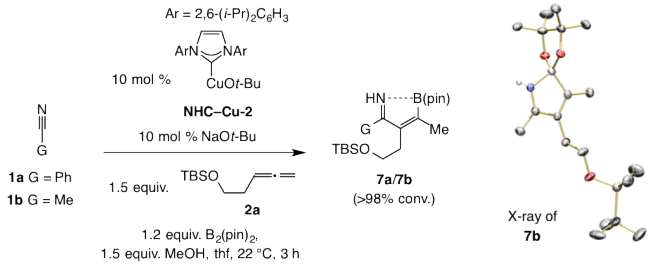

In an $N_2$-filled glove box, an oven-dried 2-dram vial was charged with [1,3-bis(2,6-diisopropylphenyl)imidazol-2-ylidene]CuO*t*-Bu (**NHC–Cu-2**) (6 mg, 0.050 mmol) and NaO*t*-Bu (10 mg, 0.0914 mmol), and thf was added (1 mL). In a separate vial, $B_2(pin)_2$ (304.2 mg, 1.1980 mmol), allene **2a** (360 μL, 1.500 mmol), MeOH (60 μL, 1.500 mmol) and PhCN (104 μL, 1.000 mmol) were dissolved in thf (5 mL) and the resulting solution was added to the vial containing the Cu complex. The mixture was allowed to stir for 3 h, resulting in a clear colorless solution. A sample of the mixture was transferred to a J-young NMR tube and reaction progress was monitored by $^1$H NMR spectroscopy, through irradiation of the thf signals with a PRESAT pulse sequence. α,β-Unsaturated ketimine **7a** was formed quantitatively (>98% conv.). The sample was brought back to the glove box and the solution was transferred to the original vial, and the volatiles were removed in vacuo. In a glove box, the resulting colorless oil was loaded onto dry silica gel (in a column). Subsequent chromatography (5:1 hexanes:$Et_2O$ to wash away non-polar impurities), flushing of the column with $Et_2O$ (20 mL), and removal of the volatiles in vacuo afforded ketimine **7a** as colorless oil (339 mg, 0.790 mmol, 79 % yield). (Note: Various amounts of pinacol impurity were present as well. The ketimine is moisture-sensitive and must be handled with care.)

### 2.3.1 2-(2-((*tert*-Butyldimethylsilyl)oxy)ethyl)-1-phenyl-3-(4,4,5,5-tetramethyl-1,3,2-dioxaborolan-2-yl)but-3-en-1-imine (7a)

**$^1$H NMR ($C_6D_6$, 500 MHz):** δ 7.67 (s, 1H), 6.93 (m, 1H), 6.90 – 6.75 (m, 4H), 3.32 (dd, *J* = 8.4, 7.2 Hz, 2H), 2.47 (t, *J* = 7.8 Hz, 2H), 2.12 (s, 3H), 1.34 (s, 12H), 0.83 (s, 9H), -0.11 (s, 6H). **$^{13}$C NMR ($C_6D_6$, 126 MHz):** δ 182.6, 133.6, 130.7, 130.5, 128.3, 126.7, 79.3, 62.1, 29.0, 25.9, 25.8, 25.7, 24.8, 18.0, 16.2, –5.7. The carbon atom bearing the boron substituent was not detected due to quadrupolar effects. **$^{11}$B NMR ($C_6D_6$, 160 MHz):** δ 10.00. Attempts at obtaining an IR spectrum and mass spec data were unsuccessful due to rapid decomposition. Pinacol is usually present in varying amounts.

Based on an analogous procedure, ketimine **7b** (16.0 mg, 0.043 mmol, 44 % yield) was synthesized, and the corresponding single crystals suitable for X-ray diffraction were obtained by preparing a concentrated solution in hexanes (0.5 mL), which was kept for 12–16 h in the freezer of the glove box at –40 °C. Crystallization occurs with pinacol present in the unit cell (omitted for clarity in the ORTEP figure).

### 2.3.2 3-(2-((*tert*-Butyldimethylsilyl)oxy)ethyl)-4-(4,4,5,5-tetramethyl-1,3,2-dioxaborolan-2-yl)pent-4-en-2-imine (7b)

**$^1$H NMR ($C_6D_6$, 500 MHz):** δ 7.61 (s, 1H), 3.36 (t, *J* = 7.3 Hz, 2H), 2.23 (t, *J* = 7.3 Hz, 2H), 2.01 (s, 3H), 1.43 (d, *J* = 1.2 Hz, 3H), 1.33 (s, 12H), 0.90 (s, 9H), –0.01 (s, 6H). **$^{13}$C NMR ($C_6D_6$, 126 MHz):** δ 183.9, 131.8, 79.1, 62.6, 33.6, 28.4, 25.7, 18.4, 18.1, 15.4, –5.6. The carbon directly attached to the boron atom could not be detected due to quadrupolar effects. **$^{11}$B NMR ($C_6D_6$, 160 MHz):** δ 9.37. Attempts at obtaining an IR spectrum and mass spec data were unsuccessful due to rapid decomposition.

# 3 Studies Regarding N-H Ketimines Reduction

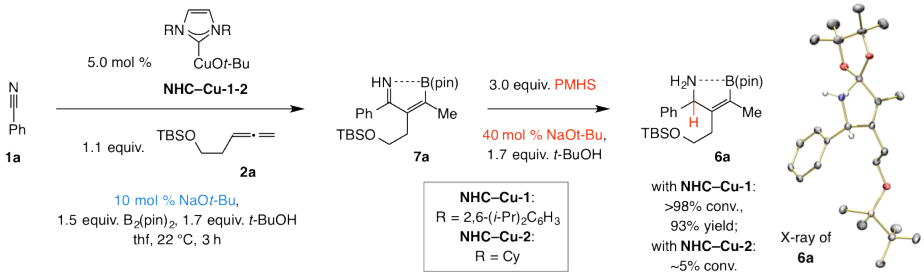


In an $N_2$-filled glove box, an oven-dried 2-dram vial was charged with [1,3-bis(cyclohexyl)imidazol-2-ylidene]CuO*t*-Bu (**NHC–Cu-1**) (1.1 mg, 0.0029 mmol) and NaO*t*-Bu (0.6 mg, 0.006 mmol), and thf was added (0.3 mL). In a separate vial, $B_2(pin)_2$ (22.1 mg, 0.0870 mmol), allene **2a** (21.0 μL, 0.0870 mmol), *t*-BuOH (9.5 μL, 0.099 mmol) and PhCN (6.0 mg, 0.058 mmol) were dissolved in thf (0.3 mL) and then added to the vial containing the Cu complex. The mixture was transferred to a J-young NMR tube and reaction progress was monitored by $^1$H NMR spectroscopy through irradiation of the thf signals with a PRESAT pulse sequence. The reaction reached >98% conv to ketimine **7a** in 3 h. The sample was brought back to the glove box and transferred to a vial containing NaO*t*-Bu (2.4 mg, 0.025 mmol), *t*-BuOH (9.5 μL, 0.099 mmol) and PMHS (10.5 μL, 0.174 mmol). The mixture was placed in an NMR tube and additional thf was used for complete transfer (total volume, ~1 mL). $^1$H NMR spectroscopy indicated >98% conversion to **6a** within 1.5 h. The resulting colorless oil was purified by silica gel chromatography ($CH_2Cl_2$:MeOH=100:1 (20 mL) to 60:1 (40mL)). The samples containing the desired product (as judged by tlc analysis) were collected and concentrated in vacuo to afford white solid residue. At this point, removal of residual pinacol was needed. Thus, the solid residue was placed under vacuum (~ 1 mtorr) and heated to 60 °C for 14 h to afford pure **6a** as white solid (23.3 mg, 0.054 mmol, 93% yield. Single crystals suitable for x-ray diffraction were obtained by preparation of a saturated solution in hexanes at ambient temperature and storage for 12–16 h in a freezer at –20 °C.

### 3.1.1 (*E*)-2-(2-((*tert*-Butyldimethylsilyl)oxy)ethyl)-1-phenyl-3-(4,4,5,5-tetramethyl-1,3,2-dioxaborolan-2-yl)but-2-en-1-amine (6a)

**m.p.** (white solid) = decomposition (140 °C); **IR (neat):** 2956 (w), 2928 (m), 2855 (w), 1254 (m), 1181 (s), 1085 (m), 1047 (s), 833 (s), 774 (s), 732 (m), 701 (m); **$^1$H NMR ($CDCl_3$, 500 MHz)**: δ 7.42–7.27 (m, 5H), 4.53 (s, 1H), 3.36 (td, *J* = 10.1, 6.6 Hz, 1H), 3.02 (td, *J* = 10.2, 5.6 Hz, 1H), 2.19–2.13 (m, 2H), 1.77 (s, 3H), 1.17 (s, 12H), 0.77 (s, 9H), –0.11 (s, 3H), –0.13 (s, 3H); **$^{13}$C NMR ($CDCl_3$, 125 MHz)**: δ 141.2, 137.8, 129.3, 128.6, 127.8, 64.1, 61.9, 31.9, 26.1, 25.4, 18.4, 13.3, –5.21, –5.22. The carbon directly attached to the boron atom could not be detected due to quadrupolar effects; **$^{11}$B NMR ($CDCl_3$, 160 MHz)**: δ 12.43; **HRMS (DART)**: Calcd for $C_{24}H_{43}BNO_3Si$ $[M+H]^+$: 432.31052, Found: 370.30970.

Amine **6b** (from reaction with MeCN) was obtained in 82% yield through the use of the same procedure.

### 3.1.2 (*E*)-3-(2-((*tert*-Butyldimethylsilyl)oxy)ethyl)-4-(4,4,5,5-tetramethyl-1,3,2-dioxaborolan-2-yl)pent-3-en-2-amine (6b)

**m.p.** (white solid) = 105–107 °C; **IR (neat):** 3195 (w), 2954 (m), 2854 (w), 1603 (w), 1461 (w), 1253 (m), 1153 (s), 1092 (m), 1032 (s), 832 (s), 772 (s), 735 (m); **$^1$H NMR ($CDCl_3$, 400 MHz)**: δ 3.75–3.63 (m, 1H), 3.50 (dd, *J* = 8.9, 6.9 Hz, 2H), 2.39–2.29 (m, 1H), 2.25–2.13 (m, 1H), 1.61 (d, *J* = 1.7 Hz, 3H), 1.29 (d, *J* = 6.7 Hz, 3H), 1.15 (s, 12H), 0.88 (s, 9H), 0.04 (s, 3H), 0.03 (s, 3H); **$^{13}$C NMR ($CDCl_3$, 100 MHz):** δ 140.0, 139.0, 79.2, 62.3, 54.9, 31.0, 26.1, 25.9, 25.7, 21.2, 18.4, 13.2, –5.1; **$^{11}$B NMR ($CDCl_3$, 160 MHz)**: δ 11.73; **HRMS (DART)**: Calcd for $C_{19}H_{41}BNO_3Si$ $[M+H]^+$: 370.2949, Found: 370.2957.

## 3.2 Examination of the Role of NaO*t*-Bu in CuH-Catalyzed Ketimine Reduction

### 3.2.1 Spectroscopic investigation of catalytic reactions with and without NaO*t*-Bu

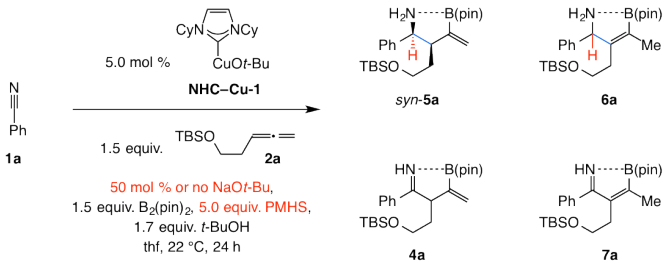


In an $N_2$-filled glove box, an oven-dried 2-dram vial was charged with [1,3-bis(cyclohexyl)imidazol-2-ylidene]CuO*t*-Bu (**NHC–Cu-1**) (1.1 mg, 0.0030 mmol), NaO*t*-Bu (2.8 mg, 0.029 mmol) and *t*-BuOH (19.0 μL, 0.199 mmol), thf was added (0.3 mL), and the solution was allowed to stir for 15 min. In a separate vial, a solution of PMHS (17.4 μL, 0.290 mmol), $B_2(pin)_2$ (22.1 mg, 0.0870 mmol), allene **2a** (21 μL, 0.0879 mmol) and PhCN (6.0 mg, 0.058 mmol) was prepared (0.3 mL thf). The solutions were mixed and then transferred to a J-young NMR tube. Upon mixing, the mixture turned yellow. Reaction progress was monitored by $^1$H NMR spectroscopy over 24 h with a PRESAT pulse sequence for irradiation of the solvent peaks.

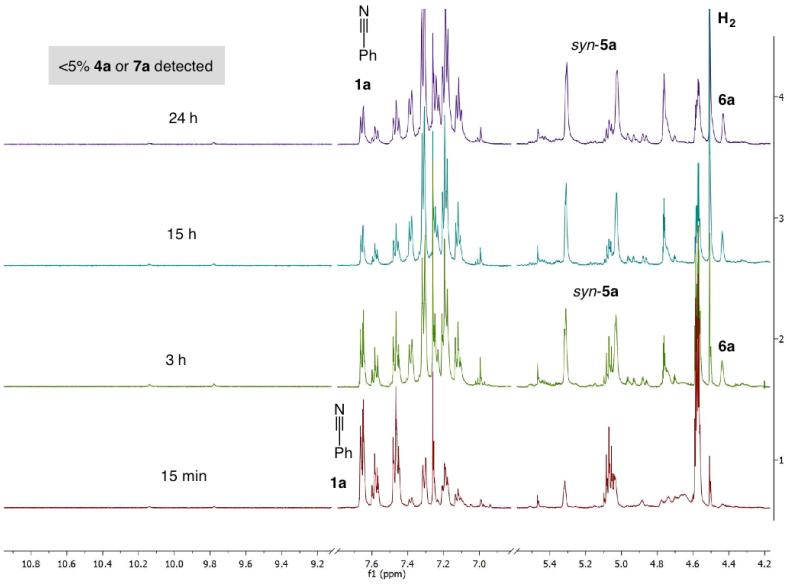


**Fig. S5.** Examination of a catalytic allyl addition/ketimine reduction process in the presence of NaO*t*-Bu. Highlighted peaks correspond to *syn*-**5a** (aryl CH, $H_2$C=C–Bpin), **4a** and **7a** (N*H*), and **6a** (*H*(Ph)C$NH_2$).

Analysis by $^{1}$H NMR spectroscopy (Fig. S5) revealed that *syn*-**5a** is generated throughout, whereas only trace amounts (<5%) of **4a** and **7a** are formed. Since **4a** does not accumulate as the transformation progresses, it can be deduced that reduction of **4a** to afford ***syn*-5a** is significantly faster than its formation in the presence of 50 mol% NaO*t*-Bu. In addition to *syn*-**5a**, isomerized amine **6a** was detected (~15% conv. from reduction of ketimine **7a**).

These observations stand in contrast to the experiment performed in the absence of NaO*t*-Bu (Fig. S6). Under these conditions, **4a** was formed as the main product along with just <10% *syn*-**5a** (see Figure 2B, the manuscript). Congruent with the experiments in Section 3 of the Supplementary Material, **4a** isomerizes over time to generate **7a**, but there is none of amine **6a** could be observed under the same conditions.

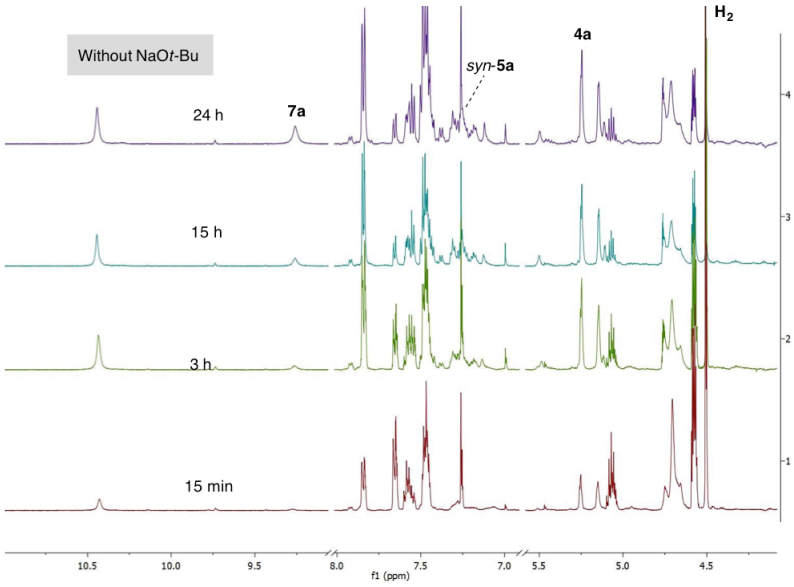


**Fig. S6.** Investigation of a catalytic allyl addition/ketimine reduction process in the absence of NaO*t*-Bu. Highlighted signals correspond to *syn*-**5a** (aryl C–H), **4a** (NH and $H_2$C=C-Bpin), and **7a** (N*H*).

After establishing that reduction of **4a** and **7a** are fast in the presence of NaO*t*-Bu, we investigated the role of this metal alkoxide in the ketimine reduction step. Accordingly, β-boryl-ketimine **7a** was prepared (see Section 3.1) and subjected to stoichiometric amounts of NHC–Cu-H without any NaO*t*-Bu or *t*-BuOH. The instability of ketimine **4a** towards isomerization precluded its isolation and examination.

### 3.2.2 Spectroscopic analysis of addition of a Cu–H complex to a β-boryl ketimine

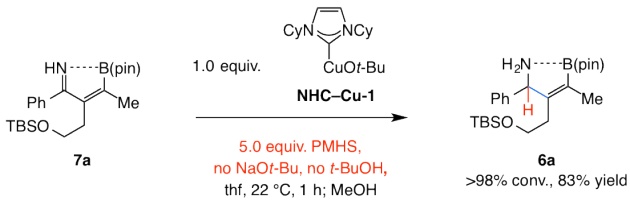


In an $N_2$-filled glove box, an oven-dried 2-dram vial was charged with [1,3-bis(cyclohexyl)imidazol-2-ylidene]CuO*t*-Bu (**NHC–Cu-1**) (11.1 mg, 0.0300 mmol) and the mixture was dissolved in thf-$d_8$ (0.3 mL). A separate vial was loaded with a freshly prepared solution of ketimine **7a** (0.0300 mmol in 0.3 mL or thf), which was prepared as detailed in Section 3.1. The precise solution concentration of **7a** was determined through analysis of the

corresponding $^1$H NMR spectrum (with $PhCH_2Ph$ as the internal standard). To this mixture was added PMHS (5.4 μL, 0.090 mmol) by syringe. The solutions were mixed and then transferred to a J-young NMR tube and the course of the reaction was monitored by $^1$H NMR spectroscopy, which indicated completion in 1 h. The reaction was then quenched by the addition of MeOH (1 mL), the volatiles were removed in vacuo, and the resulting colorless oil was purified by silica gel chromatography (4:1–2:1 hexanes:EtOAc), affording **6a** as off-white solid (10.8 mg, 83% yield).

In the absence of NaO*t*-Bu or *t*-BuOH, based on spectroscopic analysis ($^1$H NMR; Fig. S7), there was full conversion to amine **6a** within 1 h (50 % conv. in 10 min). This finding indicates that CuH-catalyzed ketimine reduction – unlike the abovementioned catalytic experiments – is efficient with stoichiometric amounts Cu–H complex present.

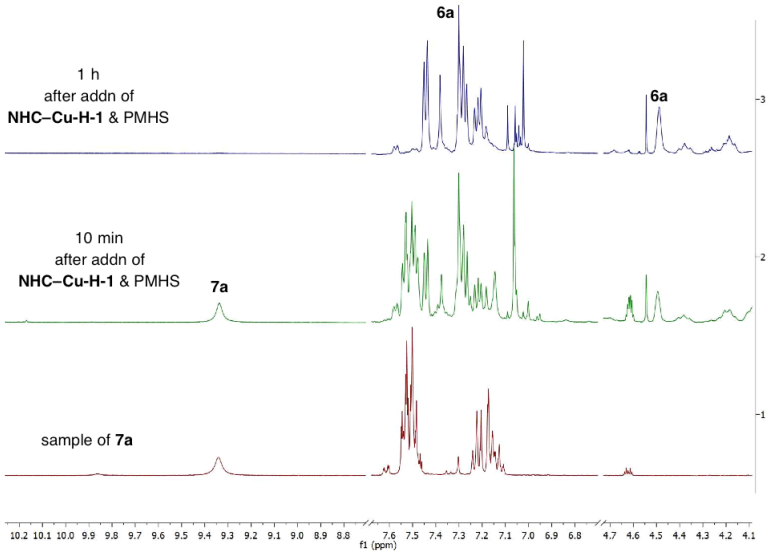


**Fig. S7.** The $^1$H NMR spectrum for reaction of a stoichiometric amount of **NHC–Cu–H-1** with ketimine **7a**.

Based on the above data, it can be concluded that the presence of NaO*t*-Bu does not impact the addition of a Cu–H complex to α,β-unsaturated ketimine **7a**. Thus, the positive influence of the metal alkoxide must be on another step of the catalytic cycle. It is likely, as illustrated in Fig. S8, that the positive impact of the metal alkoxide is to accelerate regeneration of the catalytic active Cu–H complex by facilitating its release (i.e., **S1 → S2**).

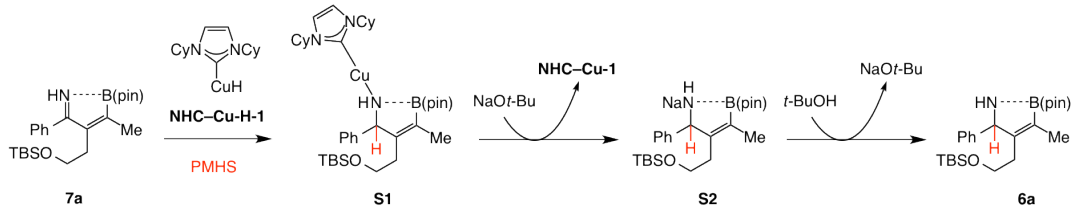


**Fig. S8.** The role of a metal alkoxide in regeneration of the Cu–H catalyst.

## 3.3 Reduction of an N-H ketimine without a neighboring boryl unit

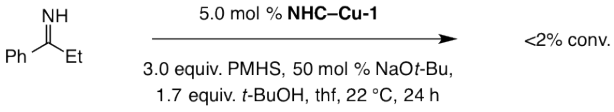

In an $N_2$-filled glove box, an oven-dried 2-dram vial was charged with [1,3-bis(2,6-diisopropylphenyl)imidazol-2-ylidene]CuO*t*-Bu (**NHC–Cu-2**) (2.6 mg, 0.005 mmol) or [1,3-bis(cyclohexyl)imidazol-2-ylidene]CuO*t*-Bu (1.9 mg, 0.005 mmol) and NaO*t*-Bu (4.8 mg, 0.050 mmol), and thf was added (0.5 mL). In a separate vial, 1-phenylpropan-1-imine (17.0 mg, 0.100 mmol), *t*-BuOH (16.3 μL, 0.170 mmol) and PMHS (30.0 μL, 0.500 mmol) were dissolved in thf (0.5 mL) and the resulting solution was added to the vial containing the Cu complex. Upon mixing, there was significant $H_2$ evolution. The mixture was transferred to a J-young NMR tube and reaction progress was monitored by $^1$H NMR analysis, through irradiation of the thf signals with a PRESAT pulse sequence. 1-Phenylpropan-1-imine was recovered quantitatively, while *t*-BuOH was consumed entirely, likely due to reaction with **NHC–Cu–H** to generate $H_2$. Furthermore, the above experiment was performed in the presence $B_2(pin)_2$ and *t*-BuO–B(pin) (1.0 equiv. of each), entities that are present in solution of a catalytic process. As before, there was <5% conversion to the amine.

## 3.4 Studies regarding CuH-catalyzed multicomponent processes

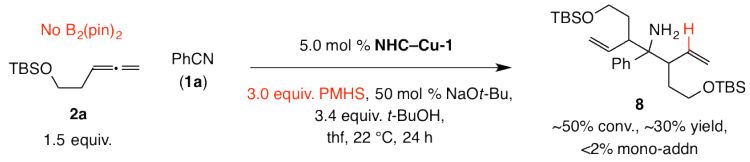


In an $N_2$-filled glove box, an oven-dried 2-dram vial was charged with [1,3-bis(cyclohexyl)imidazol-2-ylidene]CuO*t*-Bu (**NHC–Cu-1**) (1.9 mg, 0.005 mmol) and NaO*t*-Bu (4.8 mg, 0.050 mmol), and thf was added (0.5 mL). In a separate vial, PhCN (10.0 μL, 0.100 mmol), allene **2a** (36 μL, 0.150 mmol) and *t*-BuOH (32.5 μL, 0.340 mmol) were added by syringe as a thf solution (0.5 mL). The solutions were then combined and allowed to stir at 22 °C for 24 h. At this time, based on $^1$H NMR analysis, ~55% of the nitrile was consumed. Removal of the volatiles followed by silica gel chromatography afforded **8** as a mixture of stereoisomers. The identity of **8** was ascertained through analysis of its $^1$H NMR spectrum and by mass spectrometry: **HRMS (DART):** Calcd for $C_{29}H_{53}NO_2Si_2$ $[M+H]^+$: 504.3693, Found: 504.3708.

# 4 Determination of Relative Rates of Formation and Relative Reactivity of Cu–B(pin) and Cu–H Complexes

## 4.1 Relative rates of Cu–B(pin) versus Cu–H complex generation:

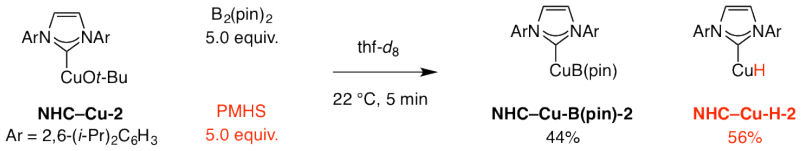


***a. With equal amounts of $B_2(pin)_2$ and PMHS.*** In an $N_2$-filled glove box, an oven-dried 2-dram vial was charged with [1,3-bis(2,6-diisopropylphenyl)imidazol-2-ylidene]CuO*t*-Bu (**NHC–Cu-2**) (10.0 mg, 0.0190 mmol) and thf-$d_8$ was introduced (0.2 mL). In a separate vial, a solution of PMHS (6 μL, 0.0950 mmol), $B_2(pin)_2$ (24.2 mg, 0.0950 mmol) was prepared in thf-$d_8$ (0.4 mL). The solutions were mixed and transferred to a J-young NMR tube. Upon

mixing, the solution turned yellow, as expected based on previous reports regarding **NHC–Cu-H-2** (*43*). Reaction progress was monitored by $^1$H NMR spectroscopy for 10 min (Fig. S9). Product analysis by $^1$H NMR spectroscopy indicated **NHC–Cu-H-2** and **NHC–Cu-B(pin)-2** at nearly similar rates (56:44). The identity of the Cu–B(pin) and Cu–H complexes was confirmed by independent synthesis, namely, by treatment of **NHC–Cu-2** with $B_2(pin)_2$ and PHMS, respectively. Unidentified decomposition products were observable after an additional 10 min, is in line with the reported level of stability for these two Cu-based complexes (*42*). These experiments were reproduced in $C_6D_6$, for which the chemical shifts for **NHC–Cu-B(pin)-2** and **NHC–Cu-H-2** have been previously reported (*42,43*).

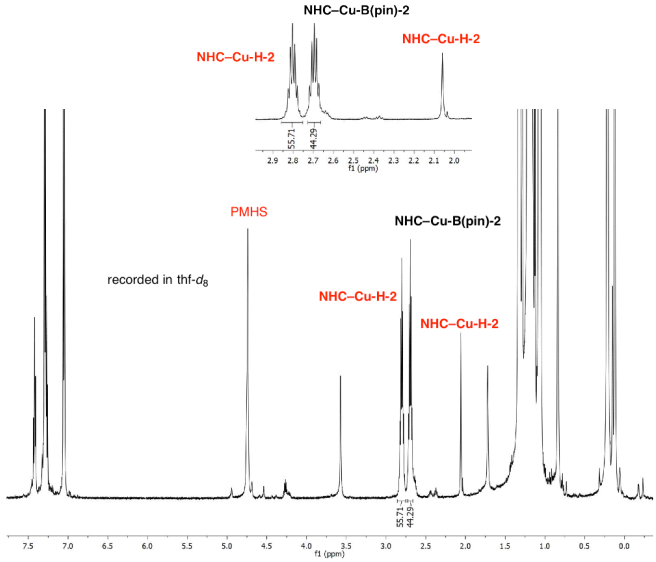


**Fig. S9.** Relative rates of Cu–B(pin) and a Cu–H complex formation with equal amounts of $B_2(pin)_2$ and PMHS.

After 10 min, the sample was brought back to the glove box and charged with *t*-BuOH (10 μL, 0.1727 mmol), causing rapid decrease of the intensity of the peaks attributed to **NHC–Cu-H-2**, while those corresponding to **NHC–Cu-B(pin)-2** grew in size (Fig. S10). This was

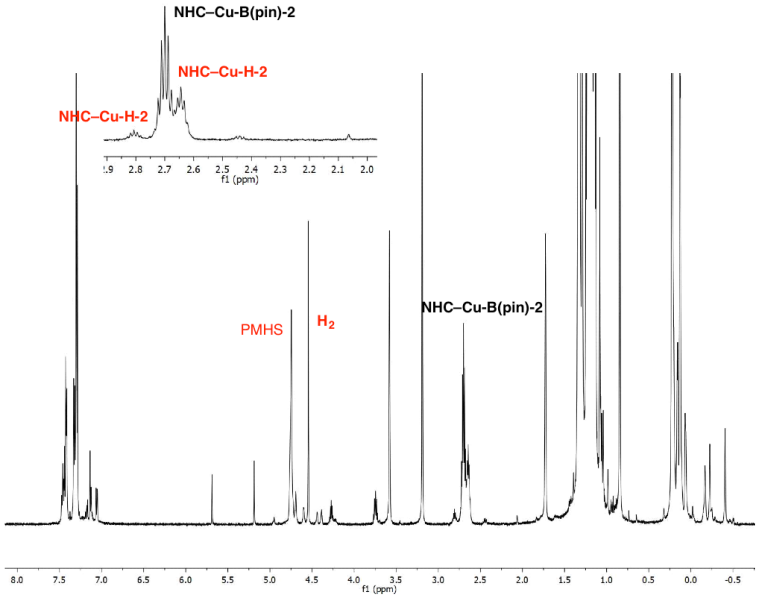


**Fig. S10.** Investigation of the relative rates of reactions of a Cu–B(pin) and a Cu–H complex (generated with equal amounts of $B_2(pin)_2$ and PMHS) with *t*-BuOH.

accompanied by $H_2$ evolution, which was also observable by $^1$H NMR spectroscopy.

The signals corresponding to various side products became more dominant after 20 min. Decomposition is probably because the Cu-based complexes are not stable for more than a limited period of time at 22 °C. It is unlikely that *t*-BuOH facilitates byproduct formation. This is because, when alcohol was added to the mixture of PMHS and $B_2(pin)_2$ (vs. being introduced after 10 min), there was minimal decomposition and **Cu-B(pin)-2** was the only species formed.

The above experiments thus illustrate that **NHC–Cu-H-2** and **NHC–Cu-B(pin)-2** are formed in similar rates when PMHS and $B_2(pin)_2$ are present in equal amounts. These studies further demonstrate that **NHC–Cu-H-2** reacts selectively with *t*-BuOH, whereas **NHC–Cu-B(pin)-2** does not do so at an appreciable rate. *These studies bear the significant implication that, even if PMHS and $B_2(pin)_2$ were simultaneously present, **NHC–Cu-B(pin)-2** can be made to accumulate selectively by means of a nonproductive cycle.*

***b. With amounts of $B_2(pin)_2$ and PMHS reflecting the catalytic conditions.*** Similar experiments were performed but in the presence of $B_2(pin)_2$ and PMHS amounts in the presence of $Ph_2CH_2$ as the internal standard, which reflect the catalytic conditions (i.e., excess PMHS; see Fig. 3A in the manuscript).

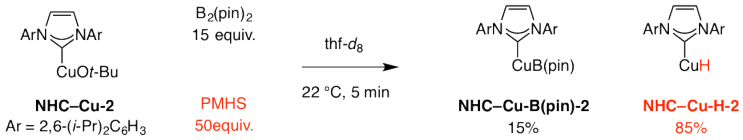


The same procedure as described above was used, except for different ratios of $B_2(pin)_2$ and PMHS. Product analysis through $^1$H NMR spectroscopy (Fig. S11) indicated the formation of **NHC–Cu-H-2** and **NHC–Cu-B(pin)-2** in 15:85 ratio (vs. 56:44 when equal amounts were used). *These experiments show that, under conditions that are similar to those used for a catalytic process, **NHC–Cu-H-2** is formed faster than **NHC–Cu-B(pin)-2**.*

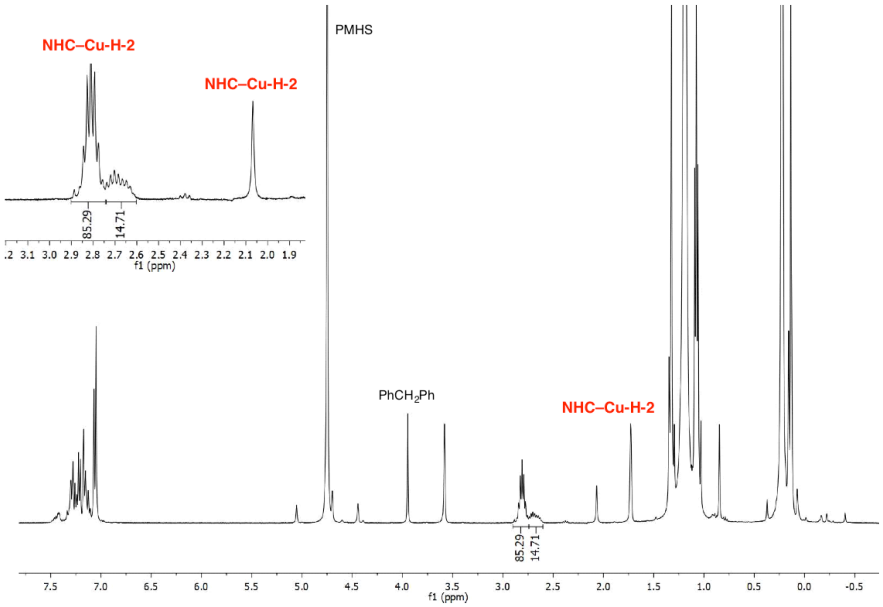


**Fig. S11.** Investigation of the relative rates of formation of a Cu–B(pin) and a Cu–H complex with 15:50 ratio of $B_2(pin)_2$:PMHS (to emulate the catalytic conditions).

As before, addition of *t*-BuOH led to rapid disappearance of the peaks for **NHC–Cu-H-2** and increase in area for those corresponding to **NHC–Cu-B(pin)-2** (Fig. S12), along with detectable $H_2$ evolution, and formation of byproducts upon standing at 22 °C.

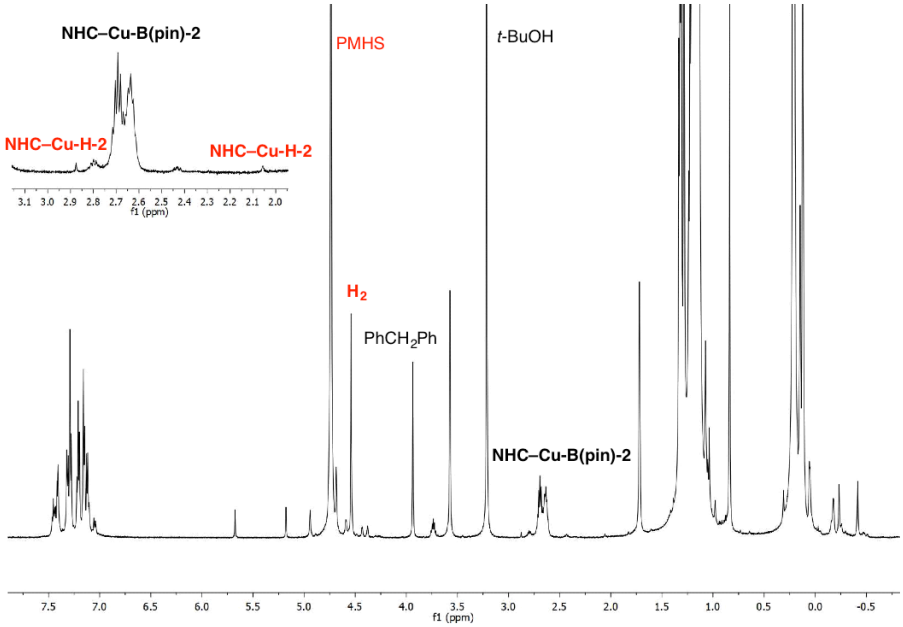


**Fig. S12.** Investigation of the relative rates of reactions of a Cu–B(pin) and a Cu–H complex (generated with equal amounts of $B_2(pin)_2$ and PMHS) with *t*-BuOH.

## 4.2 Relative rates of Cu–B(pin) and Cu–H addition to a monosubstituted allene

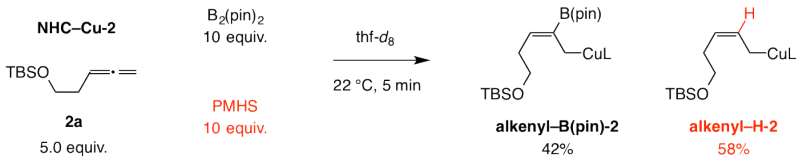


In an $N_2$-filled glove box, an oven-dried 2-dram vial was charged with [1,3-bis(2,6-diisopropylphenyl)imidazol-2-ylidene]CuO*t*-Bu (**NHC–Cu-2**) (6.0 mg, 0.0114 mmol) and thf-$d_8$ was added (0.2 mL). In a separate vial, a thf-$d_8$ (0.4 mL) solution containing PMHS (6.9 μL, 0.1140 mmol), $B_2(pin)_2$ (28.9 mg, 0.1140 mmol), allene **2a** (11.4 mg, 0.0571 mmol) and $PhCH_2Ph$ as the internal standard (2.8 mg, 0.0166 mmol) was prepared. The solutions were mixed (becoming yellow) and transferred to a J-young NMR tube. The solution turned intense yellow upon mixing, fading away in less than one min to become colorless.

Reaction progress was monitored through $^1H$ NMR spectroscopy in the presence of $Ph_2CH_2$ as the internal standard (Fig. S13). These studies show that **alkenyl–H-2** is formed slightly faster than **alkenyl–B(pin)-2** in the absence of an alcohol. The identity of the assigned species was deduced based on their coupling patterns as well as from independent synthesis of **alkenyl–B(pin)-2** and **alkenyl–H-2**, obtained by reaction of **NHC–Cu-2** with $B_2(pin)_2$ and PHMS, respectively, and their ensuing addition to allene **2a**.

It merits mention that the spectrum for **alkenyl–H-2** indicates that it exists as a single isomer. It is however likely that this represents an *E*/*Z* isomeric mixture that undergoes chemical exchange at a rate that is faster than the NMR timescale.

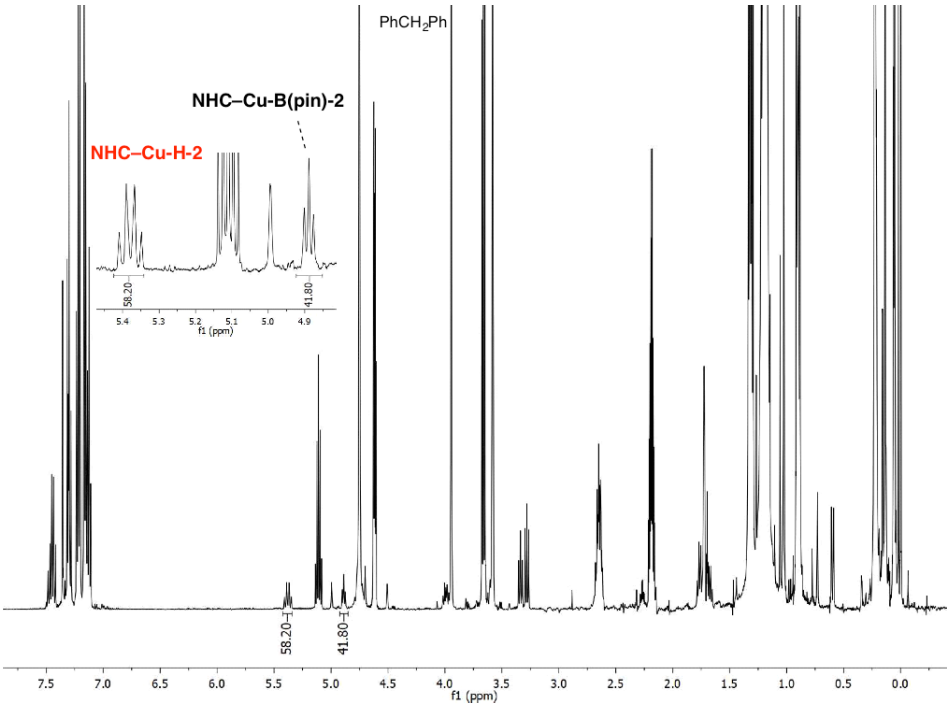


**Fig. S13.** Investigation of the relative rates of addition of a Cu–B(pin) and a Cu–H complex to an allene.

The ratio of **alkenyl–B(pin)-2** and **alkenyl–H-2** is similar that of **NHC–Cu-B(pin)-2** and **NHC–Cu-H-2** in the experiments described previously (Section 4.1). This fact suggests that under these conditions, reaction of **NHC–Cu-2** with $B_2(pin)_2$ and PMHS is considerably more facile than the addition of he corresponding Cu–B(pin) and Cu–H complexes to **2a**, and, as a result the initial ratio of **NHC–Cu-B(pin)-2** and **NHC–Cu-H-2** is retained.

Similar studies were carried out under conditions that more closely resemble those used in a catalytic process (see Fig. 3A of the manuscript). Here, due to larger amounts of PMHS, a higher concentration of **alkenyl–H-2** was observed.

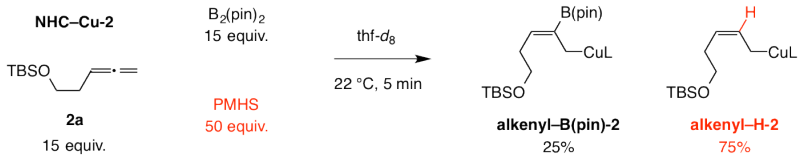


## 4.3 Relative rates of addition of Cu–allyl species derived from Cu–B(pin) and Cu–H to PhCN

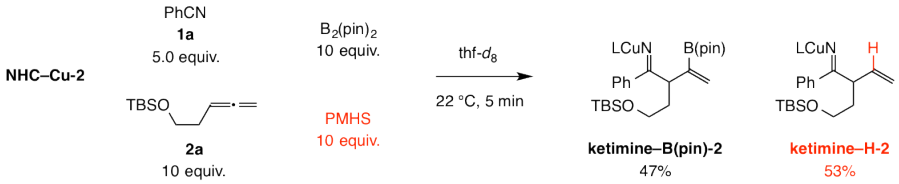


In an $N_2$-filled glove box, an oven-dried 2-dram vial was charged with [1,3-bis(2,6-diisopropylphenyl)imidazol-2-ylidene]CuO*t*-Bu (**NHC–Cu-2**) (6.0 mg, 0.0114 mmol) and thf-$d_8$ was added (0.2 mL). In a separate vial, a solution was prepared consisting of PMHS (7.0 μL, 0.1140 mmol), $B_2(pin)_2$ (28.9 mg, 0.1140 mmol), **2a** (30 μL, 0.1140 mmol), PhCN (5.9 μL, 0.0570 mmol), and $PhCH_2Ph$ (internal standard; 2.8 mg, 0.0166 mmol). The

solutions were transferred to a J-young NMR tube. The solution turned yellow upon mixing, fading away in <1 min.

Reaction progress was monitored through $^1$H NMR spectroscopy (Fig. S14) in the presence of $Ph_2CH_2$ as the internal standard. These studies show that **ketimine–B(pin)-2** and **ketimine–H-2** are formed at similar rates. The identity of these Cu-based species was deduced from their coupling patterns and by means of independent synthesis of **ketimine–H-2**. Characterization data for **ketimine–B(pin)-2** were provided in Section 3.

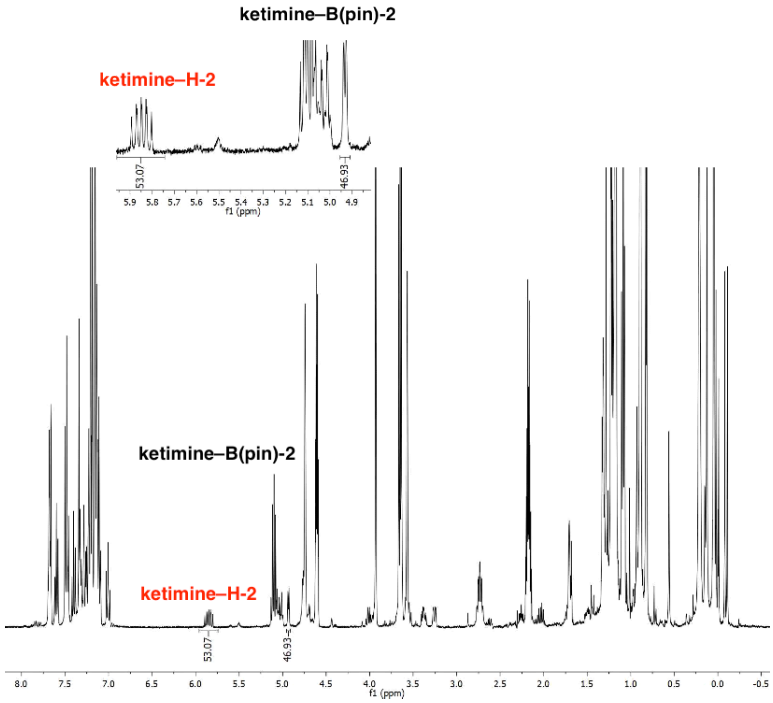


**Fig. S14.** Investigation of relative rates of reaction of a NHC–Cu–allyl complex with PhCN. The allylmetal reagent was derived from addition of a Cu–B(pin) and a Cu–H complex (generated with equal amounts of $B_2(pin)_2$ and PMHS) to an allene.

The ratio of **ketimine–B(pin)-2** and **ketimine–H-2** is close in value to that for and **Cu–B(pin)-2**:**NHC–Cu-H-2** obtained through the abovementioned studies. As before, this fact suggests that under these conditions, reaction of **NHC–Cu-2** with $B_2(pin)_2$ and PMHS is considerably more facile than the addition of the corresponding Cu–B(pin) and Cu–H complexes to **2a**, and, as a result the initial ratio of **NHC–Cu-B(pin)-2** and **NHC–Cu-H-2** may be retained.

Similar studies were carried out under conditions that more closely resemble those used in a catalytic process (Fig. S15; see Fig. 3A of the manuscript). The results were similar to those described above.

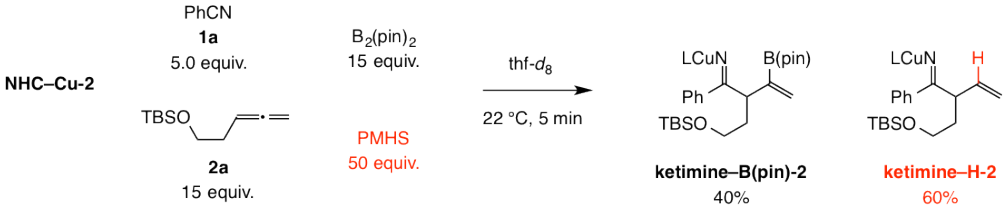

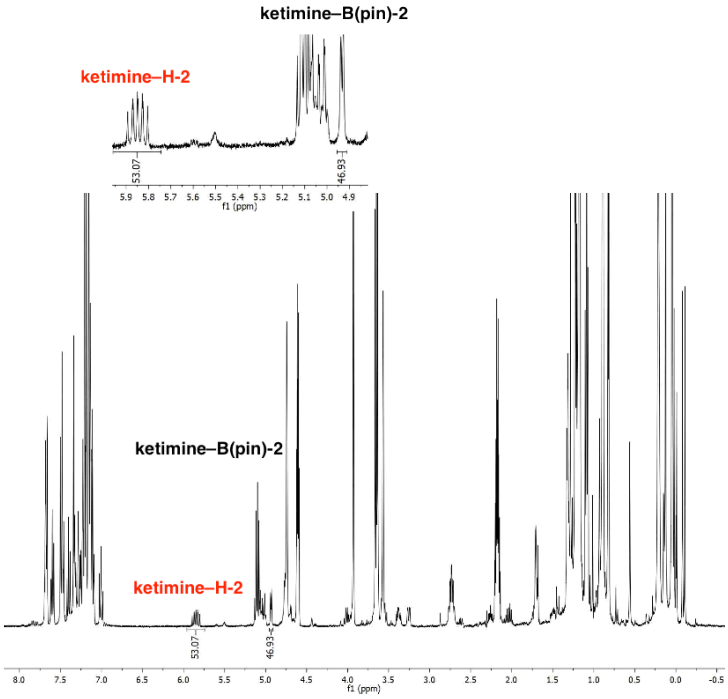


**Fig. S15.** Investigation of the relative rates of reaction of NHC–Cu–allyl species with PhCN. The allylmetal reagent was derived from addition of a Cu–B(pin) and a Cu–H complex (more PMHS vs. $B_2(pin)_2$) to an allene.

## 5 Investigations Involving a Bisphosphine–Cu Complex

We have also explored reactions involving the optimal ligand (*R*)-(–)-1-[(*S*)-2-(dicyclohexylphosphino)ferrocenyl]ethyldi-*t*-butylphosphine (**phos-3**). The corresponding Cu-based complex was prepared in situ by treatment of **phos-3** with [CuO*t*-Bu]$_4$ (*53*).

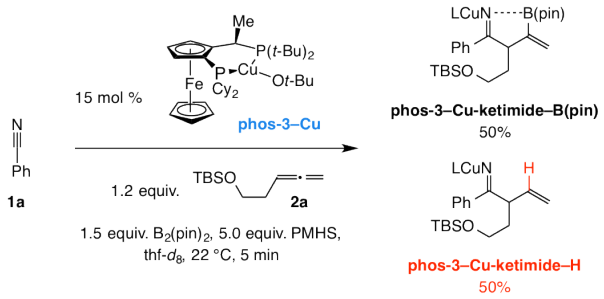


In an $N_2$-filled glove box, an oven-dried 2-dram vial was charged with copper(I)–*t*-butoxide (2.0 mg, 0.0015 mmol) and **phos-3** (8.3 mg, 0.0015 mmol), and thf was added (0.3 mL); this solution was allowed to stir for 15 min. In a separate vial, a thf solution (0.3 mL) of PMHS (30.0 μL, 0.5000 mmol), $B_2(pin)_2$ (38.1 mg, 0.1500 mmol), **2a** (28.7 μL, 0.1200 mmol) and PhCN (10.3 mg, 0.1000 mmol) was prepared. The solutions were mixed, causing the color change to orange, and then transferred to a J-young NMR tube.

Reaction progress was monitored through $^1$H NMR spectroscopy (Fig. S16). Integration of the peaks versus pre-measured (reference) amount of PhCN indicated >98% conv. to an equal mixture of **phos-3–ketimide–B(pin)** and **phos-3–ketimide–H**. These signals were assigned in analogy to the aforementioned NHC–Cu complexes. The $^{31}$P NMR spectrum of this mixture proved to be highly complicated probably as a result of fluxional processes that broaden the peaks and therefore difficult to interpret.

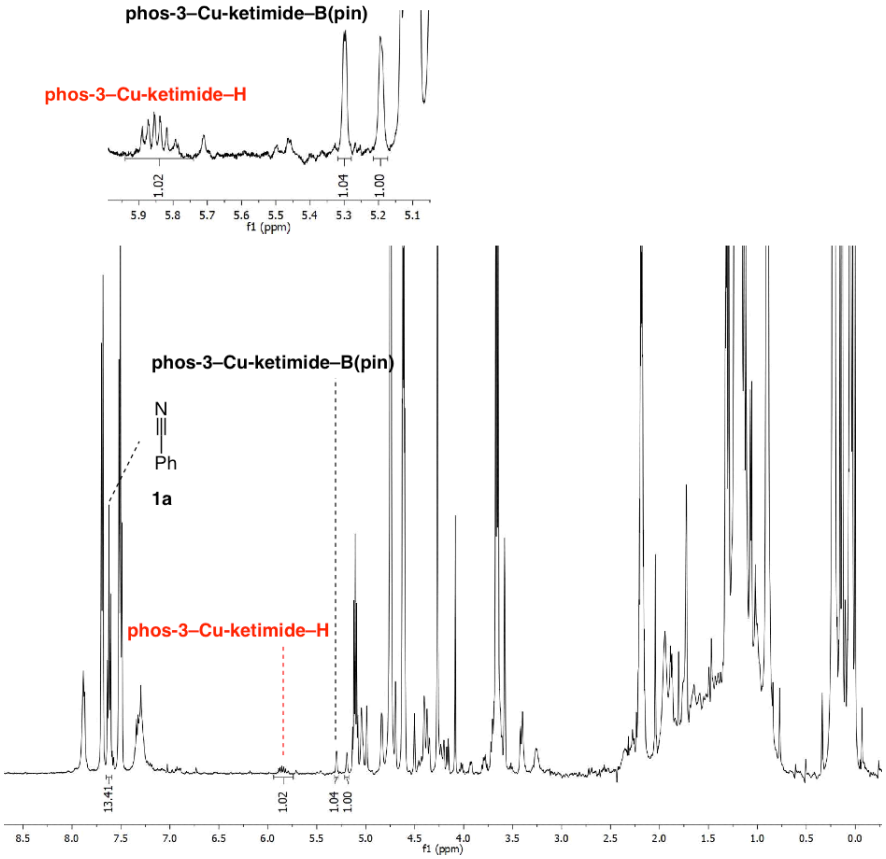


**Fig. S16.** Investigation of the relative rates of reaction of **phos-3**–Cu–allyl species with PhCN.

The sample was placed in the glove box, and *t*-BuOH (32.0 μL, 0.3400 mmol) was added by syringe. Analysis of the $^1$H NMR spectrum (Fig. S17) indicated significant $H_2$ evolution, along with formation of *syn*-**5a** and **7a**. Notably, NH ketimine peaks, probably arising from protonolysis of **phos-3–ketimide–H**, can be observed. However, we have not been able to isolate any of the byproducts.

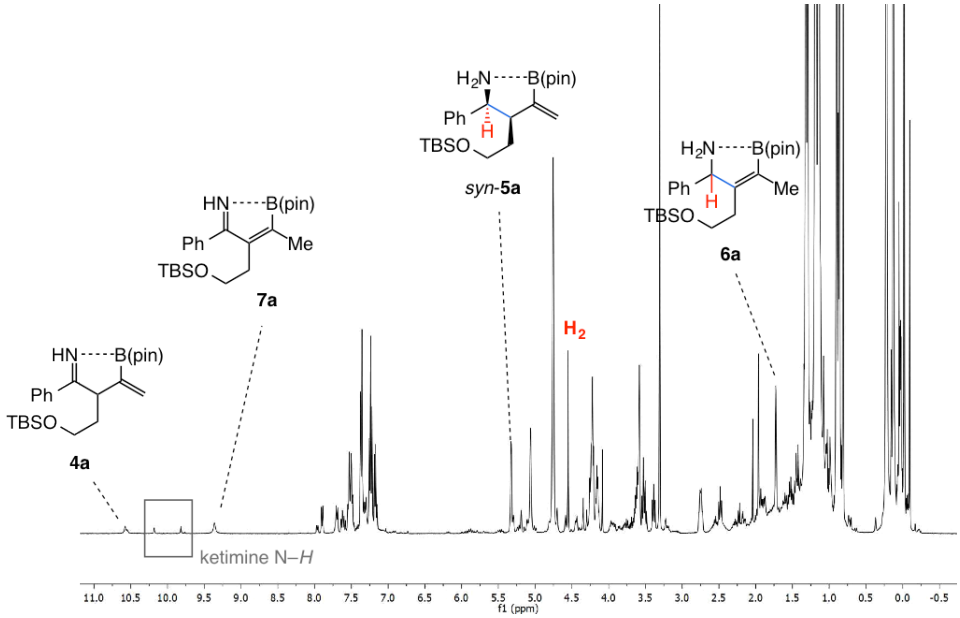


**Fig. S17.** Investigation of the reaction of Cu-ketimides shown in Fig. 16 with *t*-BuOH.

**NOTE:** Throughout this document, the % yield values correspond to isolated and purified products (±5%). In three instances, as will be noted, small impurities cannot be removed (**5l**, pg 33; **9a-b**, pg 40).

## 6 NHC–Cu-Catalyzed Synthesis of *syn*-Homoallylic Amines

In a $N_2$-filled glove box, an oven-dried 2-dram vial (4 mL, 17 × 38 mm) with a magnetic stir bar was charged with imidazolium salt precursor to **NHC–Cu-1** (2.3 mg, 0.0055 mmol), CuCl (0.5 mg, 0.0050 mmol), NaO*t*-Bu (4.8 mg, 0.050 mmol) and thf (0.5 mL). The vial was sealed and the solution was allowed to stir at 22 °C for 1 h. A solution containing $B_2(pin)_2$ (30.5 mg, 0.120 mmol), nitrile **1a** (10.3 mg, 0.100 mmol), allene **2a** (23.8 mg, 0.120 mmol)**,** *t*-BuOH (24.7 mg, 0.330 mmol), PMHS (30.0 mg, 0.500 mmol) and thf (0.4 mL) was added to the original mixture and the vial was removed from the glove box. The solution was allowed to stir at 22 °C for 24 h, after which the reaction was quenched by allowing the mixture to pass through a short plug of celite and silica gel, followed by elution with 10:1 $Et_2O$:MeOH (2 × 10 mL). The filtrate was concentrated in vacuo to afford yellow oil, which was purified by chromatography ($CH_2Cl_2$:MeOH:$HCO_2H$ 100:1.5:0.4 until all the pinacol was removed as judged by tlc, followed by 100:6.0:0.2). NOTE: The silica gel used was flushed with 2% v/v solution of formic acid in $CH_2Cl_2$ (3 × 3 mL). To remove the formic acid, the samples containing the desired product (as judged by thin layer chromatography (tlc) analysis) were collected and then allowed to stir over $K_2CO_3$ (500 mg) for 15 min. The suspension was filtered through a short plug of sand and the volatiles were removed in vacuo to afford yellow oil and white solid. Diethyl ether (5 mL) was added and the suspension was allowed to pass through a pad of celite. Evaporation of the volatiles delivered *rac*-**5a** as light-yellow oil (20.0 mg, 0.046 mmol, 46% yield).

## 7 Diastereo- and Enantioselective Synthesis of *syn*-Homoallylic Amines

In a $N_2$-filled glove box, an oven-dried vial (4 mL, 17 × 38 mm) containing a magnetic stir bar was charged with **phos-3** (3.1 mg, 0.0055 mmol), CuMes (0.9 mg, 0.0050 mmol) and thf (0.5 mL). The vessel was sealed with a cap and the solution was allowed to stir at 22 °C for 10 min. Methanol (5.5 mg, 0.17 mmol) was added and the mixture was allowed to stir for 10 min at 22 °C. At this point, NaOMe (2.7 mg, 0.050 mmol) was added and the vial was re-sealed with a cap [phenolic open top cap with white polytetrafluoroethylene (PTFE)/white silicone septum]. The vessel was then removed from the glove box. The resulting suspension was allowed to cool to –50 °C, followed by drop-wise addition of a solution containing $B_2(pin)_2$ (30.5 mg, 0.120 mmol), nitrile **1a** (10.3 mg, 0.100 mmol), allene **2a** (23.8 mg, 0.120 mmol), *t*-BuOH (12.3 mg, 0.166 mmol), PMHS (30.0 mg, 0.500 mmol) and thf (0.4 mL). The mixture was allowed to stir at –50 °C for 10 h, after which the vessel placed in a –20 °C freezer and allowed to stand for 12 h. The reaction was quenched by passing the mixture through a short plug of celite and silica gel, followed by elution with 10:1 $Et_2O$:MeOH (2×10 mL). The filtrate was concentrated in vacuo to afford yellow oil, which was purified by column chromatography ($CH_2Cl_2$:MeOH:$HCO_2H$ 100:1.5:0.4 until all the pinacol was removed as judged by thin layer chromatography (tlc), followed by 100:6.0:0.2). NOTE: The silica gel used must be flushed with 2% v/v solution of formic acid in $CH_2Cl_2$ (3 × 3 mL). To

remove the formic acid, the samples containing the desired product (as judged by tlc analysis) were collected and then allowed to stir over solid $K_2CO_3$ (500 mg) for 15 min. The suspension was filtered through a short plug of sand and the volatiles were removed in vacuo to afford yellow oil and white solid. Diethyl ether (5 mL) was added and the suspension was allowed to pass through a pad of celite. Removal of the volatiles in vacuo afforded *syn*-**5a** as colorless oil (32.8 mg, 0.076 mmol, 76% yield).

### 7.1.1 (1*S*,2*R*)-2-(2-((*tert*-Butyldimethylsilyl)oxy)ethyl)-1-phenyl-3-(4,4,5,5-tetramethyl-1,3,2-dioxaborolan-2-yl)but-3-en-1-amine (5a)

Colorless oil; **IR (neat)**: 3332 (w), 2956 (m), 2928 (m), 2856 (w), 1471 (w), 1361 (w), 1253 (m), 1154 (s), 1090 (s), 965 (m), 834 (s), 774 (s), 699 (m) $cm^{-1}$; **$^1$H NMR ($CDCl_3$, 500 MHz)**: δ 7.31–7.24 (m, 4H), 7.22–7.17 (m, 1H), 5.68 (d, *J* = 3.2 Hz, 1H), 5.38 (d, *J* = 3.2 Hz, 1H), 4.14 (d, *J* = 6.8 Hz, 1H), 3.57 (ddd, *J* = 10.1, 7.5, 5.2 Hz, 1H), 3.43 (dt, *J* = 10.0, 7.3 Hz, 1H), 2.71 (ddd, *J* = 9.1, 6.4, 4.6 Hz, 1H), 2.07 (br s, 2H), 1.76–1.64 (m, 2H), 1.22 (d, *J* = 3.8 Hz, 12H), 0.85 (s, 9H), –0.015 (s, 3H), –0.023 (s, 3H); **$^{13}$C NMR ($CDCl_3$, 125 MHz)**: 145.7, 143.7, 128.3, 127.2, 126.9, 82.5, 61.7, 59.1, 49.3, 31.4, 26.1, 25.1, 25.0, 18.4, –5.1, –5.2; **$^{11}$B NMR ($CDCl_3$, 160 MHz)**: δ 21.50; **HRMS (DART)**: Calcd for $C_{24}H_{43}BNO_3Si$ $[M+H]^+$: 432.3105. Found: 432.3114; **Specific rotation**: $[\alpha]_D^{20}$ –2.9 (*c* 1.04, $CHCl_3$) for an enantiomerically enriched sample of 95:5 e.r.

Enantiomeric purity was determined by HPLC analysis in comparison with authentic racemic material of the derived acetamide; Chiralcel OD-H column, 95:5 hexanes/*i*-PrOH, 0.3 mL/min, 220 nm.

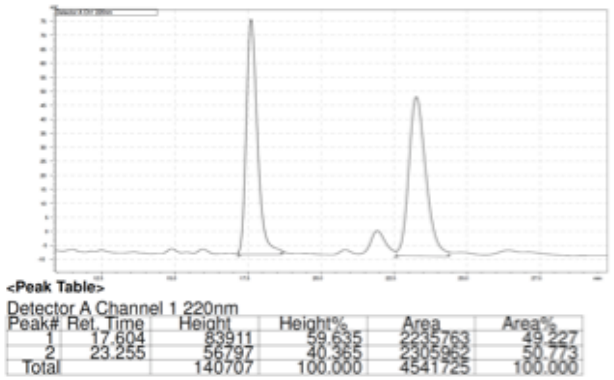

<Peak Table>
Detector A Channel 1 220nm

| Peak# | Ret. Time | Height | Height% | Area | Area% |
|---|---|---|---|---|---|
| 1 | 17.604 | 83911 | 59.635 | 2235763 | 49.227 |
| 2 | 23.255 | 56797 | 40.365 | 2305962 | 50.773 |
| Total | | 140707 | 100.000 | 4541725 | 100.000 |

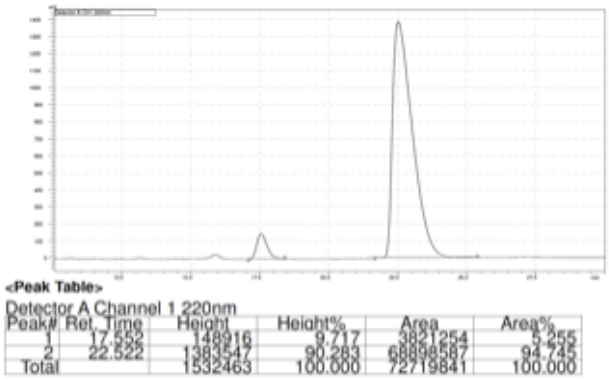

<Peak Table>
Detector A Channel 1 220nm

| Peak# | Ret. Time | Height | Height% | Area | Area% |
|---|---|---|---|---|---|
| 1 | 17.552 | 148916 | 9.717 | 3821254 | 5.255 |
| 2 | 22.522 | 1383547 | 90.283 | 68898587 | 94.745 |
| Total | | 1532463 | 100.000 | 72719841 | 100.000 |

| Retention Time | Area | Area% | Retention Time | Area | Area% |
|---|---|---|---|---|---|
| 17.604 | 2235763 | 49.227 | 17.552 | 3821254 | 5.255 |
| 23.255 | 2305962 | 50.773 | 22.522 | 68898587 | 94.745 |

### 7.1.2 (1*S*,2*R*)-2-(2-((*tert*-Butyldimethylsilyl)oxy)ethyl)-3-(4,4,5,5-tetramethyl-1,3,2-dioxaborolan-2-yl)-1-(o-tolyl)but-3-en-1-amine (5b)

Colorless oil; **IR (neat)**: 3038 (w), 2956 (m), 2929 (m), 2857 (m), 1604 (w), 1471 (w), 1361 (w), 1253 (m), 1155 (s), 1084 (s), 1055 (s), 966 (m), 835 (s), 774 (s) $cm^{-1}$; **$^1$H NMR ($CDCl_3$, 500 MHz)**: δ 7.32 (d, *J* = 7.7 Hz, 1H), 7.17 (dt, *J* = 8.0, 4.3 Hz, 1H), 7.11 (d, *J* = 4.4 Hz, 2H), 5.71 (d, *J* = 3.1 Hz, 1H), 5.49 (d, *J* = 3.2 Hz, 1H), 4.34 (d, *J* = 6.2 Hz, 1H), 3.59–3.49 (m, 1H), 3.41 (dt, *J* = 9.9, 7.3 Hz, 1H), 2.77 (dt, *J* =10.3, 4.4 Hz, 1H), 2.35 (s, 3H), 2.27–1.98 (br s, 2H), 1.74–1.57 (m, 2H), 1.21 (d, *J* = 3.4 Hz, 12H), 0.83 (s, 9H), –0.04 (s 3H), –0.06 (s,

3H); **$^{13}$C NMR ($CDCl_3$, 100 MHz)**: δ 147.6, 140.9, 135.6, 130.7, 126.8, 126.3, 126.2, 125.9, 82.3, 61.5, 55.3, 46.4, 30.9, 26.1, 25.2, 25.0, 19.7, 18.4, –5.1, –5.2; **$^{11}$B NMR ($CDCl_3$, 160 MHz)**: δ 22.33; **HRMS (DART)**: Calcd for $C_{25}H_{44}BNO_3Si$ $[M+H]^+$: 446.3262. Found: 446.3246; **Specific rotation**: $[\alpha]_D^{20}$ –12.6 (*c* 0.69, $CHCl_3$) for an enantiomerically enriched sample of 93.5:6.5 e.r.

Enantiomeric purity was determined by HPLC analysis in comparison with authentic racemic material of the derived acetamide; Chiralcel OD-H column, 95:5 hexanes/*i*-PrOH, 0.3 mL/min, 220 nm.

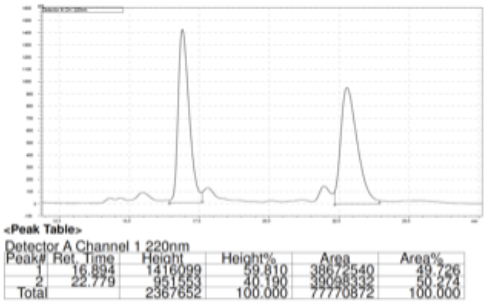

<Peak Table>
Detector A Channel 1 220nm

| Peak# | Ret. Time | Height | Height% | Area | Area% |
|---|---|---|---|---|---|
| 1 | 16.894 | 1416099 | 59.810 | 38672540 | 49.726 |
| 2 | 22.779 | 951553 | 40.190 | 39098332 | 50.274 |
| Total | | 2367652 | 100.000 | 77770872 | 100.000 |

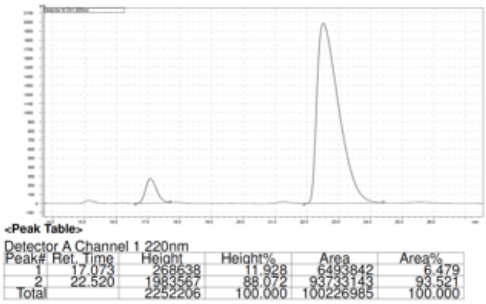

<Peak Table>
Detector A Channel 1 220nm

| Peak# | Ret. Time | Height | Height% | Area | Area% |
|---|---|---|---|---|---|
| 1 | 17.073 | 268638 | 11.928 | 6493842 | 6.479 |
| 2 | 22.520 | 1983567 | 88.072 | 93733143 | 93.521 |
| Total | | 2252206 | 100.000 | 100226985 | 100.000 |

| Retention Time | Area | Area% | Retention Time | Area | Area% |
|---|---|---|---|---|---|
| 16.894 | 38672540 | 49.726 | 17.073 | 6493842 | 6.479 |
| 22.779 | 39098332 | 50.274 | 22.520 | 93733143 | 93.521 |

### 7.1.3 (1*S*,2*R*)-1-(Benzo[*d*][1,3]dioxol-5-yl)-2-(2-((*tert*-butyldimethylsilyl)oxy)ethyl)-3-(4,4,5,5-tetramethyl-1,3,2-dioxaborolan-2-yl)but-3-en-1-amine (5c)

Colorless oil; **IR (neat)**: 3043 (w), 2954 (m), 2929 (m), 2885 (w), 2857 (m), 1709 (w), 1608 (w), 1504 (m), 1443 (m), 1361 (m), 1249 (s), 1154 (m), 1087 (s), 1039 (s), 938 (m), 834 (s), 810 (m), 774 (s), 733 (m) $cm^{-1}$; **$^1$H NMR ($CDCl_3$, 500 MHz)**: δ 6.79 (s, 1H), 6.70 (d, *J* = 1.0 Hz, 2H), 5.90 (s, 2H), 5.70 (d, *J* = 3.3 Hz, 1H), 5.39 (d, *J* = 3.3 Hz, 1H), 4.04 (d, *J* = 7.0 Hz, 1H), 3.57 (dt, *J* = 10.0, 6.3 Hz, 1H), 3.43 (dt, *J* = 10.0, 7.4 Hz, 1H), 2.61 (dt, *J* = 7.5, 7.0 Hz, 1H), 1.91 (br s, 2H), 1.76–1.68 (m, 2H), 1.22 (d, *J* = 5.2 Hz, 12H), 0.86 (s, 9H), –0.006 (s, 3H), –0.008 (s, 3H); **$^{13}$C NMR ($CDCl_3$, 125 MHz)**: δ 147.6, 146.3, 145.0, 138.3, 128.2, 120.4, 107.9, 107.8, 100.9, 82.7, 61.8, 58.9, 49.7, 31.7, 26.1, 25.1, 24.9, 18.5, –5.10, –5.14; **$^{11}$B NMR ($CDCl_3$, 160 MHz)**: δ 26.04; **HRMS (DART):** Calcd for $C_{25}H_{42}BNO_5Si$ $[M+H]^+$: 476.2998. Found: 476.3007; **Specific rotation**: $[\alpha]_D^{20}$ +7.8 (*c* 1.04, $CHCl_3$) for an enantiomerically enriched sample of 96:4 e.r.

Enantiomeric purity was determined by HPLC analysis in comparison with authentic racemic material of the derived acetamide; Chiralcel OD-H column, 95:5 hexanes/*i*-PrOH, 0.3 mL/min, 220 nm.

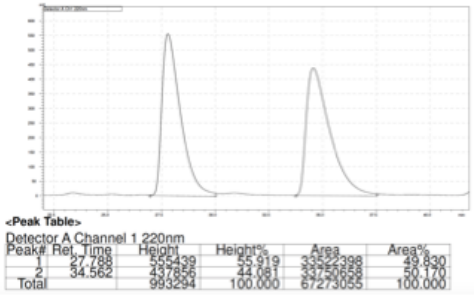

<Peak Table>
Detector A Channel 1 220nm

| Peak# | Ret. Time | Height | Height% | Area | Area% |
|---|---|---|---|---|---|
| 1 | 27.788 | 555439 | 55.919 | 33522398 | 49.830 |
| 2 | 34.562 | 437855 | 44.081 | 33750658 | 50.170 |
| Total | | 993294 | 100.000 | 67273055 | 100.000 |

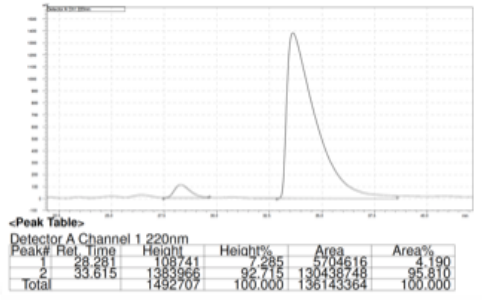

<Peak Table>
Detector A Channel 1 220nm

| Peak# | Ret. Time | Height | Height% | Area | Area% |
|---|---|---|---|---|---|
| 1 | 28.281 | 108741 | 7.285 | 5704616 | 4.190 |
| 2 | 33.615 | 1383966 | 92.715 | 130438748 | 95.810 |
| Total | | 1492707 | 100.000 | 136143364 | 100.000 |

| Retention Time | Area | Area% | Retention Time | Area | Area% |
|---|---|---|---|---|---|
| 27.788 | 33522398 | 49.830 | 28.281 | 5704616 | 4.190 |
| 34.562 | 33750658 | 50.170 | 33.615 | 130438748 | 95.810 |

### 7.1.4 (1*S*,2*R*)-2-(2-((*tert*-Butyldimethylsilyl)oxy)ethyl)-3-(4,4,5,5-tetramethyl-1,3,2-dioxaborolan-2-yl)-1-(3-(trifluoromethyl)phenyl)but-3-en-1-amine (5d)

The general procedure (see above) was modified: 2.5 equiv. MeOH and 7.0 equiv. PMHS were used (vs. 1.7 equiv. MeOH and 5.0 equiv. PMHS).

Light yellow oil; **IR (neat)**: 3051(w), 2996 (m), 2929 (m), 2887 (w), 2858 (m), 1610 (w), 1416 (m), 1327 (s), 1253 (m), 1162 (s), 1125 (s), 1096 (s), 1073 (s), 967 (m), 902 (m), 833 (s), 804 (m), 775 (s), 701 (s), 662 (m), 576 (w) $cm^{-1}$; **$^1$H NMR ($CDCl_3$, 500 MHz)**: δ 7.55 (s, 1H), 7.48 (d, *J* = 7.7 Hz, 1H), 7.44 (d, *J* = 8.3 Hz, 1H), 7.38 (t, *J* = 7.6 Hz, 1H), 5.76 (d, *J* = 3.2 Hz, 1H), 5.41 (d, *J* = 2.9 Hz, 1H), 4.18 (d, *J* = 6.9 Hz, 1H), 3.57 (ddd, *J* = 10.1, 7.5, 4.8 Hz, 1H), 3.42 (dt, *J* = 10.1, 7.5 Hz, 1H), 2.65 (ddd, *J* = 10.6, 6.9, 3.9 Hz, 1H), 1.86–1.71 (m, 2H), 1.61 (br s, 2H), 1.23 (d, *J* = 11.6 Hz, 12H), 0.85 (s, 9H), −0.01 (s, 3H), −0.02 (s, 3H); **$^{13}$C NMR ($CDCl_3$, 125 MHz)**: δ 146.3, 142.8, 130.8, 130.6, 130.4 (q, *J* = 31.9 Hz), 128.6, 124.4 (q, *J* = 272.3 Hz), 124.3 (q, *J* = 3.9 Hz), 123.5 (q, *J* = 3.8 Hz), 83.3, 61.6, 58.7, 50.1, 31.6, 26.1, 25.0, 24.8, 18.4, −5.1, −5.2; **$^{19}$F NMR ($CDCl_3$, 376 MHz)**: δ −62.53 (s); **$^{11}$B NMR ($CDCl_3$, 160 MHz)**: δ 28.96; **HRMS (DART)**: Calcd for $C_{25}H_{41}BF_3NO_3Si$ $[M+H]^+$: 500.2979. Found: 500.2990; **Specific rotation**: $[\alpha]_D^{20}$ +7.8 (*c* 0.68, $CHCl_3$) for an enantiomerically enriched sample of 94:6 e.r.

Enantiomeric purity was determined by HPLC analysis in comparison with authentic racemic material of the derived acetamide; Chiralcel OD-H column, 98:2 hexanes/*i*-PrOH, 1.0 mL/min, 220 nm.

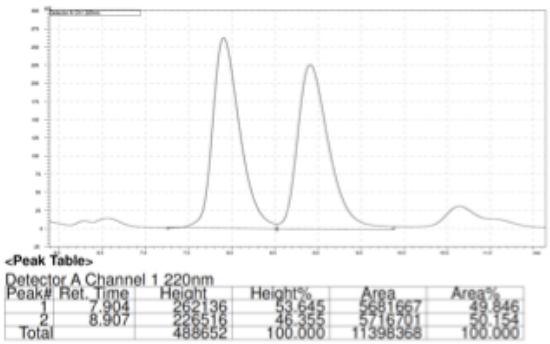


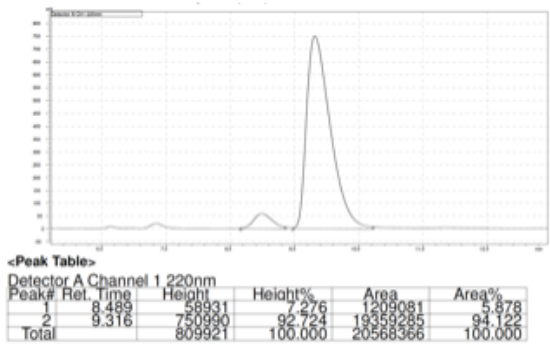


| Retention Time | Area | Area% | Retention Time | Area | Area% |
|---|---|---|---|---|---|
| 7.904 | 5681667 | 49.846 | 8.489 | 1209081 | 5.878 |
| 8.907 | 5716701 | 50.154 | 9.316 | 19359285 | 94.122 |

### 7.1.5 (1*S*,2*R*)-2-(2-((*tert*-Butyldimethylsilyl)oxy)ethyl)-1-(2,4-difluorophenyl)-3-(4,4,5,5-tetramethyl-1,3,2-dioxaborolan-2-yl)but-3-en-1-amine (5e)

Colorless oil; **IR (neat)**: 3389 (w), 2956 (m), 2929 (m), 2857 (w), 1617 (m), 1505 (m), 1430 (w), 1362 (m), 1254 (m), 1140 (m), 1094 (s), 966 (m), 835 (s), 775 (s) $cm^{-1}$; **$^1$H NMR ($CDCl_3$, 500 MHz)**: δ 7.30–7.22 (m, 1H), 6.81–6.73 (m, 1H), 6.74–6.65 (m, 1H), 5.70 (d, *J* = 3.3 Hz, 1H), 5.42 (d, *J* = 3.3 Hz, 1H), 4.27 (d, *J* = 8.1 Hz, 1H), 3.58 (ddd, *J* = 10.0, 7.8, 4.7

Hz, 1H), 3.44 (dt, *J* = 10.0, 7.5 Hz, 1H), 2.65 (ddd, *J* = 9.6, 8.0, 3.4 Hz, 1H), 1.95–1.86 (m, 1H), 1.84–1.67 (m, 3H), 1.21 (d, *J* = 8.6 Hz, 12H), 0.86 (s, 9H), 0.00 (s, 6H); **$^{13}$C NMR ($CDCl_3$, 100 MHz)**: δ 161.8 (dd, *J* = 247.0, 12.5 Hz), 160.6 (dd, *J* = 248.1, 12.0 Hz), 143.1, 130.8, 129.9 (dd, *J* = 9.1, 7.3 Hz), 128.1 (d, *J* = 12.9 Hz), 111.0 – 110.7 (m), 103.7 (t, *J* = 26.0 Hz), 83.1, 61.7, 53.8, 49.7, 32.7, 26.1, 25.0, 24.8, 18.4, –5.1, –5.2; **$^{19}$F NMR ($CDCl_3$, 376 MHz)**: two peaks overlap with each other, δ –113.16 to –113.29 (m); **$^{11}$B NMR ($CDCl_3$, 160 MHz)**: δ 28.47; **HRMS (DART):** Calcd for $C_{24}H_{41}BF_2NO_3Si$ $[M+H]^+$: 468.2817. Found: 468.2924**; Specific rotation**: $[\alpha]_D^{20}$ –2.4 (*c* 0.75, $CHCl_3$) for an enantiomerically enriched sample of 95:5 e.r.

Enantiomeric purity was determined by HPLC analysis by comparison with authentic racemic material of the derived benzyl amide; Chiralcel OZ-H column, 98:2 hexanes/*i*-PrOH, 1.0 mL/min, 220 nm.

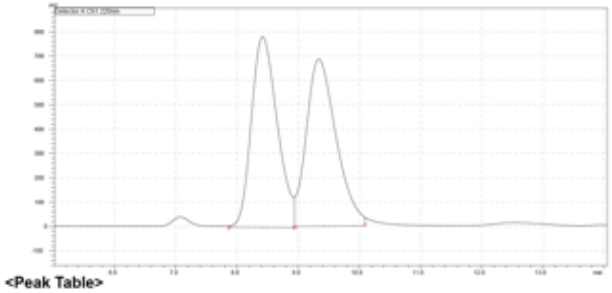

<Peak Table>
Detector A Channel 1 220nm

| Peak# | Ret. Time | Height | Height% | Area | Area% |
|---|---|---|---|---|---|
| 1 | 8.418 | 783790 | 53.283 | 23055950 | 49.726 |
| 2 | 9.337 | 687217 | 46.717 | 23310398 | 50.274 |
| Total | | 1471006 | 100.000 | 46366348 | 100.000 |

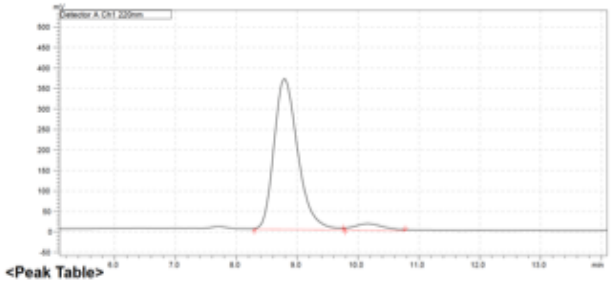

<Peak Table>
Detector A Channel 1 220nm

| Peak# | Ret. Time | Height | Height% | Area | Area% |
|---|---|---|---|---|---|
| 1 | 8.790 | 367177 | 95.873 | 10023950 | 94.864 |
| 2 | 10.162 | 15806 | 4.127 | 542717 | 5.136 |
| Total | | 382983 | 100.000 | 10566667 | 100.000 |

| Retention Time | Area | Area% | Retention Time | Area | Area% |
|---|---|---|---|---|---|
| 8.418 | 23055950 | 49.726 | 8.790 | 10023950 | 94.864 |
| 9.337 | 23310398 | 50.274 | 10.162 | 542717 | 5.136 |

### 7.1.6 (1*S*,2*R*)-1-(4-Bromophenyl)-2-(2-((*tert*-butyldimethylsilyl)oxy)ethyl)-3-(4,4,5,5-tetramethyl-1,3,2-dioxaborolan-2-yl)but-3-en-1-amine (5f)

Colorless oil; **IR (neat)**: 2955 (m), 2928 (m), 2856 (m), 1362 (w), 1253 (m), 1155 (m), 1087 (s), 1010 (m), 838 (s), 775 (m) $cm^{-1}$; **$^1$H NMR ($CDCl_3$, 400 MHz)**: δ 7.38 (d, *J* = 8.4 Hz, 1H), 7.15 (d, *J* = 8.4 Hz, 1H), 5.74 (d, *J* = 3.2 Hz, 1H), 5.40 (d, *J* = 3.2 Hz, 1H), 4.07 (d, *J* = 6.8 Hz, 1H), 3.56 (ddd, *J* = 10.0, 6.8, 5.7 Hz, 1H), 3.41 (dt, *J* = 10.1, 7.4 Hz, 1H), 2.63 (q, *J* = 7.0 Hz, 1H), 1.84–1.67 (m, 4H), 1.22 (d, *J* = 4.5 Hz, 12H), 0.86 (s, 9H), –0.01 (s, 3H), –0.02 (s, 3H); **$^{13}$C NMR ($CDCl_3$, 100 MHz)**: δ 143.6, 131.2, 129.7, 129.1, 120.5, 83.1, 61.7, 58.5, 49.5, 31.6, 26.1, 25.1, 24.9, 18.4, –5.1, –5.2. The carbon directly attached to the boron atom could not be detected due to quadrupolar effects; **$^{11}$B NMR ($CDCl_3$, 160 MHz)**: δ 24.95; **HRMS (DART)**: Calcd for $C_{24}H_{42}BBrNO_3Si$ $[M+H]^+$: 510.2210. Found: 510.2224; **Specific rotation**: $[\alpha]_D^{20}$ +6.7 (c 0.88, $CHCl_3$) for an enantiomerically enriched sample of 94:6 e.r.

Enantiomeric purity was determined by HPLC analysis in comparison with authentic racemic material of the derived acetamide; Chiralcel OD-H column, 99:1 hexanes/*i*-PrOH, 0.3 mL/min, 220 nm.

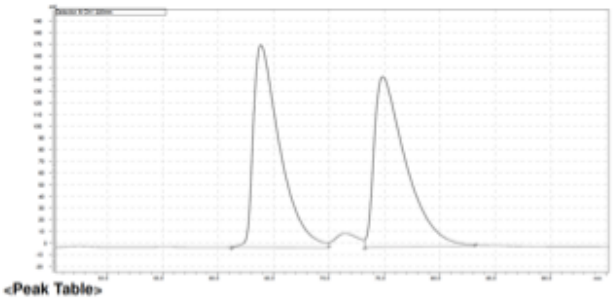

<Peak Table>
Detector A Channel 1 220nm

| Peak# | Ret. Time | Height | Height% | Area | Area% |
|---|---|---|---|---|---|
| 1 | 63.860 | 172947 | 54.274 | 28723713 | 49.966 |
| 2 | 74.845 | 145711 | 45.726 | 28762571 | 50.034 |
| Total | | 318659 | 100.000 | 57486284 | 100.000 |

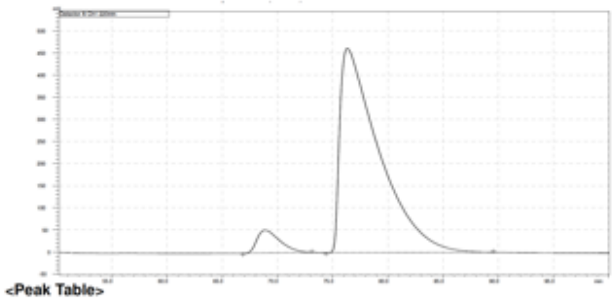

<Peak Table>
Detector A Channel 1 220nm

| Peak# | Ret. Time | Height | Height% | Area | Area% |
|---|---|---|---|---|---|
| 1 | 68.884 | 51971 | 10.102 | 7497723 | 6.180 |
| 2 | 76.327 | 462494 | 89.898 | 113819632 | 93.820 |
| Total | | 514466 | 100.000 | 121317355 | 100.000 |

| Retention Time | Area | Area% | Retention Time | Area | Area% |
|---|---|---|---|---|---|
| 63.860 | 28723713 | 49.966 | 68.884 | 7497723 | 6.180 |
| 74.845 | 28762571 | 50.034 | 76.327 | 113819632 | 93.820 |

### 7.1.7 (1*S*,2*R*)-2-(2-((*tert*-Butyldimethylsilyl)oxy)ethyl)-1-(4-methoxyphenyl)-3-(4,4,5,5-tetramethyl-1,3,2-dioxaborolan-2-yl)but-3-en-1-amine (5g)

Colorless oil; **IR (neat)**: 2955 (m), 2929 (m), 2856 (w), 1515 (m), 1252 (s), 1155 (s), 1086 (s), 833 (s), 775 (m) $cm^{-1}$; **$^1$H NMR ($CDCl_3$, 400 MHz)**: δ 7.18 (d, *J* = 8.6 Hz, 2H), 6.81 (d, *J* = 8.7 Hz, 2H), 5.64 (d, *J* = 3.3 Hz, 1H), 5.35 (d, *J* = 3.3 Hz, 1H), 4.11 (d, *J* = 6.9 Hz, 1H), 3.77 (s, 3H), 3.57 (ddd, *J* = 10.1, 7.7, 5.1 Hz, 1H), 3.44 (dt, *J* = 10.0, 7.3 Hz, 1H), 2.69 (ddd, *J* = 10.4, 6.5, 4.6 Hz, 1H), 2.20 (br s, 2H), 1.79–1.55 (m, 2H), 1.21 (s, 12H), 0.85 (s, 9H), –0.01 (s, 3H), –0.02 (s, 3H); **$^{13}$C NMR ($CDCl_3$, 100 MHz):** δ 158.6, 146.8, 135.3, 128.4, 125.9, 113.7, 82.2, 61.8, 58.5, 55.4, 49.1, 31.5, 26.2, 25.1, 25.0, 18.5, –5.1, –5.2; **$^{11}$B NMR ($CDCl_3$, 128 MHz)**: δ 23.68; **HRMS (DART)**: Calcd for $C_{25}H_{45}BNO_4Si$ $[M+H]^+$: 462.3211. Found: 462.3216; **Specific rotation**: $[\alpha]_D^{20}$ +2.9 (*c* 0.57, $CHCl_3$) for an enantiomerically enriched sample of 96:4 e.r.

Enantiomeric purity was determined by HPLC analysis in comparison with authentic racemic material of the derived acetamide; Chiralcel OD-H column, 95:5 hexanes/*i*-PrOH, 0.3 mL/min, 220 nm.

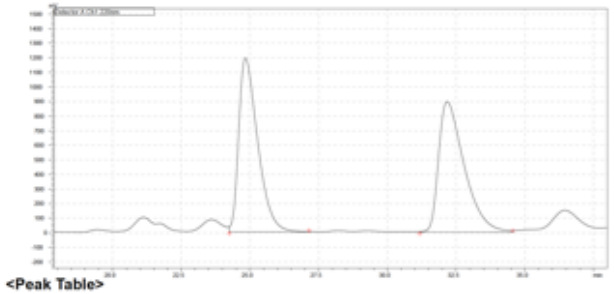

<Peak Table>
Detector A Channel 1 220nm

| Peak# | Ret. Time | Height | Height% | Area | Area% |
|---|---|---|---|---|---|
| 1 | 24.839 | 1191421 | 57.081 | 57275152 | 49.726 |
| 2 | 32.177 | 895825 | 42.919 | 57906127 | 50.274 |
| Total | | 2087246 | 100.000 | 115181279 | 100.000 |

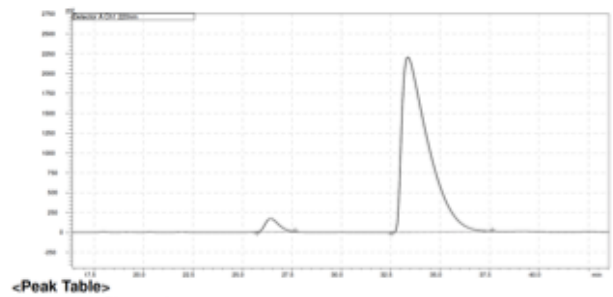

<Peak Table>
Detector A Channel 1 220nm

| Peak# | Ret. Time | Height | Height% | Area | Area% |
|---|---|---|---|---|---|
| 1 | 26.420 | 167523 | 7.061 | 8073768 | 3.842 |
| 2 | 33.362 | 2204959 | 92.939 | 202060084 | 96.158 |
| Total | | 2372482 | 100.000 | 210133852 | 100.000 |

| Retention Time | Area | Area% | Retention Time | Area | Area% |
|---|---|---|---|---|---|
| 24.839 | 57275152 | 49.726 | 26.420 | 8073768 | 3.842 |
| 32.177 | 57906127 | 50.274 | 33.362 | 202060084 | 96.158 |

### 7.1.8 Methyl 4-((1*S*,2*R*)-1-amino-2-(2-((*tert*-butyldimethylsilyl)oxy)ethyl)-3-(4,4,5,5-tetramethyl-1,3,2-dioxaborolan-2-yl)but-3-en-1-yl)benzoate (5h)

The general procedure was modified: 2.5 equiv. MeOH was used (vs. 1.7 equiv.).

Light yellow oil; **IR (neat):** 2953 (m), 2929 (m), 2857 (w), 1724 (s), 1612 (m), 1279 (s), 1253 (m), 1156 (m), 1088 (s), 835 (s), 774 (s) $cm^{-1}$; **$^1$H NMR ($CDCl_3$, 500 MHz):** δ 7.94 (d, *J* = 8.4 Hz, 2H), 7.34 (d, *J* = 8.3 Hz, 2H), 5.73 (d, *J* = 3.2 Hz, 1H), 5.39 (d, *J* = 3.2 Hz, 1H), 4.16 (d, *J* = 6.9 Hz, 1H), 3.89 (s, 3H), 3.55 (ddd, *J* = 10.0, 7.1, 5.2 Hz, 1H), 3.41 (dt, *J* = 10.0, 7.4 Hz, 1H), 2.66 (ddd, *J* = 9.2, 6.8, 5.0 Hz, 1H), 1.80–1.66 (m, 4H), 1.23 (d, *J* = 8.2 Hz, 12H), 0.85 (s, 9H), –0.02 (s, 3H), –0.03 (s, 3H); **$^{13}$C NMR ($CDCl_3$, 125 MHz):** δ 167.2, 150.3, 143.2, 130.2, 129.6, 128.6, 127.3, 83.1, 61.6, 58.9, 52.1, 49.8, 31.6, 26.1, 25.1, 24.8, 18.4, –5.1, –5.2; **$^{11}$B NMR ($CDCl_3$, 160 MHz):** δ 27.90; **HRMS (DART):** Calcd for $C_{26}H_{45}BNO_5Si$ $[M+H]^+$: 490.3160. Found: 490.3137; **Specific rotation**: $[\alpha]_D^{20}$ +7.8 (*c* 0.62, $CHCl_3$) for an enantiomerically enriched sample of 95.5:4.5 e.r.

Enantiomeric purity was determined by HPLC analysis in comparison with authentic racemic material of the derived benzyl amide; Chiralcel OZ-H column, 95:5 hexanes/*i*-PrOH, 0.3 mL/min, 220 nm.

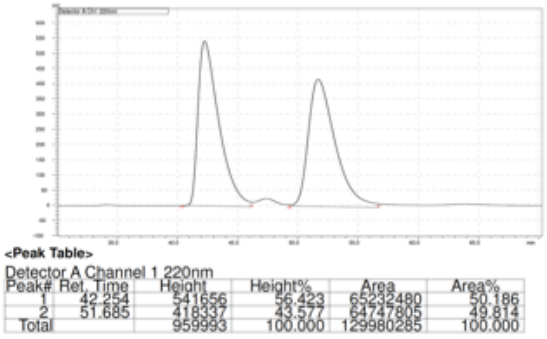

<Peak Table>
Detector A Channel 1 220nm

| Peak# | Ret. Time | Height | Height% | Area | Area% |
|---|---|---|---|---|---|
| 1 | 42.254 | 541656 | 56.423 | 65232480 | 50.186 |
| 2 | 51.685 | 418337 | 43.577 | 64747805 | 49.814 |
| Total | | 959993 | 100.000 | 129980285 | 100.000 |

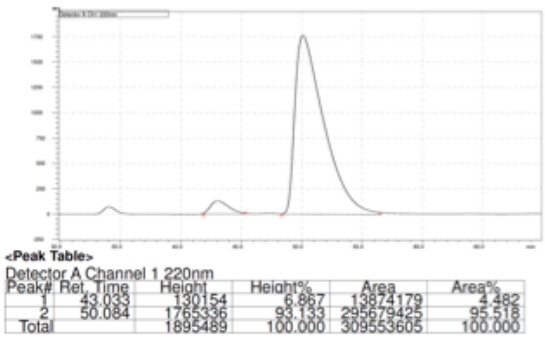

<Peak Table>
Detector A Channel 1 220nm

| Peak# | Ret. Time | Height | Height% | Area | Area% |
|---|---|---|---|---|---|
| 1 | 43.033 | 130154 | 6.867 | 13874179 | 4.482 |
| 2 | 50.084 | 1765336 | 93.133 | 295679425 | 95.518 |
| Total | | 1895489 | 100.000 | 309553605 | 100.000 |

| Retention Time | Area | Area% | Retention Time | Area | Area% |
|---|---|---|---|---|---|
| 42.254 | 65232480 | 50.186 | 43.033 | 13874179 | 4.482 |
| 51.685 | 64747805 | 49.814 | 50.084 | 295679425 | 95.518 |

### 7.1.9 (1*S*,2*R*)-2-(2-((*tert*-Butyldimethylsilyl)oxy)ethyl)-1-(pyridin-2-yl)-3-(4,4,5,5-tetramethyl-1,3,2-dioxaborolan-2-yl)but-3-en-1-amine (5i)

The general procedure (see above) was modified: 11.0 mol% **phos-3** and 10.0 mol% CuMes were used (vs. 5.5 mol% **phos-3** and 5.0 mol% CuMes). Moreover, the reaction was run at –50 °C and kept at this temperature for 20 h. The solution was allowed to warm to –20 °C and kept at this temperature for 24 h.

Light yellow oil; **IR (neat)**: 3268 (w), 3038 (w), 2954 (m), 2928 (m), 2856 (m), 1594 (w), 1473 (w), 1251 (m), 1154 (m), 1079 (s), 964 (m), 907 (m), 832 (s), 773 (s), 747 (m) $cm^{-1}$; **$^1$H NMR ($CDCl_3$, 500 MHz)**: δ 8.55 (d, *J* = 4.9 Hz, 1H), 7.64 (td, *J* = 7.7, 1.8 Hz, 1H), 7.22 (d, *J* = 7.6 Hz, 1H), 7.17 (ddd, *J* = 7.4, 4.9, 1.1 Hz, 1H), 5.47 (d, *J* = 3.4 Hz, 1H), 5.30 (d, *J* = 3.4 Hz, 1H), 4.29 (d, *J* = 6.6 Hz, 1H), 3.54–3.49 (m, 1H), 3.48–3.41 (m, 1H), 2.76 (ddd, *J* = 10.5, 6.5, 3.5 Hz, 1H), 1.62–1.50 (m, 1H), 1.38–1.30 (m, 1H), 1.20 (s, 12H), 0.83 (s, 9H), –0.03 (s, 3H), –0.06 (s, 3H); **$^{13}$C NMR ($CDCl_3$, 100 MHz)**: δ 159.9, 152.0, 148.5, 136.7, 122.33,

122.31, 121.9, 81.2, 61.1, 59.6, 49.0, 31.3, 26.1, 25.4, 25.3, 18.4, –5.1, –5.2; **$^{11}$B NMR (CDCl$_3$, 160 MHz):** δ 16.31; **HRMS (DART)**: Calcd for $C_{23}H_{42}BN_2O_3Si$ $[M+H]^+$: 433.3052. Found: 433.3031; **Specific rotation**: $[\alpha]_D^{20}$ +2.7 (*c* 0.48, $CHCl_3$) for an enantiomerically enriched sample of 95:5 e.r.

Enantiomeric purity was determined by HPLC analysis in comparison with authentic racemic material of the derived benzyl amide; Chiralcel OZ-H column, 98:2 hexanes/*i*-PrOH, 1.0 mL/min, 220 nm.

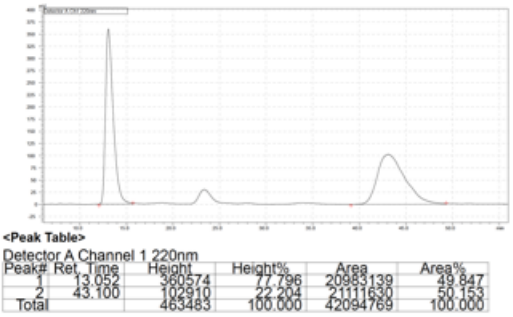

<Peak Table>
Detector A Channel 1 220nm

| Peak# | Ret. Time | Height | Height% | Area | Area% |
|---|---|---|---|---|---|
| 1 | 13.052 | 360574 | 77.796 | 20983139 | 49.847 |
| 2 | 43.100 | 102910 | 22.204 | 21111630 | 50.153 |
| Total | | 463483 | 100.000 | 42094769 | 100.000 |

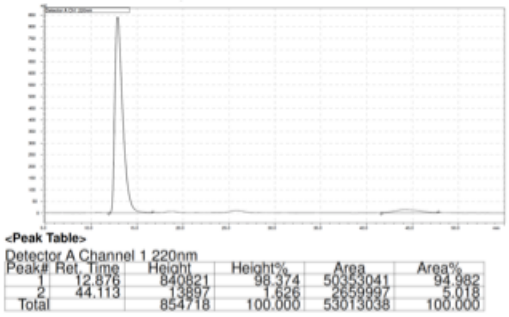

<Peak Table>
Detector A Channel 1 220nm

| Peak# | Ret. Time | Height | Height% | Area | Area% |
|---|---|---|---|---|---|
| 1 | 12.876 | 840821 | 98.374 | 50353041 | 94.982 |
| 2 | 44.113 | 13897 | 1.626 | 2659997 | 5.018 |
| Total | | 854718 | 100.000 | 53013038 | 100.000 |

| Retention Time | Area | Area% | Retention Time | Area | Area% |
|---|---|---|---|---|---|
| 13.052 | 20983139 | 49.847 | 12.876 | 50353041 | 94.982 |
| 43.100 | 21111630 | 50.153 | 44.113 | 2659997 | 5.018 |

### 7.1.10 *tert*-Butyl 3-((1*S*,2*R*,*E*)-1-amino-5-phenyl-2-(1-(4,4,5,5-tetramethyl-1,3,2-dioxaborolan-2-yl)vinyl)pent-4-en-1-yl)-1*H*-indole-1-carboxylate (5j)

Light yellow oil**; IR (neat):** 3316 (w), 2975 (m), 2929 (w), 1733 (s), 1598 (w), 1452 (m), 1370 (m),1220 (m), 1153 (s), 1084 (m), 963 (m), 907 (m), 730 (s), 692 (m) $cm^{-1}$; **$^1$H NMR (CDCl$_3$, 500 MHz)**: δ 8.15 (br s, 1H), 7.81 (d, *J* = 7.8 Hz, 1H), 7.52 (s, 1H), 7.31 (t, *J* = 7.7 Hz, 1H), 7.25–7.18 (m, 5H), 7.18–7.11 (m, 1H), 6.26 (d, *J* = 15.8 Hz, 1H), 6.05 (dt, *J* = 15.2, 7.0 Hz, 1H), 5.87 (d, *J* = 3.0 Hz, 1H), 5.63 (d, *J* = 3.0 Hz, 1H), 4.49 (d, *J* = 5.5 Hz, 1H), 3.02 (dt, *J* = 10.0, 4.9 Hz, 1H), 2.62–2.52 (m, 1H), 2.51–2.44 (m, 1H), 1.86 (br s, 2H), 1.65 (s, 9H), 1.27 (d, *J* = 5.6 Hz, 12H); **$^{13}$C NMR (CDCl$_3$, 125 MHz)**: δ 149.9, 143.7, 138.0, 136.0, 130.8, 130.0, 129.8, 129.4, 128.5, 126.8, 126.0, 124.4, 124.0, 123.1, 122.4, 120.1, 115.4, 83.5, 83.2, 51.8, 50.4, 31.5, 28.4, 25.3, 24.9; **$^{11}$B NMR (CDCl$_3$, 160 MHz)**: δ 27.26; **HRMS (DART)**: Calcd for $C_{32}H_{42}BN_2O_4$ $[M+H]^+$: 529.3238. Found: 529.3265; **Specific rotation**: $[\alpha]_D^{20}$ +33.8 (*c* 0.64, $CHCl_3$) for an enantiomerically enriched sample of 96:4 e.r.

Enantiomeric purity was determined by HPLC analysis in comparison with authentic racemic material of the derived acetamide; Chiralcel OD-H column, 96:4 hexanes/*i*-PrOH, 0.3 mL/min, 220 nm.

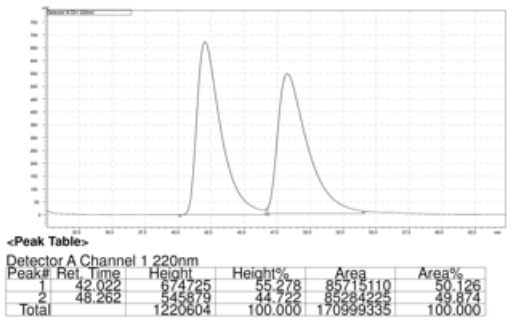

<Peak Table>
Detector A Channel 1 220nm

| Peak# | Ret. Time | Height | Height% | Area | Area% |
|---|---|---|---|---|---|
| 1 | 42.022 | 674725 | 55.278 | 85715110 | 50.126 |
| 2 | 48.262 | 545879 | 44.722 | 85284225 | 49.874 |
| Total | | 1220604 | 100.000 | 170999335 | 100.000 |

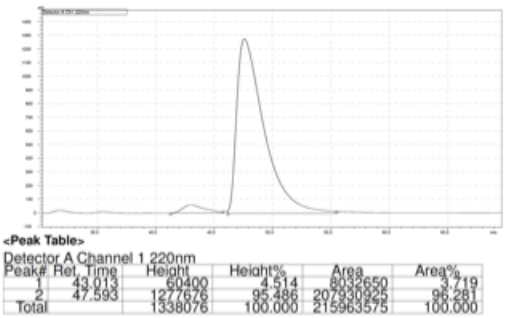

<Peak Table>
Detector A Channel 1 220nm

| Peak# | Ret. Time | Height | Height% | Area | Area% |
|---|---|---|---|---|---|
| 1 | 43.013 | 60400 | 4.514 | 8032650 | 3.719 |
| 2 | 47.593 | 1277676 | 95.486 | 207930925 | 96.281 |
| Total | | 1338076 | 100.000 | 215963575 | 100.000 |

| Retention Time | Area | Area% | Retention Time | Area | Area% |
|---|---|---|---|---|---|
| 42.022 | 85715110 | 50.126 | 43.013 | 8032650 | 3.719 |
| 48.262 | 85284225 | 49.874 | 47.593 | 207930925 | 96.281 |

### 7.1.11 (1*S*,2*R*,*E*)-5-Phenyl-2-(1-(4,4,5,5-tetramethyl-1,3,2-dioxaborolan-2-yl)vinyl)-1-(thiophen-2-yl)pent-4-en-1-amine (5k)

Yellow oil; **IR (neat):** 3313 (w), 3025 (w), 2971 (m), 2926 (w), 1598 (w), 1370 (m), 1306 (m), 1154 (s), 963 (m), 854 (m), 738 (m), 693 (s) $cm^{-1}$; **$^1$H NMR ($CDCl_3$, 400 MHz)**: δ 7.31–7.27 (m, 3H), 7.26–7.23 (m, 1H), 7.20–7.14 (m, 2H), 6.94–6.88 (m, 2H), 6.34 (d, *J* = 15.8 Hz, 1H), 6.12 (dt, *J* = 15.7, 7.1 Hz, 1H), 5.82 (d, *J* = 3.2 Hz, 1H), 5.51 (d, *J* = 3.2 Hz, 1H), 4.48 (d, *J* = 6.9 Hz, 1H), 2.72 (dt, *J* = 7.1, 6.9 Hz, 1H), 2.59–2.52 (m, 2H), 1.84 (br s, 2H), 1.25 (s, 12H); **$^{13}$C NMR ($CDCl_3$, 100 MHz)**: 149.4, 143.1, 138.0, 131.0, 130.7, 129.8, 128.5, 126.9, 126.5, 126.1, 123.8, 123.7, 83.2, 55.1, 54.4, 33.1, 25.1, 24.9; **$^{11}$B NMR ($CDCl_3$, 160 MHz)**: δ 27.71; **HRMS (DART)**: Calcd for $C_{23}H_{31}BNO_2S$ $[M+H]^+$: 396.2169. Found: 396.2158; **Specific rotation**: $[\alpha]_D^{20}$ +20.4 (*c* 1.06, $CHCl_3$) for an enantiomerically enriched sample of 97:3 e.r.

Enantiomeric purity was determined by HPLC analysis in comparison with authentic racemic material of the derived benzyl amide; Chiralcel OD-H column, 95:5 hexanes/*i*-PrOH, 0.3 mL/min, 220 nm.

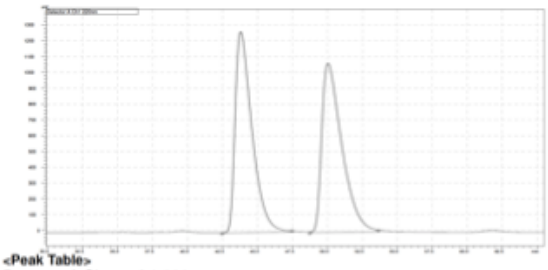

<Peak Table>
Detector A Channel 1 220nm

| Peak# | Ret. Time | Height | Height% | Area | Area% |
|---|---|---|---|---|---|
| 1 | 43.792 | 1272371 | 54.317 | 106244806 | 49.957 |
| 2 | 50.047 | 1070120 | 45.683 | 105426745 | 50.043 |
| Total | | 2342492 | 100.000 | 212671551 | 100.000 |

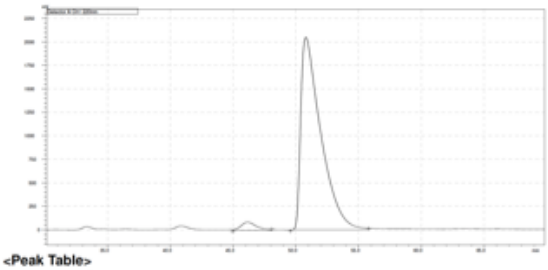

<Peak Table>
Detector A Channel 1 220nm

| Peak# | Ret. Time | Height | Height% | Area | Area% |
|---|---|---|---|---|---|
| 1 | 46.148 | 86570 | 4.049 | 7460737 | 3.174 |
| 2 | 50.800 | 2051533 | 95.951 | 227561593 | 96.826 |
| Total | | 2138104 | 100.000 | 235022329 | 100.000 |

| Retention Time | Area | Area% | Retention Time | Area | Area% |
|---|---|---|---|---|---|
| 43.792 | 106244806 | 49.957 | 46.148 | 7460737 | 3.174 |
| 50.047 | 105426745 | 50.043 | 50.800 | 227561593 | 96.826 |

### 7.1.12 (3*R*,4*R*,*E*)-4-(2-((*tert*-Butyldimethylsilyl)oxy)ethyl)-1-phenyl-5-(4,4,5,5-tetramethyl-1,3,2-dioxaborolan-2-yl)hexa-1,5-dien-3-amine (5l)

The general procedure was modified: 2.5 equiv. MeOH was used (vs. 1.7 equiv.). The isolated product contains small amount of impurities derived from over-reduction of the styrenyl alkene. These compounds, which contain an alkyl side chain **2H-5l** cannot be removed by silica gel chromatography.

Light yellow oil; **IR (neat)**: 3313 (w), 3025 (w), 2971 (m), 2926 (w), 1598 (w), 1370 (m), 1306 (m), 1154 (s), 963 (m), 854 (m), 738 (m), 693 (s) $cm^{-1}$; **$^1$H NMR ($CDCl_3$, 400 MHz)**: δ 7.38–7.32 (m, 2H), 7.32–7.27 (m, 2H), 7.24–7.18 (m, 1H), 6.48 (d, *J* = 15.9 Hz, 1H), 6.20 (dd, *J* = 15.9, 7.9 Hz, 1H), 5.70 (d, *J* = 3.2 Hz, 1H), 5.46 (d, *J* = 3.6 Hz, 1H), 3.76–3.65 (m, 2H), 3.55 (dt, *J* = 10.2, 6.8 Hz, 1H), 2.61 (td, *J* = 6.7, 6.0 Hz, 1H), 1.92–1.63 (m, 4H), 1.20

(s, 12H), 0.89 (s, 9H), 0.04 (s, 6H); **$^{13}$C NMR ($CDCl_3$, 125 MHz)**: δ 137.0, 131.5, 130.9, 128.6, 127.7, 126.6, 124.9, 82.0, 61.6, 57.8, 48.1, 32.2, 26.2, 25.20, 25.17, 18.5, –5.08, –5.10. The carbon directly attached to the boron atom could not be detected due to quadrupolar effects; **$^{11}$B NMR ($CDCl_3$, 160 MHz)**: δ 21.13; **HRMS (DART)**: Calcd for $C_{26}H_{45}BNO_3Si$ $[M+H]^+$: 458.3262. Found: 458.3265; **Specific rotation**: $[\alpha]_D^{20}$ +5.1 (*c* 0.28, $CHCl_3$) for an enantiomerically enriched sample of 95:5 e.r.

Enantiomeric purity was determined by HPLC analysis in comparison with authentic racemic material of the derived benzyl amide; Chiralcel OD-H column, 95:5 hexanes/*i*-PrOH, 0.3 mL/min, 254 nm.

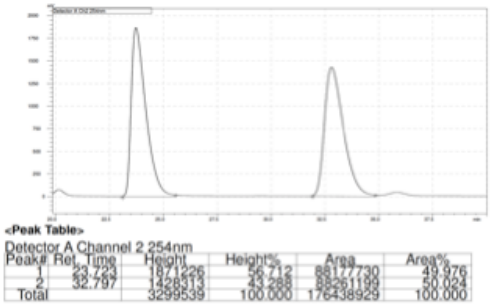

<Peak Table>
Detector A Channel 2 254nm

| Peak# | Ret. Time | Height | Height% | Area | Area% |
|---|---|---|---|---|---|
| 1 | 23.723 | 1971426 | 56.712 | 88177730 | 49.976 |
| 2 | 32.797 | 1428113 | 43.288 | 88261199 | 50.024 |
| Total | | 3299539 | 100.000 | 176438929 | 100.000 |

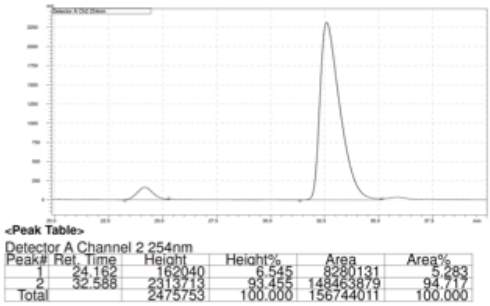

<Peak Table>
Detector A Channel 2 254nm

| Peak# | Ret. Time | Height | Height% | Area | Area% |
|---|---|---|---|---|---|
| 1 | 24.162 | 162040 | 6.545 | 8280131 | 5.283 |
| 2 | 32.588 | 2313713 | 93.455 | 148463879 | 94.717 |
| Total | | 2475753 | 100.000 | 156744011 | 100.000 |

| Retention Time | Area | Area% | Retention Time | Area | Area% |
|---|---|---|---|---|---|
| 23.723 | 88177730 | 49.976 | 24.162 | 8280131 | 5.283 |
| 32.797 | 88261199 | 50.024 | 32.588 | 148463879 | 94.717 |

### 7.1.13 (3*R*,4*R*)-3-(2-((*tert*-Butyldimethylsilyl)oxy)ethyl)-2-(4,4,5,5-tetramethyl-1,3,2-dioxaborolan-2-yl)hepta-1,6-dien-4-amine (5m)

Colorless oil (2.0% loading was used); **IR (neat)**: 3312 (w), 3040 (w), 2957 (m), 2929 (m), 2857 (w), 1604 (w), 1370 (w), 1253 (m), 1154 (s), 1096 (s), 1061 (m), 1014 (m), 833 (s), 775 (s) $cm^{-1}$; **$^1$H NMR ($CDCl_3$, 500 MHz)**: δ 5.70 (dtd, *J* = 17.1, 9.7, 5.0 Hz, 1H), 5.43 (s, 1H), 5.26–5.16 (m, 3H), 3.72 (dt, *J* = 10.1, 6.1 Hz, 1H), 3.62–3.50 (m, 3H), 3.17–3.09 (m, 1H), 2.56 (dt, *J* = 7.0, 6.5 Hz, 1H), 2.30 (dt, *J* = 14.3, 4.5 Hz, 1H), 1.98 (dt, *J* = 14.0, 10.3 Hz, 1H), 1.86–1.76 (m, 1H), 1.61–1.51 (m, 1H), 1.16 (d, J = 8.8 Hz, 12H), 0.88 (s, 9H), 0.04 (s, 6H); **$^{13}$C NMR ($CDCl_3$, 100 MHz)**: δ 153.8, 135.1, 119.6, 117.5, 80.3, 62.3, 53.9, 46.2, 34.2, 30.8, 26.2, 25.6, 25.1, 18.5, –5.17, –5.19; **$^{11}$B NMR ($CDCl_3$, 160 MHz)**: δ 13.08; **HRMS (DART)**: Calcd for $C_{21}H_{43}BNO_3Si$ $[M+H]^+$: 396.3100. Found: 396.3104; **Specific rotation**: $[\alpha]_D^{20}$ +14.9 (*c* 0.59, $CHCl_3$) for an enantiomerically enriched sample of 93.5:6.5 e.r.

Enantiomeric purity was determined by HPLC analysis in comparison with authentic racemic material of the derived benzyl amide; Chiralcel OZ-H column, 98:2 hexanes/*i*-PrOH, 0.3 mL/min, 254 nm.

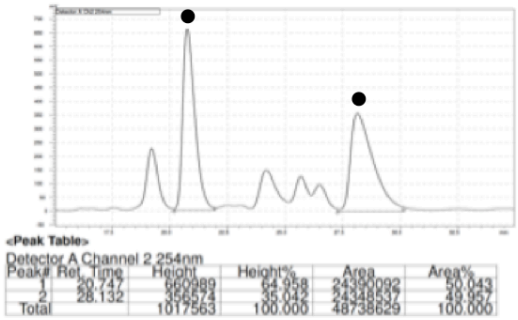


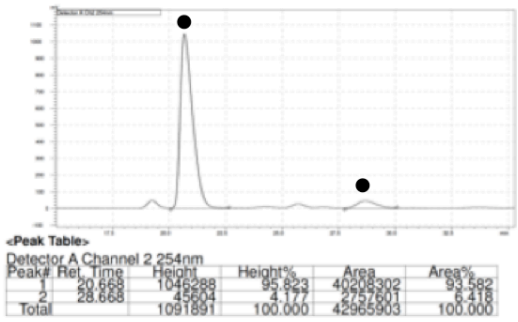


| Retention Time | Area | Area% | Retention Time | Area | Area% |
|---|---|---|---|---|---|
| 20.747 | 24390092 | 50.043 | 20.668 | 40208302 | 93.582 |
| 28.132 | 24348537 | 49.957 | 28.668 | 2757601 | 6.418 |

### 7.1.14 (2*R*,3*S*,4*R*)-4-(2-((*tert*-Butyldimethylsilyl)oxy)ethyl)-2-phenyl-5-(4,4,5,5-tetramethyl-1,3,2-dioxaborolan-2-yl)hex-5-en-3-amine (5n)

Colorless oil; **IR (neat)**: 3211 (w), 2956 (m), 2929 (m), 2857 (m), 1602 (w), 1471 (m), 1254 (m), 1154 (s), 1094 (s), 1041 (m), 936 (s), 833 (m), 774 (s) $cm^{-1}$; **$^{1}$H NMR ($CDCl_3$, 400 MHz)**: δ 7.37 – 7.29 (m, 2H), 7.27 – 7.22 (m, 1H), 7.21 – 7.14 (m, 2H), 5.41 (d, *J* = 3.2 Hz, 1H), 5.32 (d, *J* = 3.2 Hz, 1H), 3.81 (dt, *J* = 10.2, 5.6 Hz, 1H), 3.62 (ddd, *J* = 10.2, 7.3, 5.0 Hz, 1H), 3.05 (dd, *J* = 10.7, 5.0 Hz, 1H), 2.93 – 2.80 (m, 1H), 2.81 – 2.63 (m, 2H), 1.79 – 1.59 (m, 2H), 1.26 (d, *J* = 6.8 Hz, 3H), 1.07 (d, *J* = 10.4 Hz, 12H), 0.91 (s, 9H), 0.09 (s, 3H), 0.07 (s, 3H); **$^{13}$C NMR ($CDCl_3$, 100 MHz)**: δ 155.5, 14340, 129.2, 127.4, 127.2, 118.4, 80.2, 61.7, 60.5, 44.0, 42.0, 29.6, 26.2, 25.4, 25.3, 19.0, 18.6, –5.3, –5.2; **$^{11}$B NMR ($CDCl_3$, 160 MHz)**: δ 12.95; **HRMS (DART)**: Calcd for $C_{19}H_{47}NO_3BSi$ $[M+H]^+$: 460.3413. Found: 460.3391; **Specific rotation:** $[\alpha]_D^{20}$ +0.296 (*c* 0.8459, $CHCl_3$) for an enantiomerically enriched sample of 98:2 e.r.

Enantiomeric purity was determined by HPLC analysis in comparison with authentic racemic material of the derived benzyl amide; Chiralcel OD-H column, 96:4 hexanes/*i*-PrOH, 0.3 mL/min, 220 nm.

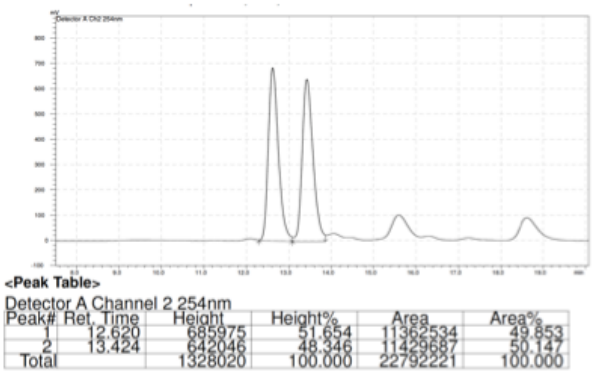


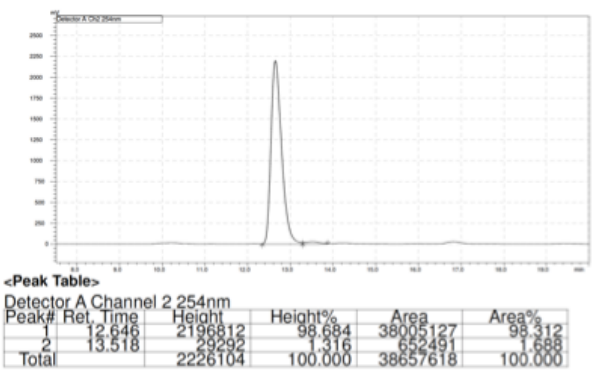


| Retention Time | Area | Area% | Retention Time | Area | Area% |
|---|---|---|---|---|---|
| 12.620 | 11362534 | 49.853 | 12.646 | 38005127 | 98.312 |
| 13.424 | 11429687 | 50.147 | 13.518 | 652491 | 1.688 |

### 7.1.15 (2*R*,3*R*)-3-(2-((*tert*-Butyldimethylsilyl)oxy)ethyl)-4-(4,4,5,5-tetramethyl-1,3,2-dioxaborolan-2-yl)pent-4-en-2-amine (5o)

Colorless oil (2.0% loading was used); **IR (neat)**: 3210 (w), 2958 (m), 2929 (m), 2857 (m), 1604 (w), 1471 (m), 1253 (m), 1155 (s), 1094 (s), 1041 (m), 905 (m), 834 (s), 755 (s) $cm^{-1}$; **$^1$H NMR ($CDCl_3$, 400 MHz)**: δ 5.51–5.47 (m, 1H), 5.30–5.26 (m, 1H), 3.70 (ddd, *J* = 10.1, 6.8, 5.9 Hz, 1H), 3.55 (dt, *J* = 10.2, 6.8 Hz, 1H), 3.26 (dq, *J* = 6.6, 6.8 Hz, 1H), 2.86 (br s, 2H), 2.46 (dt, *J* = 7.2, 6.7 Hz, 1H), 1.84–1.73 (m, 1H), 1.62–1.51 (m, 1H), 1.18 (d, *J* = 4.2 Hz, 12H), 1.06 (d, *J* = 6.7 Hz, 3H), 0.88 (s, 9H), 0.039 (s, 3H), 0.036 (s, 3H); **$^{13}$C NMR ($CDCl_3$, 100 MHz)**: δ 119.2, 80.7, 61.9, 50.7, 47.4, 31.2, 26.1, 25.5, 25.3, 18.5, 17.6, –5.15, –5.18. The carbon directly attached to the boron atom could not be detected due to quadrupolar effects; **$^{11}$B NMR ($CDCl_3$, 160 MHz)**: δ 15.27; **HRMS (DART)**: Calcd for $C_{19}H_{41}NO_3BSi$ $[M+H]^+$: 370.2949. Found: 370.2965; **Specific rotation:** $[\alpha]_D^{20}$ +5.0 (*c* 0.59, $CHCl_3$) for an enantiomerically enriched sample of 94:6 e.r.

Enantiomeric purity was determined by HPLC analysis in comparison with authentic racemic material of the derived benzyl amide; Chiralcel OZ-H column, 99:1 hexanes/*i*-PrOH, 1.0 mL/min, 220 nm.

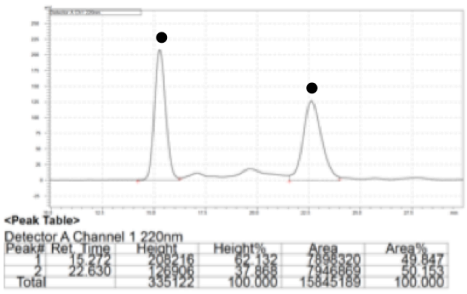

<Peak Table>
Detector A Channel 1 220nm

| Peak# | Ret. Time | Height | Height% | Area | Area% |
|---|---|---|---|---|---|
| 1 | 15.272 | 208516 | 62.132 | 7898320 | 49.847 |
| 2 | 22.630 | 126606 | 37.868 | 7946869 | 50.153 |
| Total | | 335122 | 100.000 | 15845189 | 100.000 |

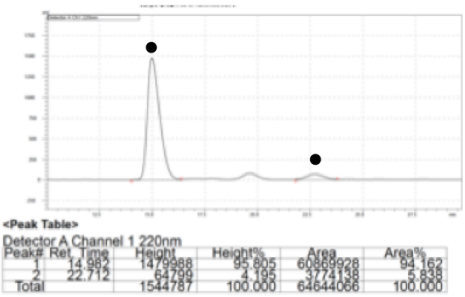

<Peak Table>
Detector A Channel 1 220nm

| Peak# | Ret. Time | Height | Height% | Area | Area% |
|---|---|---|---|---|---|
| 1 | 14.982 | 1479988 | 95.805 | 60869928 | 94.162 |
| 2 | 22.712 | 64799 | 4.195 | 3774138 | 5.838 |
| Total | | 1544787 | 100.000 | 64644066 | 100.000 |

| Retention Time | Area | Area% | Retention Time | Area | Area% |
|---|---|---|---|---|---|
| 15.272 | 7898320 | 49.847 | 14.982 | 60869928 | 94.162 |
| 22.630 | 7946869 | 50.153 | 22.712 | 3774138 | 5.838 |

### 7.1.16 (3*S*,4*R*)-4-(2-((*tert*-Butyldimethylsilyl)oxy)ethyl)-2,2-dimethyl-5-(4,4,5,5-tetramethyl-1,3,2-dioxaborolan-2-yl)hex-5-en-3-amine (5p)

Colorless oil; **IR (neat)**: 3332 (w), 3079 (w), 2956 (m), 2929 (m), 2857 (w), 1472 (w), 1361 (w), 1253 (m), 1156 (m), 1092 (s), 909 (w), 834 (s), 737 (m) $cm^{-1}$; **$^1$H NMR ($CDCl_3$, 500 MHz)**: δ 5.42 (d, *J* = 3.4 Hz, 1H), 5.28 (d, *J* = 3.4 Hz, 1H), 3.63 (ddd, *J* = 9.9, 6.9, 4.2 Hz, 1H), 3.51 (ddd, *J* = 9.9, 8.4, 5.9 Hz, 1H), 2.66 (dt, *J* = 11.8, 3.4 Hz, 1H), 2.60 (d, *J* = 4.0 Hz, 1H), 2.49 (br s, 2H), 1.79–1.71 (m, 1H), 1.57–1.48 (m, 1H), 1.19 (d, *J* = 6.4 Hz, 12H), 0.99 (s, 9H), 0.88 (s, 9H), 0.030 (s, 3H), 0.026 (s, 3H); **$^{13}$C NMR ($CDCl_3$, 125 MHz)**: δ 153.3, 120.4, 81.1, 65.0, 61.3, 44.8, 34.2, 30.3, 27.6, 26.1, 25.3, 25.2, 18.4, –5.1, –5.2; **$^{11}$B NMR ($CDCl_3$, 160 MHz)**: δ 16.94; **HRMS (DART)**: Calcd for $C_{22}H_{47}BNO_3Si$ $[M+H]^+$: 412.3418. Found: 412.3441; **Specific rotation**: $[\alpha]_D^{20}$ –15.5 (*c* 0.61, $CHCl_3$) for an enantiomerically enriched sample of >99:1 e.r.

Enantiomeric purity was determined by HPLC analysis in comparison with authentic racemic material of the derived benzyl amide; Chiralcel OZ-H column, 98:2 hexanes/*i*-PrOH, 0.3 mL/min, 220 nm.

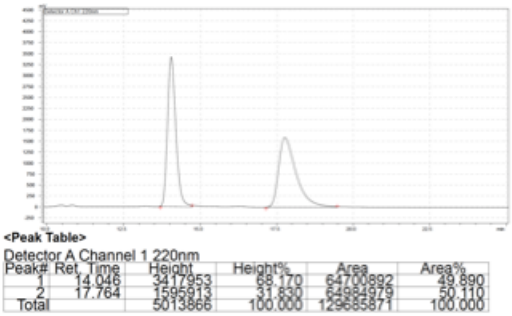

<Peak Table>
Detector A Channel 1 220nm

| Peak# | Ret. Time | Height | Height% | Area | Area% |
|---|---|---|---|---|---|
| 1 | 14.046 | 3417953 | 68.170 | 64700892 | 49.890 |
| 2 | 17.764 | 1595913 | 31.830 | 64984979 | 50.110 |
| Total | | 5013866 | 100.000 | 129685871 | 100.000 |

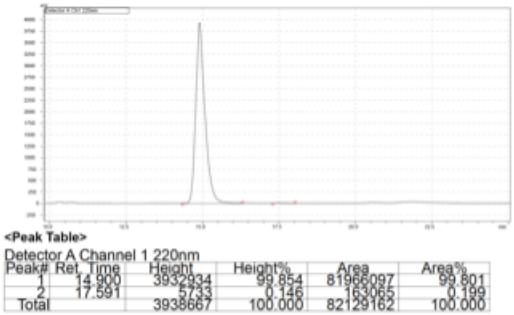

<Peak Table>
Detector A Channel 1 220nm

| Peak# | Ret. Time | Height | Height% | Area | Area% |
|---|---|---|---|---|---|
| 1 | 14.900 | 3932934 | 99.854 | 81966097 | 99.801 |
| 2 | 17.591 | 5733 | 0.146 | 163065 | 0.199 |
| Total | | 3938667 | 100.000 | 82129162 | 100.000 |

| Retention Time | Area | Area% | Retention Time | Area | Area% |
|---|---|---|---|---|---|
| 14.046 | 64700892 | 49.890 | 14.900 | 81966097 | 99.801 |
| 17.764 | 64984979 | 50.110 | 17.591 | 163065 | 0.199 |

### 7.1.17 (1*S*,2*R*)-2-Methyl-1-phenyl-3-(4,4,5,5-tetramethyl-1,3,2-dioxaborolan-2-yl)but-3-en-1-amine (5q)

The general procedure was modified: 1.5 equiv allene **2b** was used (vs. 1.2 equiv.).

Colorless oil; **IR (neat)**: 3356 (w), 3032 (m), 2966 (m), 2927 (m), 1604 (m), 1414 (m), 1114 (s), 1063 (m), 964 (m), 877 (w), 700 (m) $cm^{-1}$; **$^{1}$H NMR ($CDCl_3$, 500 MHz)**: δ 7.32–7.28 (m, 4H), 7.24–7.19 (m, 1H), 5.69 (d, *J* = 3.0 Hz, 1H), 5.43 (d, *J* = 3.0 Hz, 1H), 4.17 (d, *J* = 6.1 Hz, 1H), 2.79 (dq, *J* = 6.9, 6.1 Hz, 1H), 1.90 (br s, 2H), 1.25 (d, *J* = 2.6 Hz, 12H), 0.95 (d, *J* = 6.9 Hz, 3H); **$^{13}$C NMR ($CDCl_3$, 125 MHz)**: δ 143.8, 128.3, 127.1, 126.9, 126.0, 82.7, 59.2, 45.9, 25.2, 25.0, 13.9. The carbon directly attached to the boron atom could not be detected due to quadrupolar effects; **$^{11}$B NMR ($CDCl_3$, 160 MHz)**: δ 25.41; **HRMS (DART):** Calcd for $C_{17}H_{27}BNO_2$ $[M+H]^+$: 288.2135. Found: 288.2146; **Specific rotation**: $[\alpha]_D^{20}$ +26.9 (*c* 0.38, $CHCl_3$) for an enantiomerically enriched sample of 93:7 e.r.

Enantiomeric purity was determined by HPLC analysis in comparison with authentic racemic material of the derived acetamide; Chiralcel OD-H column, 95:5 hexanes/*i*-PrOH, 0.3 mL/min, 220 nm.

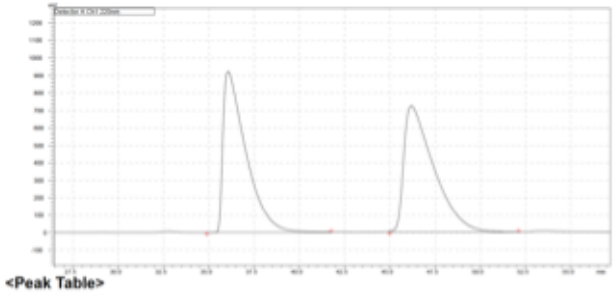

<Peak Table>
Detector A Channel 1 220nm

| Peak# | Ret. Time | Height | Height% | Area | Area% |
|---|---|---|---|---|---|
| 1 | 36.065 | 923166 | 56.055 | 81155293 | 49.275 |
| 2 | 46.186 | 723740 | 43.945 | 83544129 | 50.725 |
| Total | | 1646906 | 100.000 | 164699422 | 100.000 |

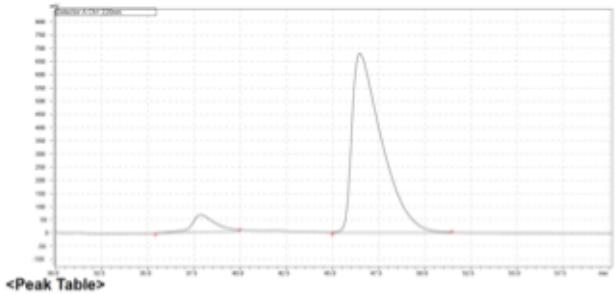

<Peak Table>
Detector A Channel 1 220nm

| Peak# | Ret. Time | Height | Height% | Area | Area% |
|---|---|---|---|---|---|
| 1 | 37.861 | 64652 | 8.676 | 5800763 | 7.021 |
| 2 | 46.469 | 680546 | 91.324 | 76814950 | 92.979 |
| Total | | 745198 | 100.000 | 82615713 | 100.000 |

| Retention Time | Area | Area% | Retention Time | Area | Area% |
|---|---|---|---|---|---|
| 36.065 | 81155293 | 49.275 | 37.861 | 5800763 | 7.021 |
| 46.186 | 83544129 | 50.725 | 46.469 | 76814950 | 92.979 |

### 7.1.18 (1*S*,2*S*)-1,2-Diphenyl-3-(4,4,5,5-tetramethyl-1,3,2-dioxaborolan-2-yl)but-3-en-1-amine (5r)

Light yellow oil; **IR (neat)**: 3334 (w), 3059 (w), 2973 (m), 2931 (w), 1602 (w), 1454 (m), 1360 (m), 1309 (m), 1153 (s), 1072 (s), 1007 (m), 909 (m), 755 (m), 701 (s) $cm^{-1}$; **$^{1}$H NMR ($CDCl_3$, 500 MHz)**: δ 7.40 (d, *J* = 8.0 Hz, 2H), 7.34 (d, *J* = 7.9 Hz, 2H), 7.30–7.26 (m, 4H), 7.23–7.17 (m, 2H), 5.61 (d, *J* = 3.0 Hz, 1H), 5.49 (d, *J* = 3.0 Hz, 1H), 4.74 (d, *J* = 9.8 Hz, 1H), 3.78 (d, *J* = 9.8 Hz, 1H), 1.64 (s, 2H), 1.18 (s, 12H); **$^{13}$C NMR ($CDCl_3$, 125 MHz)**: δ 144.0, 142.6, 129.8, 129.1, 128.5, 128.3, 127.9, 127.2, 126.6, 83.1, 61.1, 58.5, 25.1, 24.8. The carbon directly attached to the boron atom could not be detected due to quadrupolar effects; **$^{11}$B NMR ($CDCl_3$, 160 MHz)**: δ 27.37; **HRMS (DART)**: Calcd for $C_{22}H_{29}BNO_2$ $[M+H]^+$: 350.2291. Found: 350.2290; **Specific rotation**: $[\alpha]_D^{20}$ +9.1 (*c* 0.53, $CHCl_3$) for an enantiomerically enriched sample of 97.5:2.5 e.r.

Enantiomeric purity was determined by HPLC analysis in comparison with authentic racemic material of the derived acetamide; Chiralcel OD-H column, 90:10 hexanes/*i*-PrOH, 0.3 mL/min, 220 nm.

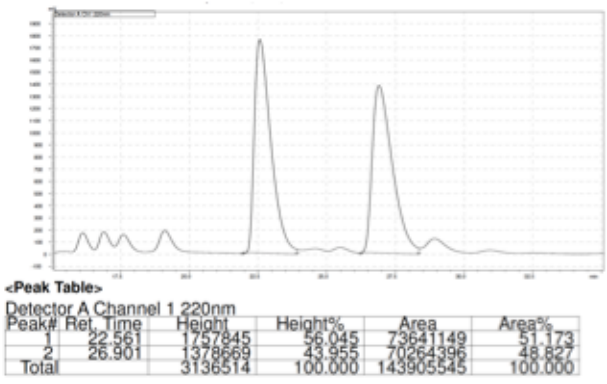

<Peak Table>
Detector A Channel 1 220nm

| Peak# | Ret. Time | Height | Height% | Area | Area% |
|---|---|---|---|---|---|
| 1 | 22.561 | 1757845 | 56.045 | 73641149 | 51.173 |
| 2 | 26.901 | 1378669 | 43.955 | 70264396 | 48.827 |
| Total | | 3136514 | 100.000 | 143905545 | 100.000 |

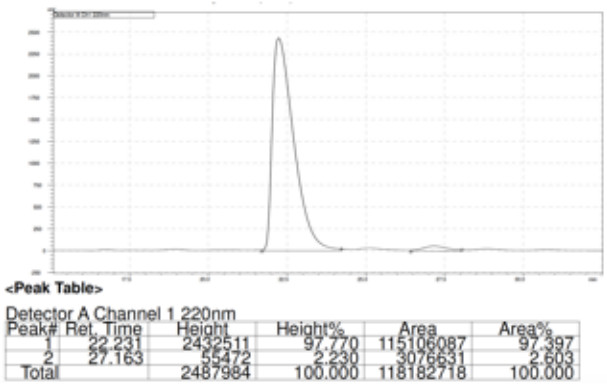

<Peak Table>
Detector A Channel 1 220nm

| Peak# | Ret. Time | Height | Height% | Area | Area% |
|---|---|---|---|---|---|
| 1 | 22.231 | 2432511 | 97.770 | 115106087 | 97.397 |
| 2 | 27.163 | 55472 | 2.230 | 3076631 | 2.603 |
| Total | | 2487984 | 100.000 | 118182718 | 100.000 |

| Retention Time | Area | Area% | Retention Time | Area | Area% |
|---|---|---|---|---|---|
| 22.561 | 73641149 | 51.173 | 22.231 | 115106087 | 97.397 |
| 26.901 | 70264396 | 48.827 | 27.163 | 3076631 | 2.603 |

# 8 Enantioselective Synthesis of *anti*-Homoallylic N-H Amines

**Table S1.** Screening of Various Reducing Agents and Conditions for *anti*-Selective Ketimine Reduction

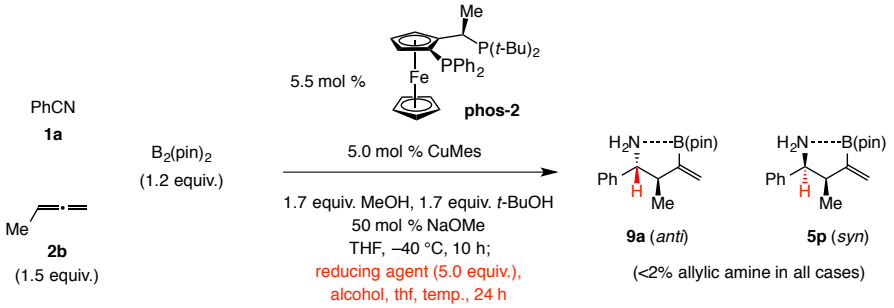


| Entry | Reducing Agent | Alcohol (equiv.) | Temp (°C) | Conv. (%); Yield (%) | **9a**:**5p** | e.r. |
|---|---|---|---|---|---|---|
| 1 | $NaCNBH_3$ | MeOH (3.4) | –40 | 48; 42 | 17:83 | 89:11 (**9a**) |
| 2 | $NaBH_4$ | MeOH (3.4) | –40 | >98; 68 | 36:64 | 98:2 (**9a**); 93:7 (**5p**) |
| 3 | $LiAlH_4$ | none | –40 | >98; 52 | 50:50 | 98:2 (**9a**); 98:2 (**5p**) |
| 4 | $LiBH_4$ | none | –40 | >98; 49 | 71:29 | 98:2 (**9a**); 98:2 (**5p**) |
| 5 | $LiBH_4$ | MeOH (3.4) | –40 | ND | 75:25 | ND |
| 6 | $LiBH_4$ | MeOH (200) | –40 | ND | 83:17 | ND |
| 7 | $LiBH_4$ | MeOH (200) | –78 | >98; 56 | 94:6 | 98:2 (**9a**) |
| 8 | $LiBH_4$ | EtOH (200) | –78 | ND | 56:44 | ND |
| 9 | $LiBH_4$ | *i*-PrOH (200) | –78 | ND | 51:49 | ND |
| 10 | $LiBH_4$ | MeOH (200) | –78 | >98; 66 | 97:3 | 97:3 (**9a**) |

Reactions were performed under $N_2$ atm. Conv. and diastereomeric ratios were determined by spectroscopic ($^1$H NMR) analysis of the unpurified reaction mixtures (±2%). Yields correspond to isolated and purified products (±5%). Enantioselectivity was determined by HPLC analysis (±1%). For entry 10, $Et_2O$ was used as the solvent, and the mixture was subjected to vacuum prior to being charged with $LiBH_4$ and MeOH. ND, not determined.

**Table S2.** Screening of Various Lewis acidic Additives for *anti*-Selective Ketimine Reduction

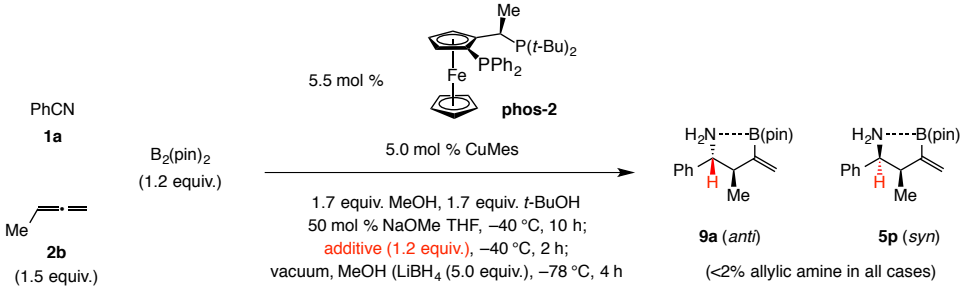


| Entry | Additive | Conv. (%); Yield (%) | **9a**:**5p** | e.r. |
|---|---|---|---|---|
| 1 | none | >98; 49 | 84:16 | 97:3 |
| 2 | $AlCl_3$ | 90; 63 | 93:7 | 91:9 |
| 3 | $Al(Os\text{-}Bu)_3$ | 81; ND | 79:21 | ND |
| 4 | $Al(OTf)_3$ | >98; 63 | 99:1 | 99:1 |
| 5 | $Zn(OMe)_2$ | >98; ND | 81:19 | ND |
| 6 | $Zn(OTf)_2$ | >98; 15 | 92:8 | 99:1 |
| 7 | $TiCl_4$ | 94; 53 | 86:14 | 86:14 |
| 8 | $CeCl_3{\cdot}7H_2O$ | >98; complex mix. | ND | ND |

Reactions were performed under $N_2$ atm. Conv. and diastereomeric ratios were determined by spectroscopic ($^1$H NMR) analysis of the unpurified reaction mixtures (±2%). Yields correspond to isolated and purified products (±5%). Enantioselectivity was determined by HPLC analysis (±1%). ND, not determined.

**Typical procedure:** In a $N_2$-filled glove box, an oven-dried vial (4 mL, 17 × 38 mm) was charged with **phos-2** (3.0 mg, 0.0055 mmol), CuMes (0.9 mg, 0.0050 mmol) and $Et_2O$ (0.50 mL). The solution was kept at 22 °C for 10 min (homogeneous solution, no stirring needed), after which MeOH (5.5 mg, 0.170 mmol) was added and the mixture was retained at 22 °C for another 10 min before being placed in a –40 °C freezer. In a separate oven-dried vial containing a stir bar, nitrile **1a** (10.3 mg, 0.10 mmol), allene **2b** (5.0 M in thf, 30 μL, 0.15 mmol), $B_2(pin)_2$ (30.5 mg, 0.12 mmol) and $Et_2O$ (0.40 mL) were added and the mixture was allowed to cool in a –40 °C freezer. Once the latter solution was sufficiently cooled, it was charged with the solution of the copper complex in a drop-wise manner. The resulting solution was allowed to remain at –40 °C for 10 h, after which it was treated with aluminum triflate (56.9 mg, 0.120 mmol), and allowed to stir for 2 h at –40 °C. After the vessel was removed from the glove box, the solution, while placed in an ice bath, was concentrated in vacuo. Methanol (0.8 mL) was then added and the solution, while being allowed to stir rigorously vigorous stirring, was cooled to –78 °C; slight warming up might be needed for the residues dissolve fully. With the solution kept at –78 °C, lithium borohydride (2.0 M in thf, 0.25 mL, 0.50 mmol) was added slowly over 5 min. CAUTION: Exothermic reaction. The mixture was allowed to stir for 4 h at –78 °C, after which the reaction was quenched by the addition of a saturated solution of aqueous ammonium chloride (1.0 mL) and a saturated solution of aqueous potassium sodium tartrate (1.0 mL). The mixture was allowed to stir for 30 min at 22 °C, washed with $CH_2Cl_2$ (5 × 2.0 mL) and the combined organic layers were concentrated in vacuo to give yellow oil, which was purified by silica gel chromatography ($CH_2Cl_2$:MeOH:$HCO_2H$ 100:1.5:0.4 and after removal of pinacol, 100:6.0:0.2). NOTE: Silica gel used was flushed with 2% v/v solution of formic acid in $CH_2Cl_2$ (3×3 mL). To remove formic acid, the samples containing the desired product (as judged by tlc analysis) were collected and allowed to stir for 15 min over $K_2CO_3$ (500 mg). The suspension was filtered through a short plug of sand and the volatiles were removed in vacuo to afford tan solid. Diethyl ether (5 mL) was added and the suspension was passed through a pad of celite. Removal of the volatiles in vacuo afforded **9a** as white solid (18.9 mg, 0.066 mmol, 66% yield).

### 8.1.1 (1*R*,2*R*)-2-Methyl-1-phenyl-3-(4,4,5,5-tetramethyl-1,3,2-dioxaborolan-2-yl)but-3-en-1-amine (9a)

Due to slight decomposition of this compound upon purification/recording of the NMR spectrum, boron containing impurities (~2–5 %) are present and are inseparable by silica gel chromatography. White solid; **m.p.** 144–145 °C; IR (neat): 3206 (w), 3046 (m), 2968 (s), 2928 (m), 1605 (w), 1457 (m), 1228 (m), 1158 (s), 1117 (s), 1059 (m), 962 (m), 907 (m), 757 (m), 700 (m) $cm^{-1}$; **$^1$H NMR ($CDCl_3$, 400 MHz)**: δ 7.44–7.28 (m, 5H), 5.47 (t, *J* = 2.7 Hz, 1H), 5.30 (t, *J* = 2.7 Hz, 1H), 4.12 (br s, 2H), 3.52 (d, *J* = 11.8 Hz, 1H), 2.77–2.66 (m, 1H), 1.15 (d, *J* = 8.5 Hz, 12H), 0.88 (d, *J* = 6.5 Hz, 3H); **$^{13}$C NMR ($CDCl_3$, 100 MHz)**: δ 157.9, 140.1, 129.1, 128.5, 127.5, 115.1, 80.2, 63.4, 45.1, 25.7, 25.4, 14.0; **$^{11}$B NMR ($CDCl_3$, 160 MHz)**: δ 11.14; **HRMS (DART)**: Calcd for $C_{17}H_{27}BNO_2$ $[M+H]^+$: 288.2194. Found: 288.2142; **specific rotation**: $[\alpha]_D^{20}$ +12.7 (*c* 0.58, $CHCl_3$) for an enantiomerically enriched sample of 97:3 e.r.

Enantiomeric purity was determined by HPLC analysis in comparison with authentic racemic material of the derived acetamide; Chiralcel OD-H column, 97:3 hexanes/*i*-PrOH, 0.3 mL/min, 220 nm.

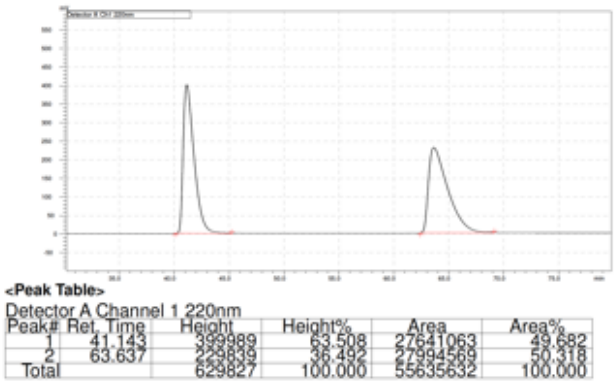

<Peak Table>
Detector A Channel 1 220nm

| Peak# | Ret. Time | Height | Height% | Area | Area% |
|---|---|---|---|---|---|
| 1 | 41.143 | 399989 | 63.508 | 27641063 | 49.682 |
| 2 | 63.637 | 229838 | 36.492 | 27994569 | 50.318 |
| Total | | 629827 | 100.000 | 55635632 | 100.000 |

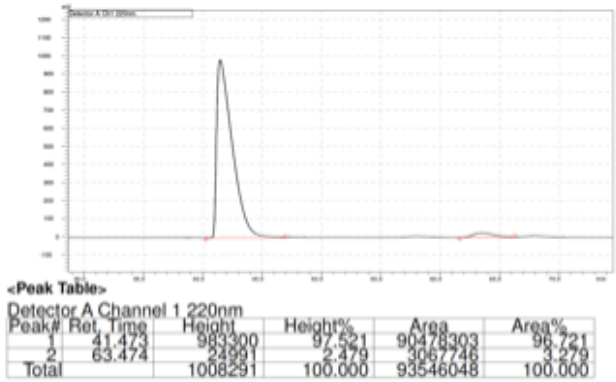

<Peak Table>
Detector A Channel 1 220nm

| Peak# | Ret. Time | Height | Height% | Area | Area% |
|---|---|---|---|---|---|
| 1 | 41.473 | 983300 | 97.521 | 90478303 | 96.721 |
| 2 | 63.474 | 24991 | 2.479 | 3067746 | 3.279 |
| Total | | 1008291 | 100.000 | 93546048 | 100.000 |

| Retention Time | Area | Area% | Retention Time | Area | Area% |
|---|---|---|---|---|---|
| 41.143 | 27641063 | 49.682 | 41.473 | 90478303 | 96.721 |
| 63.637 | 27994569 | 50.318 | 63.474 | 3067746 | 3.279 |

### 8.1.2 (1*R*,2*R*)-2-(2-((*tert*-Butyldimethylsilyl)oxy)ethyl)-1-phenyl-3-(4,4,5,5-tetramethyl-1,3,2-dioxaborolan-2-yl)but-3-en-1-amine (9b)

The general procedure was modified: 1.2 equiv of **2a** was used (vs. 1.5 equiv.). Due to slight decomposition of this compound upon purification/recording of the NMR spectrum, boron containing impurities (~2–5 %) are present and are inseparable by silica gel chromatography. White Solid; **m.p.** 119–121 °C; **IR (neat)**: 3045 (w), 2957 (m), 2928 (m), 2856 (w), 1605 (w), 1462 (m), 1361 (m), 1252 (m), 1156 (s), 1091 (s), 1007 (m), 963 (m), 835 (s), 774 (s), 700 (s) $cm^{-1}$; **$^1$H NMR ($CDCl_3$, 400 MHz)**: δ 7.43–7.39 (m, 2H), 7.39–7.34 (m, 2H), 7.33–7.28 (m, 1H), 5.55 (t, *J* = 2.5 Hz, 1H), 5.40 (t, *J* = 2.4 Hz, 1H), 3.69 (d, *J* = 11.3 Hz, 1H), 3.47 (ddd, *J* = 10.2, 9.0, 5.3 Hz, 1H), 3.33 (ddd, *J* = 10.1, 8.5, 6.7 Hz, 1H), 2.77–2.67 (m, 1H), 1.83–1.69 (m, 1H), 1.50–1.40 (m, 1H), 1.14 (d, *J* = 9.0 Hz, 12H), 0.79 (s, 9H), –0.09 (s, 3H), –0.11 (s, 3H); **$^{13}$C NMR ($CDCl_3$, 100 MHz)**: δ 154.5, 141.2, 129.0, 128.3, 127.7, 117.7, 80.7, 61.7, 61.4, 47.4, 33.2, 26.1, 25.6, 25.2, 18.4, –5.22, –5.23; **$^{11}$B NMR ($CDCl_3$, 160 MHz)**: δ 14.59; **HRMS (DART)**: Calcd for $C_{24}H_{43}BNO_3Si$ $[M+H]^+$: 432.3100. Found: 432.3093; **specific rotation**: $[\alpha]_D^{20}$ +0.5 (*c* 2.01, $CHCl_3$) for an enantiomerically enriched sample of 99:1 e.r.

Enantiomeric purity was determined by HPLC analysis in comparison with authentic racemic material of the derived acetamide; Chiralcel OD-H column, 98:2 hexanes/*i*-PrOH, 0.3 mL/min, 220 nm.

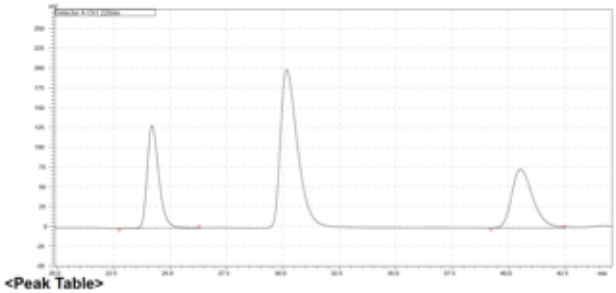

<Peak Table>
Detector A Channel 1 220nm

| Peak# | Ret. Time | Height | Height% | Area | Area% |
|---|---|---|---|---|---|
| 1 | 24.193 | 129595 | 63.593 | 4658310 | 49.145 |
| 2 | 40.521 | 74195 | 36.407 | 4820368 | 50.855 |
| Total | | 203790 | 100.000 | 9478679 | 100.000 |

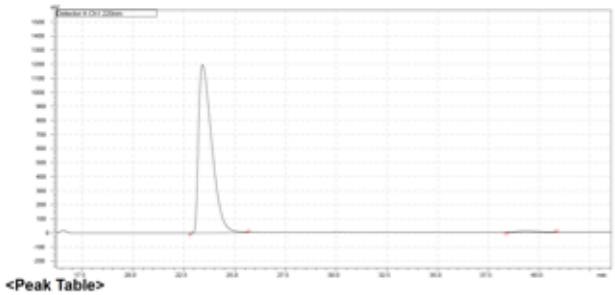

<Peak Table>
Detector A Channel 1 220nm

| Peak# | Ret. Time | Height | Height% | Area | Area% |
|---|---|---|---|---|---|
| 1 | 23.417 | 1195688 | 99.236 | 54101316 | 98.804 |
| 2 | 39.334 | 9203 | 0.764 | 654748 | 1.196 |
| Total | | 1204891 | 100.000 | 54756065 | 100.000 |

| Retention Time | Area | Area% | Retention Time | Area | Area% |
|---|---|---|---|---|---|
| 24.193 | 4658310 | 49.145 | 23.417 | 54101316 | 98.804 |
| 40.521 | 4820368 | 50.855 | 39.334 | 654748 | 1.196 |

### 8.1.3 (1*R*,2*R*)-2-(2-((*tert*-Butyldimethylsilyl)oxy)ethyl)-1-(pyridin-3-yl)-3-(4,4,5,5-tetramethyl-1,3,2-dioxaborolan-2-yl)but-3-en-1-amine (9c)

The general procedure was modified in the following manner: after the addition of the allyl moiety, $Et_2O$ was removed in vacuo, the mixture was re-dissolved in MeOH and then $Al(OTf)_3$ was added. Removal of the volatiles in the presence of $Al(OTf)_3$ resulted in extensive epimerization was (66:34 vs. 99:1 e.r.). Light yellow solid; **m.p.** = 110 °C, decomposition; **IR (neat)**: 3049 (w), 2958 (s), 2929 (m), 2857 (m), 1579 (w), 1472 (m), 1385 (m), 1254 (s), 1158 (s), 1094 (s), 836 (s), 776 (s), 715 (m); **$^1$H NMR ($CDCl_3$, 500 MHz)**: δ 8.55 (d, J = 2.4 Hz, 1H), 8.51 (dd, J = 4.8, 1.7 Hz, 1H), 7.73 (dt, J =7.9, 2.0 Hz, 1H), 7.28–7.25 (m, 1H), 5.86 (d, J = 3.2 Hz, 1H), 5.61 (d, J = 3.1 Hz, 1H), 3.96 (d, J = 9.6 Hz, 1H), 3.51–3.44 (m, 1H), 3.35 (ddd, J = 10.1, 7.7, 6.9 Hz, 1H), 2.57 (td, J = 9.8, 3.6 Hz, 1H), 2.12 (br s, 2H), 1.72–1.63 (m, 1H), 1.41–1.32 (m, 1H), 1.24 (s, 12H), 0.81 (s, 9H), –0.07 (s, 3H), –0.09 (s, 3H); **$^{13}$C NMR ($CDCl_3$, 100 MHz)**: δ 149.8, 149.0, 139.3, 135.0, 128.7, 123.7, 82.7, 61.3, 57.3, 50.2, 33.8, 26.1, 25.1, 18.4, −5.21, −5.23. The peak for the carbon bearing the boron atom could not be detected due to quadrupolar effects; **$^{11}$B NMR ($CDCl_3$, 160 MHz)**: δ 26.24; **HRMS (DART)**: Calcd for $C_{23}H_{42}BN_2O_3Si[M+H]^+$: 433.3052. Found: 433.3038; **specific rotation**: $[\alpha]_D^{20}$ +10.0 (*c* 1.16, $CHCl_3$) for an enantiomerically enriched sample of 99:1 e.r.

Enantiomeric purity was determined by HPLC analysis in comparison with authentic racemic material of the derived acetamide; Chiralcel OZ-H column, 90:10 hexanes/*i*-PrOH, 0.3 mL/min, 220 nm.

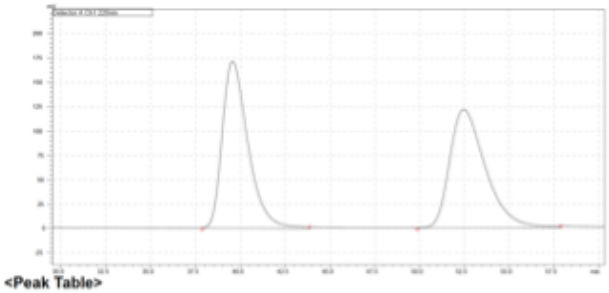

<Peak Table>
Detector A Channel 1 220nm

| Peak# | Ret. Time | Height | Height% | Area | Area% |
|---|---|---|---|---|---|
| 1 | 39.548 | 171544 | 58.427 | 17225930 | 50.440 |
| 2 | 52.476 | 122058 | 41.573 | 16925283 | 49.560 |
| Total | | 293602 | 100.000 | 34151213 | 100.000 |

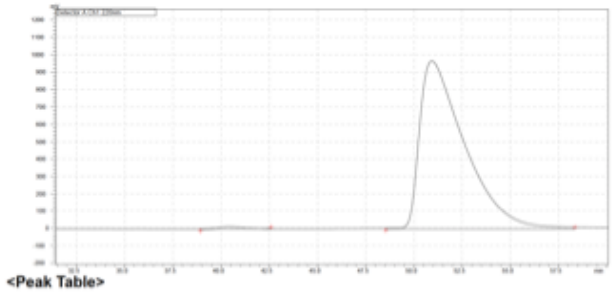

<Peak Table>
Detector A Channel 1 220nm

| Peak# | Ret. Time | Height | Height% | Area | Area% |
|---|---|---|---|---|---|
| 1 | 40.449 | 11721 | 1.197 | 1117948 | 0.709 |
| 2 | 50.929 | 967465 | 98.803 | 156623917 | 99.291 |
| Total | | 979186 | 100.000 | 157741866 | 100.000 |

| Retention Time | Area | Area% | Retention Time | Area | Area% |
|---|---|---|---|---|---|
| 39.548 | 17225930 | 50.440 | 40.449 | 1117948 | 0.709 |
| 52.476 | 16925283 | 49.560 | 50.929 | 156623917 | 99.291 |

### 8.1.4 (3*S*,4*R*,*E*)-4-(2-((*tert*-Butyldimethylsilyl)oxy)ethyl)-1-phenyl-5-(4,4,5,5-tetramethyl-1,3,2-dioxaborolan-2-yl)hexa-1,5-dien-3-amine (9d)

The general procedure was modified: 1.2 equiv. **2a** was used (vs. 1.5 equiv.). White solid; **m.p.** 129–131 °C; **IR (neat):** 3191 (w), 2957 (m), 2928 (m), 2857 (w), 1600 (w), 1471 (w), 1384 (m), 1360 (m), 1253 (m), 1157 (s), 1098 (s), 1007 (m), 903 (w), 834 (s), 776 (s), 748 (m), 692 (m) $cm^{-1}$; **$^1$H NMR ($CDCl_3$, 400 MHz)**: δ 7.40–7.29 (m, 5H), 6.57 (d, J = 15.8 Hz, 1H), 6.18 (dd, J = 15.9, 8.4 Hz, 1H), 5.60 (s, 1H), 5.43 (s, 1H), 3.66 (ddd, J = 10.2, 8.6, 5.6 Hz, 1H), 3.58 (ddd, J = 10.1, 8.2, 6.8 Hz, 1H), 3.39 (dd, J = 9.2, 8.7 Hz, 1H), 3.22 (br s, 2H), 2.45–2.35 (m, 1H), 1.86–1.76 (m, 1H), 1.76–1.66 (m, 1H), 1.20 (s, 12H), 0.84 (s, 9H), –0.01 (s, 3H), –0.02 (s, 3H); **$^{13}$C NMR ($CDCl_3$, 100 MHz)**: δ 136.5, 133.2, 130.3, 128.7, 128.0, 126.64, 126.61, 81.1, 61.7, 59.6, 47.5, 33.6, 26.1, 25.4, 25.4, 18.5, –5.1. The signal for the carbon bearing the boron atom could not be detected due to quadrupolar effects; **$^{11}$B NMR ($CDCl_3$, 160 MHz)**: δ 15.21; **HRMS (DART)**: Calcd for $C_{26}H_{45}BNO_3Si$ $[M+H]^+$: 458.3256. Found: 458.3253; **specific rotation**: $[\alpha]_D^{20}$ –6.0 (*c* 0.40, $CHCl_3$) for an enantiomerically enriched sample of 99:1 e.r.

Enantiomeric purity was determined by HPLC analysis in comparison with an authentic racemic sampe of the derived benzyl amide; Chiralcel OD-H column, 95:5 hexanes/*i*-PrOH, 0.3 mL/min, 254 nm.

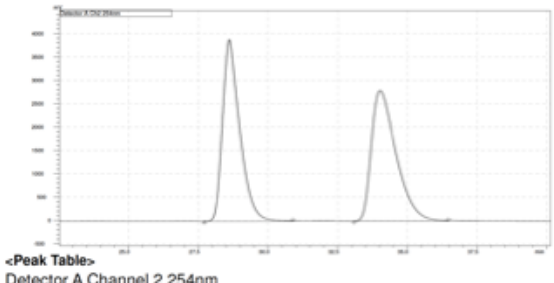

<Peak Table>
Detector A Channel 2 254nm

| Peak# | Ret. Time | Height | Height% | Area | Area% |
|---|---|---|---|---|---|
| 1 | 28.611 | 3892724 | 58.133 | 166461963 | 48.986 |
| 2 | 34.018 | 2796598 | 41.807 | 173355322 | 51.014 |
| Total | | 6689322 | 100.000 | 339817286 | 100.000 |

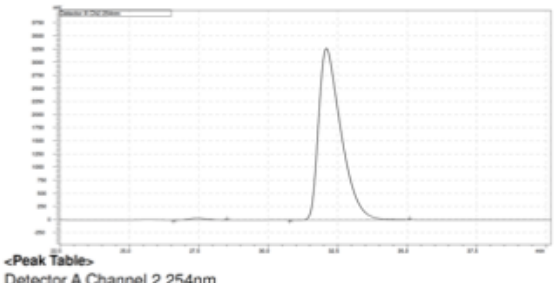

<Peak Table>
Detector A Channel 2 254nm

| Peak# | Ret. Time | Height | Height% | Area | Area% |
|---|---|---|---|---|---|
| 1 | 27.442 | 38287 | 1.156 | 1767855 | 0.955 |
| 2 | 32.094 | 3274768 | 98.844 | 183288703 | 99.045 |
| Total | | 3313055 | 100.000 | 185056558 | 100.000 |

| Retention Time | Area | Area% | Retention Time | Area | Area% |
|---|---|---|---|---|---|
| 28.611 | 166461963 | 48.986 | 27.442 | 1767855 | 0.955 |

| | | | | | |
|---|---|---|---|---|---|
| 34.018 | 173355322 | 51.014 | 32.094 | 183288703 | 99.045 |

### 8.1.5 (2*S*,3*R*)-3-(2-((*tert*-Butyldimethylsilyl)oxy)ethyl)-4-(4,4,5,5-tetramethyl-1,3,2-dioxaborolan-2-yl)pent-4-en-2-amine (9e)

The general procedure was modified: 1.2 equiv. of **2a** was used (vs. 1.5 equiv.). White solid; **m.p.** = 136 °C, decomposition; **IR (neat)**: 3208 (w), 2961 (s), 2929 (s), 2857 (m), 1603 (w), 1462 (m), 1384 (m), 1361 (m), 1255 (m), 1137 (s), 1097 (s), 1042 (m), 835 (s), 775 (m) $cm^{-1}$; **$^1$H NMR ($CDCl_3$, 500 MHz)**: δ 5.41 (t, J= 2.3 Hz, 1H), 5.26 (t, J= 2.4 Hz, 1H), 3.74–3.68 (m, 1H), 3.58 (dt, J = 10.0, 6.8 Hz, 1H), 3.25–3.17 (m, 2H), 2.87 (dq, J = 8.5, 6.4 Hz, 1H), 2.18–2.12 (m, 1H), 1.82–1.72 (m, 1H), 1.72–1.64 (m, 1H), 1.25 (d, J = 6.3 Hz, 3H), 1.18 (s, 12H), 0.88 (s, 9H), 0.03 (s, 6H); **$^{13}$C NMR ($CDCl_3$, 100 MHz)**: δ 117.4, 80.3, 61.5, 52.7, 48.9, 33.9, 26.1, 25.52, 25.49, 20.6, 18.4, −5.11, −5.13. The carbon directly attached to the boron atom could not be detected due to quadrupolar effects; **$^{11}$B NMR ($CDCl_3$, 160 MHz)**: δ 13.09; **HRMS (DART)**: Calcd for $C_{19}H_{41}BNO_3Si$ $[M+H]^+$: 370.2943. Found: 370.2930; **specific rotation**: $[\alpha]_D^{20}$ +6.6 (*c* 0.34, $CHCl_3$) for an enantiomerically enriched sample of 96:4 e.r.

Enantiomeric purity was determined by HPLC analysis in comparison with authentic racemic material of the derived benzyl amide; Chiralcel OD-H column, 98:2 hexanes/i-PrOH, 0.3 mL/min, 220 nm.

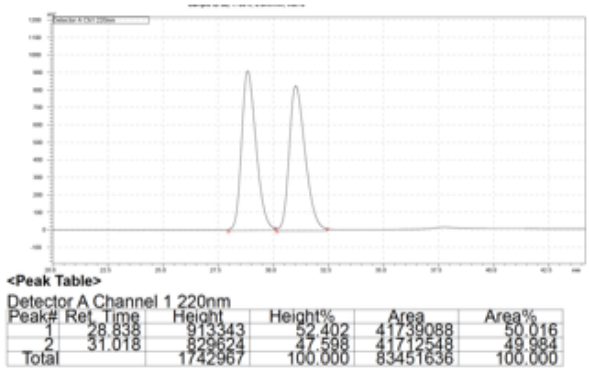


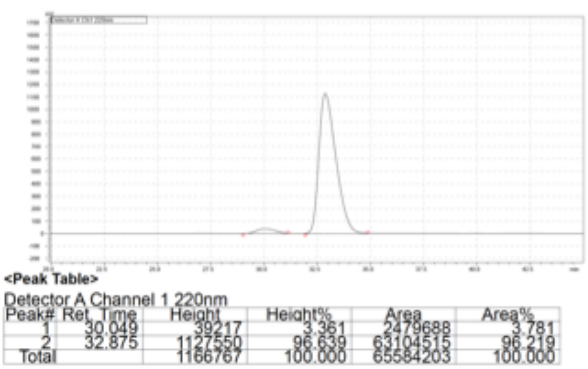


| Retention Time | Area | Area% | Retention Time | Area | Area% |
|---|---|---|---|---|---|
| 28.838 | 41739088 | 50.016 | 30.049 | 2479688 | 3.781 |
| 31.018 | 41712548 | 49.984 | 32.875 | 63104515 | 96.219 |

### 8.1.6 Methyl (4*S*,5*R*)-4-amino-5-(2-((*tert*-butyldimethylsilyl)oxy)ethyl)-6-(4,4,5,5-tetramethyl-1,3,2-dioxaborolan-2-yl)hept-6-enoate (9f)

The general procedure was modified: 1.2 equiv. of **2a** was used (vs. 1.5 equiv.). Light yellow oil; **IR (neat)**: 3048 (w), 2996 (s), 2857 (m), 1741 (s), 1683 (s), 1436 (w), 1362 (m), 1252 (m), 1158 (s), 1095 (s), 839(s), 967 (w), 775 (m) $cm^{-1}$; **$^1$H NMR ($CDCl_3$, 400 MHz)**: δ 5.49 (s, 1H), 5.31 (s, 1H), 3.74–3.64 (m, 4H), 3.56 (dt, J = 10.2, 6.7 Hz, 1H), 2.80 (td, J = 7.7, 3.9 Hz, 1H), 2.54–2.37 (m, 2H), 2.30 (dd, J = 6.4, 4.8 Hz, 1H), 2.04–1.94 (m, 1H), 1.80–1.61 (m, 3H), 1.18 (s, 12H), 0.87 (s, 9H), 0.03 (s, 6H); **$^{13}$C NMR ($CDCl_3$, 100 MHz)**: δ 174.2, 119.9, 80.8, 61.4, 56.2, 52.0, 47.6, 34.6, 31.3, 29.3, 26.1, 25.4, 25.3, 18.4, −5.14, −5.16. The carbon directly attached to the boron atom could not be detected due to quadrupolar effects; **$^{11}$B NMR ($CDCl_3$, 160 MHz)**: δ 15.22; **HRMS (DART)**: Calcd for $C_{22}H_{45}BNO_5Si$ $[M+H]^+$:

442.3155. Found: 442.3150; **specific rotation**: $[\alpha]_D^{20}$ −1.6 (*c* 0.59, $CHCl_3$) for an enantiomerically enriched sample of 98.5:1.5 e.r.

Enantiomeric purity was determined by HPLC analysis in comparison with authentic racemic material of the derived benzyl amide; Chiralcel OZ-H column, 98:2 hexanes/*i*-PrOH, 0.3 mL/min, 220 nm.

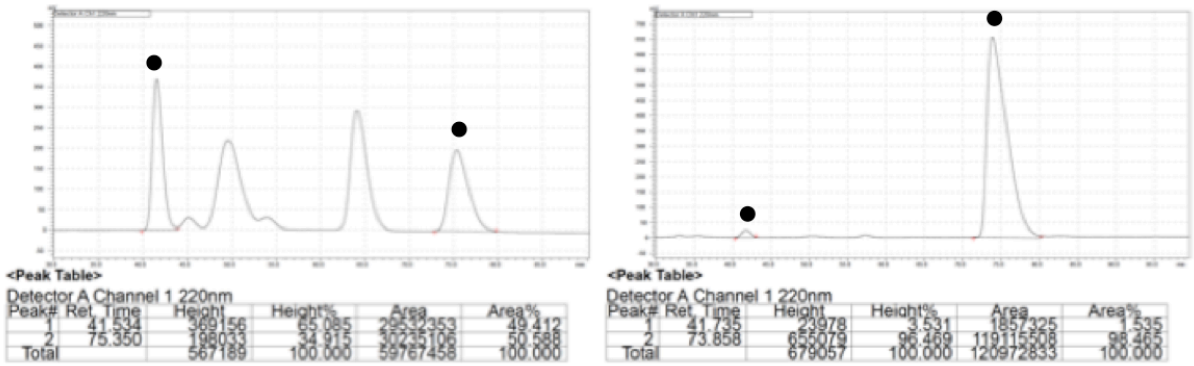


| Retention Time | Area | Area% | Retention Time | Area | Area% |
|---|---|---|---|---|---|
| 41.534 | 29532353 | 49.412 | 41.735 | 1857325 | 1.535 |
| 75.350 | 30235106 | 50.588 | 73.858 | 119115508 | 98.465 |

### 8.1.7 (1*S*,2*R*)-2-(2-((*tert*-Butyldimethylsilyl)oxy)ethyl)-1-cyclohexyl-3-(4,4,5,5-tetramethyl-1,3,2-dioxaborolan-2-yl)but-3-en-1-amine (9g)

The general procedure was modified: 1.2 equiv. of **2a** was used (vs. 1.5 equiv.). Light yellow oil; **IR (neat)**: 3206 (w), 3043 (w), 2926 (s), 2855 (m), 1597 (w), 1447 (m), 1360 (m), 1251 (m), 1157 (s), 1089 (s), 1074 (s), 1007 (m), 882 (m), 834 (s), 774 (s), 663 (w); **$^1$H NMR ($CDCl_3$, 400 MHz)**: δ 5.33 (t, *J* = 2.4 Hz, 1H), 5.20 (t, *J* = 2.5 Hz, 1H), 3.73 (dt, *J* = 10.3, 6.4 Hz, 1H), 3.62 (dt, *J* = 10.3, 6.6 Hz, 1H), 3.27 (br s, 2H), 2.63 (dd, *J* = 7.6, 5.5 Hz, 1H), 2.54–2.46 (m, 1H), 1.86–1.58 (m, 9H), 1.35–1.21 (m, 2H), 1.16 (s, 12H), 1.15–1.07 (m, 1H), 1.05–0.97 (m, 1H), 0.88 (s, 9H), 0.04 (s, 6H); **$^{13}$C NMR ($CDCl_3$, 100 MHz)**: δ 115.3, 79.9, 62.2, 61.2, 43.5, 38.1, 35.2, 31.1, 27.0, 26.5, 26.2, 26.1, 25.9, 25.7, 25.5, 18.4, −5.12, −5.14. The peak for the carbon bearing the boron atom could not be detected due to quadrupolar effects; **$^{11}$B NMR ($CDCl_3$, 160 MHz)**: δ 10.28; **HRMS (DART)**: Calcd for $C_{24}H_{49}BNO_3Si$ $[M+H]^+$: 438.3569. Found: 438.3570; **specific rotation**: $[\alpha]_D^{20}$ +1.5 (*c* 0.59, $CHCl_3$) for an enantiomerically enriched sample of 98.5:1.5 e.r.

Enantiomeric purity was determined by HPLC analysis in comparison with authentic racemic material of the derived benzyl amide; Chiralcel AZ-H column, 95:5 hexanes/*i*-PrOH, 0.3 mL/min, 254 nm.

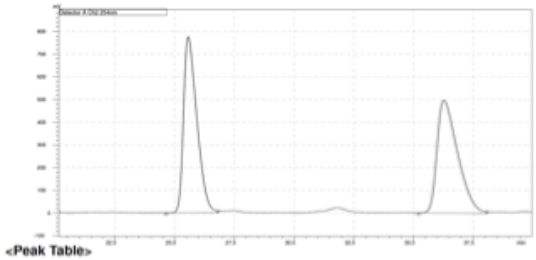


| Retention Time | Area | Area% | Retention Time | Area | Area% |
|---|---|---|---|---|---|
| 25.566 | 30109652 | 50.305 | 25.337 | 22153616 | 98.511 |
| 36.280 | 29744089 | 49.695 | 36.368 | 334859 | 1.489 |

### 8.1.8 (1*S*,2*R*)-1-Cyclohexyl-2-methyl-3-(4,4,5,5-tetramethyl-1,3,2-dioxaborolan-2-yl)but-3-en-1-amine (9h)

White solid; **m.p.** = 139–142 °C; **IR (neat)**: 3025 (w), 2958 (s), 2853 (m), 1597 (w), 1447 (m), 1313 (m), 1247 (m), 1159 (s), 1119 (s), 1048 (m), 894 (s), 795 (m), 734 (m) $cm^{-1}$; **$^{1}$H NMR ($CDCl_3$, 400 MHz)**: δ 5.26 (s, 1H), 5.15 (s, 1H), 3.37 (br s, 2H), 2.40 (s, 2H), 1.82 (t, *J* = 14.7 Hz, 2H), 1.72 (d, *J* = 12.6 Hz, 2H), 1.69–1.59 (m, 2H), 1.37–1.24 (m, 2H), 1.17 (d, *J* = 3.1 Hz, 12H), 1.15–1.03 (m, 2H), 0.99 (d, *J* = 4.7 Hz, 3H), 0.90 (qd, *J* = 12.5, 3.7 Hz, 1H); **$^{13}$C NMR (100 MHz, $CDCl_3$)** δ 158.8, 113.2, 79.8, 64.2, 40.0, 38.0, 31.6, 26.6, 26.5, 26.2, 25.7, 25.5, 14.7; **$^{11}$B NMR ($CDCl_3$, 160 MHz)**: δ 9.64; **HRMS (DART)**: Calcd for $C_{17}H_{33}BNO_2$ $[M+H]^+$: 294.2599. Found: 294.2601; **specific rotation**: $[\alpha]_D^{20}$ +11.5 (*c* 0.51, $CHCl_3$) for an enantiomerically enriched sample of 96:4 e.r.

Enantiomeric purity was determined by HPLC analysis in comparison with authentic racemic material of the derived benzyl amide; Chiralcel OZ-H column, 95:5 hexanes/*i*-PrOH, 0.3 mL/min, 220 nm.

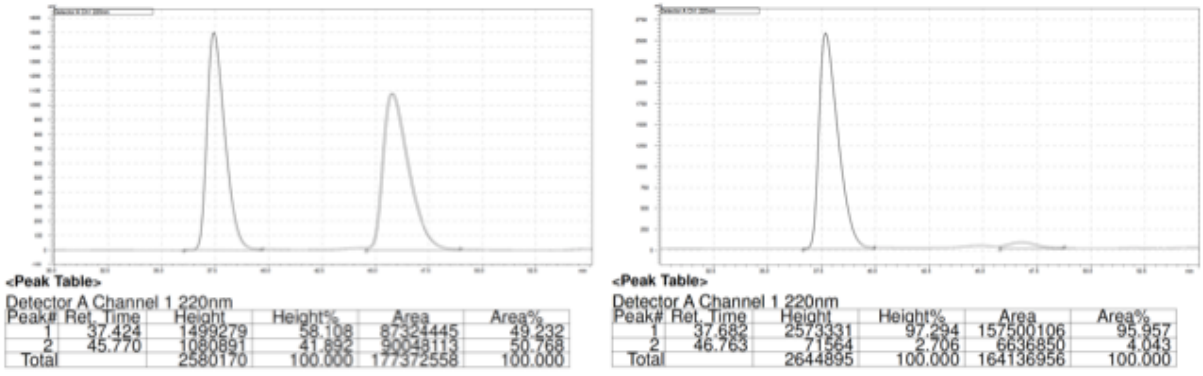


| Retention Time | Area | Area% | Retention Time | Area | Area% |
|---|---|---|---|---|---|
| 37.424 | 87324445 | 49.232 | 37.682 | 157500106 | 95.957 |
| 45.770 | 90048113 | 50.768 | 46.763 | 6636850 | 4.043 |

# 9 Determination of Absolute Configuration

The absolute configuration of is assigned based on the X-ray structure of the benzyl amide derivative of (2*S*,3*R*)-**9e**, prepared by the use of (*R*)-(–)-1-[(*S*)-2-(dicyclohexylphosphino)ferrocenyl]ethyldi-*t*-butylphosphine **((*R*)-phos-3)**. Single crystals were obtained by slow evaporation of a hexanes solution.

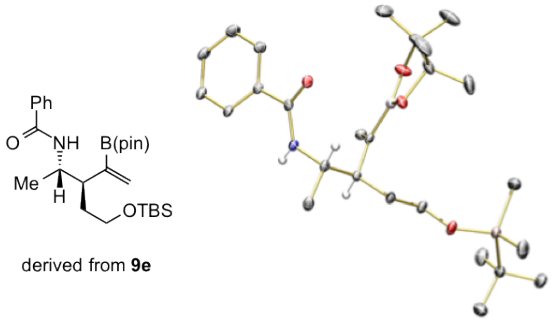


# 10 Gram-Scale Synthesis of (+)-Tangutorine

## 10.1.1 2-Iodoprop-2-en-1-ol (S4)(*54*)

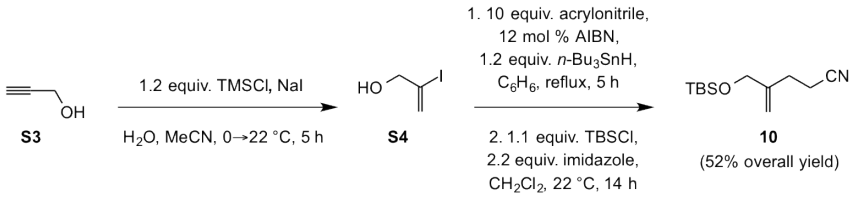


A solution of NaI (3.60 g, 24.0 mmol) in MeCN (40 mL) was allowed to cool to 0 °C and was then charged with TMSCl (3.05 mL, 24.0 mmol). The mixture was allowed to stir for 15 min at 0 °C, after which $H_2O$ (216 µL, 12.0 mmol) was added, immediately followed by propargyl alcohol **S3** (1.16 mL, 20.0 mmol). The solution was allowed to stir at 22 °C for 5 h, and then the reaction was quenched by the addition of a saturated solution of aqueous $NaHCO_3$ (100 mL). The mixture was washed with $Et_2O$ (3 × 80 mL). The combined organic layers were washed with a saturated solution of aqueous $Na_2S_2O_3$ (2 × 150 mL) and dried over $MgSO_4$. Removal of the solids through filtration and then the volatiles in vacuo afforded dark oil, which was purified by silica gel chromatography (pentane:$Et_2O$ = 9:1 → 4:1; $R_f$ = 0.25 (pentane:$Et_2O$ = 4:1)) to furnish 2-iodoprop-2-en-1-ol (**S4**) as colorless oil (2.65 g, 14.4 mmol, 72% yield). Colorless oil; **IR (neat)**: 3323 (m), 1627 (m), 1443 (w), 1398 (w), 1145 (w), 1032 (s), 900 (m) $cm^{-1}$; **$^1$H NMR ($CDCl_3$, 400 MHz)**: δ 6.39 (1H, q, *J* = 1.4 Hz), 5.87 (1H, q, *J* = 1.4 Hz, 1H), 4.18 (2H, t, *J* = 1.4 Hz), 2.03 (1H, bs); **$^{13}$C NMR ($CDCl_3$, 100 MHz)**: δ 124.6, 110.6, 71.2; **HRMS (DART)**: Calcd for $C_3H_6OI$ $[M+H]^+$: 184.9458. Found: 184.9459.

## 10.1.2 4-(((*tert*-Butyldimethylsilyl)oxy)methyl)pent-4-enenitrile (10)

A solution of **S4** (2.65 g, 14.4 mmol) and acrylonitrile (9.43 mL, 144 mmol) in benzene (72 mL) was allowed to reach gentle reflux. This solution was charged, in eight portions at interval, of 40 min, with a solution of *n*-$Bu_3SnH$ (4.60 mL, 17.3 mmol) and AIBN (284 mg, 1.73 mmol) in benzene (30 mL, 0.5 M with respect to the *n*-$Bu_3SnH$). The mixture was then allowed to stir at reflux for an additional 2 h, after which it was allowed to cool to 22 °C and

concentrated in vacuo. The resulting brown oil was dissolved with $Et_2O$ (100 mL) and $H_2O$ (200 mL), and was subsequently treated with KF (10.0 g, 172 mmol). The mixture was allowed to stir vigorously at 22 °C for 2 h, and was then washed with $Et_2O$ (3 × 80 mL). The combined organic layers were dried over $Na_2SO_4$, filtered and the volatiles were removed in vacuo to afford yellow oil, which was purified by silica gel chromatography (hexanes:EtOAc = 3:1→3:2; $R_f$ = 0.10 (hexanes:EtOAc = 3:1)) to afford the expected hydroxy-nitrile intermediate(*55,56*) as colorless oil (1.20 g, 10.8 mmol, 75% yield). Colorless oil; **IR (neat)**: 3416 (m), 2927 (m), 2858 (w), 2245 (w), 1636 (w), 1429 (m), 1065 (m), 1021 (s), 910 (m) $cm^{-1}$; **$^1$H NMR ($CDCl_3$, 400 MHz)**: δ 5.19 (1H, dt, J = 1.6, 0.8 Hz), 5.01 (1H, dt, J = 2.0, 0.8 Hz), 4.13 (2H, s), 2.59–2.52 (2H, m), 2.45 (2H, t, J = 7.3 Hz), 1.64 (1H, s); **$^{13}$C NMR ($CDCl_3$, 100 MHz)**: δ 145.0, 119.4, 113.0, 65.8, 28.7, 16.3; **HRMS (DART)**: Calcd for $C_6H_{10}NO$ $[M+H]^+$: 112.0757. Found: 112.0751.

The abovementioned primary alcohol (1.20 g, 10.8 mmol) was dissolved in $CH_2Cl_2$ (60 mL) and the solution was charged with imidazole (16.2 g, 23.8 mmol) and TBSCl (1.79 g, 11.9 mmol) at 22 °C. The mixture was allowed to stir for 14 h, after which the reaction was quenched by the addition of a saturated solution of aqueous $NaHCO_3$ (100 mL). The mixture was washed with $Et_2O$ (3 × 100 mL) and the combined organic layers were washed with an aqueous solution of 0.5 M HCl (100 mL) and then 10% aqueous $CuSO_4$ (100 mL). The organic layers were dried over $MgSO_4$, solids were removed by filtration and the volatiles were removed in vacuo. Purification of the resulting pale yellow oil by silica gel chromatography (hexanes:$Et_2O$ = 40:1→20:1; $R_f$ = 0.08 (hexanes:$Et_2O$ = 40:1) afforded nitrile **10** as colorless oil (2.36 g, 10.5 mmol, 97% yield). Colorless oil; **IR (neat)**: 2930 (m), 2857 (m), 2246 (w), 1738 (w), 1472 (w), 1265 (m), 1112 (m), 1084 (m), 838 (s), 777 (m) $cm^{-1}$; **$^1$H NMR ($CDCl_3$, 400 MHz)**: δ 5.14 (1H, s,), 5.01 (1H, d, J = 0.9 Hz), 4.11 (2H, s), 2.53 (2H, td, J = 7.4, 1.0 Hz), 2.40 (2H, t, *J* = 7.4 Hz), 0.90 (9H, s), 0.07 (6H, s); **$^{13}$C NMR ($CDCl_3$, 101 MHz)**: δ 145.0, 119.5, 111.9, 66.0, 28.7, 26.0, 18.4, 16.3, –5.3; **HRMS (DART)**: Calcd for $C_{12}H_{24}NOSi$ $[M+H]^+$: 226.1622. Found: 226.1631.

### 10.1.3 *tert*-Butyl hexa-4,5-dienoate (11)

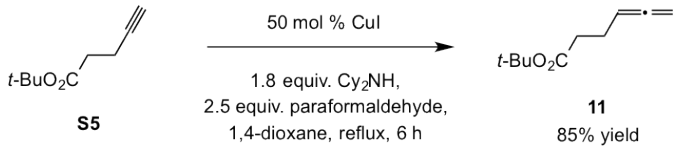


A solution was first prepared that consisted of *tert*-butyl pent-4-ynoate[57] **S5** (5.30 g, 34.4 mmol), CuI (3.28 g, 17.2 mmol) and paraformaldehyde (2.58 g, 86.0 mmol) in 1,4-dioxane (50 mL). This solution was charged (at 22 °C) with $Cy_2NH$ (12.3 mL, 61.9 mmol), and the mixture was allowed to stir for 3 h at reflux, after which it was allowed to cool to 22 °C. Solids were removed by filtration through a short pad of silica ($Et_2O$ was used for washing). The filtrate was diluted with $Et_2O$ (100 mL) and poured into aqueous solution of 1.0 M HCl (200 mL). The phases were separated and the aqueous layer was washed with $Et_2O$ (3 × 50 mL). The combined organic layers were washed with a saturated solution of aqueous $NaHCO_3$ (100 mL), dried over $MgSO_4$, filtered and concentrated under reduced pressure. Purification of the resulting brown oil by silica gel chromatography (hexanes:$Et_2O$ = 20:1; $R_f$ = 0.28 (hexanes:$Et_2O$ = 20:1)) delivered allene **11** as colorless oil (4.92 g, 29.2 mmol, 85%

yield). Colorless oil; **IR (neat)**: 2976 (w), 2928 (w), 1955 (w), 1726 (s), 1454 (m), 1255 (m), 1145 (s), 845 (m) $cm^{-1}$; **$^1$H NMR ($CDCl_3$, 400 MHz)**: δ 5.16 (1H, p, *J* = 6.5 Hz), 4.70 (2H, dt, *J* = 6.5, 3.4 Hz), 2.39–2.30 (2H, m), 2.33–2.21 (2H, m), 1.45 (9H, s); **$^{13}$C NMR ($CDCl_3$, 150 MHz)**: δ 208.5, 172.5, 89.1, 80.4, 75.9, 34.8, 28.3, 28.2, 23.6; **HRMS (DART)**: Calcd for $C_{10}H_{17}O_2$ $[M+H]^+$: 169.1223. Found: 169.1219.

### 10.1.4 *tert*-Butyl (4*R*,5*R*)-5-amino-8-(((*tert*-butyldimethylsilyl)oxy)methyl)-4-(1-(4,4,5,5-tetramethyl-1,3,2-dioxaborolan-2-yl)vinyl)non-8-enoate (12)

In a glove box, an oven-dried 250 mL round-bottom flask containing a magnetic stir bar was charged with **phos-3** (78.1 mg, 0.141 mmol), CuMes (23.4 mg, 0.128 mmol) and thf (10 mL). The solution was allowed to stir at 22 °C for 10 min, after which *i*-PrOH (1.22 mL, 16.0 mmol) was added and the mixture was allowed to stir for 10 min. At this point, NaOMe (17.3 mg, 0.320 mmol) was added and the vial removed from the glove box. In parallel, a solution of $B_2(pin)_2$ (1.95 g, 7.68 mmol), nitrile **10** (1.44 g, 6.40 mmol), allene **11** (1.29 g, 7.68 mmol), and PMHS (1.92 mL, 32.0 mmol) in thf (20 mL) was prepared. The two solutions were removed from the glove box and allowed to cool to –5 °C, after which they were mixed and the resulting solution was allowed to stir for 16 h (at –5 °C). The reaction was then quenched by the addition of a saturated solution of aqueous $NaHCO_3$ (200 mL). The aqueous layer was separated and washed with $CH_2Cl_2$ (3 × 200 mL). The combined organic layers were dried over $Na_2SO_4$, filtered and concentrated under reduced pressure. Purification of the resulting yellow oil by silica gel chromatography ($CH_2Cl_2$:MeOH = 80:1→20:1; $R_f$ = 0.48 ($CH_2Cl_2$:MeOH = 8:1)). NOTE: The silica gel must be conditioned with 2% v/v solution of formic acid in $CH_2Cl_2$ (300 mL). To remove the formic acid, the samples containing the desired product (judged by tlc analysis) were collected and allowed to stir over $K_2CO_3$ (32 g) for 15 min. The suspension was filtered through a short plug of sand and the volatiles were removed in vacuo to afford yellow oil and white solid. Diethyl ether (5 mL) was added and the suspension was allowed to pass through a pad of celite. Evaporation of the volatiles afforded **12** as colorless oil (2.68 g, 5.12 mmol, 80% yield, d.r. >98:2, e.r. = 95:5). Colorless oil; **IR (neat)**: 3211 (w), 3037 (w), 2954 (m), 2927 (m), 2855 (w), 1725 (m), 1460 (w), 1364 (m), 1251 (m), 1149 (s), 1109 (s), 1005 (m), 964 (m), 903 (m), 834 (s), 774 (s), 732 (m) $cm^{-1}$; **$^1$H NMR ($CDCl_3$, 400 MHz)**: δ 5.49 (1H, s), 5.28 (1H, s), 5.04 (1H, d, *J* = 1.6 Hz), 4.83 (1H, d, *J* = 1.6 Hz), 4.06 (2H, s), 2.96 (1H, dt, *J* = 9.4, 5.3 Hz), 2.85 (2H, bs), 2.33–2.18 (2H, m), 2.19–1.99 (3H, m), 1.79–1.52 (3H, m), 1.54–1.44 (1H, m), 1.42 (9H, s), 1.16 (12H, s), 0.89 (9H, s), 0.05 (6H, s); **$^{13}$C NMR ($CDCl_3$, 100 MHz)**: δ 173.3, 148.0, 120.9, 109.6, 80.9, 80.1, 65.9, 55.4, 49.4, 33.4, 29.8, 28.3, 26.0, 25.4, 25.2, 22.6, 18.5, –5.2, –5.2; **$^{11}$B NMR ($CDCl_3$, 160 MHz)**: δ 16.0; **HRMS (DART)**: Calcd for $C_{28}H_{55}BNO_5Si$ $[M+H]^+$: 524.3937. Found: 524.3936; **specific rotation:** $[\alpha]_D^{20}$ = +1.8 (*c* 2.4, $CHCl_3$) for an enantiomerically enriched sample of 95:5 e.r.

Enantiomeric purity was determined by HPLC analysis of the *N*-benzoylated product in comparison with authentic racemic material; Chiralcel OZ-H column, hexanes:*i*-PrOH = 98:2, 0.3 mL/min, 220 nm.

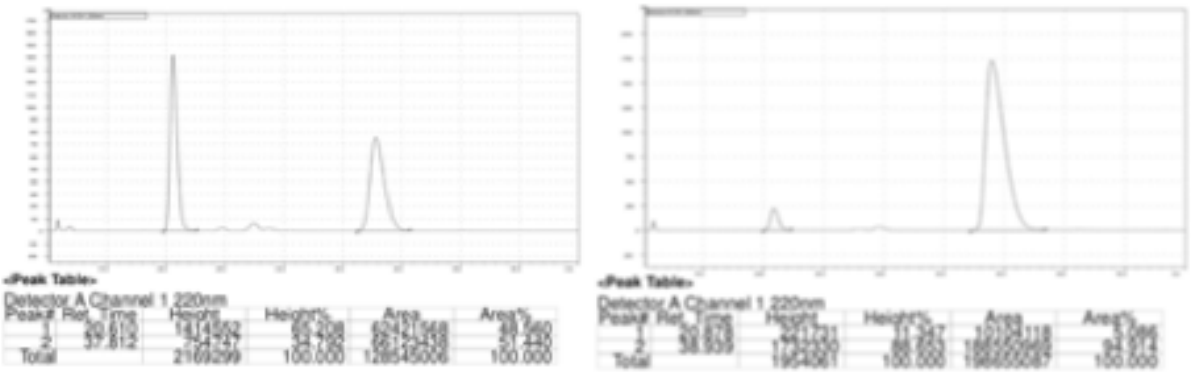

| Retention Time | Area | Area% | Retention Time | Area | Area% |
|---|---|---|---|---|---|
| 20.610 | 62421568 | 48.560 | 20.878 | 10104118 | 5.086 |
| 37.812 | 66123438 | 51.440 | 38.939 | 188550969 | 94.914 |

### 10.1.5 2-(1*H*-Indol-3-yl)acetaldehyde (14)(*58*)

Tryptophol (2.42 g, 15.0 mmol) was dissolved in dimethylsulfoxide (60 mL) and the resulting solution was treated with freshly prepared IBX (4.62 g, 16.5 mmol) at 22 °C. The mixture was allowed to stir for 2 h at 22 °C, after which it was diluted with water (250 mL). The solids were then removed by filtration, and the filtrate was washed with $Et_2O$ (3 x 100 mL). The combined organic layers were dried over $Na_2SO_4$, filtered, and concentrated under reduced pressure to provide 2-(1*H*-indol-3-yl)acetaldehyde **14** (1.74 g, 10.9 mmol, 73% yield) as yellow oil. NOTE: The aldehyde decomposes rapidly and must be used immediately.

### 10.1.6 (5*R*,6*R*)-1-(2-(1*H*-Indol-3-yl)ethyl)-6-(3-(((*tert*-butyldimethylsilyl)oxy) methyl)but-3-en-1-yl)-5-vinylpiperidin-2-one (15)

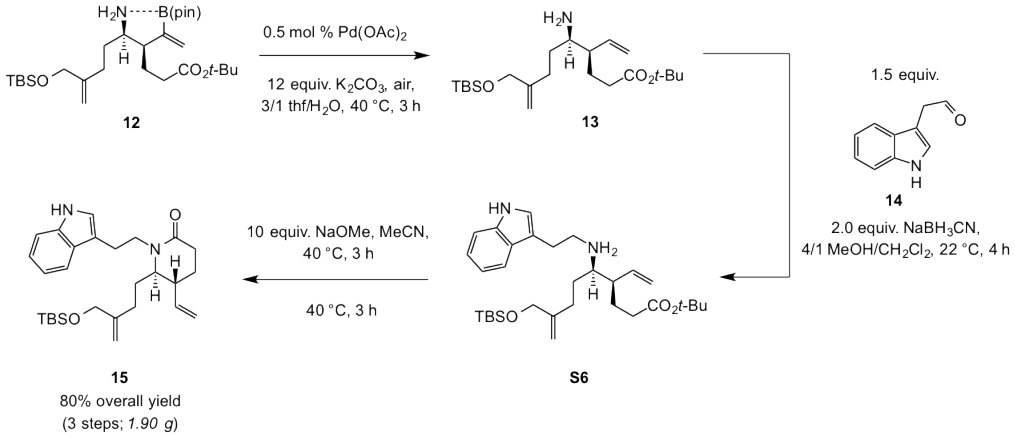


To a solution of amine **12** (2.68 g, 5.12 mmol) and $Pd(OAc)_2$ (5.70 mg, 25.6 μmol) in thf (30.7 mL) at 22 °C was added a 6 M solution of aqueous $K_2CO_3$ (10.2 mL, 61.4 mmol). A balloon filled with air was attached to the vessel after which the mixture was allowed to warm to 40 °C and was kept at this temperature for 3 h, after which it was allowed to cool to 22 °C. The mixture was then diluted with $H_2O$ (30 mL) and washed with $CH_2Cl_2$ (3 × 100 mL). The combined organic layers were dried over $Na_2SO_4$, filtered and concentrated under reduced pressure, affording amine **13** as yellow oil, which was used directly without

purification. NOTE: The amine must be used immediately as it has strong tendency to be converted to the corresponding lactam.

Amine **13** was dissolved in MeOH (10 mL) and 2-(1*H*-indol-3-yl)acetaldehyde **14** (815 mg, 5.12 mmol) was dissolved in $CH_2Cl_2$ (1.5 mL). These two solutions were mixed (at 22 °C) and after 10 min, the mixture was charged with $NaCNBH_3$ (643 mg, 10.2 mmol) and allowed to stir for 2 h. At this point, a second portion of **14** (408 mg, 2.56 mmol), dissolved in $CH_2Cl_2$ (1.0 mL), was added. The mixture was allowed to stir for 1 h and the volatiles were removed in vacuo. The resulting yellow oil was dissolved in $CH_2Cl_2$ (5 mL) and filtered through a short pad of celite ($CH_2Cl_2$ was used for washing). The filtrate was concentrated in vacuo to afford amine **S6**, which was used directly without further purification.

Amine **S6** was dissolved in MeCN (100 mL) at 22 °C, and the resulting solution was charged with NaOMe (2.77 g, 51.2 mmol). The mixture was allowed to warm to 40 °C. After 3 h, the solution was allowed to cool to 22 °C and the solution pH was adjusted to 7 by the addition of appropriate amounts of a saturated solution of aqueous $NH_4Cl$. Removal of the volatiles left behind brown oil, which was dissolved in $CH_2Cl_2$ (25 mL) and the mixture was treated with a saturated solution of aqueous $NH_4Cl$ (25 mL). After the phases were separated, the aqueous phase was washed with $CH_2Cl_2$ (2 × 20 mL), and the combined organic layers were dried over $Na_2SO_4$, filtered and the volatiles were removed in vacuo to afford orange oil. Purification by silica gel chromatography (100% $CH_2Cl_2$ to $CH_2Cl_2$:MeOH = 100:1; $R_f$ = 0.54 ($CH_2Cl_2$:MeOH = 10:1)) afforded lactam **15** as yellow oil (1.91 g, 4.10 mmol, 80% overall yield). Yellow oil; **IR (neat)**: 3413 (w), 3280 (w), 2949 (m), 2925 (s), 2852 (m), 1617 (s), 1470 (m), 1357 (w), 1252 (m), 1101 (m), 1008 (w), 836 (s), 776 (m), 739 (s) $cm^{-1}$; **$^1$H NMR ($CDCl_3$, 400 MHz)**: δ 8.03 (1H, bs), 7.69 (1H, d, *J* = 8.0 Hz), 7.36 (1H, d, *J* = 8.0 Hz), 7.19 (1H, ddd, *J* = 8.0, 7.1, 0.9 Hz), 7.12 (1H, ddd, *J* = 8.0, 7.1, 1.1 Hz), 7.04 (1H, d, *J* = 2.3 Hz), 5.67 (1H, ddd, *J* = 17.4, 10.4, 7.3 Hz), 5.15–5.01 (2H, m), 5.04 (1H, bs), 4.80 (1H, d, *J* = 1.4 Hz), 4.27–4.14 (1H, m), 4.05 (2H, s), 3.19 (1H, dt, *J* = 7.9, 3.6 Hz), 3.12–2.98 (3H, m), 2.54–2.41 (2H, m), 2.34 (1H, dt, *J* = 17.8, 6.0 Hz), 2.09–1.88 (3H, m), 1.83 (1H, tdt, *J* = 9.5, 6.4, 3.3 Hz), 1.74 (1H, tt, *J* = 9.5, 4.8 Hz), 1.65 (1H, dt, *J* = 13.4, 6.4 Hz), 0.90 (9H, s), 0.05 (6H, s); **$^{13}$C NMR ($CDCl_3$, 100 MHz)**: δ 170.2, 147.6, 139.4, 136.4, 127.7, 122.2, 122.1, 119.5, 119.1, 116.0, 113.4, 111.2, 109.5, 66.1, 61.5, 46.7, 39.2, 30.9, 29.3, 28.6, 26.0, 26.0, 23.35, 22.9, 18.5, –5.2; **HRMS (DART)**: Calcd for $C_{28}H_{43}N_2O_2Si$ $[M+H]^+$: 467.3088. Found: 467.3065; **specific rotation**: $[\alpha]_D^{20}$ +4.2 (*c* 1.0, $CHCl_3$).

### 10.1.7 (4a*R*,8a*R*)-1-(2-(1*H*-Indol-3-yl)ethyl)-6-(((*tert*-butyldimethylsilyl)oxy) methyl)-3,4,4a,7,8,8a-hexahydroquinolin-2(1*H*)-one (16)

To a solution of diene **15** (1.90 g, 4.07 mmol) in toluene (4.1 mL) at 22 °C was added (pin)BH (26 μL, 204 μmol). After gas evolution ceased, the solution was diluted with toluene (16.3 mL) and Mo complex **Mo-1** (156 mg, 204 μmol) was added. The mixture was heated to 80 °C and allowed to stir at this temperature for 1 h; it was then allowed to cool to 22 °C and the volatiles were removed in vacuo to afford brown solid. Purification by silica gel chromatography (100% $CH_2Cl_2$ to $CH_2Cl_2$:MeOH = 40:1, $R_f$ = 0.42 ($CH_2Cl_2$:MeOH = 10:1)) delivered lactam **16** as colorless solid (1.62 g, 3.70 mmol, 91% yield). NOTE: Pre-treatment of **15** with (pin)BH is necessary for high efficiency (to remove residual water). Colorless

solid; **$^1$H NMR ($CDCl_3$, 400 MHz)**: δ 8.23 (1H, bs), 7.71 (1H, d, *J* = 7.6 Hz), 7.35 (1H, d, *J* = 7.6 Hz), 7.18 (1H, t, *J* = 7.6 Hz), 7.13 (1H, t, *J* = 7.6 Hz), 7.04 (1H, s), 5.43 (1H, s), 4.02 (2H, s), 3.89 (1H, ddd, *J* = 15.6, 10.8, 5.5 Hz), 3.69 (1H, ddd, *J* = 13.5, 10.5, 5.5 Hz), 3.17–3.02 (2H, m), 2.86 (1H, ddd, *J* = 14.7, 10.3, 5.5 Hz), 2.66–2.47 (2H, m), 2.44–2.34 (1H, m), 2.30–2.15 (2H, m), 2.10–1.94 (1H, m), 1.86 (1H, ddt, *J* = 12.4, 6.1, 2.8 Hz), 1.63–1.40 (2H, m), 0.92 (9H, s), 0.07 (6H, s); **$^{13}$C NMR ($CDCl_3$, 101 MHz)**: δ 171.2, 137.5, 136.4, 127.7, 123.1, 122.1, 122.0, 119.4, 119.1, 113.6, 111.3, 66.3, 59.8, 43.2, 39.5, 33.2, 27.5, 27.3, 26.1, 25.8, 24.4, 18.6, –5.13; IR (neat): 3251 (w), 2951 (m), 2925 (s), 2852 (m), 1616 (s), 1458 (m), 1342 (w), 1257 (s), 1096 (m), 1010 (w), 836 (s), 776 (m), 739 (s) $cm^{-1}$; **HRMS (DART)**: Calcd for $C_{26}H_{39}N_2O_2Si$ $[M+H]^+$: 439.2775. Found: 439.2775; **specific rotation**: $[\alpha]_D^{20}$ +4.8 (*c* 1.0, $CHCl_3$).

### 10.1.8 (+)-Tangutorine

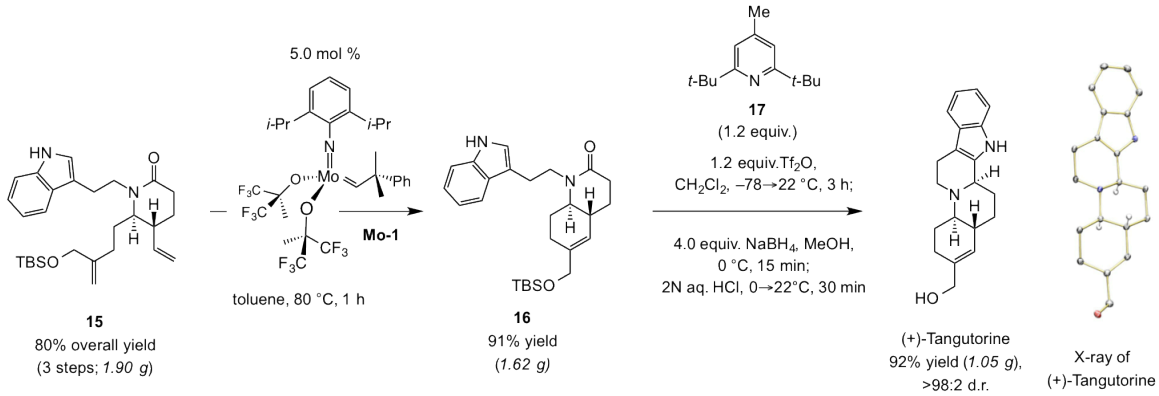


A solution of lactam **16** (1.62 g, 3.70 mmol) and 2,6-di-*tert*-butyl-4-methylpyridine (913 mg, 4.44 mmol) in $CH_2Cl_2$ (80 mL) was allowed to cool to –78 °C and then it was treated with $Tf_2O$ (746 μL, 4.44 mmol). The mixture was allowed to slowly warm to 22 °C over the course of 2.5 h and stir for an additional 30 min at 22 °C (solution color changed from yellow to dark red). The mixture was then cooled to 0 °C and charged with a solution of $NaBH_4$ (560 mg, 14.8 mmol) in MeOH (30 mL); the resulting solution was allowed to stir for 15 min at 0 °C, after which an aqueous solution of 2 M HCl (120 mL) was added and the mixture was allowed to stir vigorously for 30 min at 22 °C. The solution pH was adjusted to 8-9 by addition of appropriate amounts of an aqueous solution of 1M NaOH. After dilution with $CHCl_3$ (60 mL), the two phases were separated and the aqueous layer was washed with $CHCl_3$ (4 × 50 mL). The combined organic layers were dried over $Na_2SO_4$, filtered and concentrated under reduced pressure to afford a yellow solid. Purification by silica gel chromatography ($CHCl_3$:MeOH = 20:1→9:1; $R_f$ = 0.10 ($CHCl_3$:MeOH = 9:1)) delivered (+)-tangutorine as colorless solid (1.05 g, 3.40 mmol, 92% yield). Colorless solid; **IR (neat)**: 3203 (w), 2920 (s), 2846 (s), 1452 (m), 1376 (w), 1260 (m), 1100 (m), 1068 (s), 1030 (m), 796 (s), 737 (s) $cm^{-1}$; **$^1$H NMR (dmso-$d_6$, 500 MHz)**: δ 10.66 (1H, s), 7.35 (1H, d, *J* = 7.6 Hz), 7.28 (1H, d, *J* = 7.6 Hz), 7.01 (1H, t, *J* = 7.6 Hz), 6.93 (1H, t, *J* = 7.6 Hz), 5.31 (1H, s), 4.68 (1H, t, *J* = 5.5 Hz), 3.81 (2H, bs), 3.52 (1H, bd, *J* = 11.1 Hz), 3.40–3.31 (1H, m), 2.75–2.61 (2H, m), 2.36–2.20 (3H, m), 2.17–1.99 (4H, m), 1.87 (1H, d, *J* = 11.7 Hz), 1.53 (1H, q, *J* = 11.5 Hz), 1.37 (1H, qd, *J* = 11.5, 5.8 Hz), 1.26 (1H, qd, *J* = 12.6, 3.7 Hz); **$^1$H NMR ($CDCl_3$:$CD_3OD$ = 95:5, 400 MHz)**: δ 7.43 (1H, d, J = 7.3 Hz), 7.27 (1H, d, J = 7.3 Hz), 7.08

(1H, t, *J* = 7.3 Hz), 7.03 (1H, t, *J* = 7.2 Hz), 5.33 (1H, bs), 3.96 (1H, d, AB, *J* = 14.4 Hz), 3.93 (1H, d, AB, *J* = 14.4 Hz), 3.63–3.52 (1H, m), 3.50 (1H, bd, *J* = 10.7 Hz), 2.97–2.83 (1H, m), 2.78 (1H, bd, *J* = 14.9 Hz), 2.47–2.34 (1H, m), 2.35–2.25 (1H, m), 2.28–2.06 (5H, m), 1.89 (1H, bd, *J* = 12.2 Hz), 1.74 (1H, ddt, *J* = 12.2, 12.2, 3.0 Hz), 1.59–1.48 (1H, m), 1.38–1.26 (1H, m); **$^{13}$C NMR (dmso-$d_6$, 126 MHz)**: δ 137.2, 136.4, 136.0, 126.5, 123.9, 120.2, 118.2, 117.4, 110.9, 106.3, 64.8, 64.3, 60.5, 45.1, 31.0, 29.6, 25.8, 21.9; **$^{13}$C NMR ($CDCl_3$:$CD_3OD$ = 95:5, 101 MHz)**: δ 137.0, 136.3, 134.1, 126.8, 125.1, 121.5, 119.3, 118.1, 111.1, 107.1, 66.00, 65.4, 60.7, 44.9, 38.3, 30.6, 29.1, 26.1, 25.6, 21.4; **HRMS (DART)**: Calcd for $C_{20}H_{25}N_2O$ $[M+H]^+$: 309.1961. Found: 309.1962; **specific rotation**: $[\alpha]_D^{20}$ +98.6 (*c* 1.0, dmf).

Crystals suitable for X-ray crystallography were obtained by slowly cooling a concentrated boiling solution of (+)-tangutorine in a 9:1 mixture of $CHCl_3$:$CH_3OH$.

## 11 Density Functional Theory (DFT) Studies

DFT computations(*59,60,61,62,63,64,65,66,67,68*) were performed with the Gaussian 09/Gaussian 16 suite of programs (*69*). Geometries were optimized with the M06–L (*70*) functional and the Def2SVP basis set (*71*) in conjunction with the corresponding Coulomb fitting basis set to speed up calculations (*72*). The effect of a polar reaction medium (thf) was approximated by means of the SMD solvation model (*73*). Stationary points were probed through vibrational analysis and Gibbs free energy corrections were performed under standard conditions (298.15 K, 1.0 atm). Transition states have been verified through Intrinsic Reaction Coordinate (IRC) calculations through the use of the L(ocal) Q(uadratic) A(approximation) method (*74,75*) followed by optimization of the end points with the abovementioned optimization method. Furthermore, we probed the performance of various density functionals through single point energy calculations at the geometries optimized with the level described above by means of the SMD solvation model with thf as solvent and the larger def2-TZVPP71 basis set. Because the correct density functional is unknown, we tested several state of the art approaches (all of which account for dispersion (*76,77,78,79,80,81,82*)) that have been developed over the past decade (*59–68,83,84,85,86*): M06–L (Figs S23-1, S23-2, S24-1 and S24-2) (*70*) M06 (Figs S25-1 and S25-2),70 MN15 (Figs S26-1 and S26-2) (*66*) and ωB97XD (Figs S27-1 and S27-2) (*66*). Several conformers, generated by rotation around P–Cy bonds (see the coordinates.xyz" file), were investigated, and only the most stable of these are shown in Figs S23–S27. Every functional provided qualitatively similar results and we chose to report the MN15/Def2TZVPP$_{thf(SMD)}$//M06L/DF-Def2SVP$_{thf(SMD)}$ energies in the following section (Figs S26-1 and S26-2). A .xyz file for convenient viewing of computed geometries with the program Mercury 3.3 is appended as separate "coordinates.xyz" file (*87*).

### 11.1 Nomenclature of investigated transition states for Cu–allyl addition to nitriles

All investigated transition states for Cu-allyl addition (**ts$_{AA}$**, transition state for allyl addition) to benzonitrile as substrate are shown in Fig. S18. Complexes corresponding to **ts$_{AA}$**(major, mode A) and **ts$_{AA}$**(major, mode B) lead to the major enantiomer of the imine

intermediate (R configuration at the stereocenter), while through **ts$_{AA}$**(minor, mode A) and **ts$_{AA}$**(minor, mode B) the minor enantiomer is generated (*S* configuration). **Mode A** indicates that the allyl nucleophile is approaching from the front, whereas it approaches from the back in **mode B**. The corresponding free energy surfaces with different density functionals are shown in Figs. S23-1, S24-1, S25-1, S26-1, and S27-1.

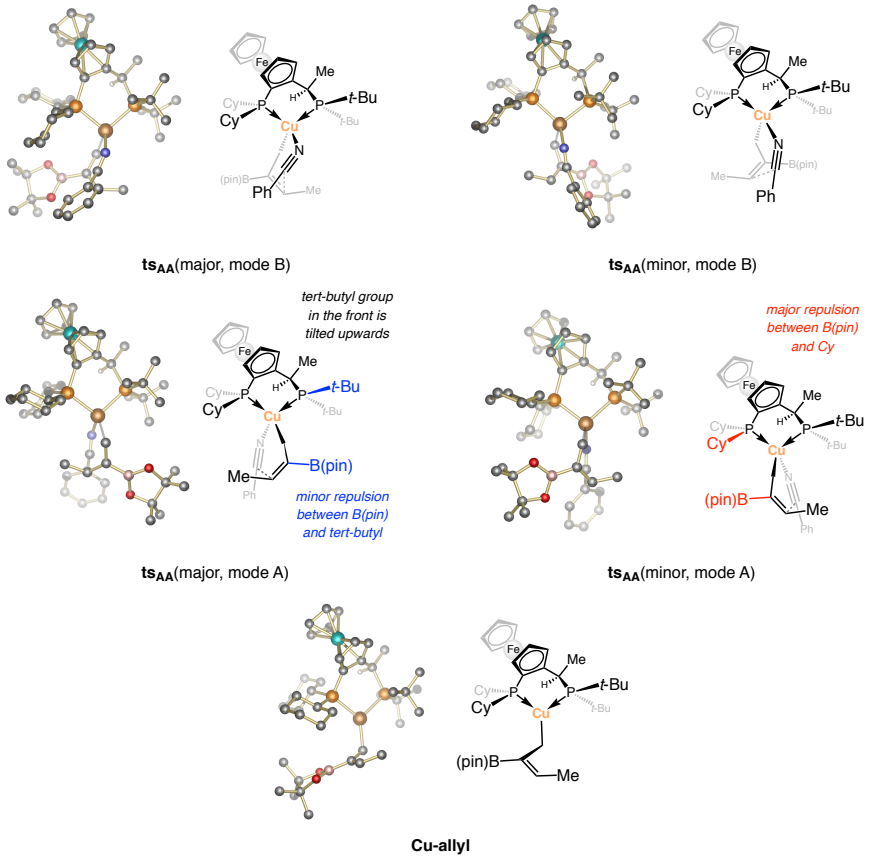


**Fig. S18.** Nomenclature and transition states investigated for Cu–allyl addition.

## 11.2 Nomenclature of investigated transition states for Cu–H addition to ketimines

All investigated transition states for Cu–H addition (**ts$_{CuHadd}$**) to the **major** (R configuration) as well as **minor** enantiomer (*S* configuration) of the imine intermediate are displayed in Fig. S19. **ts$_{CuHadd}$**(syn, major, mode A), **ts$_{CuHadd}$**(syn, major, mode B), **ts$_{CuHadd}$**(syn, minor, mode A) and **ts$_{CuHadd}$**(syn, minor, mode B) lead to the *syn* diastereomer, whereas through the corresponding ts labeled with **anti** the opposite diastereomer is generated. **Mode A** indicates that the hydride nucleophile is approaching from the rear, whereas it approaches from the front in **mode B**. The free energy surfaces with different density functionals are shown in Fig. S23-2, S24-2, S25-2, S26-2 and S27-2.

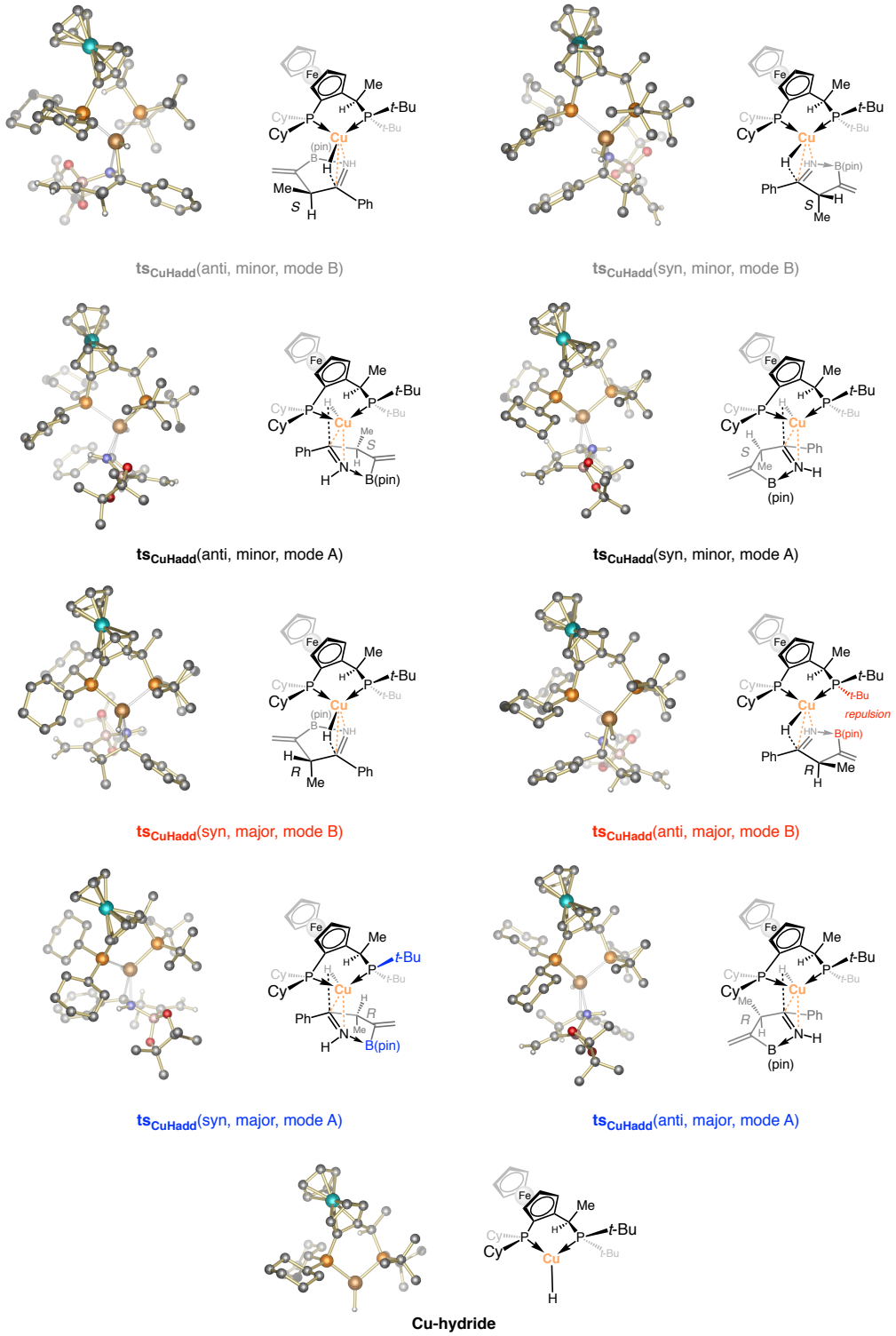


**Fig. S19.** Nomenclature and transition states investigated for Cu–H addition to major and minor enantiomer of imine intermediate.

## 11.3 Main features of the stereochemical model

Based on these DFT studies we propose the following models for enantioselective C–C bond formation (**I** vs. **II**, Fig. S20), as well as diastereoselective reduction (**III** vs. **IV**, Fig. S21).

### 11.3.1 Origin of enantioselectivity

In the transition state leading to the major enantiomer of the ketimine intermediate [**I** = **ts**$_{AA}$(major, mode A)] the nitrile coordinates to Cu from the back, while the allyl nucleophile is oriented such that the sterically demanding B(pin) moiety is placed below the *tert*-butyl group (Fig. S20a). This can easily be rationalized from the side view of the computed structure, indicating that the *tert*-butyl group in closer proximity to the nucleophile is tilted upwards (Fig. S20b). In the corresponding transition state leading to the minor enantiomer [**II** = **ts**$_{AA}$(minor, mode A)] there is repulsion between the B(pin) group and the proximal Cy substituent (Fig. S20c), as well as unfavorable interaction between the Me group on the nucleophile and the *tert*-butyl group in the back (Figs S20c and S20d). The latter interaction causes dissymmetry in the Cα–Cu–P angles (106.9° and 124.2° in **II** vs. 117.2° and 114.4° in **I**). It is probable that the upward tilted *tert*-butyl group in **I** (Fig. S20b) might also function as dispersion energy donor (DED), through selective binding of (i.e., attracting) the B(pin) moiety of the nucleophile (*88,89,90*).

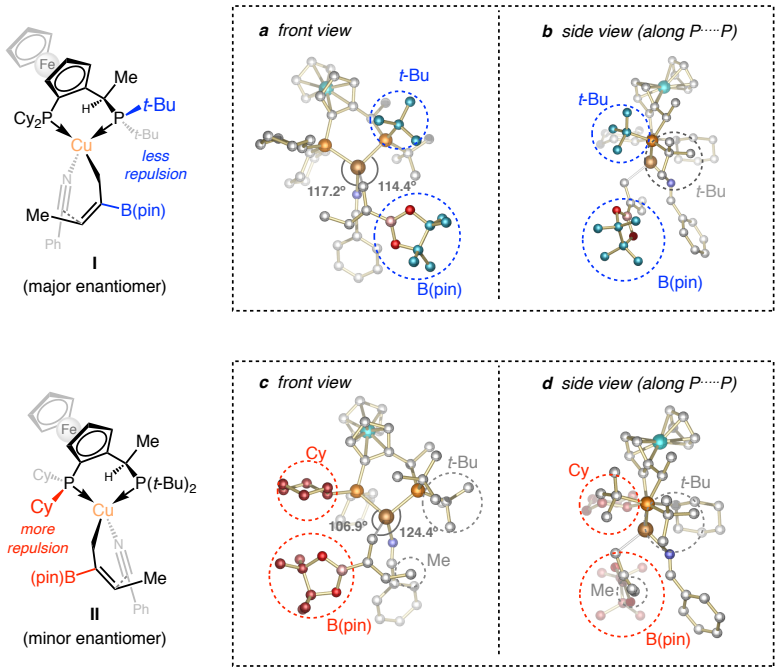


**Fig. S20.** Stereochemical model for enantioselective C–C bond formation.

### 11.3.2 Origin of diastereoselectivity during the Cu–H reduction process

In the favored transition state for Cu–H addition [**III** = **ts**$_{CuHadd}$(syn, major, mode A)], the imine intermediate approaches such that the B(pin) moiety can occupy the sterically least encumbered quadrant beneath the protruding *tert*-butyl group (Fig. S21a), and the small hydride ligand can be in close proximity to the *tert*-butyl group that is oriented downwards (Fig. S21b). In the transition state leading to the minor diastereomer [**IV** = **ts**$_{CuHadd}$(anti, major, mode B)], the methyl substituent on the substrate occupies the most accessible quadrant underneath the upward tilting *tert*-butyl group (Fig. S21d). Nonetheless, the methyl group is forced into a pseudo-equatorial position (Felkin-Anh control), causing eclipsing interaction with the *exo* methylene unit (Me–C$^1$–C$^2$–CH$_2$ dihedral angle = 24.8° in **IV**, Fig. S21c vs. 89.0° in **III**, Fig. S21a).

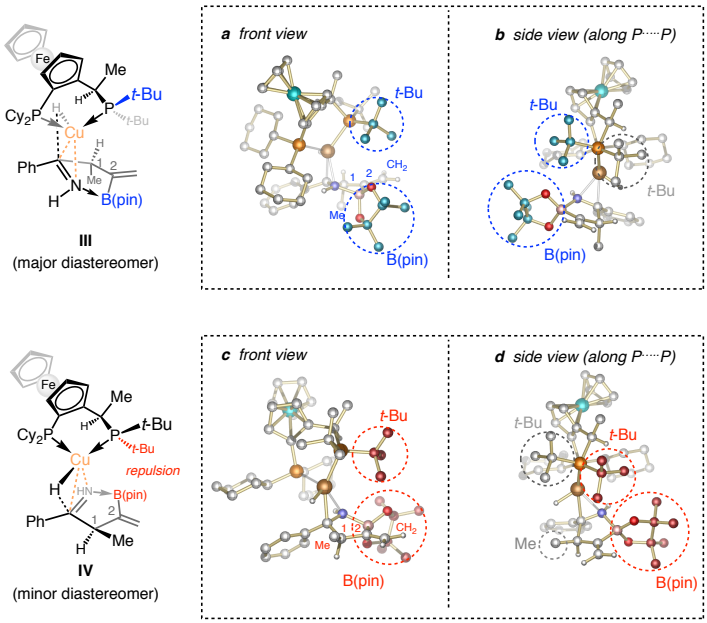


**Fig. S21.** Stereochemical model for diastereoselective addition.

### 11.3.3 Probing a match/mismatch case scenario for the Cu–H addition step

To probe a possible match/mismatch case scenario vis-à-vis Cu–H addition, we performed the multicomponent reaction with methyl-substituted allene (Fig. S22a) in presence of racemic ligand (Fig. S22b). The d.r. was diminished from 92:8 to 90:10. We provide the following rationale for why the d.r. is just slightly reduced (Fig. S22c-e).

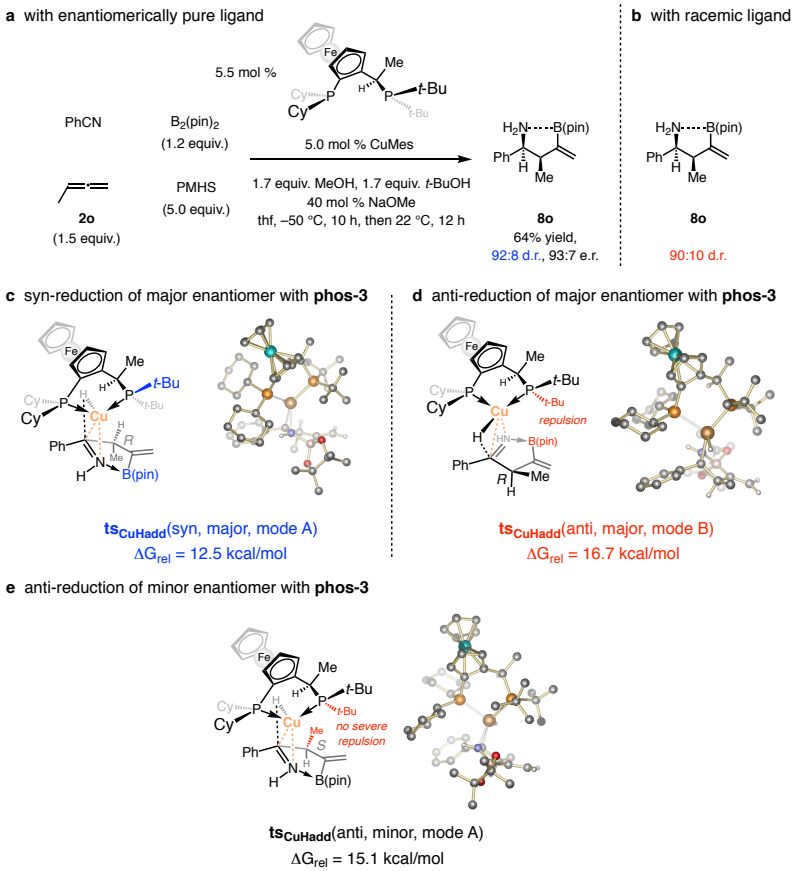


**Fig. S22.** Investigation of a match/mismatch case scenario for Cu–H reduction (free energies at the MN15/Def2TZVPP//M06L/Def2SVP$_{thf(SMD)}$ level).

Whereas *syn*-reduction of the major imine enantiomer occurs with a free energy barrier of 12.5 kcal/mol (Fig. S22c), the corresponding *anti*-reduction is significantly more challenging (16.7 kcal/mol; Fig. S22d). *Anti*-reduction in presence of larger amounts of minor imine enantiomer (generated from the opposite ligand enantiomer) is still energetically demanding (15.1 kcal/mol; Fig. S22e), but more favored compared to *anti*-reduction of the major imine enantiomer. There is likely minimal steric pressure between the small pseudo-equatorial methyl group on the substrate and the rear *t*-Bu group on the ligand (Fig. S22e). A plausible rationale accounting for competitiveness of this pathway is, as was noted above, the orientation of the B(pin) moiety, which prefers to occupy the position underneath the front *t*-Bu group on the ligand (i.e., less steric repulsion and/or attractive dispersion interaction).

## 11.4 Free energy surfaces with M06L/Def2SVP$_{thf(SMD)}$

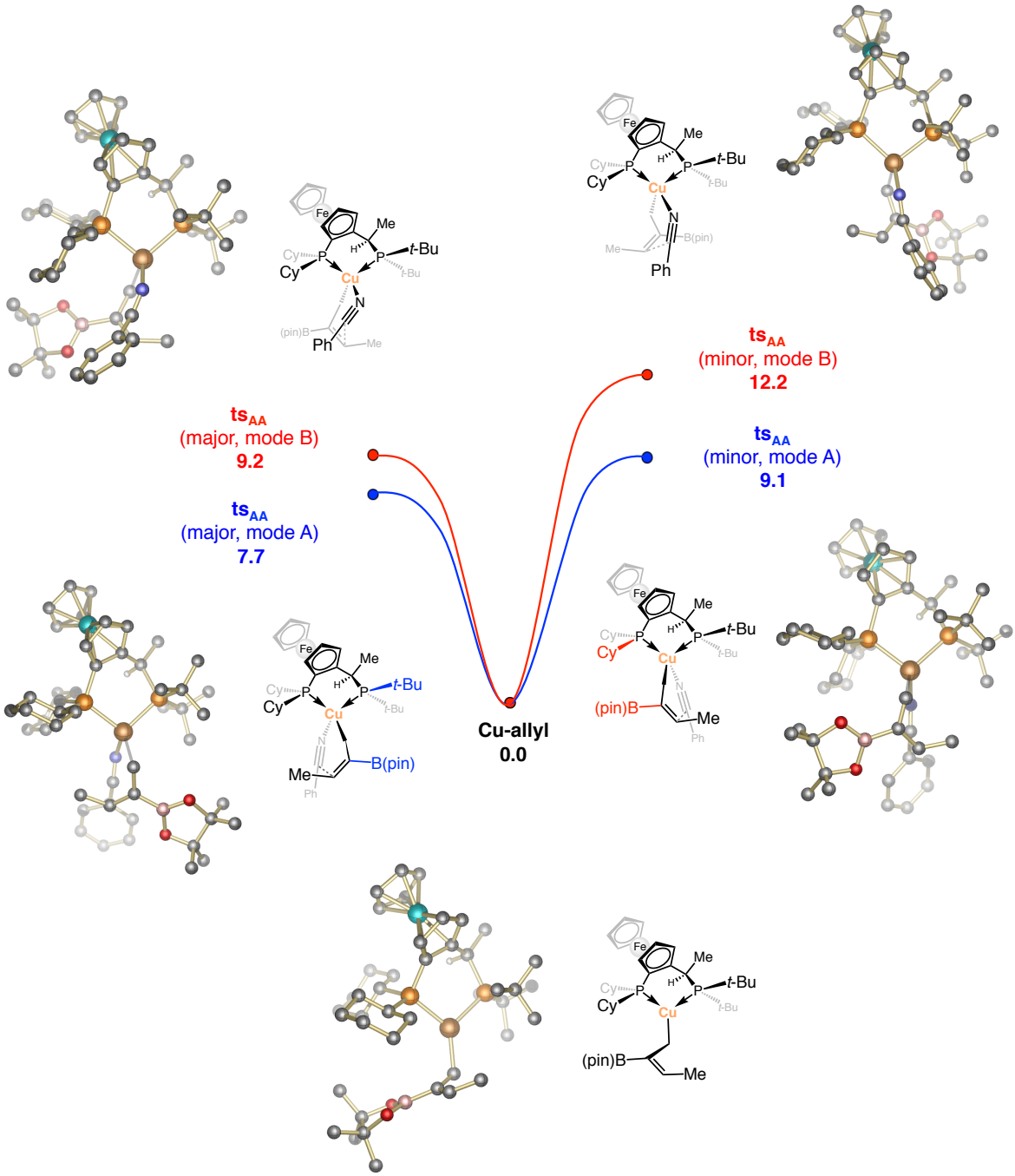


**Fig. S23-1.** Free energy surface (ΔG relative to **Cu–allyl**) for Cu–allyl addition to benzonitrile leading to major [**ts$_{AA}$**(major), left] and minor enantiomer [**ts$_{AA}$**(minor), right] at the M06L/Def2SVP$_{thf(SMD)}$ level; **ts$_{AA}$**, transition state for allyl addition; **mode A**, nucleophile in the front; **mode B**, nucleophile at the rear.

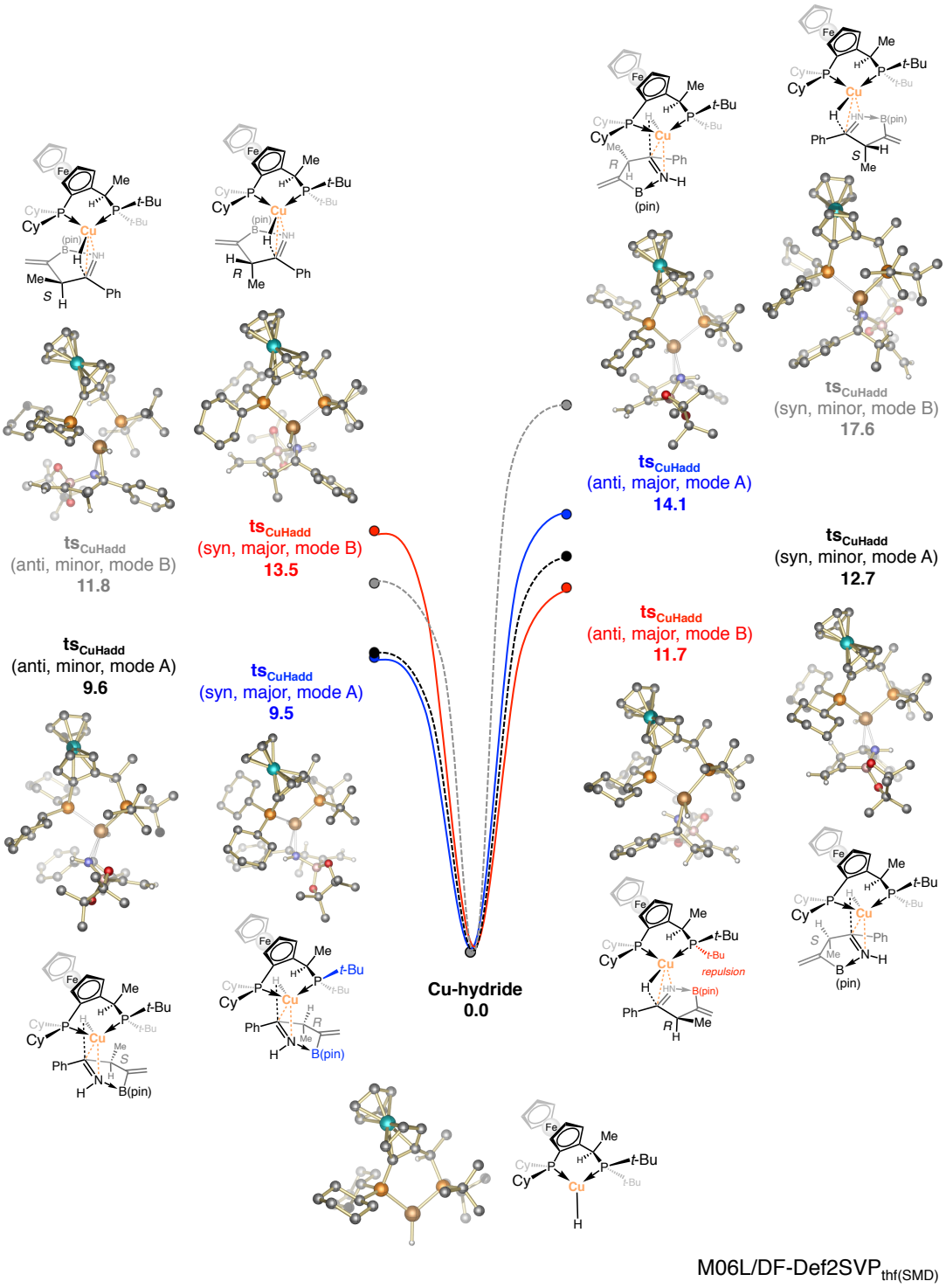


**Fig. S23-2.** Free energy surface (ΔG relative to **Cu–hydride**) for Cu–H addition to **major** (inside) and **minor** enantiomer (outside) of imine intermediate at the M06L/Def2SVP$_{thf(SMD)}$ level; **ts$_{CuHadd}$**, transition state for Cu–H addition addition; **mode A**, hydride at the rear; **mode B**, hydride in the front; **syn**, leading to *syn* diastereomer; **anti**, leading to *anti* diastereomer.

## 11.5 Free energy surfaces with M06L/Def2TZVPP//M06L/Def2SVP$_{thf(SMD)}$

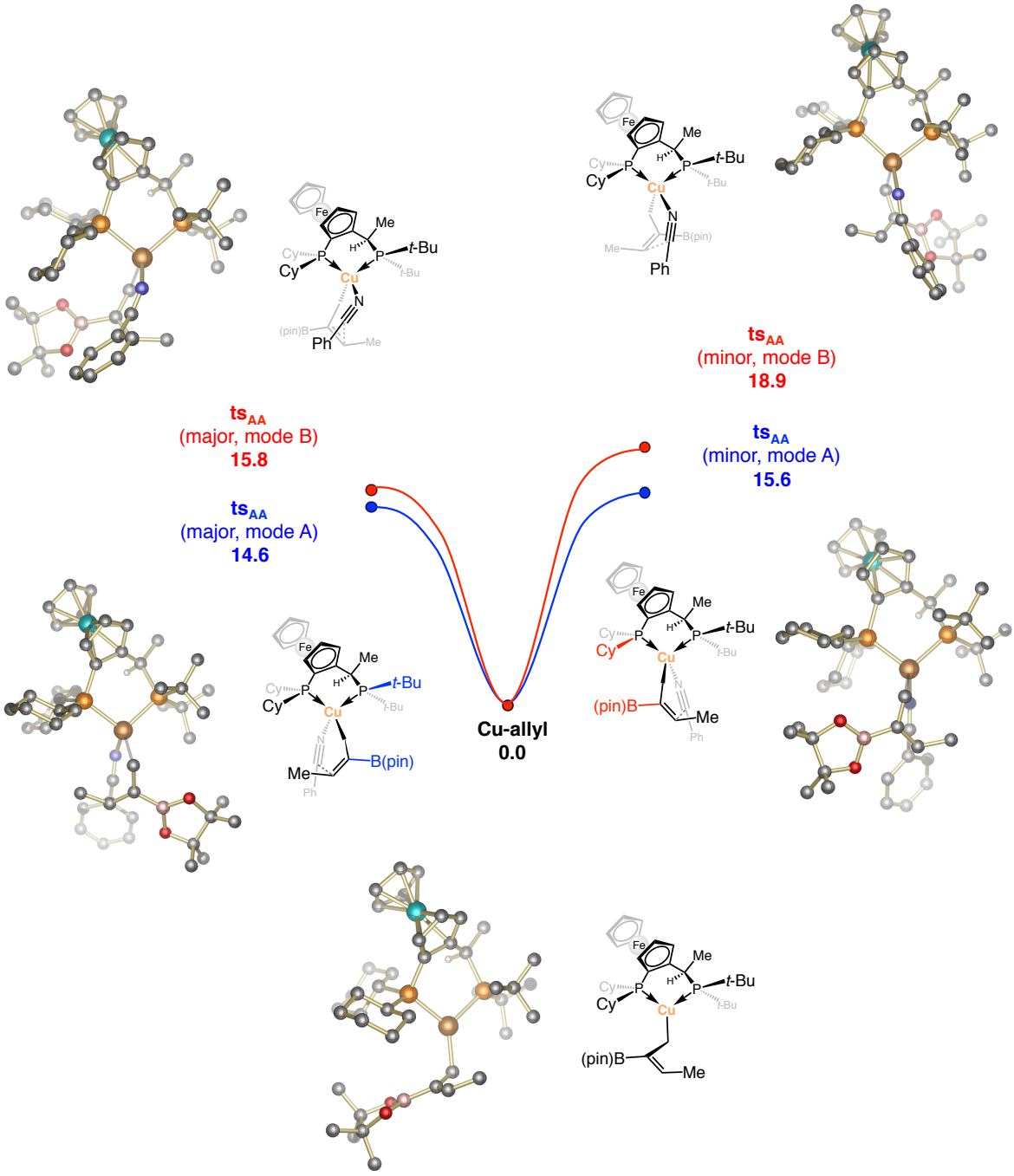


**Fig. S24-1.** Free energy surface (ΔG relative to **Cu–allyl**) for Cu–allyl addition to benzonitrile leading to major [**ts$_{AA}$**(major), left] and minor enantiomer [**ts$_{AA}$**(minor), right] at the M06L/Def2TZVPP//M06L/Def2SVP$_{thf(SMD)}$ level; **ts$_{AA}$**, transition state for allyl addition; **mode A**, nucleophile in the front; **mode B**, nucleophile in the rear.

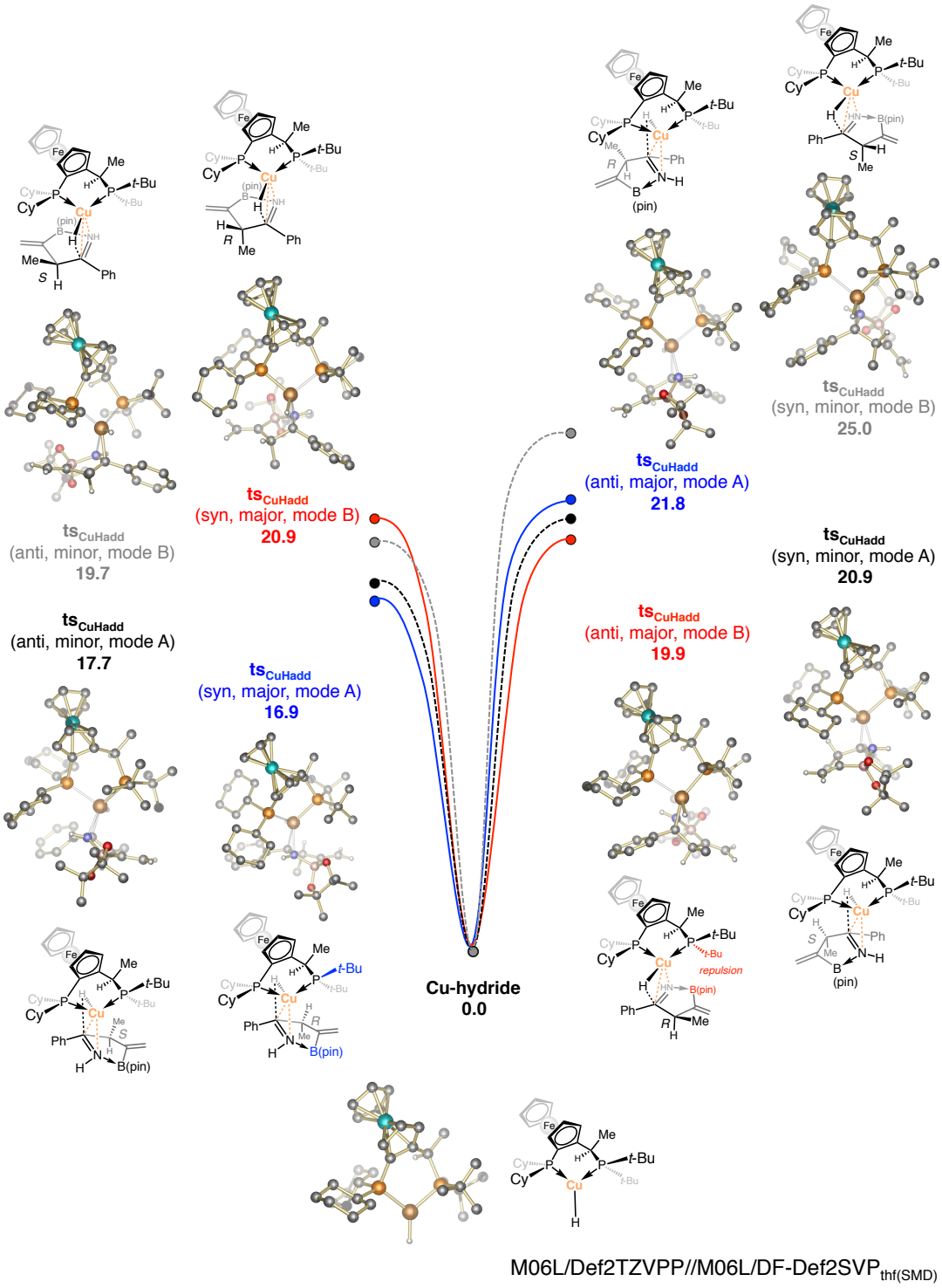


**Fig. S24-2.** Free energy surface (ΔG relative to **Cu–hydride**) for Cu–H addition to **major** (inside) and **minor** enantiomer (outside) of imine intermediate at the M06L/Def2TZVPP//M06L/Def2SVP$_{thf(SMD)}$ level; **ts$_{CuHadd}$**, transition state for Cu–H addition addition; **mode A**, hydride at the rear; **mode B**, hydride in the front; **syn**, leading to *syn* diastereomer; **anti**, leading to *anti* diastereomer.

## 11.6 Free energy surfaces with M06/Def2TZVPP//M06L/Def2SVP$_{thf(SMD)}$

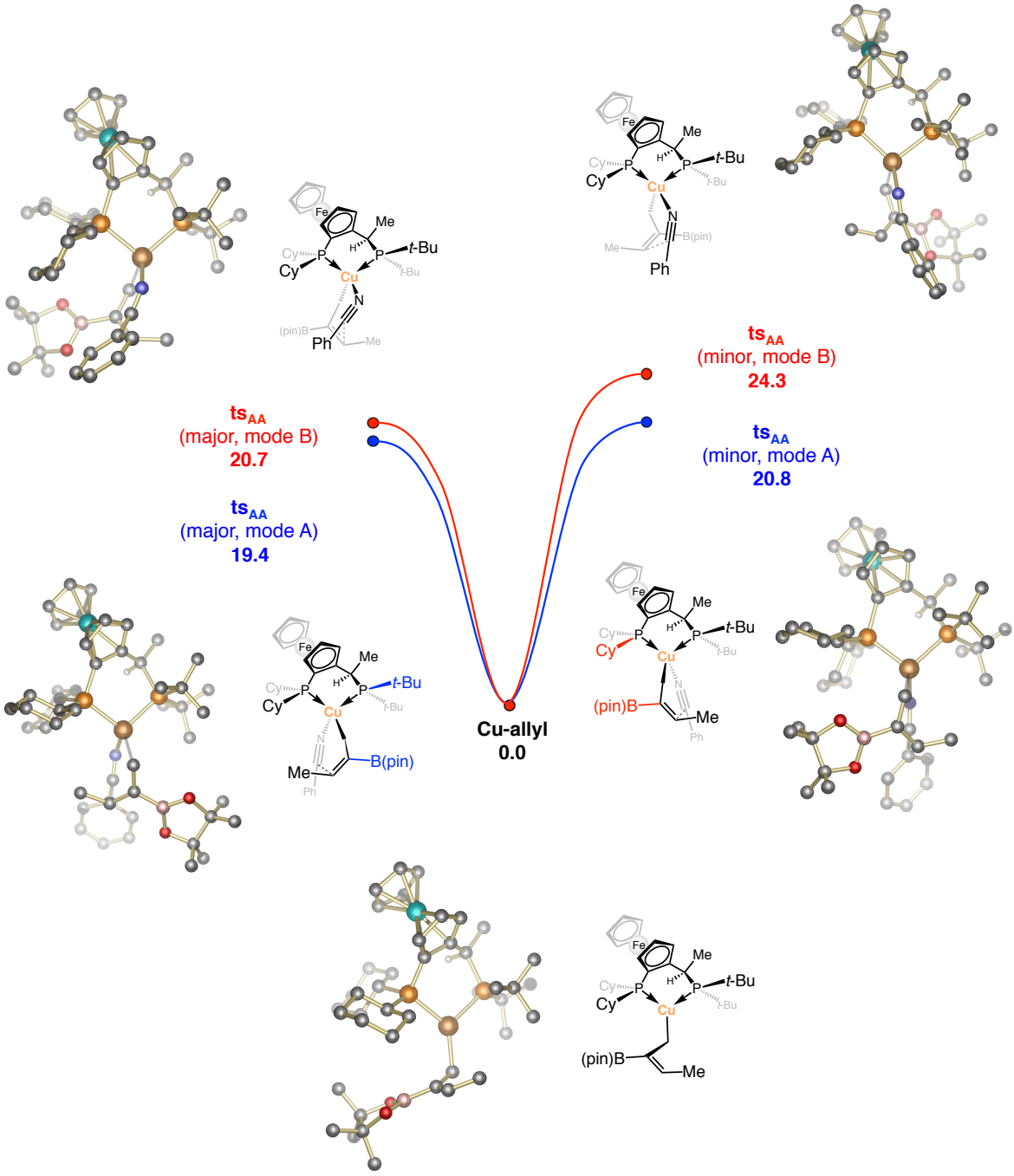


**Fig. S25-1.** Free energy surface (ΔG relative to **Cu–allyl**) for Cu–allyl addition to benzonitrile leading to major [**ts$_{AA}$**(major), left] and minor enantiomer [**ts$_{AA}$**(minor), right] at the M06/Def2TZVPP//M06L/Def2SVP$_{thf(SMD)}$ level; **ts$_{AA}$**, transition state for allyl addition; **mode A**, nucleophile in the front; **mode B**, nucleophile at the rear.

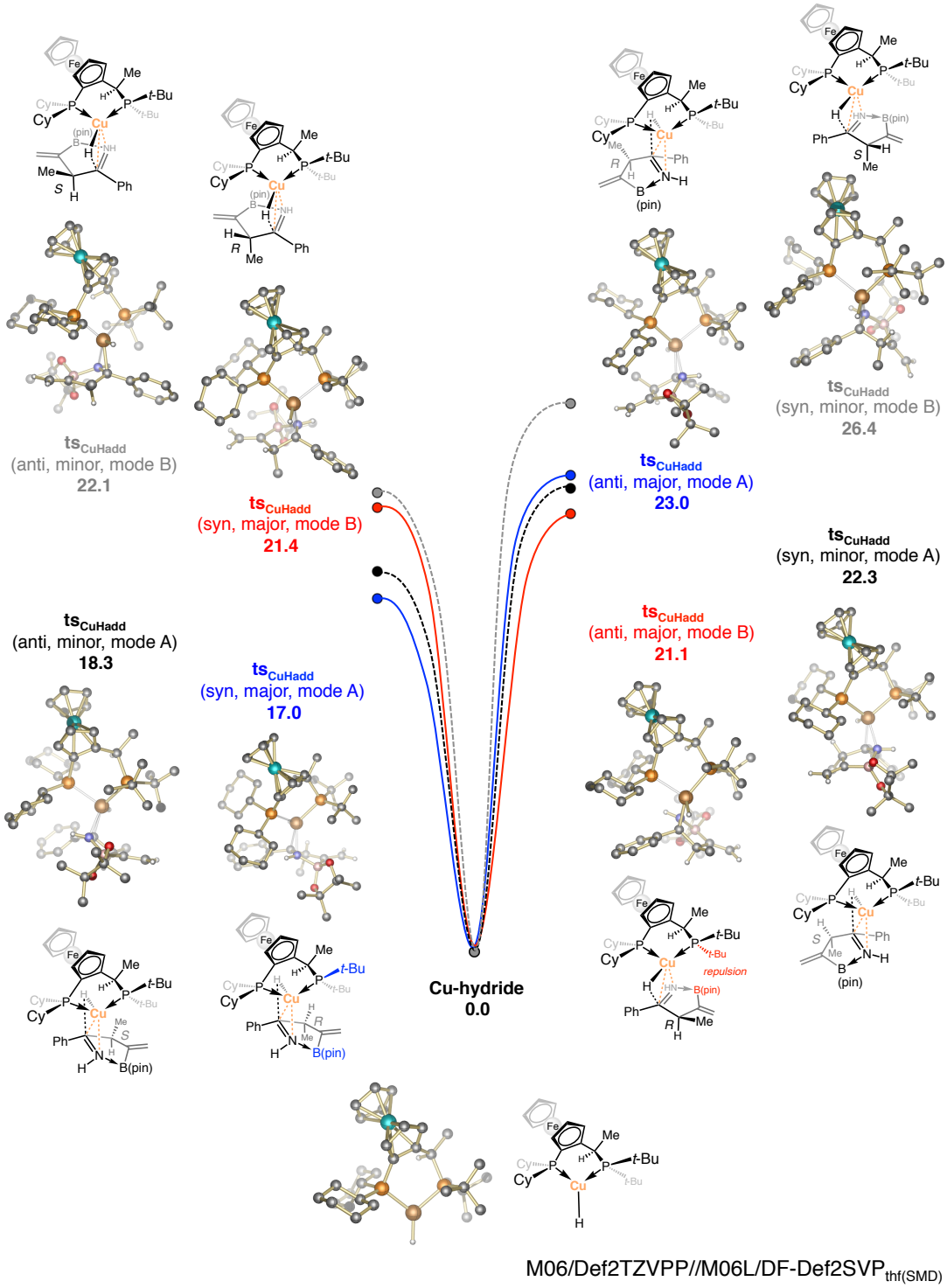


**Fig. S25-2.** Free energy surface (ΔG relative to **Cu–hydride**) for Cu–H addition to **major** (inside) and **minor** enantiomer (outside) of imine intermediate at the M06/Def2TZVPP//M06L/Def2SVP$_{thf(SMD)}$ level; **ts$_{CuHadd}$**, transition state for Cu–H addition; **mode A**, hydride at the rear; **mode B**, hydride in the front; **syn**, leading to *syn* diastereomer; **anti**, leading to *anti* diastereomer.

## 11.7 Free energy surfaces with MN15/Def2TZVPP//M06L/Def2SVP$_{thf(SMD)}$

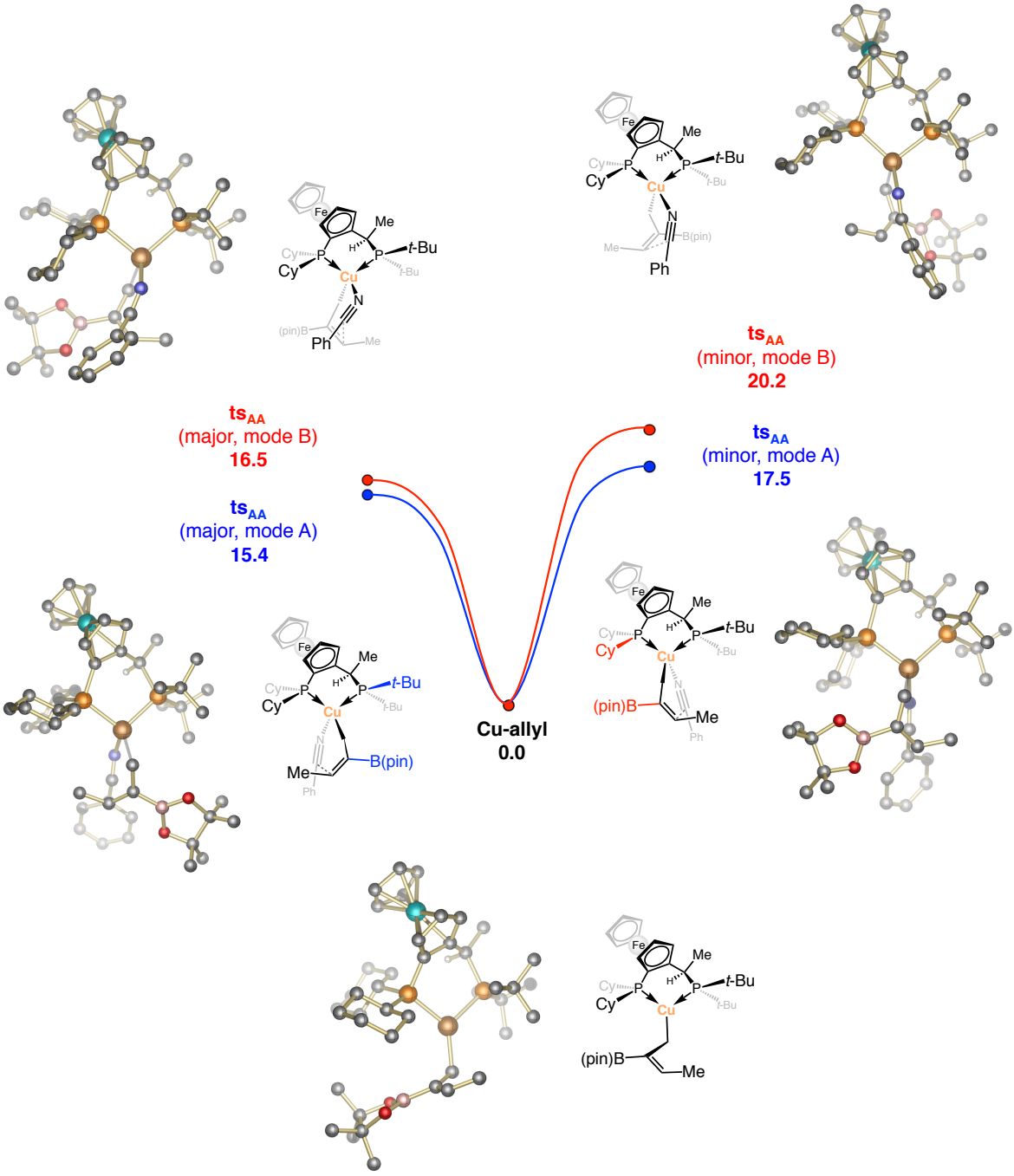


**Fig. S26-1.** Free energy surface (ΔG relative to **Cu–allyl**) for Cu–allyl addition to benzonitrile leading to major [**ts$_{AA}$**(major), left] and minor enantiomer [**ts$_{AA}$**(minor), right] at the MN15/Def2TZVPP//M06L/Def2SVP$_{thf(SMD)}$ level; **ts$_{AA}$**, transition state for allyl addition; **mode A**, nucleophile in the front; **mode B**, nucleophile at the rear.

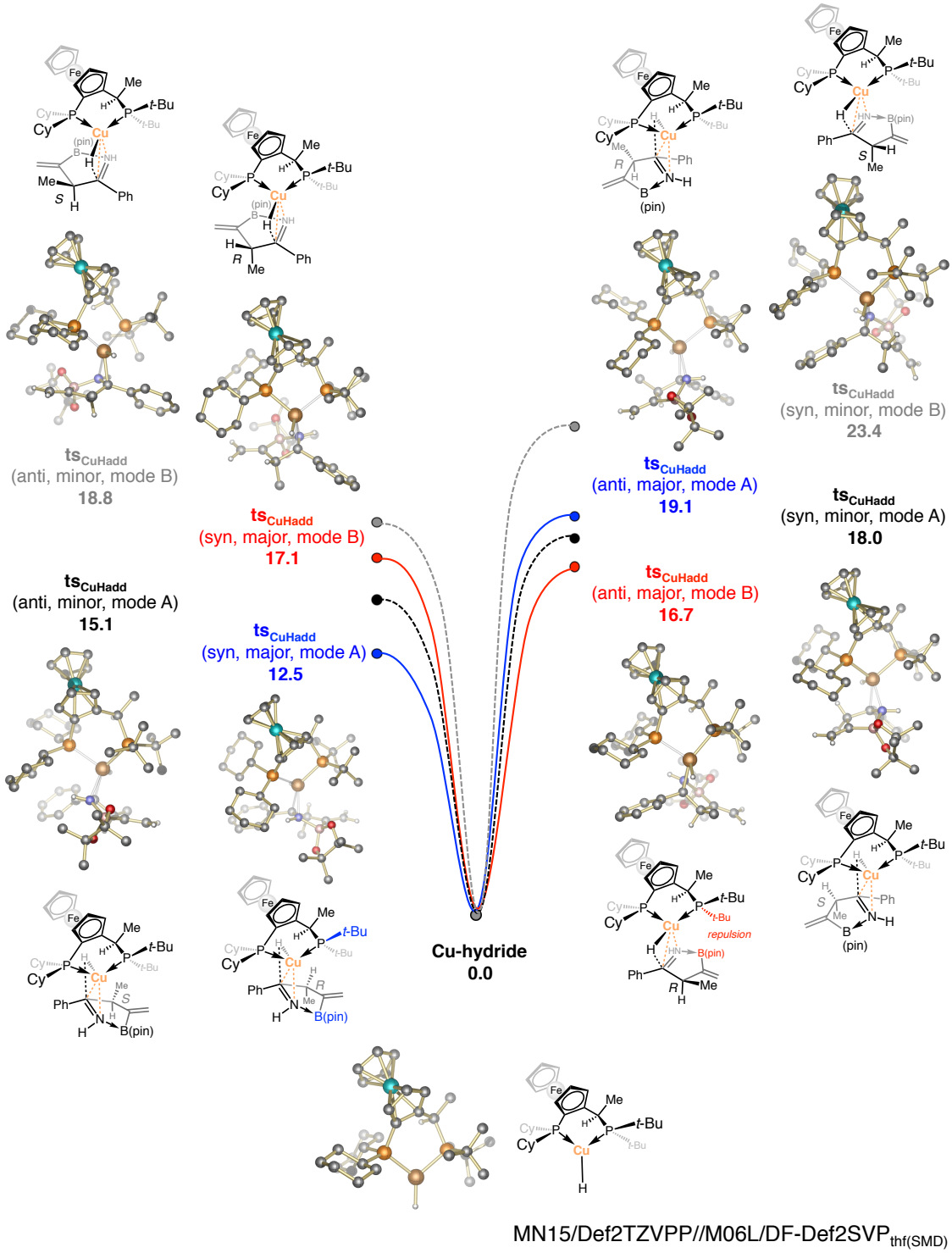


**Fig. S26-2.** Free energy surface (ΔG relative to **Cu–hydride**) for Cu–H addition to **major** (inside) and **minor** enantiomer (outside) of imine intermediate at the MN15/Def2TZVPP//M06L/Def2SVP$_{thf(SMD)}$ level; **ts$_{CuHadd}$**, transition state for Cu–H addition addition; **mode A**, hydride in the back; **mode B**, hydride in the front; **syn**, leading to *syn* diastereomer; **anti**, leading to *anti* diastereomer.

## 11.8 Free energy surfaces with ωB97XD/Def2TZVPP//M06L/Def2SVP$_{thf(SMD)}$

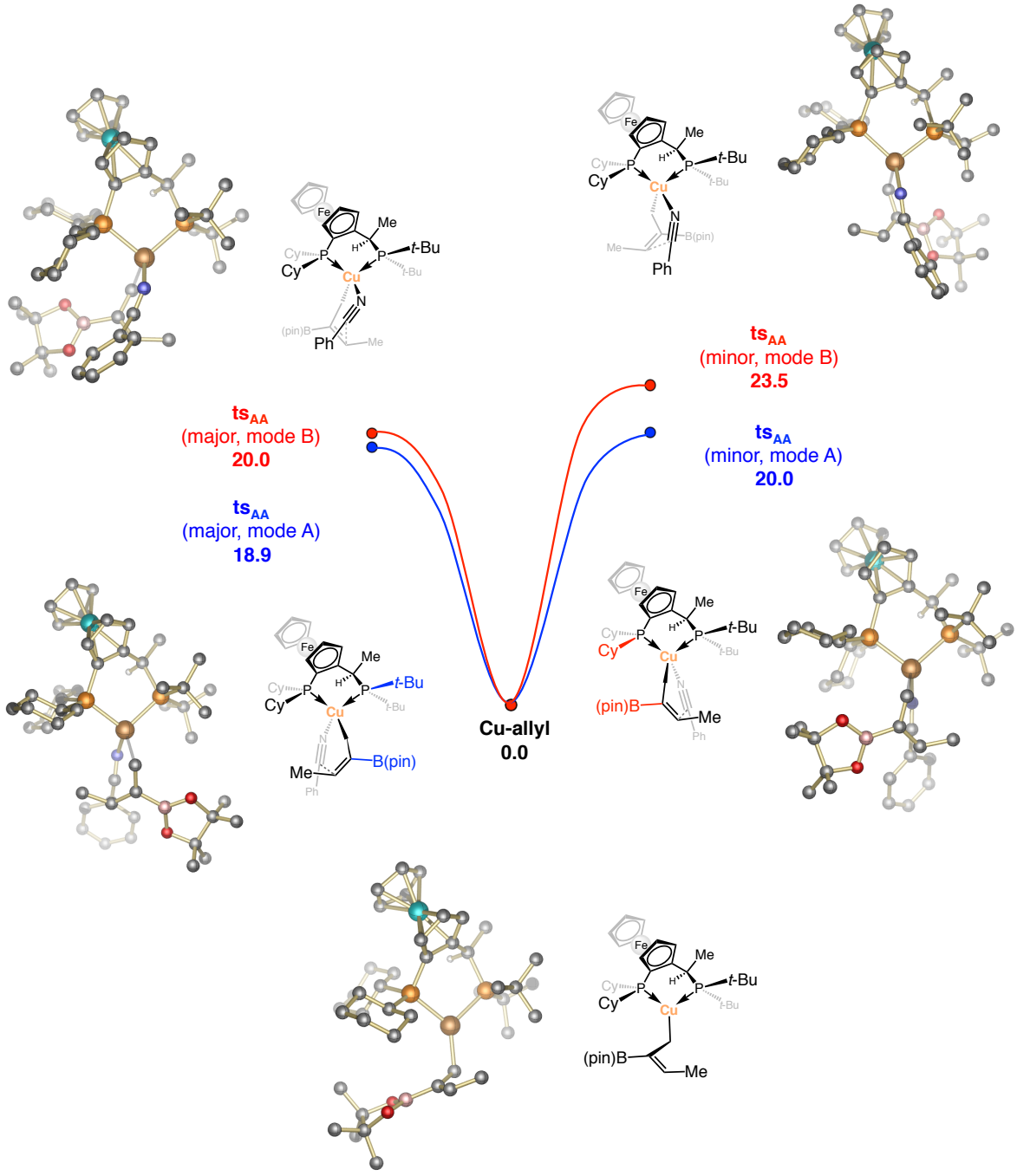


**Fig. S27-1.** Free energy surface (ΔG relative to **Cu–allyl**) for Cu–allyl addition to benzonitrile leading to major [**ts$_{AA}$**(major), left] and minor enantiomer [**ts$_{AA}$**(minor), right] at the ωB97XD/Def2TZVPP//M06L/Def2SVP$_{thf(SMD)}$ level; **ts$_{AA}$**, transition state for allyl addition; **mode A**, nucleophile in the front; **mode B**, nucleophile at the rear.

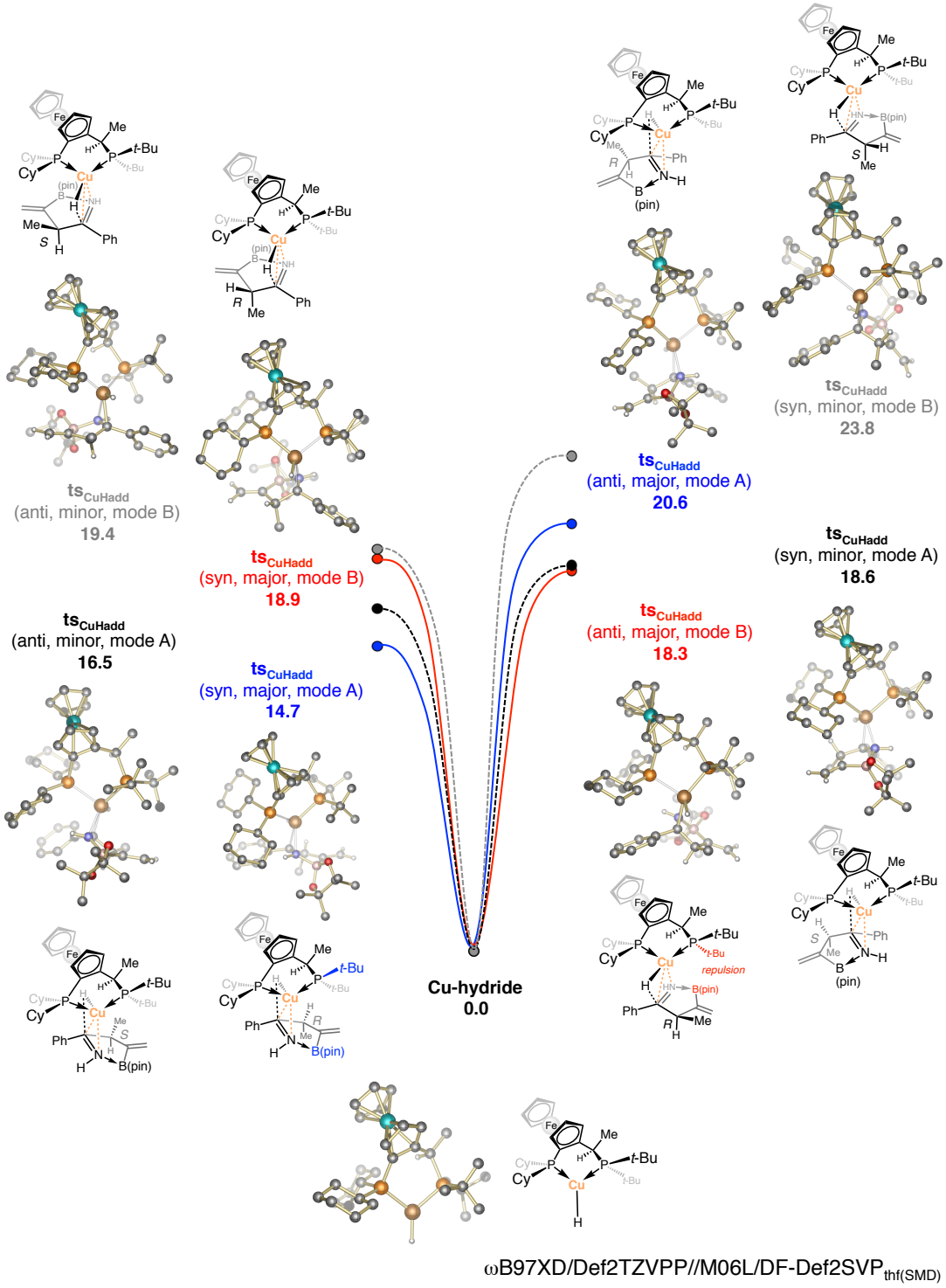


**Fig. S27-2.** Free energy surface (ΔG relative to **Cu–hydride**) for Cu–H addition to **major** (inside) and **minor** enantiomer (outside) of imine intermediate at the ωB97XD/Def2TZVPP//M06L/Def2SVP$_{thf(SMD)}$ level; **ts$_{CuHadd}$**, transition state for Cu–H addition addition; **mode A**, hydride at the rear; **mode B**, hydride in the front; **syn**, leading to *syn* diastereomer; **anti**, leading to *anti* diastereomer.

## 12 X-ray Structures

Selected single crystals suitable for X-ray crystallographic analysis were used for structural determination. The X-ray intensity data were measured at 100(2) K (Oxford Cryostream 700) on a Bruker Kappa APEX Duo diffractometer system equipped with a sealed Mo-target X-ray tube (λ = 0.71073 Å) and a high brightness IμS copper source (λ = 1.54178 Å). The crystals were mounted on a goniometer head with paratone oil. The detector was placed at a distance of 5.000 or 6.000 cm from the crystal. For each experiment, data collection strategy was determined by APEX software package and all frames were collected with a scan width of 0.5° in ω and ϕ with an exposure time of 10 or 20 s/frame.

The frames were integrated with the Bruker SAINT Software package using a narrow-frame integration algorithm to a maximum 2θ angle of 56.54° (0.75 Å resolution) for Mo data and of 134° (0.84 Å resolution) for Cu data. The final cell constants are based upon the refinement of the XYZ-centroids of several thousand reflections above 20 σ(I). Analysis of the data showed negligible decay during data collection. Data were corrected for absorption effects using the empirical method (SADABS). The structures were solved and refined by full-matrix least squares procedures on $|F^2|$ through the use of the Bruker SHELXTL (version 6.12) software package. All hydrogen atoms were included in idealized positions for structure factor calculations except for those forming hydrogen bonds or on a chiral center. Anisotropic displacement parameters were assigned to all non-hydrogen atoms, except those disordered.

### 12.1 X-ray Structure of Cu–ketimide 3b

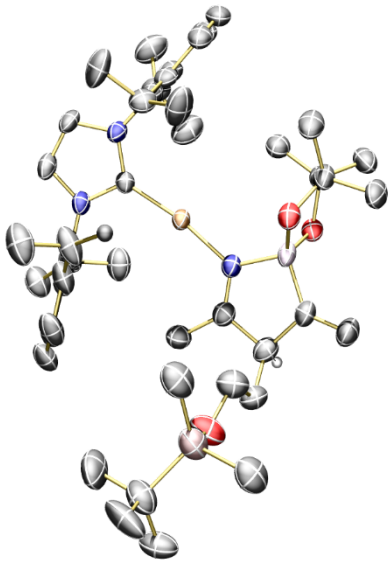

**Table S3**. Crystal data and structure refinement for Cu–ketimide **3b**

| | |
|---|---|
| Identification code | C46H73BCuN3O3Si(C6H14)1.25 |
| Empirical formula | C53.50 H90.50 B Cu N3 O3 Si |
| Formula weight | 926.22 |
| Temperature | 100(2) K |

| | | |
|---|---|---|
| Wavelength | 1.54178 Å | |
| Crystal system | Tetragonal | |
| Space group | $P4_12_12$ | |
| Unit cell dimensions | a = 16.9654(2) Å | α= 90°. |
| | b = 16.9654(2) Å | β= 90°. |
| | c = 39.6438(7) Å | γ = 90°. |
| Volume | 11410.5(3) $Å^3$ | |
| Z | 8 | |
| Density (calculated) | 1.078 $Mg/m^3$ | |
| Absorption coefficient | 1.036 $mm^{-1}$ | |
| F(000) | 4036 | |
| Crystal size | 0.440 x 0.300 x 0.220 $mm^3$ | |
| Theta range for data collection | 2.833 to 66.586°. | |
| Index ranges | -20<=h<=20, -20<=k<=20, -47<=l<=42 | |
| Reflections collected | 77417 | |
| Independent reflections | 10065 [R(int) = 0.0424] | |
| Completeness to theta = 66.586° | 99.8 % | |
| Absorption correction | Semi-empirical from equivalents | |
| Max. and min. transmission | 0.7533 and 0.6590 | |
| Refinement method | Full-matrix least-squares on $F^2$ | |
| Data / restraints / parameters | 10065 / 512 / 594 | |
| Goodness-of-fit on $F^2$ | 1.085 | |
| Final R indices [I>2sigma(I)] | R1 = 0.0545, wR2 = 0.1575 | |
| R indices (all data) | R1 = 0.0569, wR2 = 0.1609 | |
| Absolute structure parameter | 0.005(5) | |
| Extinction coefficient | n/a | |
| Largest diff. peak and hole | 0.782 and -0.460 e.$Å^{-3}$ | |

## 12.2 X-ray Structure of Cu–ketimide 3c

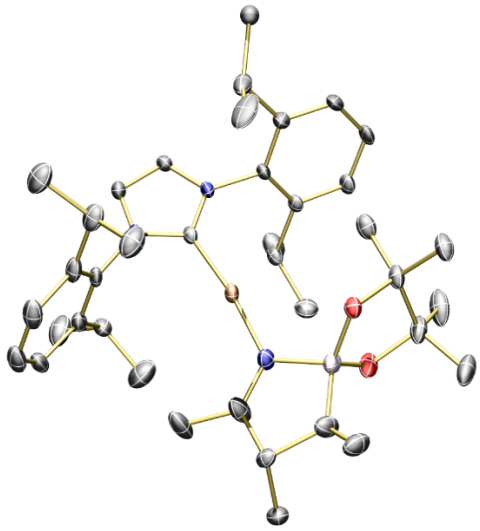

**Table S4**. Crystal data and structure refinement for Cu–ketimide **3c**

| | | |
|---|---|---|
| Identification code | Cu–ketimide **3c** | |
| Empirical formula | C43 H65 B Cu N3 O3 | |
| Formula weight | 746.33 | |
| Temperature | 100(2) K | |
| Wavelength | 1.54178 Å | |
| Crystal system | Orthorhombic | |
| Space group | $P2_12_12_1$ | |
| Unit cell dimensions | a = 12.6373(5) Å | α= 90°. |
| | b = 17.3810(7) Å | β= 90°. |
| | c = 18.9811(8) Å | γ = 90°. |
| Volume | 4169.2(3) $Å^3$ | |
| Z | 4 | |
| Density (calculated) | 1.189 $Mg/m^3$ | |
| Absorption coefficient | 1.041 $mm^{-1}$ | |
| F(000) | 1608 | |
| Crystal size | 0.320 x 0.180 x 0.160 $mm^3$ | |
| Theta range for data collection | 3.448 to 69.708°. | |
| Index ranges | -11<=h<=15, -20<=k<=20, -21<=l<=21 | |
| Reflections collected | 20788 | |
| Independent reflections | 7341 [R(int) = 0.0261] | |
| Completeness to theta = 67.679° | 97.3 % | |
| Absorption correction | Semi-empirical from equivalents | |
| Max. and min. transmission | 0.7532 and 0.6551 | |
| Refinement method | Full-matrix least-squares on $F^2$ | |

| | |
|---|---|
| Data / restraints / parameters | 7341 / 7 / 483 |
| Goodness-of-fit on $F^2$ | 1.117 |
| Final R indices [I>2sigma(I)] | R1 = 0.0480, wR2 = 0.1339 |
| R indices (all data) | R1 = 0.0494, wR2 = 0.1353 |
| Absolute structure parameter | 0.017(7) |
| Extinction coefficient | n/a |
| Largest diff. peak and hole | 0.903 and -0.566 e.Å$^{-3}$ |

## 12.3 X-ray Structure of 6a

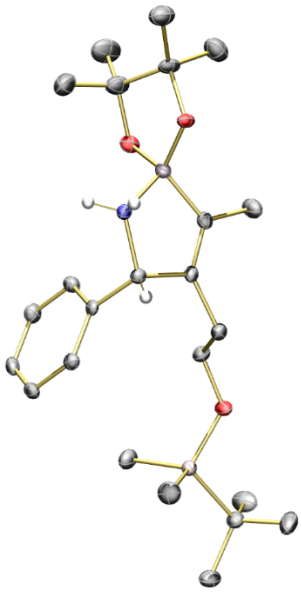

**Table S5**. Crystal data and structure refinement for amine **6a**

| | | |
|---|---|---|
| Identification code | amine **6a** | |
| Empirical formula | C24 H42 B N O3 Si | |
| Formula weight | 431.48 | |
| Temperature | 100(2) K | |
| Wavelength | 1.54178 Å | |
| Crystal system | Orthorhombic | |
| Space group | Fdd2 | |
| Unit cell dimensions | a = 20.549(2) Å | α= 90°. |
| | b = 25.2336(18) Å | β= 90°. |
| | c = 20.1814(14) Å | γ = 90°. |
| Volume | 10464.6(16) Å$^3$ | |

| | |
|---|---|
| Z | 16 |
| Density (calculated) | 1.095 $Mg/m^3$ |
| Absorption coefficient | 0.960 $mm^{-1}$ |
| F(000) | 3776 |
| Crystal size | 0.250 x 0.200 x 0.150 $mm^3$ |
| Theta range for data collection | 3.534 to 66.929°. |
| Index ranges | -24<=h<=21, -30<=k<=30, -24<=l<=24 |
| Reflections collected | 31220 |
| Independent reflections | 4617 [R(int) = 0.0366] |
| Completeness to theta = 66.929° | 99.4 % |
| Absorption correction | Semi-empirical from equivalents |
| Max. and min. transmission | 0.7528 and 0.6715 |
| Refinement method | Full-matrix least-squares on $F^2$ |
| Data / restraints / parameters | 4617 / 3 / 278 |
| Goodness-of-fit on $F^2$ | 1.041 |
| Final R indices [I>2sigma(I)] | R1 = 0.0342, wR2 = 0.0926 |
| R indices (all data) | R1 = 0.0344, wR2 = 0.0927 |
| Absolute structure parameter | 0.017(5) |
| Extinction coefficient | n/a |
| Largest diff. peak and hole | 0.443 and -0.166 $e.Å^{-3}$ |

## 12.4 X-ray Structure of 7b

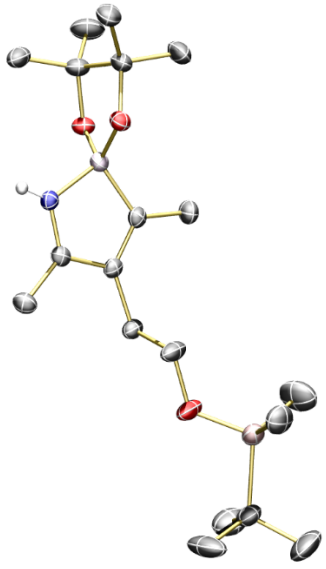

**Table S6**. Crystal data and structure refinement for imine **7b**

| | | |
|---|---|---|
| Identification code | imine **7b** | |
| Empirical formula | C25 H52 B N O5 Si | |
| Formula weight | 485.57 | |
| Temperature | 100(2) K | |
| Wavelength | 1.54178 Å | |
| Crystal system | Triclinic | |
| Space group | P-1 | |
| Unit cell dimensions | a = 10.9049(3) Å | α= 103.3850(10)°. |
| | b = 11.8140(3) Å | β= 104.6030(10)°. |
| | c = 13.9547(4) Å | γ = 106.3070(10)°. |
| Volume | 1578.81(8) $Å^3$ | |
| Z | 2 | |
| Density (calculated) | 1.021 $Mg/m^3$ | |
| Absorption coefficient | 0.885 $mm^{-1}$ | |
| F(000) | 536 | |
| Crystal size | 0.220 x 0.070 x 0.030 $mm^3$ | |
| Theta range for data collection | 3.461 to 66.741°. | |
| Index ranges | -12<=h<=12, -14<=k<=13, -16<=l<=16 | |
| Reflections collected | 22278 | |
| Independent reflections | 5557 [R(int) = 0.0301] | |
| Completeness to theta = 66.741° | 99.4 % | |
| Absorption correction | Semi-empirical from equivalents | |
| Max. and min. transmission | 0.7528 and 0.6704 | |
| Refinement method | Full-matrix least-squares on $F^2$ | |
| Data / restraints / parameters | 5557 / 3 / 322 | |
| Goodness-of-fit on $F^2$ | 1.053 | |
| Final R indices [I>2sigma(I)] | R1 = 0.0446, wR2 = 0.1217 | |
| R indices (all data) | R1 = 0.0490, wR2 = 0.1258 | |
| Extinction coefficient | n/a | |
| Largest diff. peak and hole | 0.529 and -0.241 $e.Å^{-3}$ | |

## 12.5 X-ray Structure of 9e

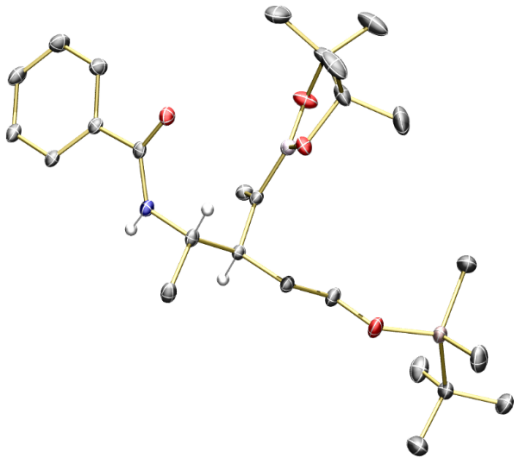

**Table S7**. Crystal data and structure refinement for benzyl amide of **(2*S*,3*R*)-9e**

| | | |
|---|---|---|
| Identification code | benzyl amide of **(2*S*,3*R*)-9e** | |
| Empirical formula | C19 H28 B N O3 | |
| Formula weight | 329.23 | |
| Temperature | 100(2) K | |
| Wavelength | 1.54178 Å | |
| Crystal system | Orthorhombic | |
| Space group | Pbca | |
| Unit cell dimensions | a = 9.8241(3) Å | α= 90°. |
| | b = 17.1434(6) Å | β= 90°. |
| | c = 22.6801(8) Å | γ = 90°. |
| Volume | 3819.7(2) Å$^3$ | |
| Z | 8 | |
| Density (calculated) | 1.145 Mg/m$^3$ | |
| Absorption coefficient | 0.598 mm$^{-1}$ | |
| F(000) | 1424 | |
| Crystal size | 0.340 x 0.060 x 0.050 mm$^3$ | |
| Theta range for data collection | 3.898 to 66.589°. | |
| Index ranges | -11<=h<=11, -19<=k<=20, -26<=l<=26 | |
| Reflections collected | 15536 | |
| Independent reflections | 3359 [R(int) = 0.0517] | |
| Completeness to theta = 66.589° | 99.5 % | |
| Absorption correction | Semi-empirical from equivalents | |

| | |
|---|---|
| Max. and min. transmission | 0.7528 and 0.6088 |
| Refinement method | Full-matrix least-squares on $F^2$ |
| Data / restraints / parameters | 3359 / 1 / 226 |
| Goodness-of-fit on $F^2$ | 1.041 |
| Final R indices [I>2sigma(I)] | R1 = 0.0431, wR2 = 0.1097 |
| R indices (all data) | R1 = 0.0571, wR2 = 0.1174 |
| Extinction coefficient | n/a |
| Largest diff. peak and hole | 0.223 and -0.173 e.Å$^{-3}$ |

## 12.6 X-ray Structure of (+)-Tangutorine

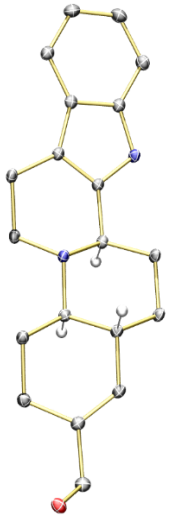

**Table S8**. Crystal data and structure refinement for (+)-tangutorine

| | | |
|---|---|---|
| Identification code | (+)-tangutorine | |
| Empirical formula | C21 H28 N2 O2 | |
| Formula weight | 340.45 | |
| Temperature | 100(2) K | |
| Wavelength | 1.54178 Å | |
| Crystal system | Orthorhombic | |
| Space group | $P2_12_12_1$ | |
| Unit cell dimensions | a = 9.9025(14) Å | α= 90°. |
| | b = 10.8161(15) Å | β= 90°. |
| | c = 17.092(2) Å | γ = 90°. |
| Volume | 1830.7(4) Å$^3$ | |
| Z | 4 | |
| Density (calculated) | 1.235 Mg/m$^3$ | |
| Absorption coefficient | 0.625 mm$^{-1}$ | |

| | |
|---|---|
| F(000) | 736 |
| Crystal size | 0.430 x 0.360 x 0.220 $mm^3$ |
| Theta range for data collection | 4.838 to 66.669°. |
| Index ranges | -11<=h<=11, -12<=k<=12, -20<=l<=20 |
| Reflections collected | 23863 |
| Independent reflections | 3253 [R(int) = 0.0442] |
| Completeness to theta = 66.669° | 100.1 % |
| Absorption correction | Semi-empirical from equivalents |
| Max. and min. transmission | 0.7528 and 0.6712 |
| Refinement method | Full-matrix least-squares on $F^2$ |
| Data / restraints / parameters | 3253 / 3 / 240 |
| Goodness-of-fit on $F^2$ | 1.116 |
| Final R indices [I>2sigma(I)] | R1 = 0.0316, wR2 = 0.0839 |
| R indices (all data) | R1 = 0.0318, wR2 = 0.0841 |
| Absolute structure parameter | 0.05(4) |
| Extinction coefficient | 0.0061(7) |
| Largest diff. peak and hole | 0.290 and -0.237 $e.Å^{-3}$ |

## 12.7 X-ray Structure of 5h

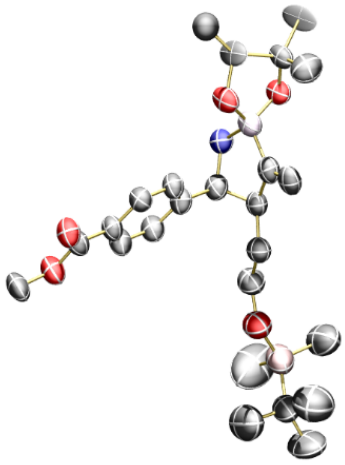

For the *syn*-homoallylic amines investigated, the strength of the N→B(pin) chelation is variable and there are some cases where the interaction might be relatively weak, as suggested by the significantly downfield $^{11}B$ NMR signal or product **5h** (27.9 ppm) or *syn*-homoallylic amines such as **5d** and **5e**, indicating a tri-coordinate species. We were able to obtain crystals suitable for X-Ray diffraction of compound **5h** by slow evaporation of a sample in hexanes. However, the structure presents significant disorder localized mostly in the pinacol and *tert*-butyl-dimethylsilyl groups. Accordingly, the data are not suitable for publication in the Cambridge Crystallographic Database. Nevertheless, data quality is sufficiently high to show that internal N→B(pin) chelation is in **5h** and likely in the other products amines, which show a broader and more downfield $^{11}B$ signal (~30 ppm).

# 13 NMR Spectra

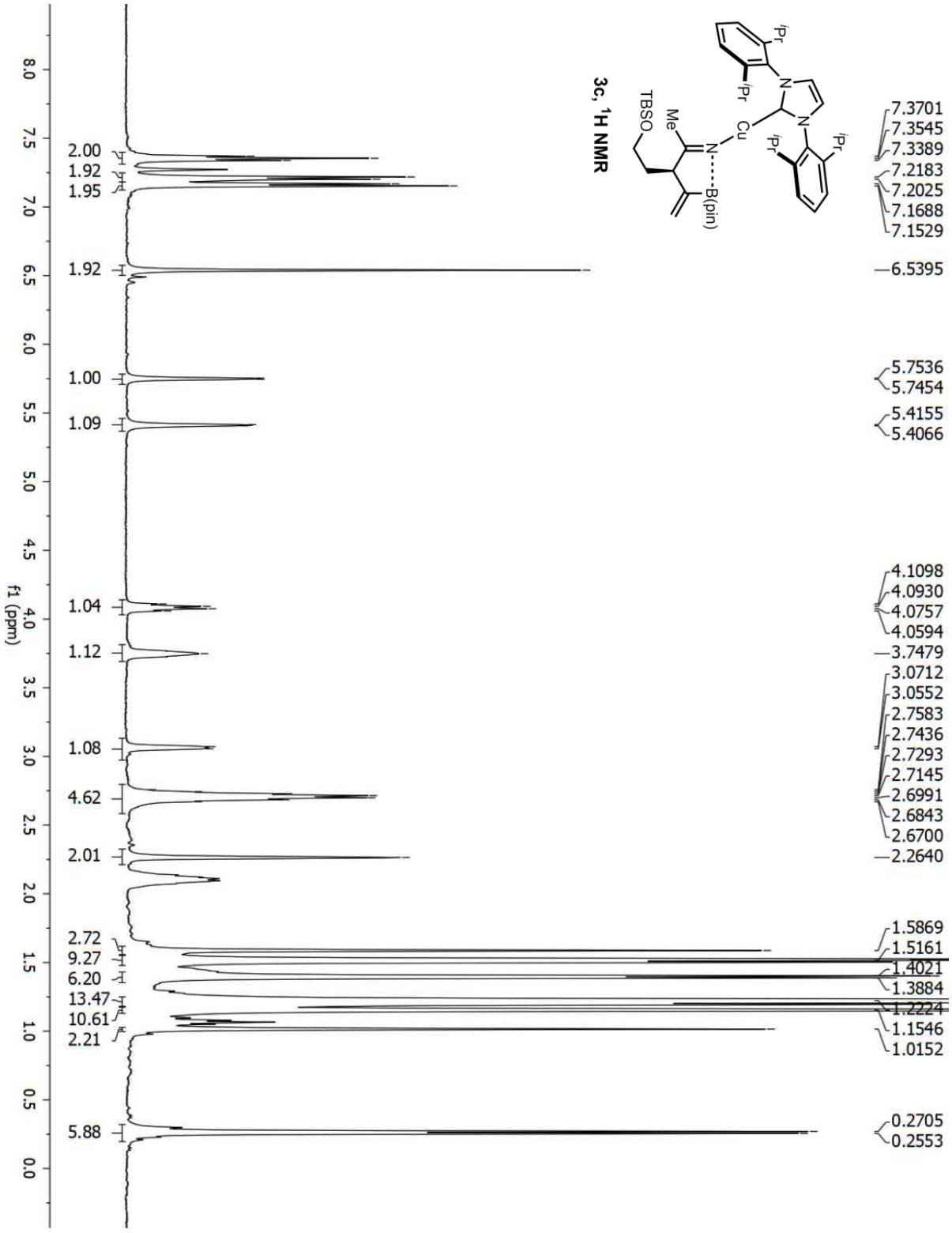

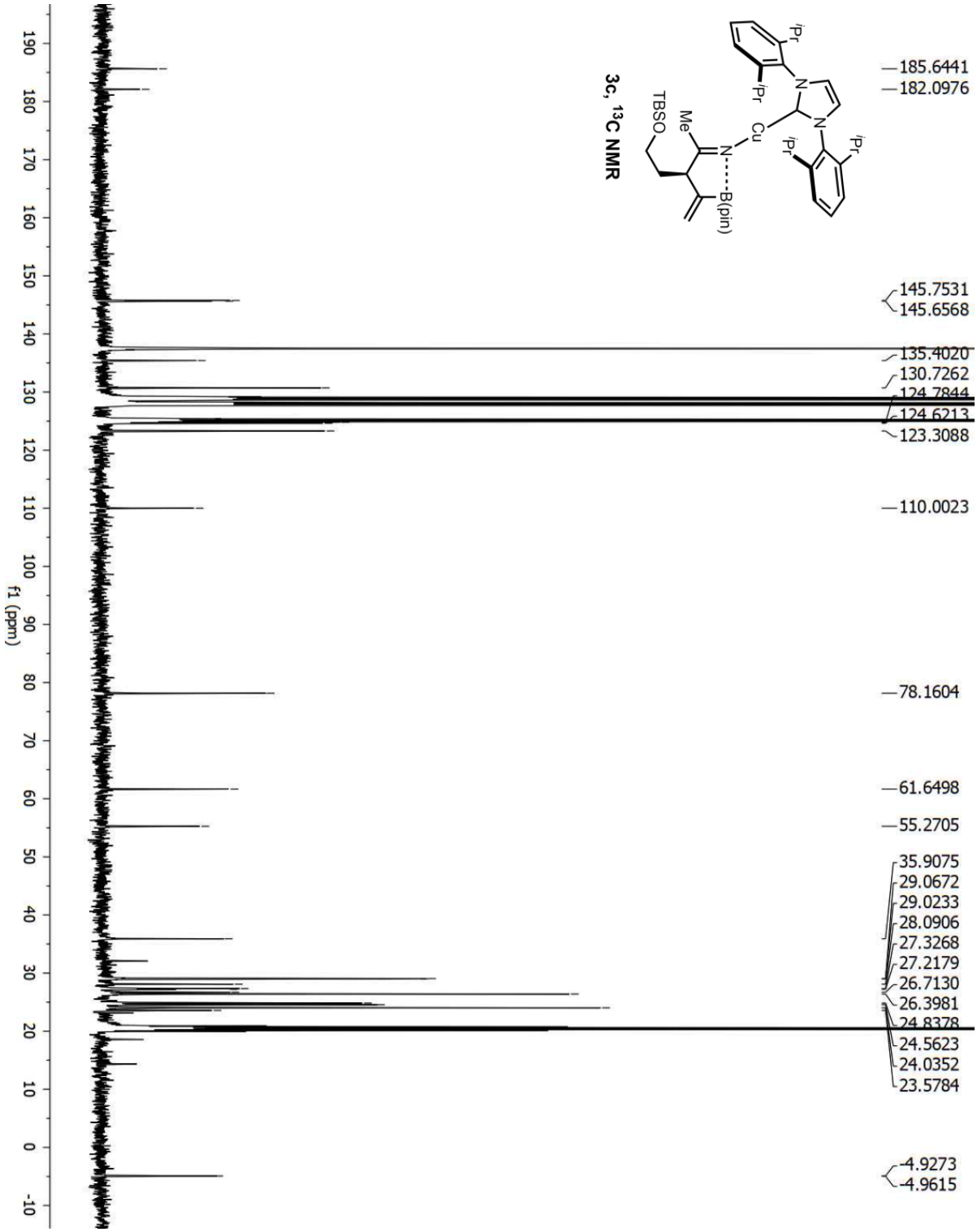
3c, $^{13}$C NMR
TBSO
Me
Cu
B(pin)
iPr
185.6441
182.0976
145.7531
145.6568
135.4020
130.7262
124.7844
124.6213
123.3088
110.0023
78.1604
61.6498
55.2705
35.9075
29.0672
29.0233
28.0906
27.3268
27.2179
26.7130
26.3981
24.8378
24.5623
24.0352
23.5784
-4.9273
-4.9615
f1 (ppm)

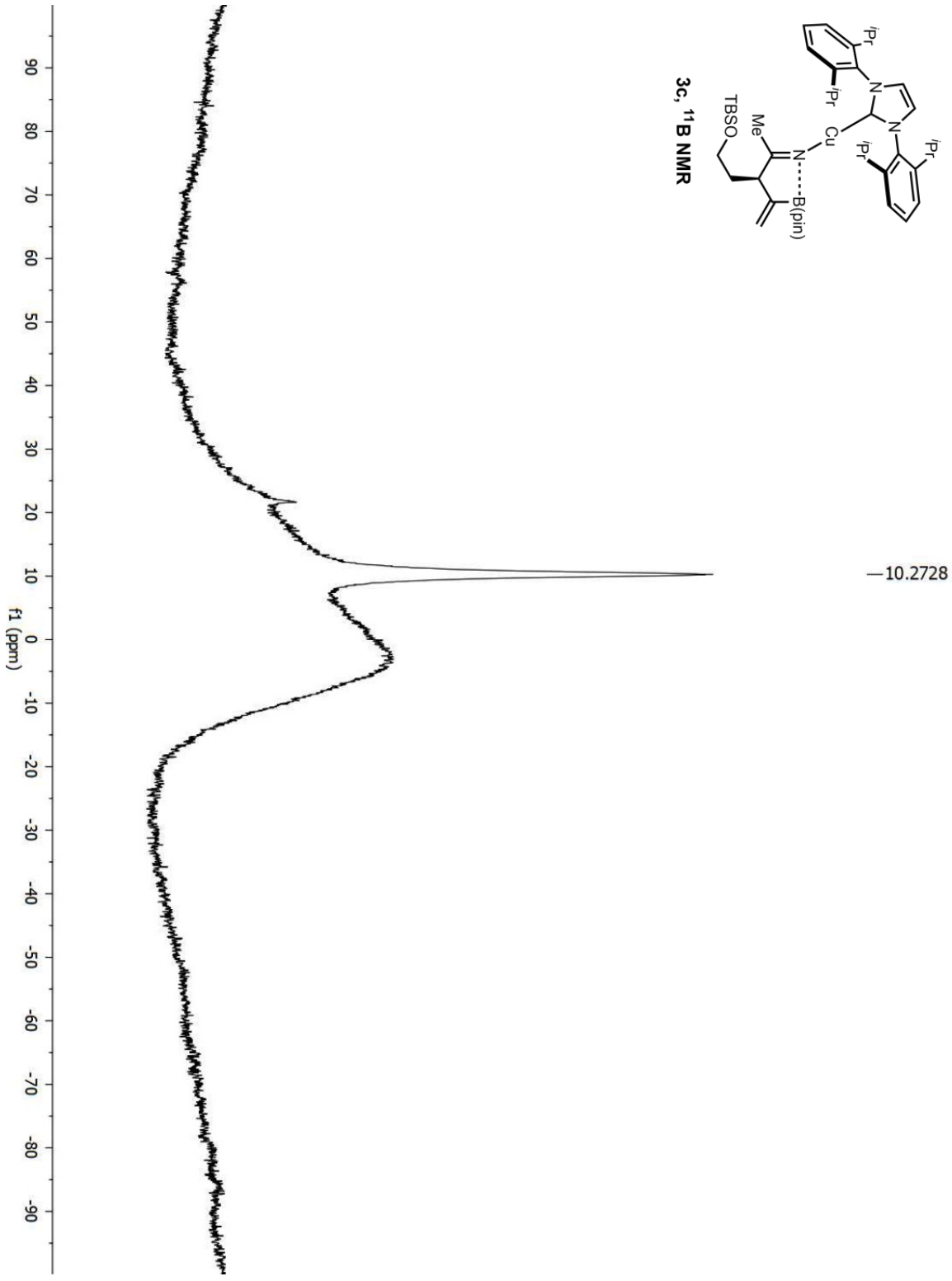
3c, $^{11}$B NMR
—10.2728
f1 (ppm)
90
80
70
60
50
40
30
20
10
0
-10
-20
-30
-40
-50
-60
-70
-80
-90
Me
TBSO
Cu
N
B(pin)

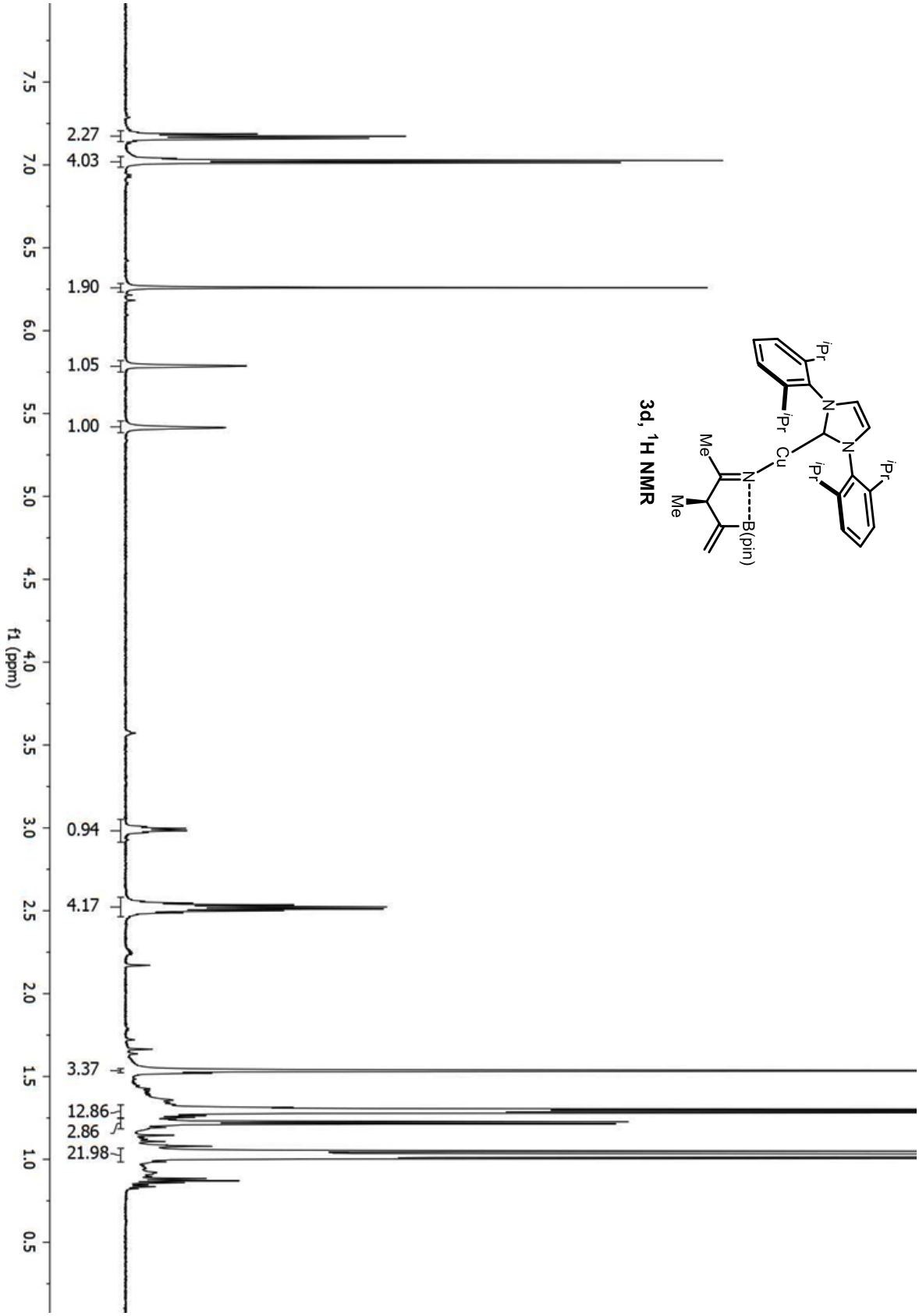
2.27
4.03
1.90
1.05
1.00
0.94
4.17
3.37
12.86
2.86
21.98
f1 (ppm)
7.5
7.0
6.5
6.0
5.5
5.0
4.5
4.0
3.5
3.0
2.5
2.0
1.5
1.0
0.5
Me
N
B(pin)
Me
Cu
N
N
iPr
iPr
iPr
iPr

**3d, $^1$H NMR**

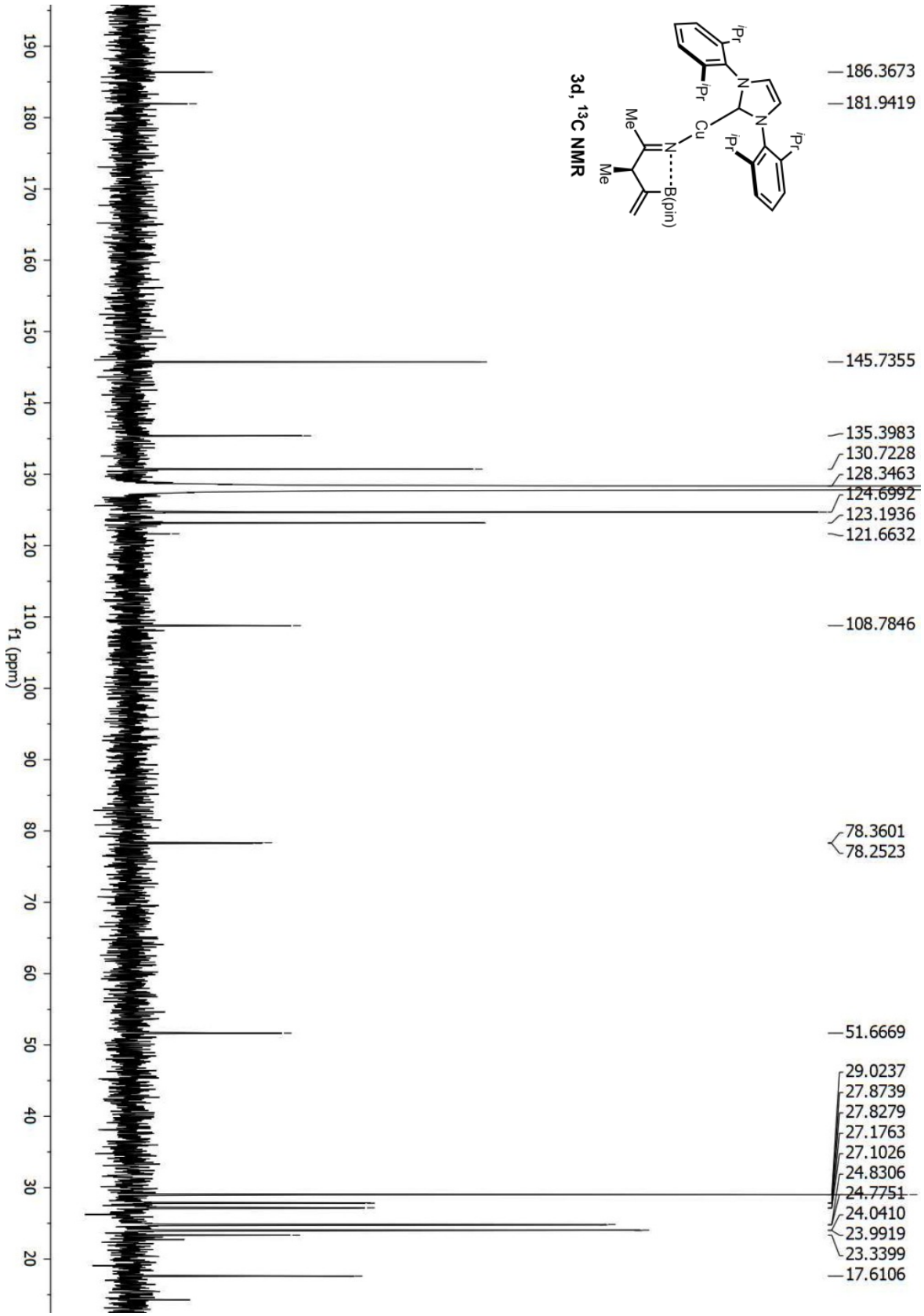
3d, $^{13}$C NMR
Me
Me
N
B(pin)
Cu
N
N
$^{i}$Pr
$^{i}$Pr
$^{i}$Pr
$^{i}$Pr
186.3673
181.9419
145.7355
135.3983
130.7228
128.3463
124.6992
123.1936
121.6632
108.7846
78.3601
78.2523
51.6669
29.0237
27.8739
27.8279
27.1763
27.1026
24.8306
24.7751
24.0410
23.9919
23.3399
17.6106
f1 (ppm)

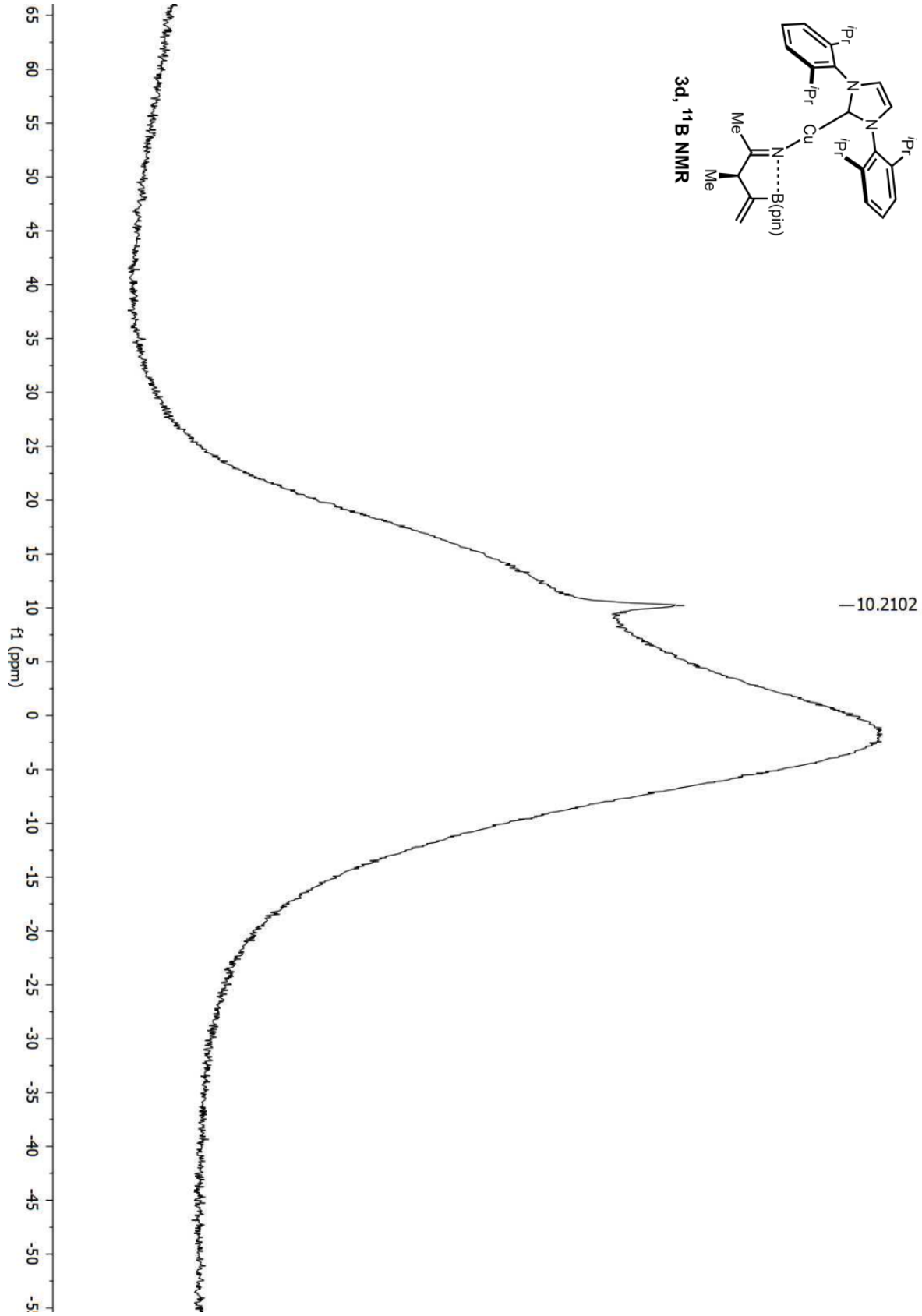
3d, $^{11}$B NMR
Me
Me
N
B(pin)
Cu
N
N
iPr
iPr
iPr
iPr
—10.2102
f1 (ppm)
65
60
55
50
45
40
35
30
25
20
15
10
5
0
-5
-10
-15
-20
-25
-30
-35
-40
-45
-50

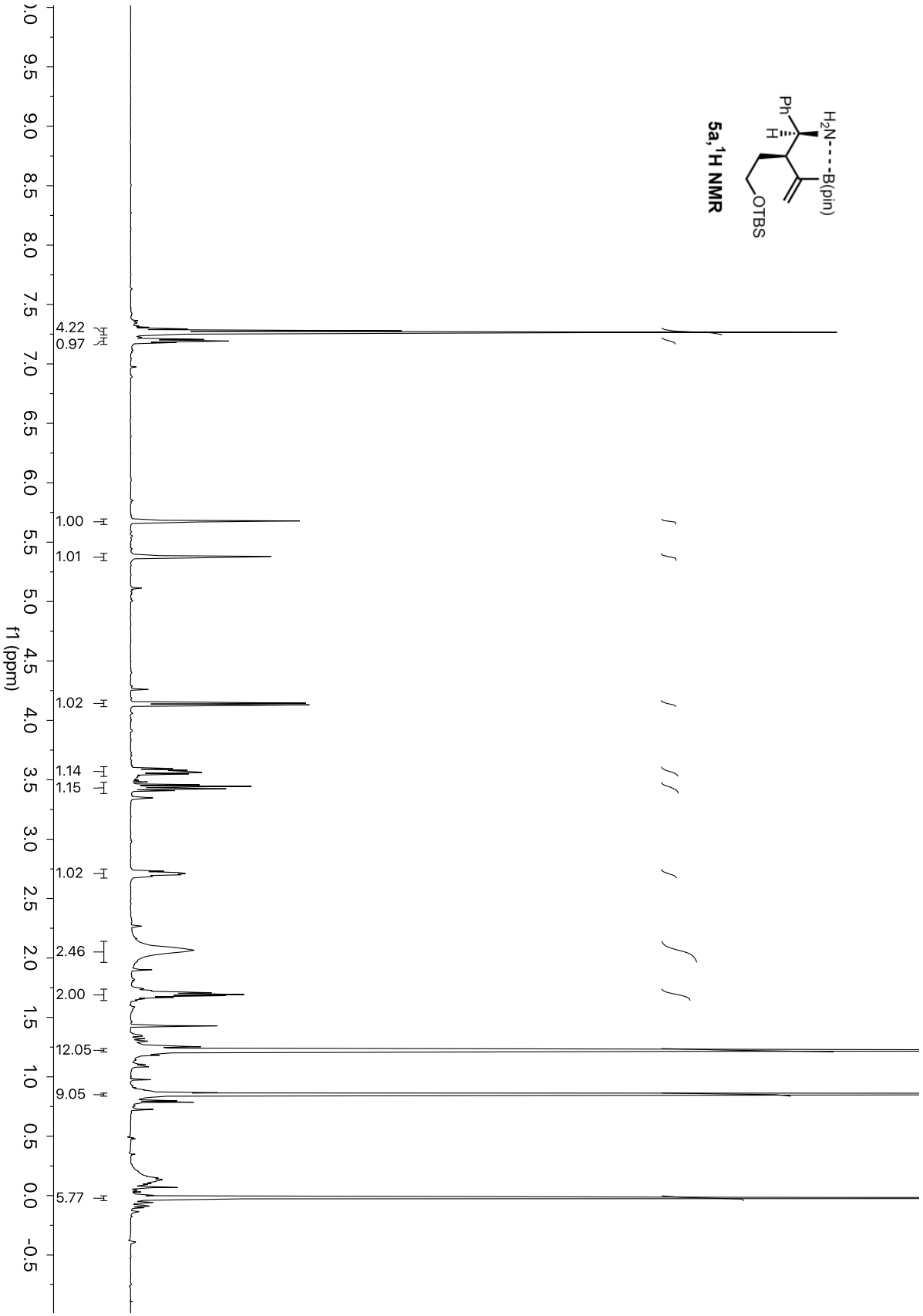
5a, $^1$H NMR
Ph
H
H$_2$N---B(pin)
OTBS
4.22
0.97
1.00
1.01
1.02
1.14
1.15
1.02
2.46
2.00
12.05
9.05
5.77
f1 (ppm)

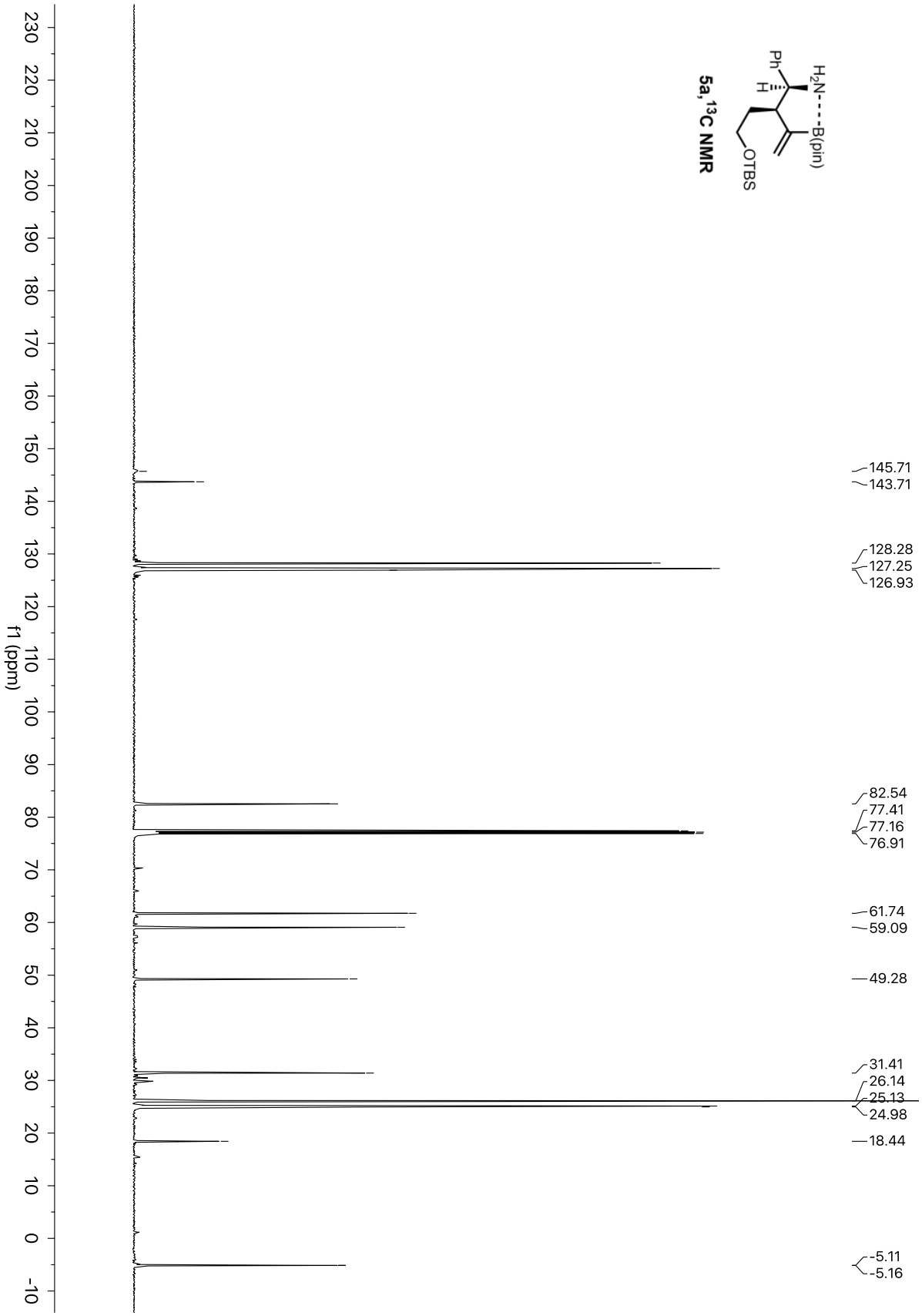
5a, 13C NMR
H2N---B(pin)
Ph
H
OTBS
145.71
143.71
128.28
127.25
126.93
82.54
77.41
77.16
76.91
61.74
59.09
49.28
31.41
26.14
25.13
24.98
18.44
-5.11
-5.16
f1 (ppm)

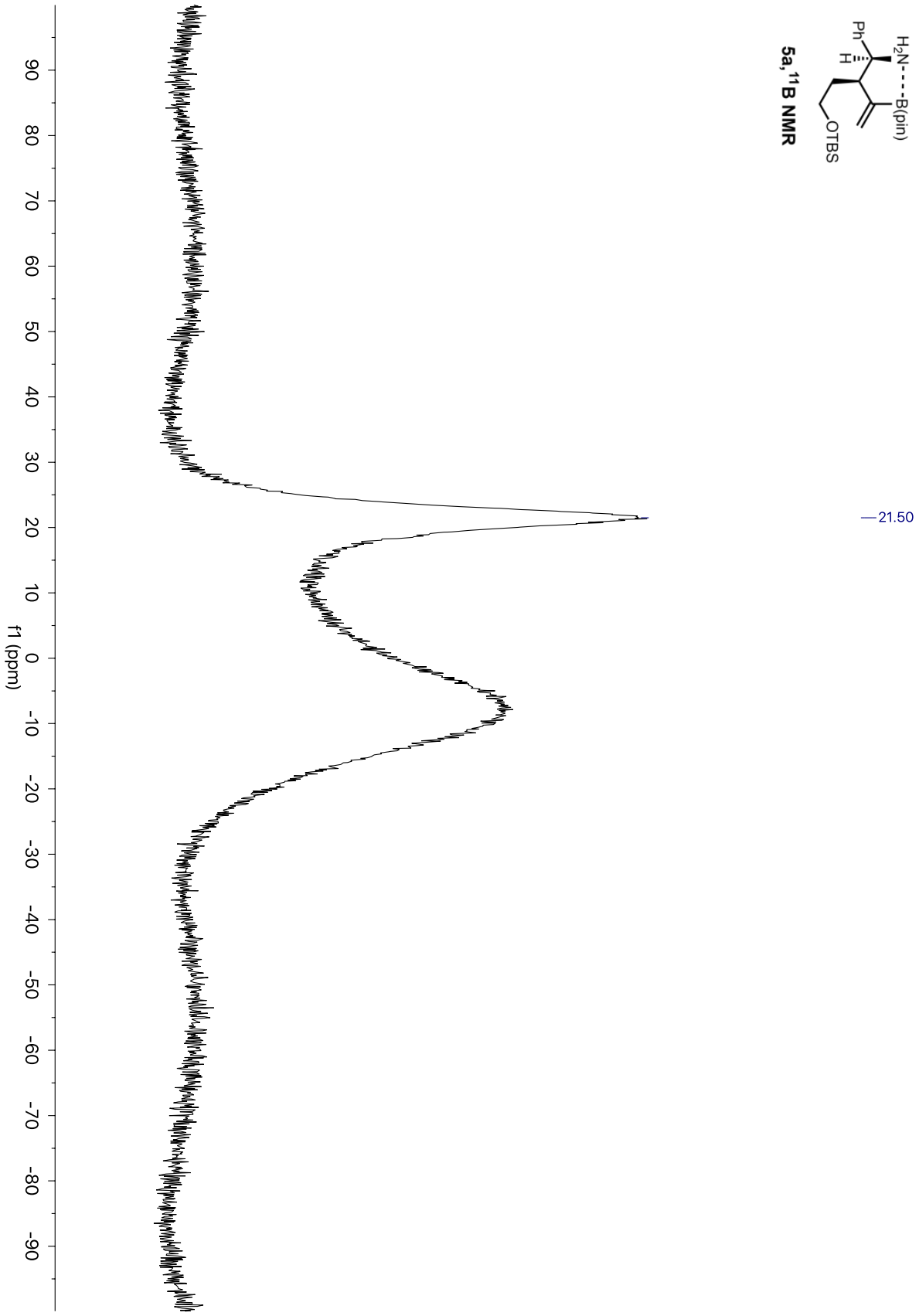
5a, $^{11}$B NMR
Ph
H
$H_2N$----B(pin)
OTBS
21.50
f1 (ppm)
90
80
70
60
50
40
30
20
10
0
-10
-20
-30
-40
-50
-60
-70
-80
-90

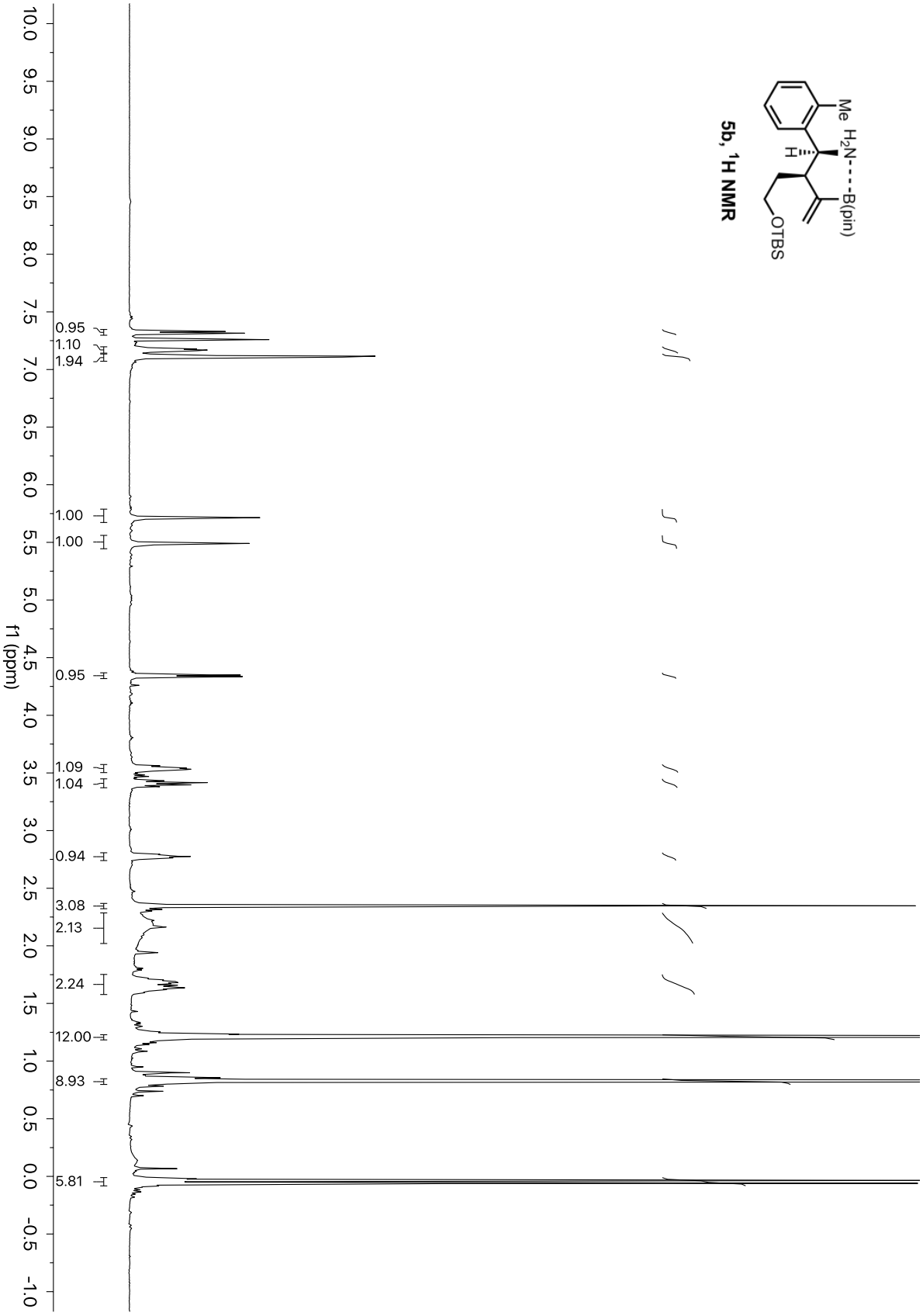
Me
H2N---B(pin)
H
OTBS
5b, 1H NMR
f1 (ppm)
10.0
9.5
9.0
8.5
8.0
7.5
7.0
6.5
6.0
5.5
5.0
4.5
4.0
3.5
3.0
2.5
2.0
1.5
1.0
0.5
0.0
-0.5
-1.0
0.95
1.10
1.94
1.00
1.00
0.95
1.09
1.04
0.94
3.08
2.13
2.24
12.00
8.93
5.81

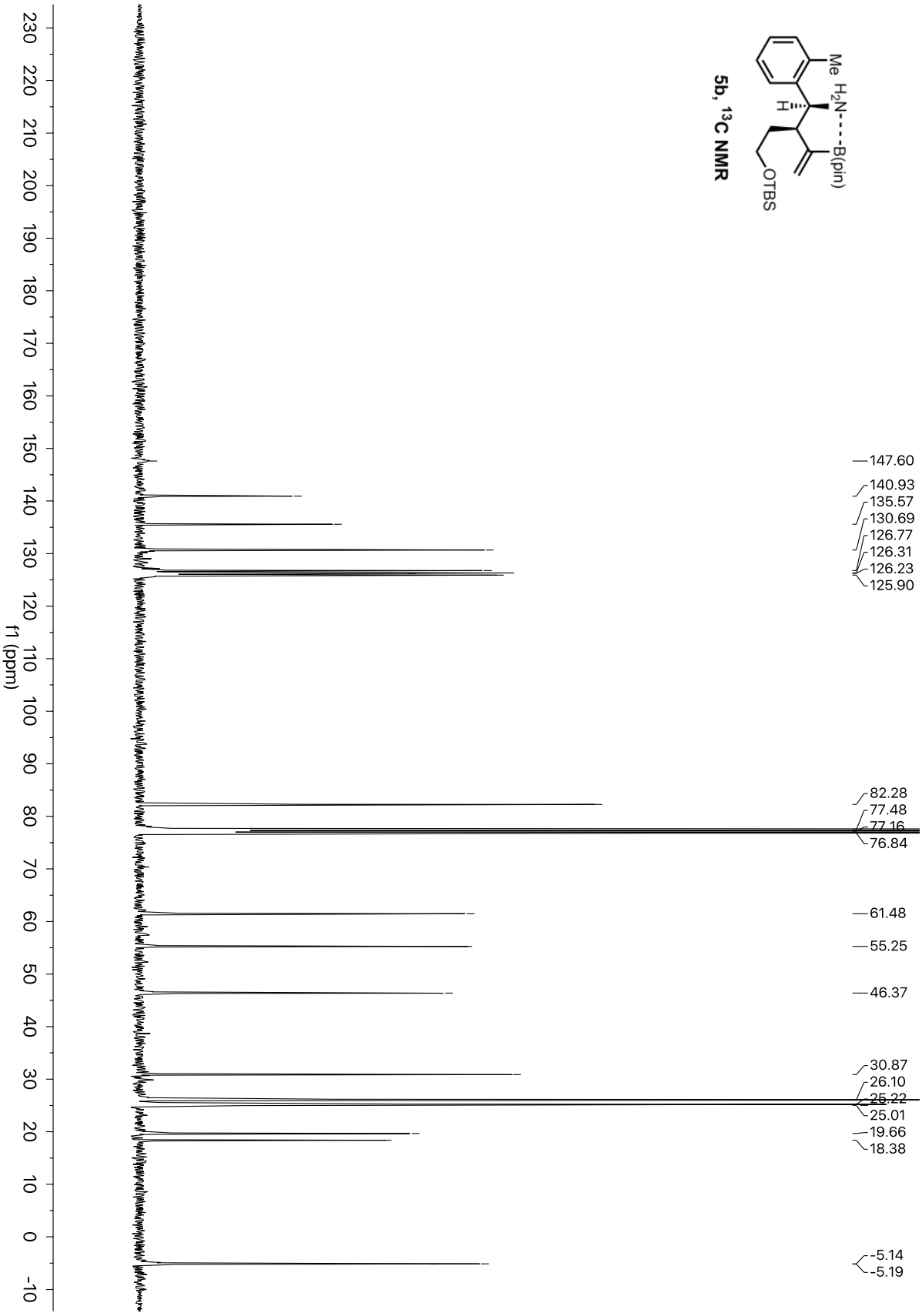
5b, $^{13}$C NMR
Me
$H_2N$---B(pin)
H
OTBS
147.60
140.93
135.57
130.69
126.77
126.31
126.23
125.90
82.28
77.48
77.16
76.84
61.48
55.25
46.37
30.87
26.10
25.22
25.01
19.66
18.38
-5.14
-5.19
f1 (ppm)
230 220 210 200 190 180 170 160 150 140 130 120 110 100 90 80 70 60 50 40 30 20 10 0 -10

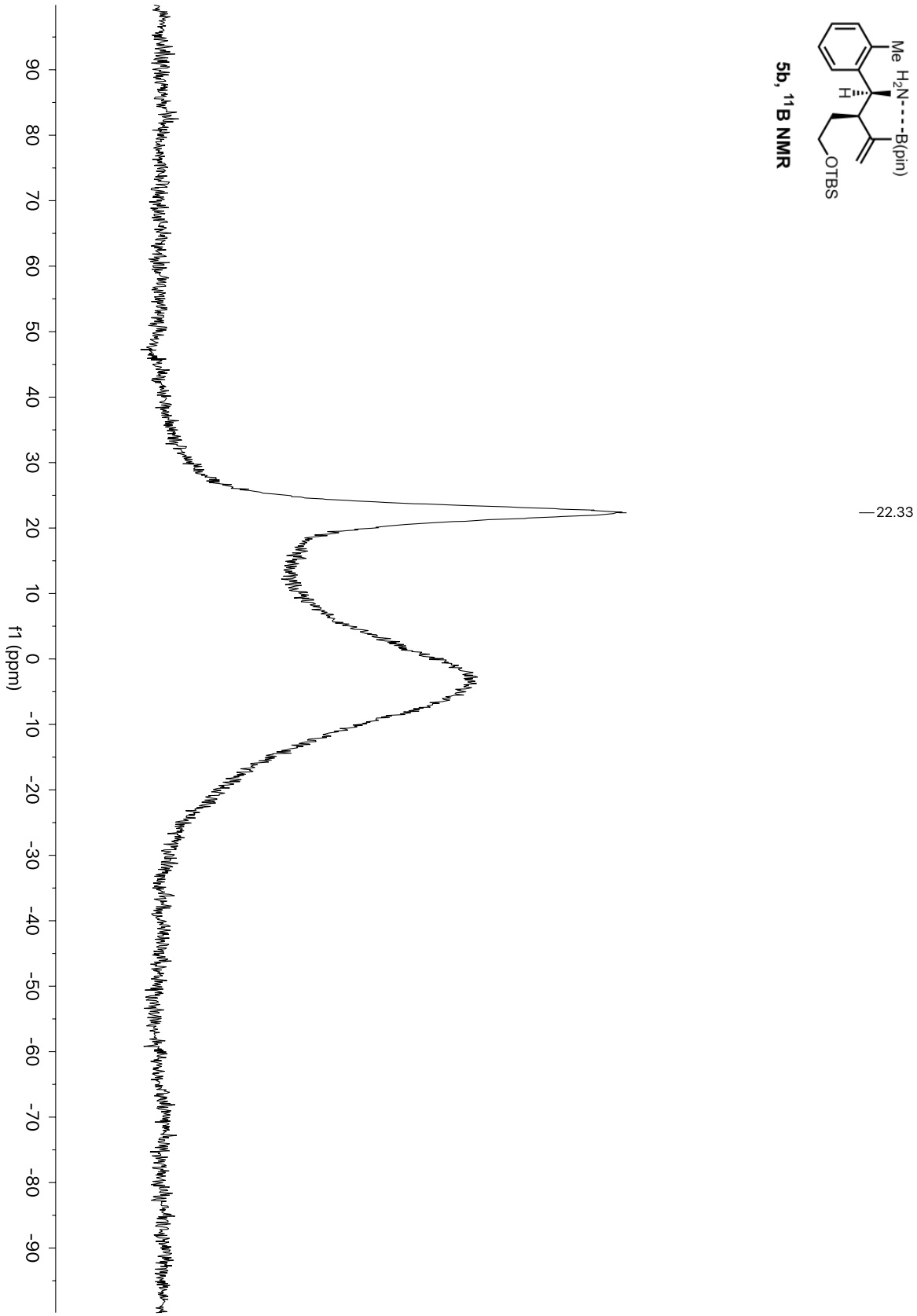
Me
H2N---B(pin)
H
OTBS
5b, 11B NMR
22.33
f1 (ppm)
90
80
70
60
50
40
30
20
10
0
-10
-20
-30
-40
-50
-60
-70
-80
-90

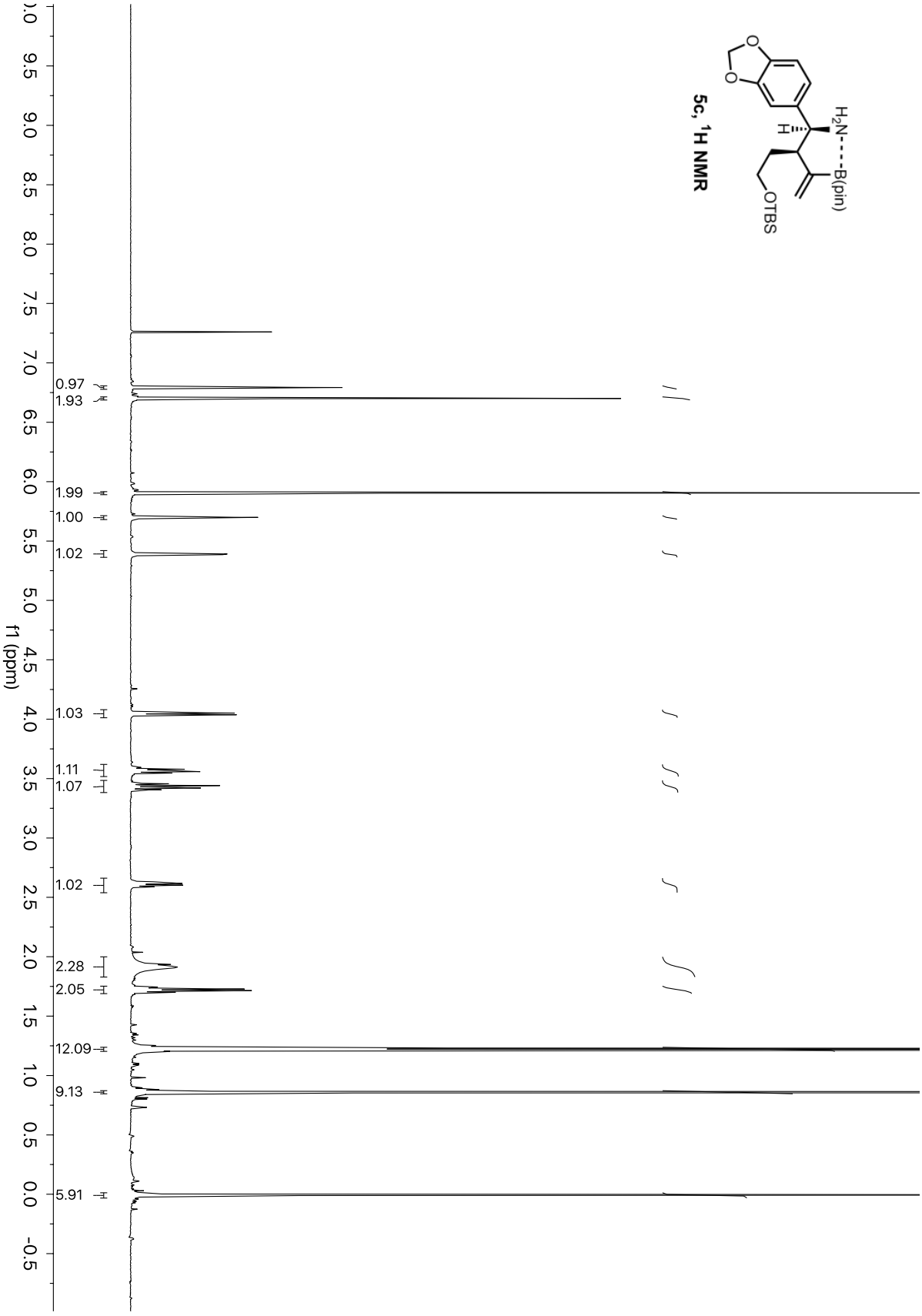
5c, 1H NMR
H2N---B(pin)
H
OTBS
f1 (ppm)
0.97
1.93
1.99
1.00
1.02
1.03
1.11
1.07
1.02
2.28
2.05
12.09
9.13
5.91

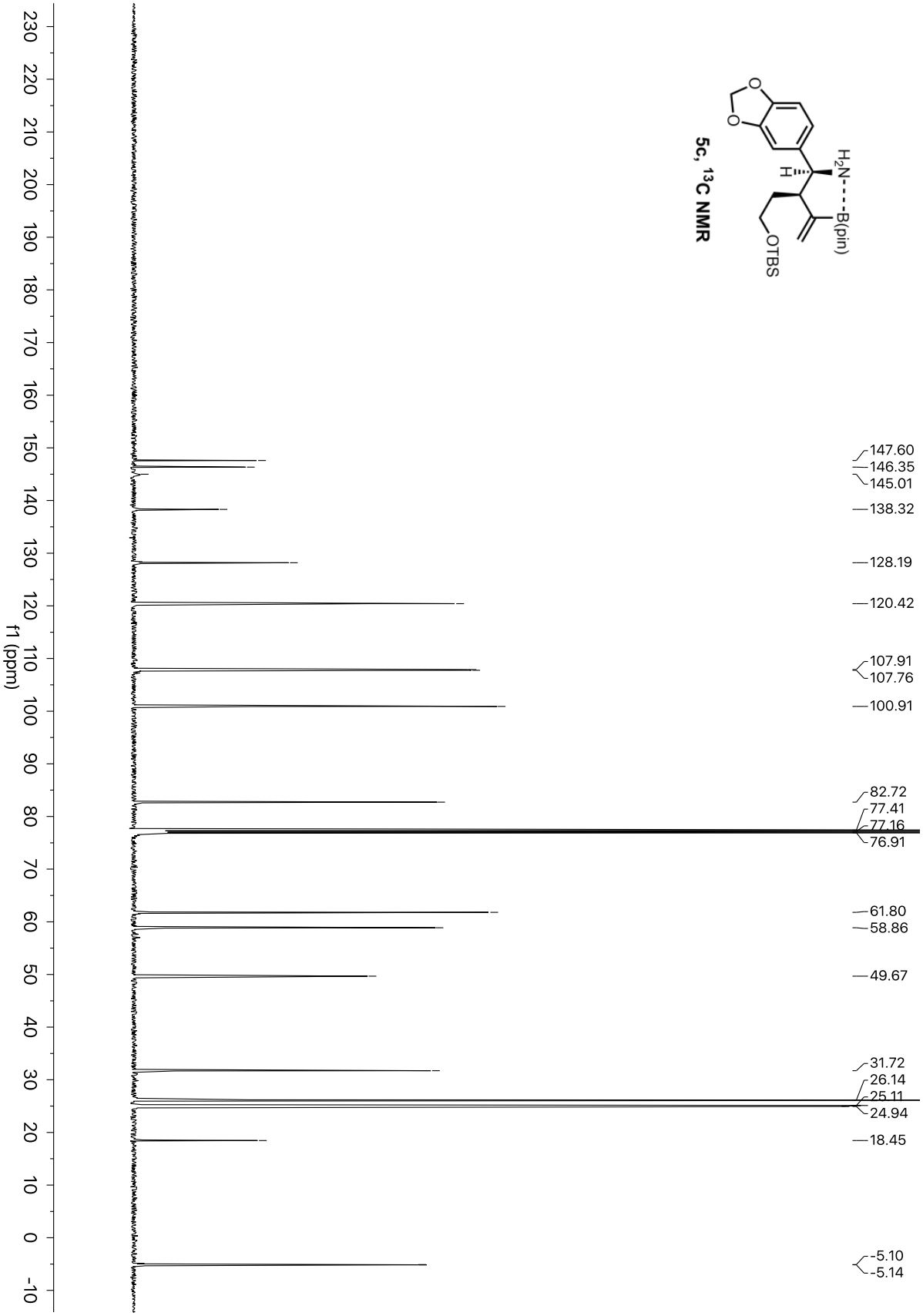
5c, $^{13}$C NMR
$H_2N$----B(pin)
H
OTBS
f1 (ppm)
230
220
210
200
190
180
170
160
150
140
130
120
110
100
90
80
70
60
50
40
30
20
10
0
-10
147.60
146.35
145.01
138.32
128.19
120.42
107.91
107.76
100.91
82.72
77.41
77.16
76.91
61.80
58.86
49.67
31.72
26.14
25.11
24.94
18.45
-5.10
-5.14

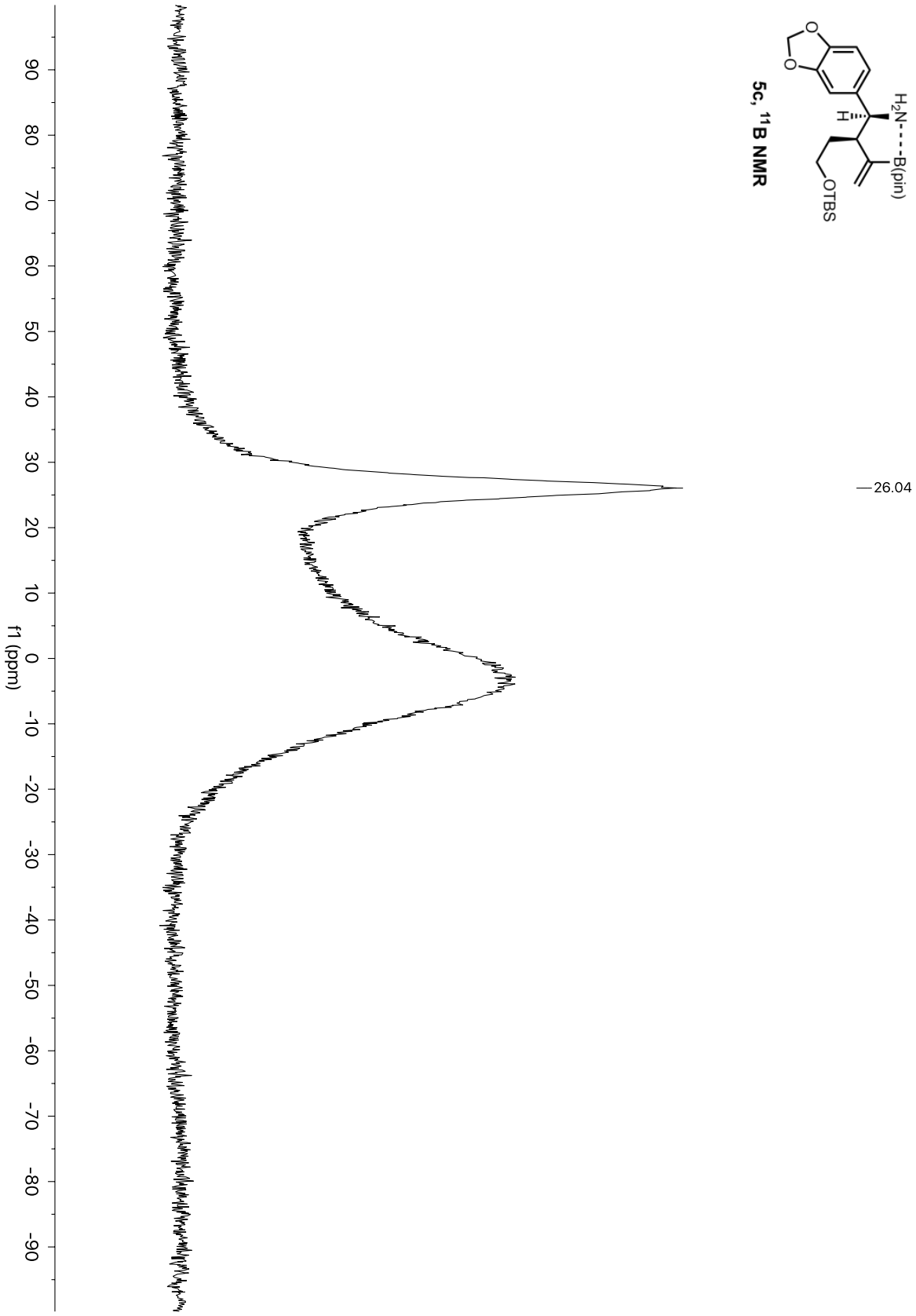
H2N---B(pin)
H
OTBS
5c, 11B NMR
26.04
90
80
70
60
50
40
30
20
10
0
-10
-20
-30
-40
-50
-60
-70
-80
-90
f1 (ppm)

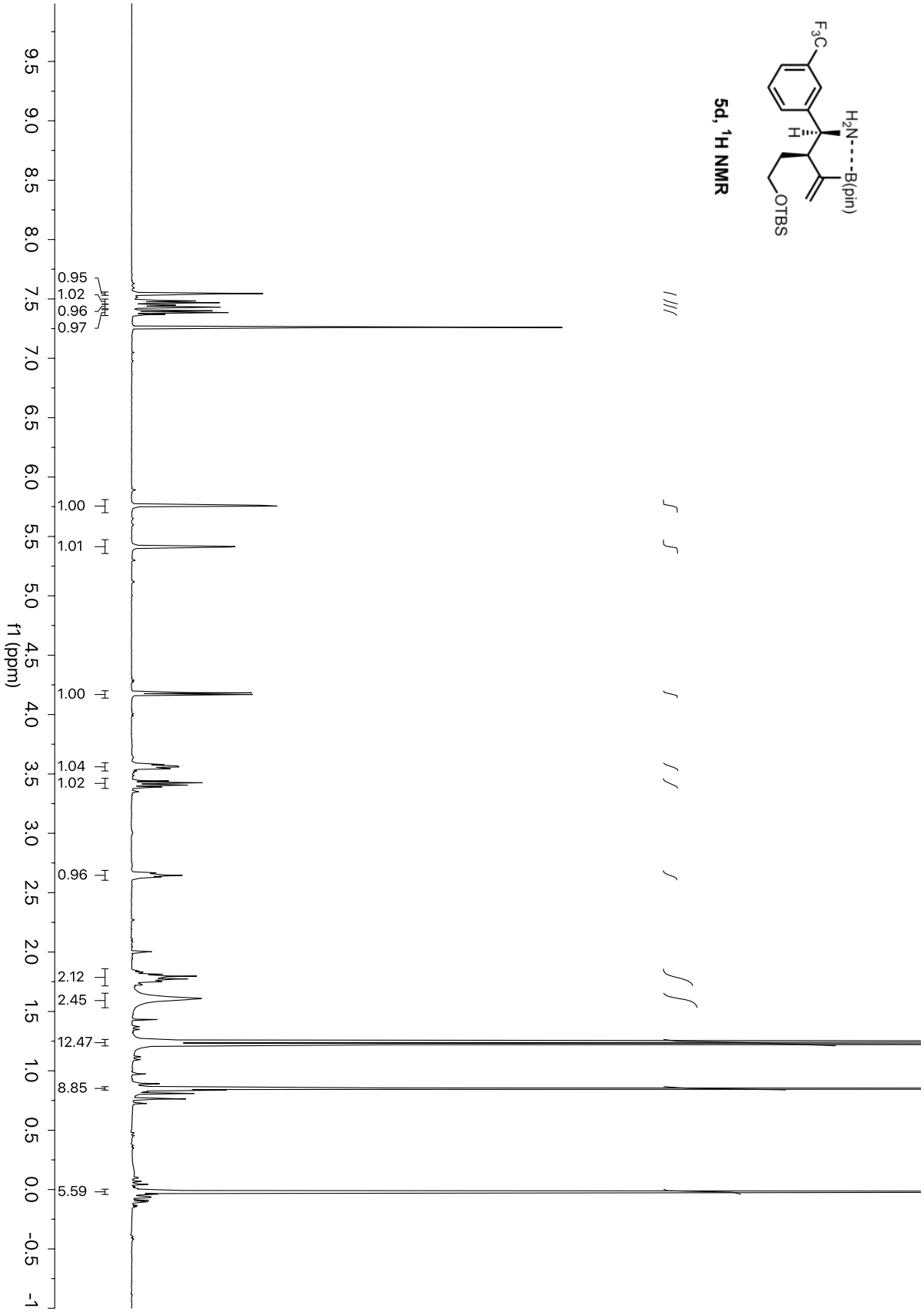
5d, $^1$H NMR
$F_3C$
$H_2N$---B(pin)
H
OTBS
f1 (ppm)
0.95
1.02
0.96
0.97
1.00
1.01
1.00
1.04
1.02
0.96
2.12
2.45
12.47
8.85
5.59

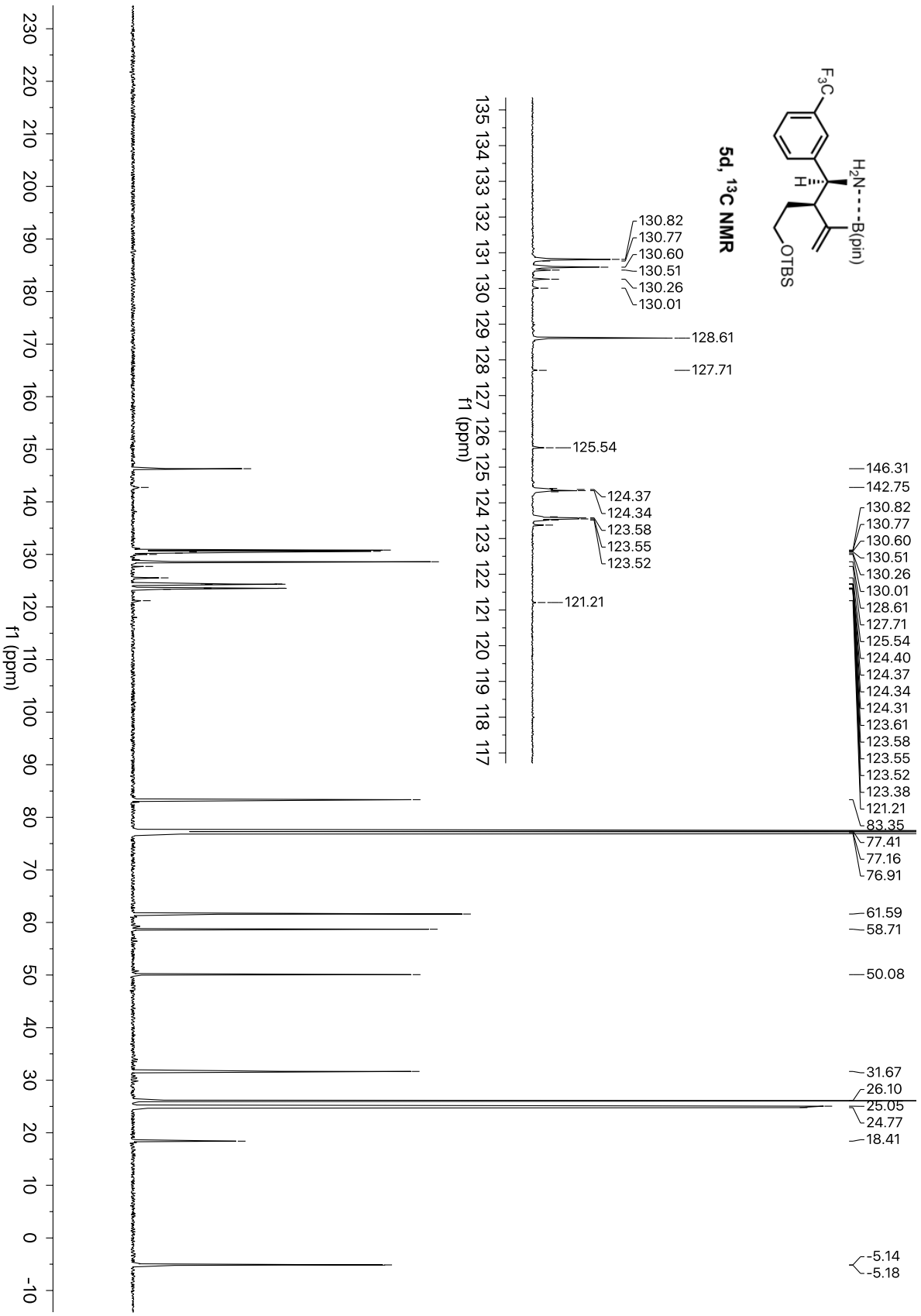
5d, 13C NMR
F3C
H2N----B(pin)
H
OTBS
f1 (ppm)
130.82
130.77
130.60
130.51
130.26
130.01
128.61
127.71
125.54
124.37
124.34
123.58
123.55
123.52
121.21
146.31
142.75
130.82
130.77
130.60
130.51
130.26
130.01
128.61
127.71
125.54
124.40
124.37
124.34
124.31
123.61
123.58
123.55
123.52
123.38
121.21
83.35
77.41
77.16
76.91
61.59
58.71
50.08
31.67
26.10
25.05
24.77
18.41
-5.14
-5.18

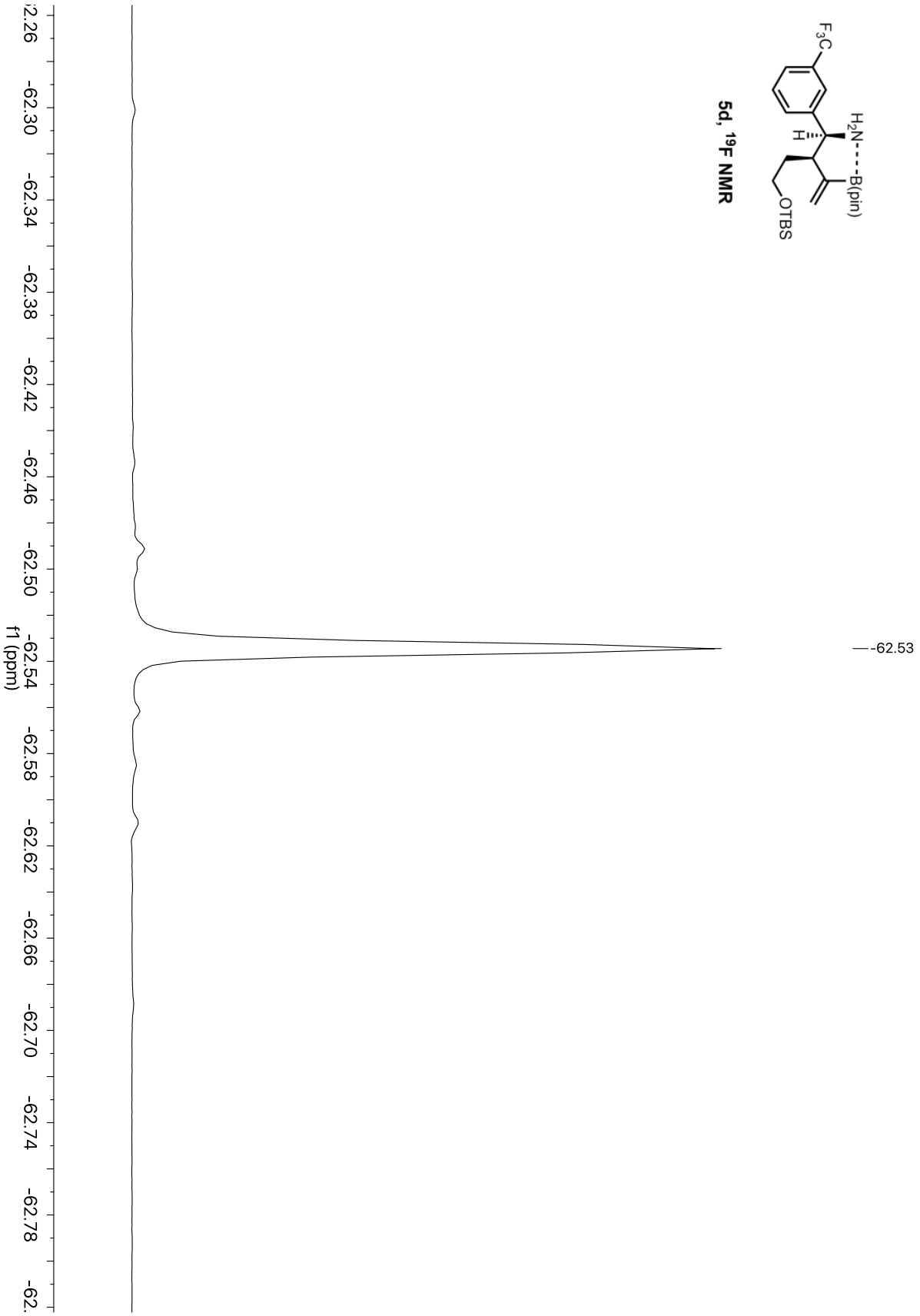
F3C
H2N---B(pin)
H
OTBS
5d, 19F NMR
-62.53
-62.26
-62.30
-62.34
-62.38
-62.42
-62.46
-62.50
-62.54
-62.58
-62.62
-62.66
-62.70
-62.74
-62.78
-62.
f1 (ppm)

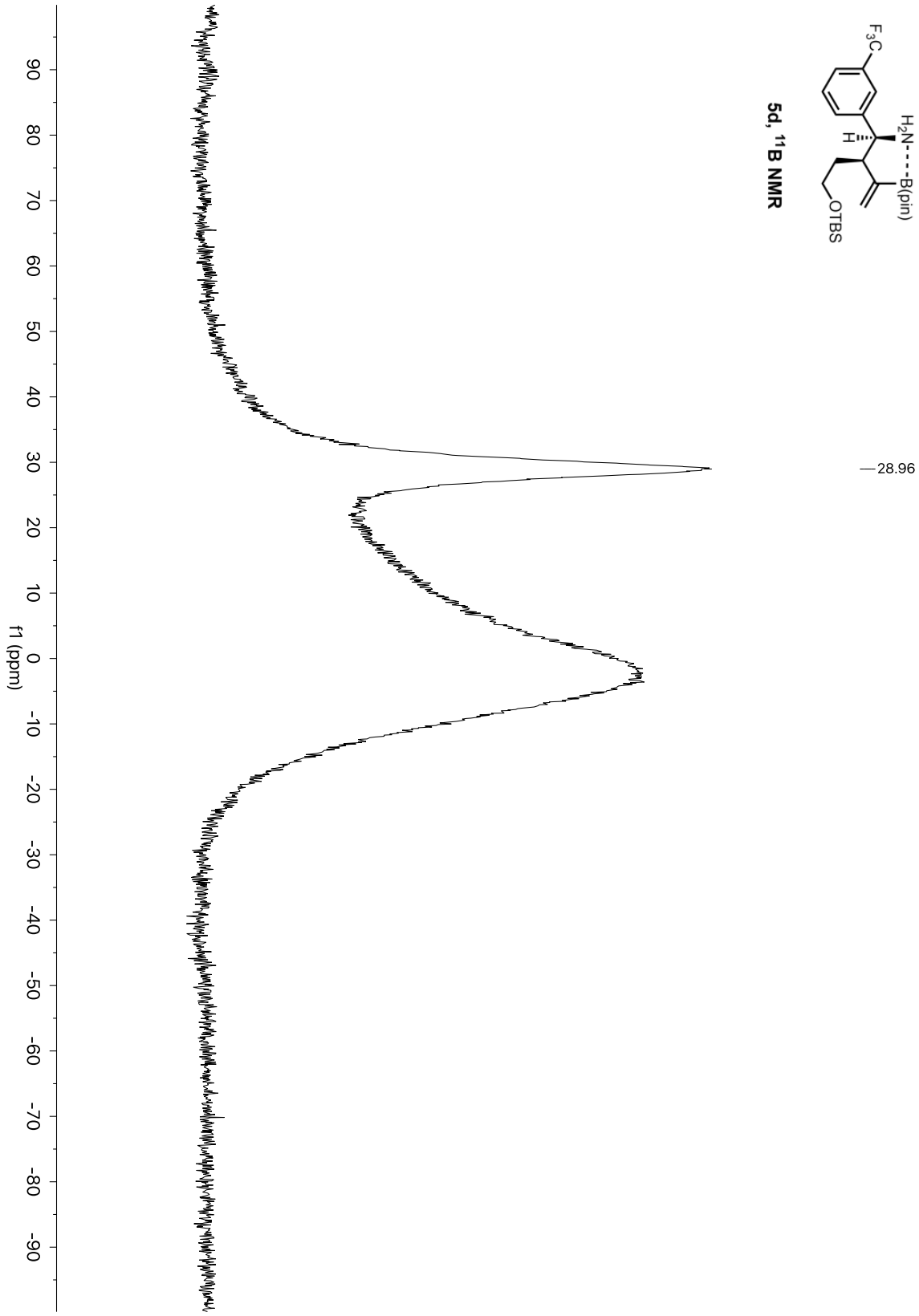
F3C
H2N---B(pin)
H
OTBS
5d, 11B NMR
28.96
90
80
70
60
50
40
30
20
10
0
-10
-20
-30
-40
-50
-60
-70
-80
-90
f1 (ppm)

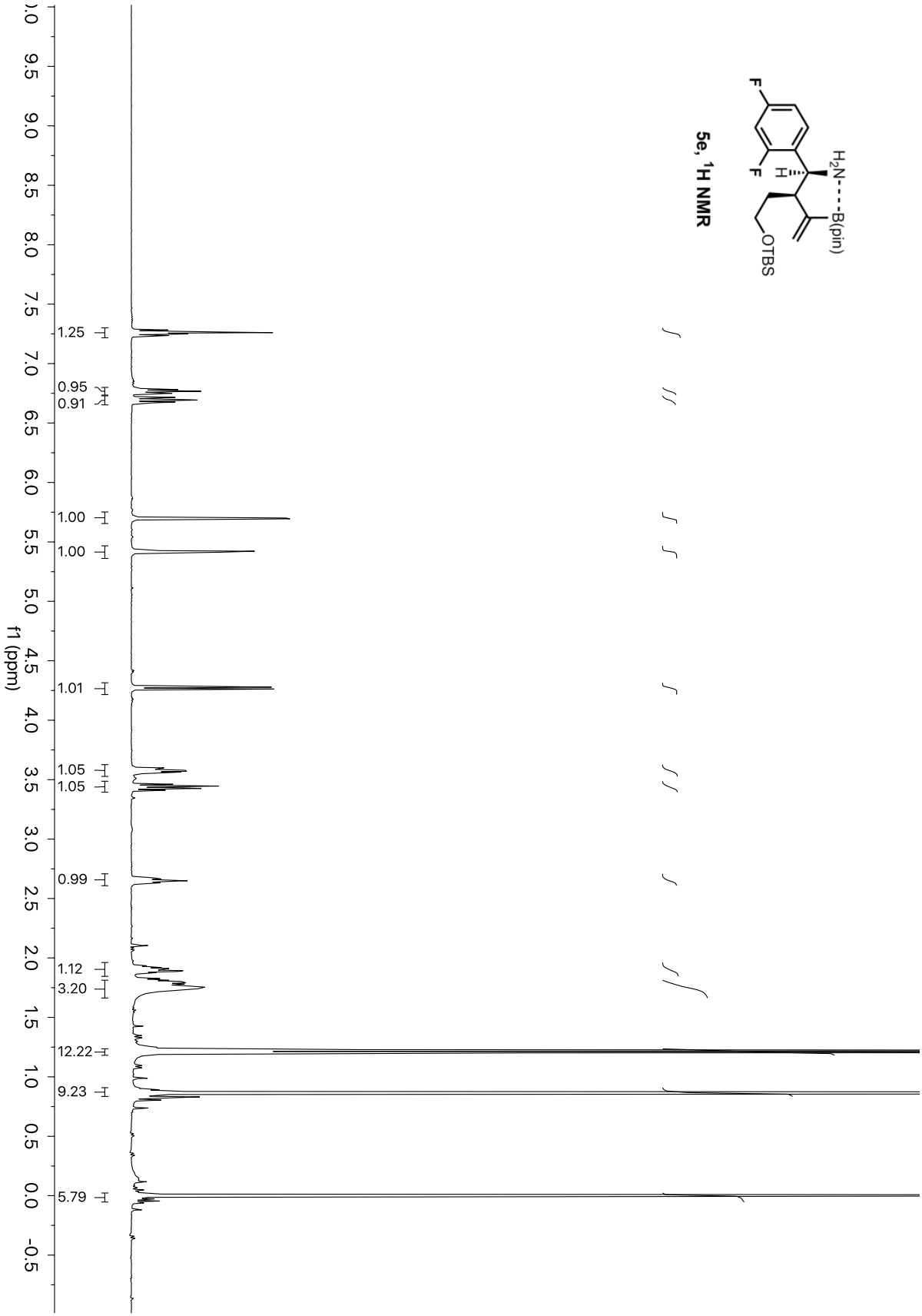
5e, 1H NMR
F
F
H
H2N---B(pin)
OTBS
f1 (ppm)
1.25
0.95
0.91
1.00
1.00
1.01
1.05
1.05
0.99
1.12
3.20
12.22
9.23
5.79

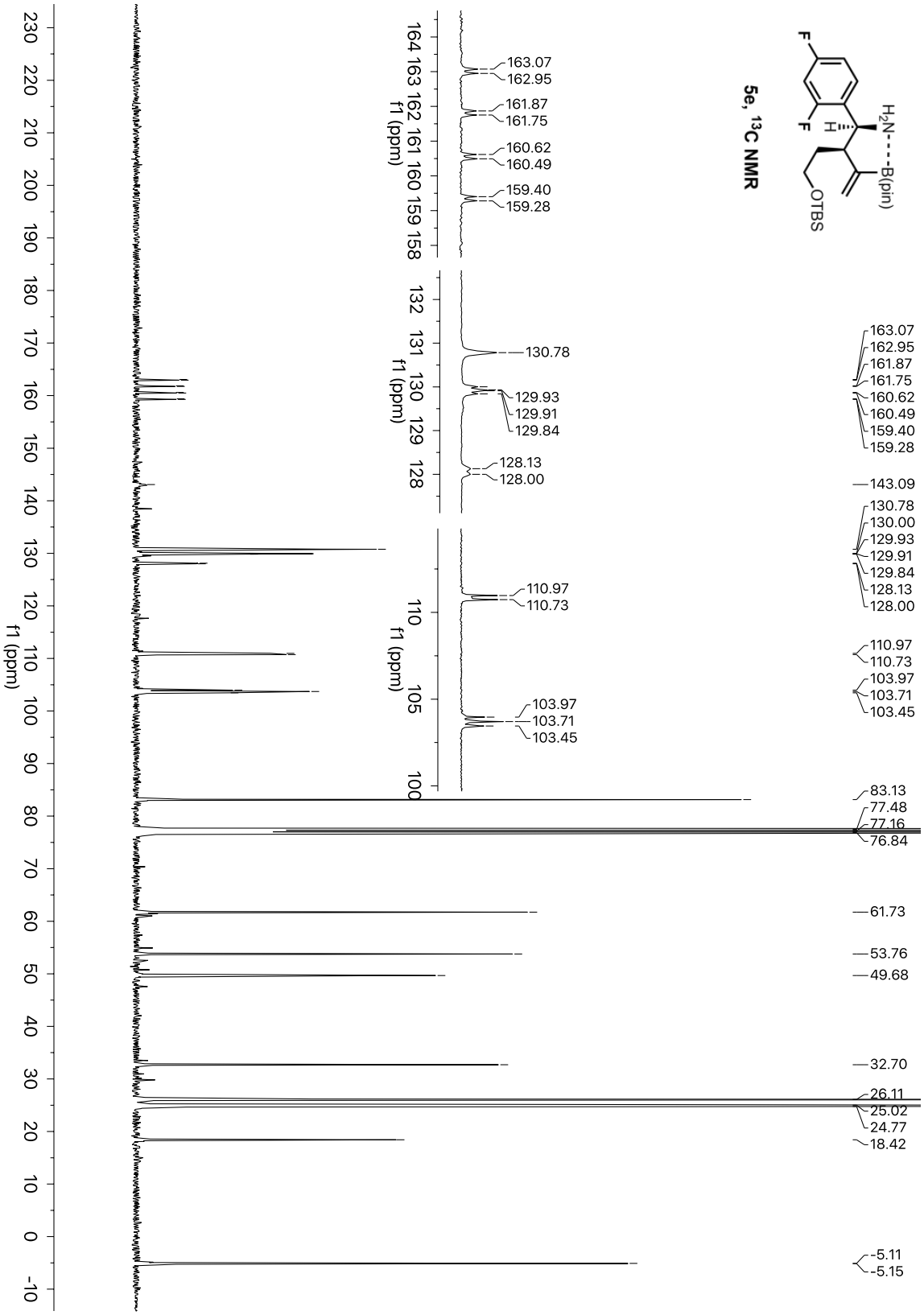
5e, $^{13}$C NMR
F
F
H
H$_2$N----B(pin)
OTBS
163.07
162.95
161.87
161.75
160.62
160.49
159.40
159.28
130.78
129.93
129.91
129.84
128.13
128.00
110.97
110.73
103.97
103.71
103.45
143.09
130.00
83.13
77.48
77.16
76.84
61.73
53.76
49.68
32.70
26.11
25.02
24.77
18.42
-5.11
-5.15
f1 (ppm)

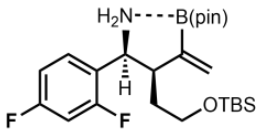
H2N----B(pin)
H
F
F
OTBS

**5e, $^{19}$F NMR**


-113.19
-113.21
-113.22
-113.24
-113.26
-113.27
-112.6
-113.0
-113.4
-113.8
-114.2
-114.6
f1 (ppm)
100
80
60
40
20
0
-20
-40
-60
-80
-100
-120
-140
-160
-180
-200
-220
-240
-260
-280
-300
f1 (ppm)

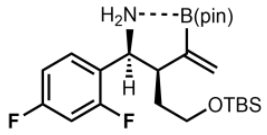
H2N----B(pin)
H
F
F
OTBS

**5e, $^{11}$B NMR**

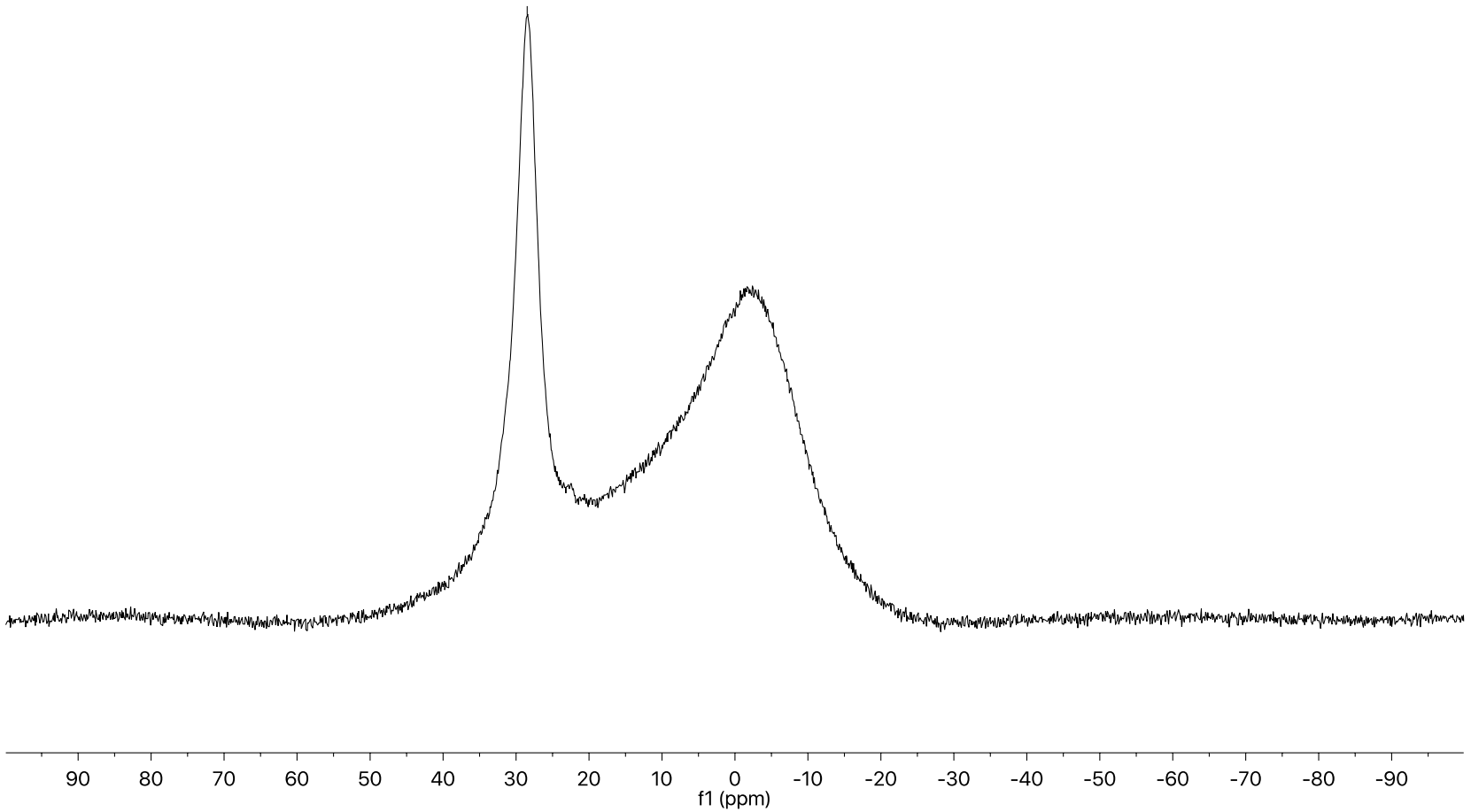
28.47
90
80
70
60
50
40
30
20
10
0
-10
-20
-30
-40
-50
-60
-70
-80
-90
f1 (ppm)

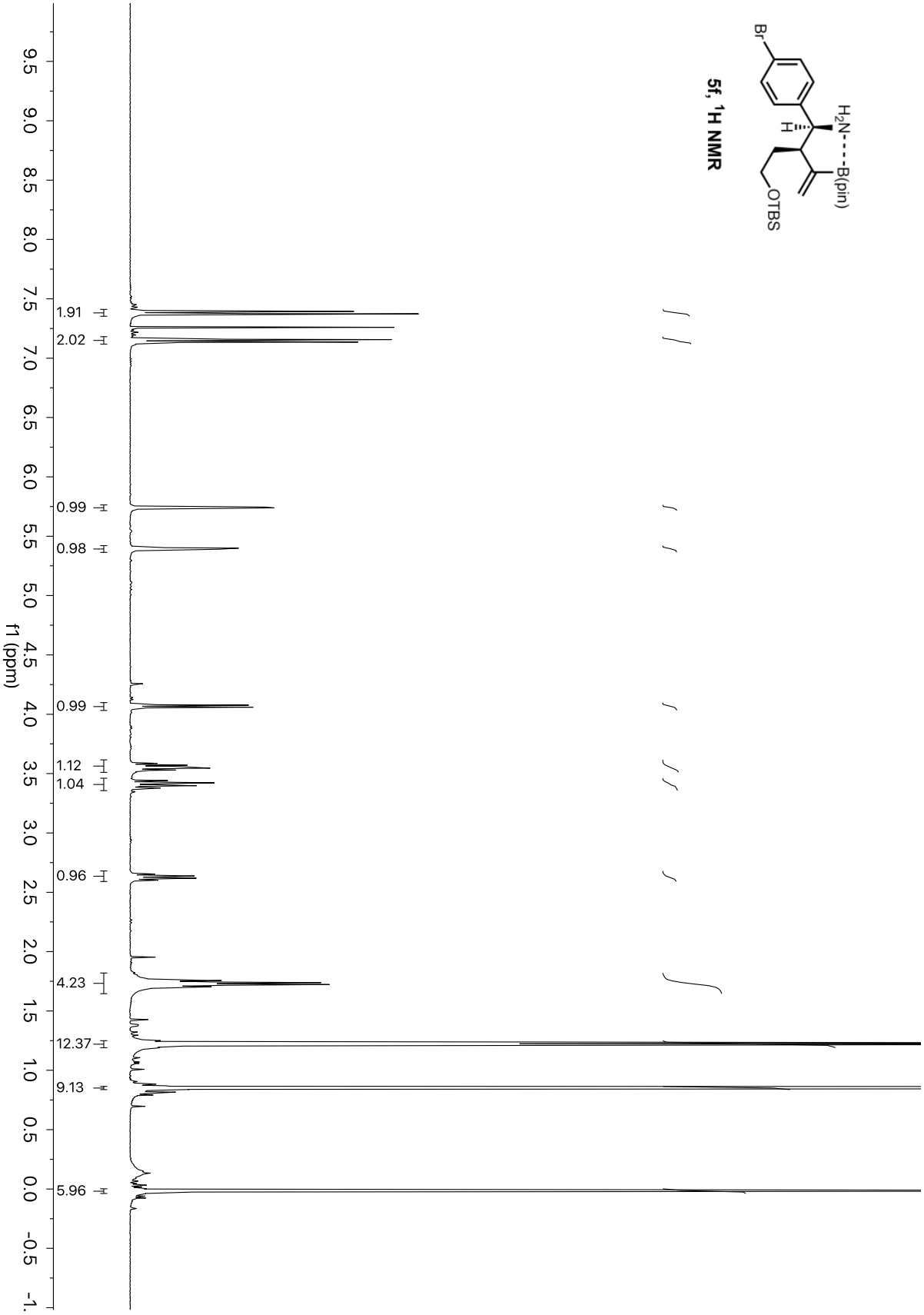
5f, 1H NMR
Br
H2N---B(pin)
H
OTBS
f1 (ppm)
1.91
2.02
0.99
0.98
0.99
1.12
1.04
0.96
4.23
12.37
9.13
5.96

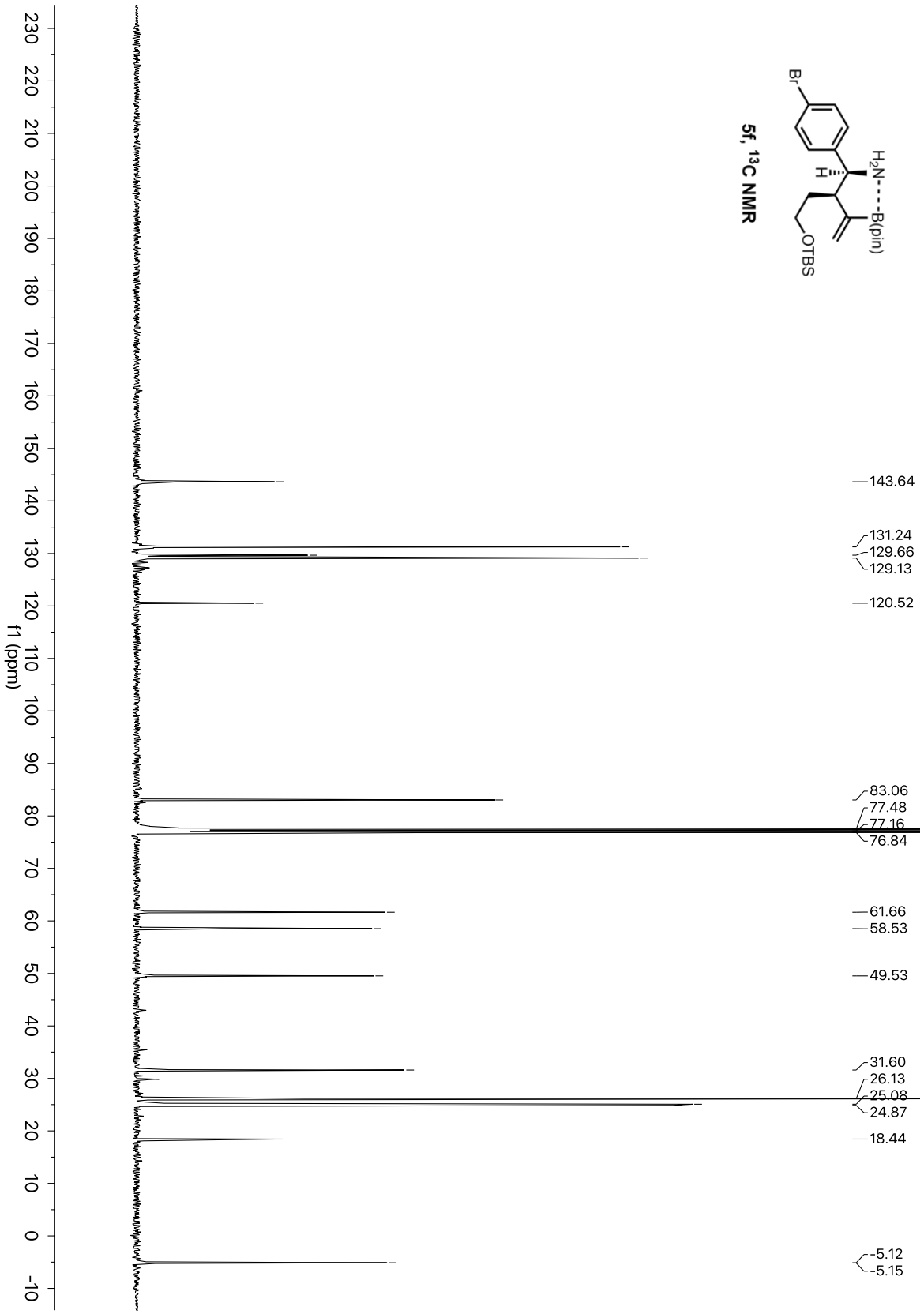
5f, $^{13}$C NMR
Br
H
$H_2N$---B(pin)
OTBS
143.64
131.24
129.66
129.13
120.52
83.06
77.48
77.16
76.84
61.66
58.53
49.53
31.60
26.13
25.08
24.87
18.44
-5.12
-5.15
f1 (ppm)
230 220 210 200 190 180 170 160 150 140 130 120 110 100 90 80 70 60 50 40 30 20 10 0 -10

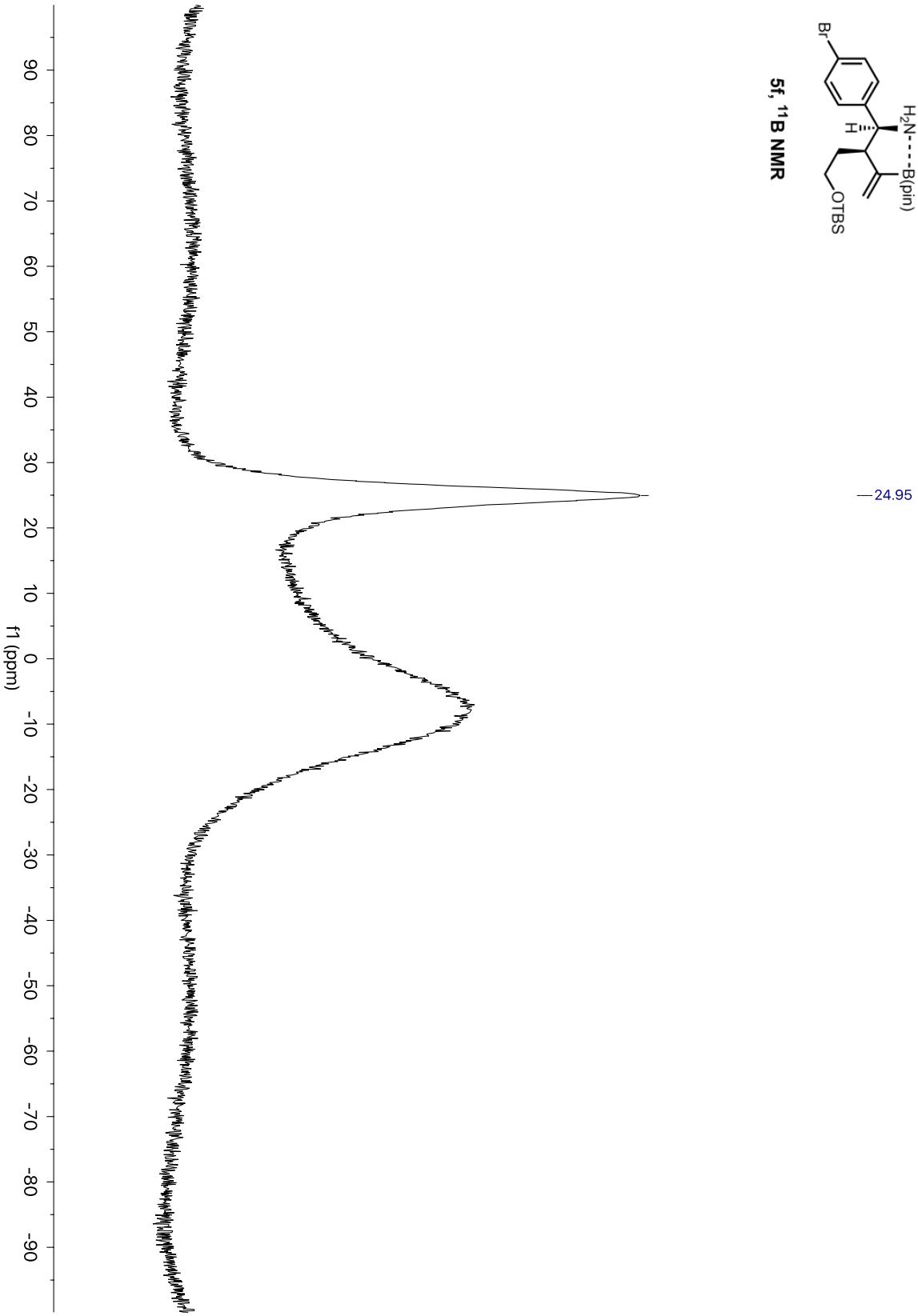
Br
H
H2N---B(pin)
OTBS
5f, 11B NMR
24.95
f1 (ppm)
90
80
70
60
50
40
30
20
10
0
-10
-20
-30
-40
-50
-60
-70
-80
-90

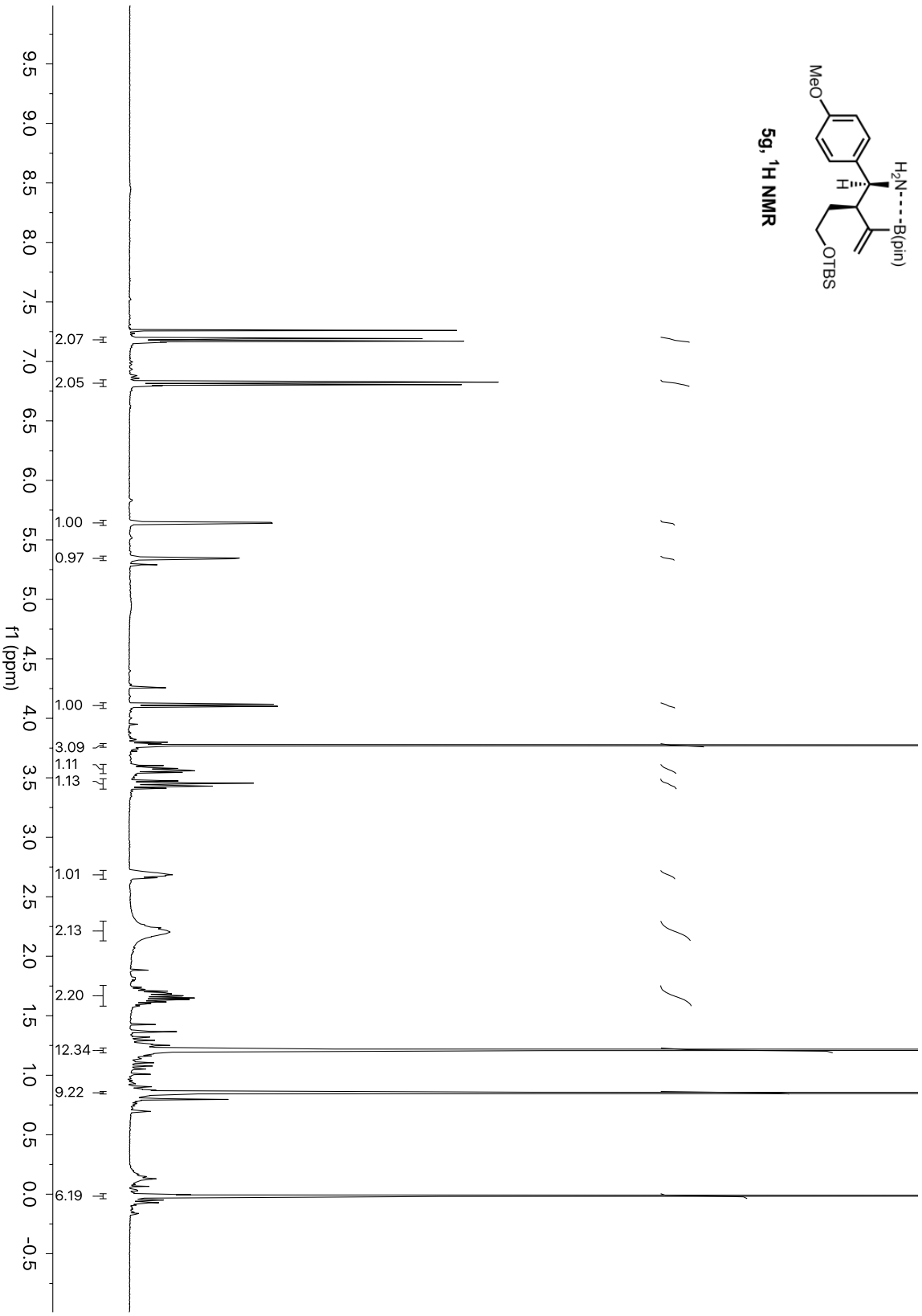
MeO
H
H2N---B(pin)
OTBS
5g, 1H NMR
f1 (ppm)
2.07
2.05
1.00
0.97
1.00
3.09
1.11
1.13
1.01
2.13
2.20
12.34
9.22
6.19

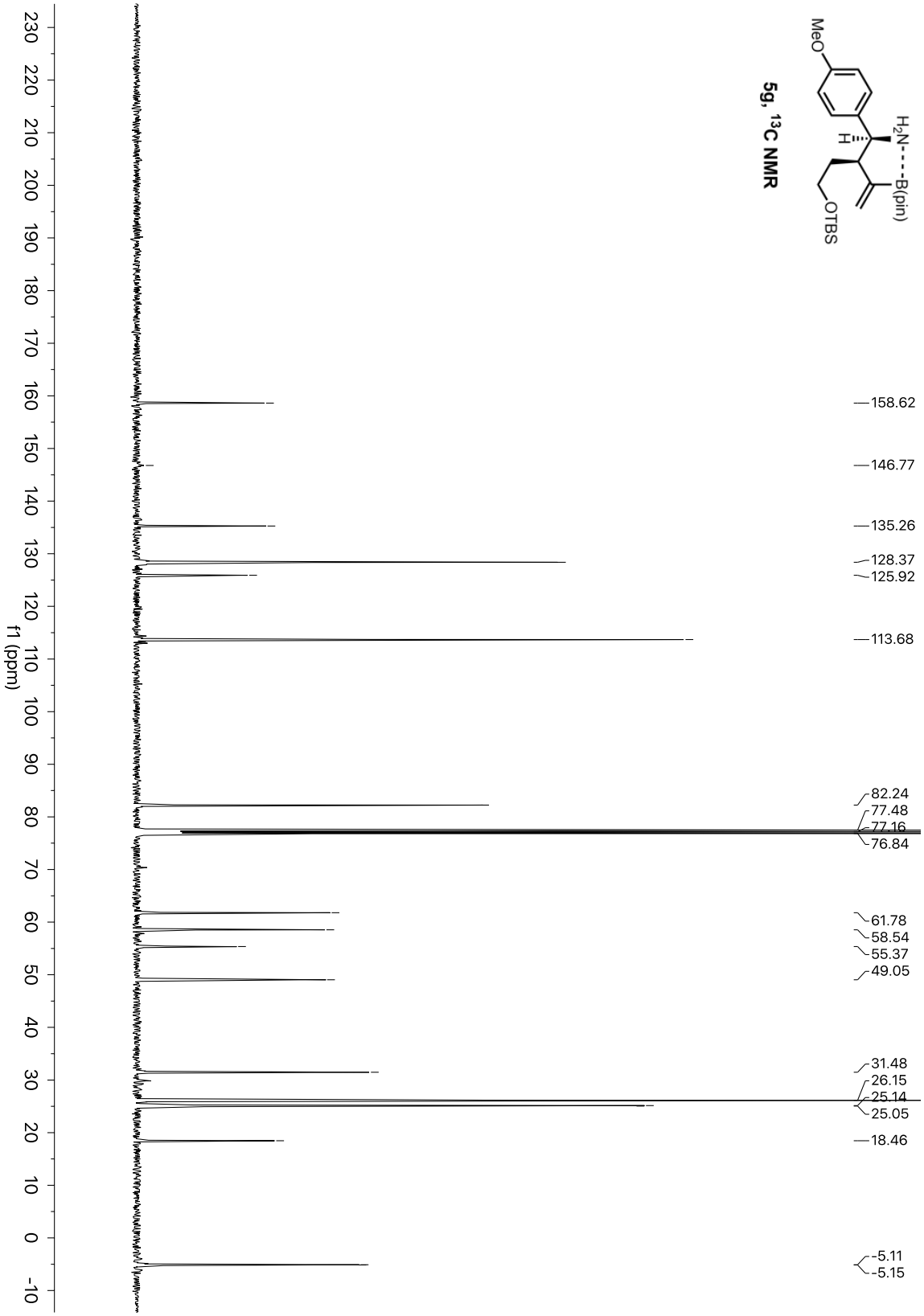
MeO
H
H2N---B(pin)
OTBS
5g, 13C NMR
158.62
146.77
135.26
128.37
125.92
113.68
82.24
77.48
77.16
76.84
61.78
58.54
55.37
49.05
31.48
26.15
25.14
25.05
18.46
-5.11
-5.15
f1 (ppm)

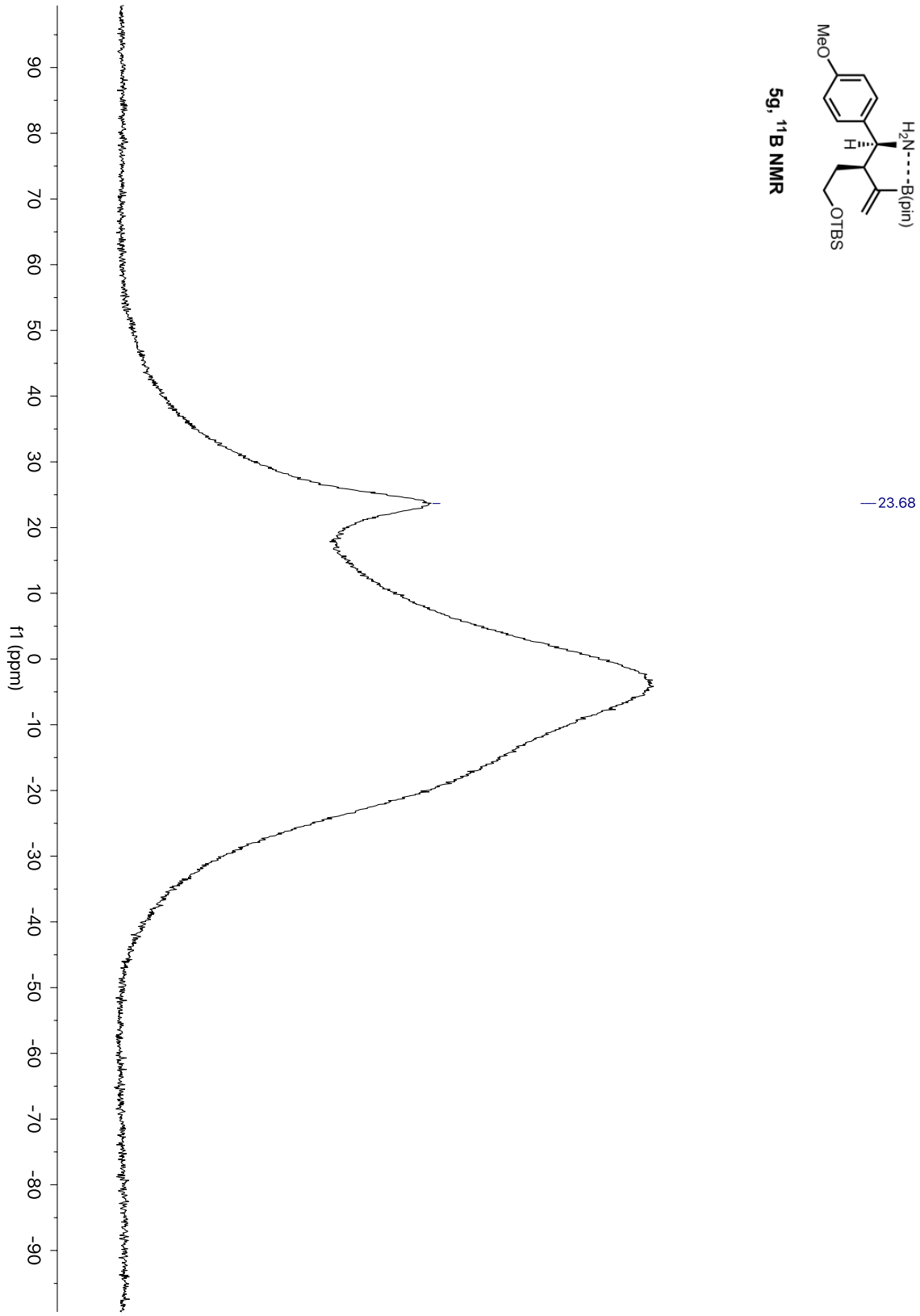
MeO
H
H2N---B(pin)
OTBS
5g, 11B NMR
23.68
f1 (ppm)
90
80
70
60
50
40
30
20
10
0
-10
-20
-30
-40
-50
-60
-70
-80
-90

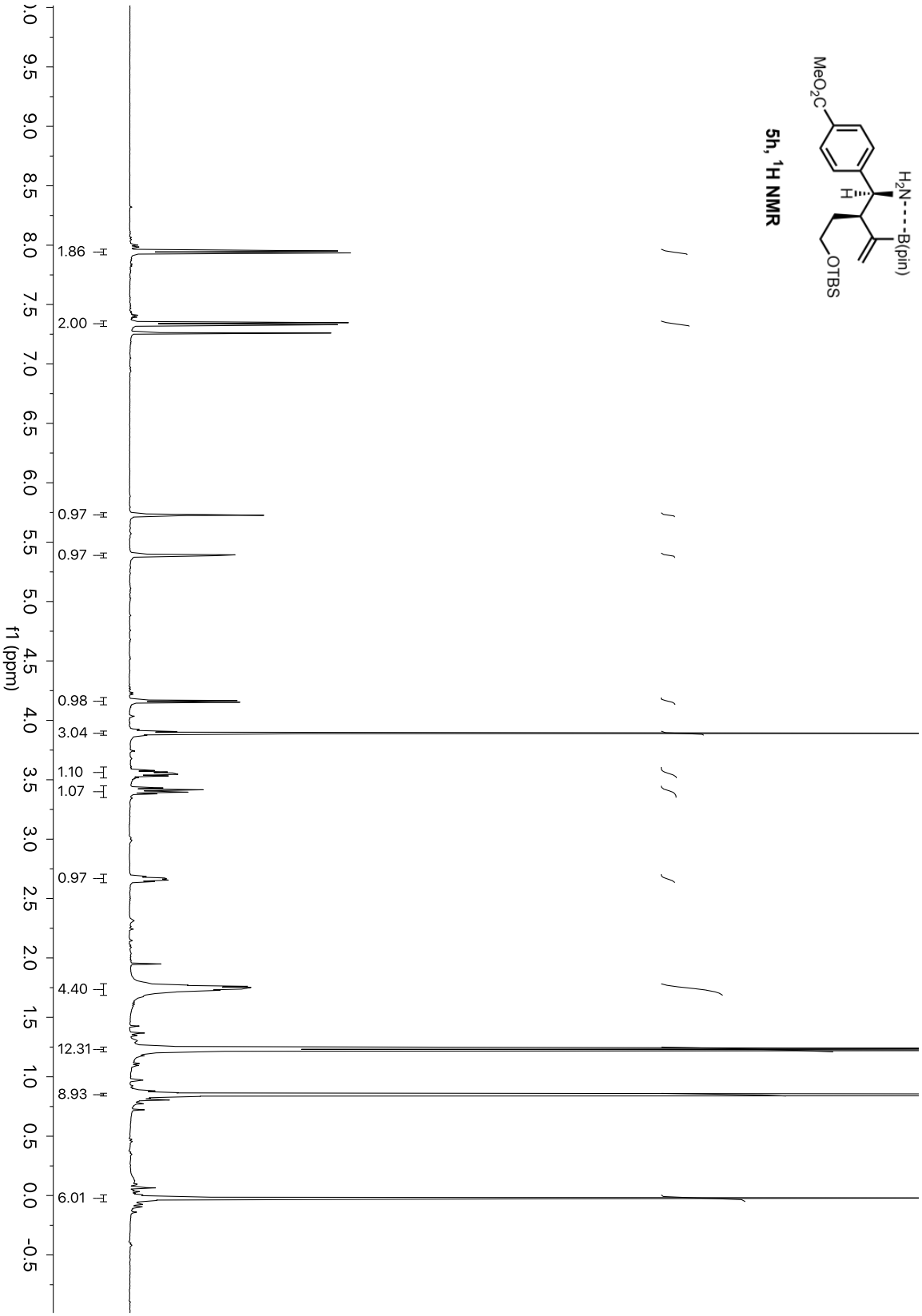
5h, $^1$H NMR
$MeO_2C$
$H_2N$---B(pin)
H
OTBS
f1 (ppm)
1.86
2.00
0.97
0.97
0.98
3.04
1.10
1.07
0.97
4.40
12.31
8.93
6.01

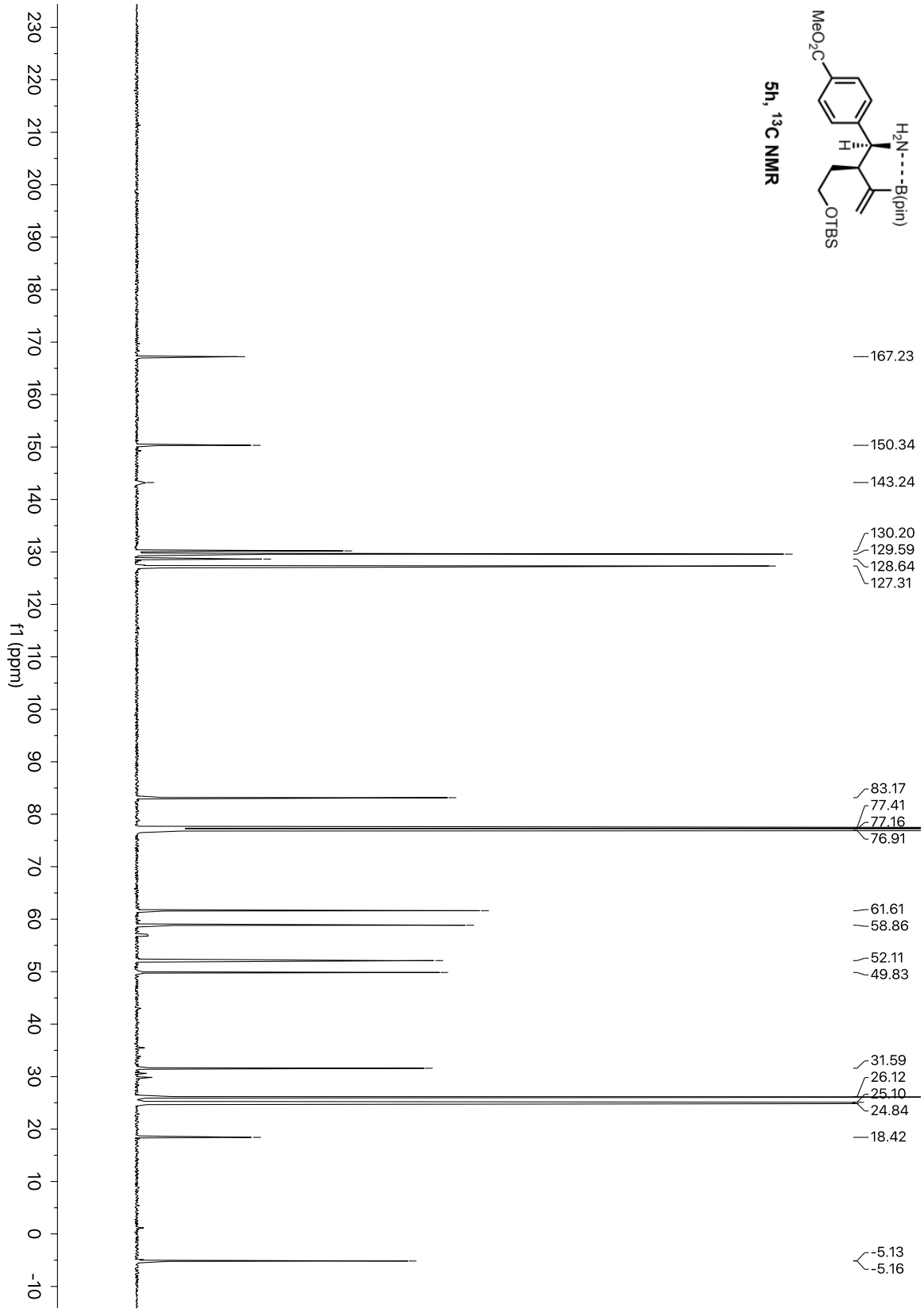
5h, $^{13}$C NMR
$MeO_2C$
$H_2N$----B(pin)
H
OTBS
167.23
150.34
143.24
130.20
129.59
128.64
127.31
83.17
77.41
77.16
76.91
61.61
58.86
52.11
49.83
31.59
26.12
25.10
24.84
18.42
-5.13
-5.16
f1 (ppm)

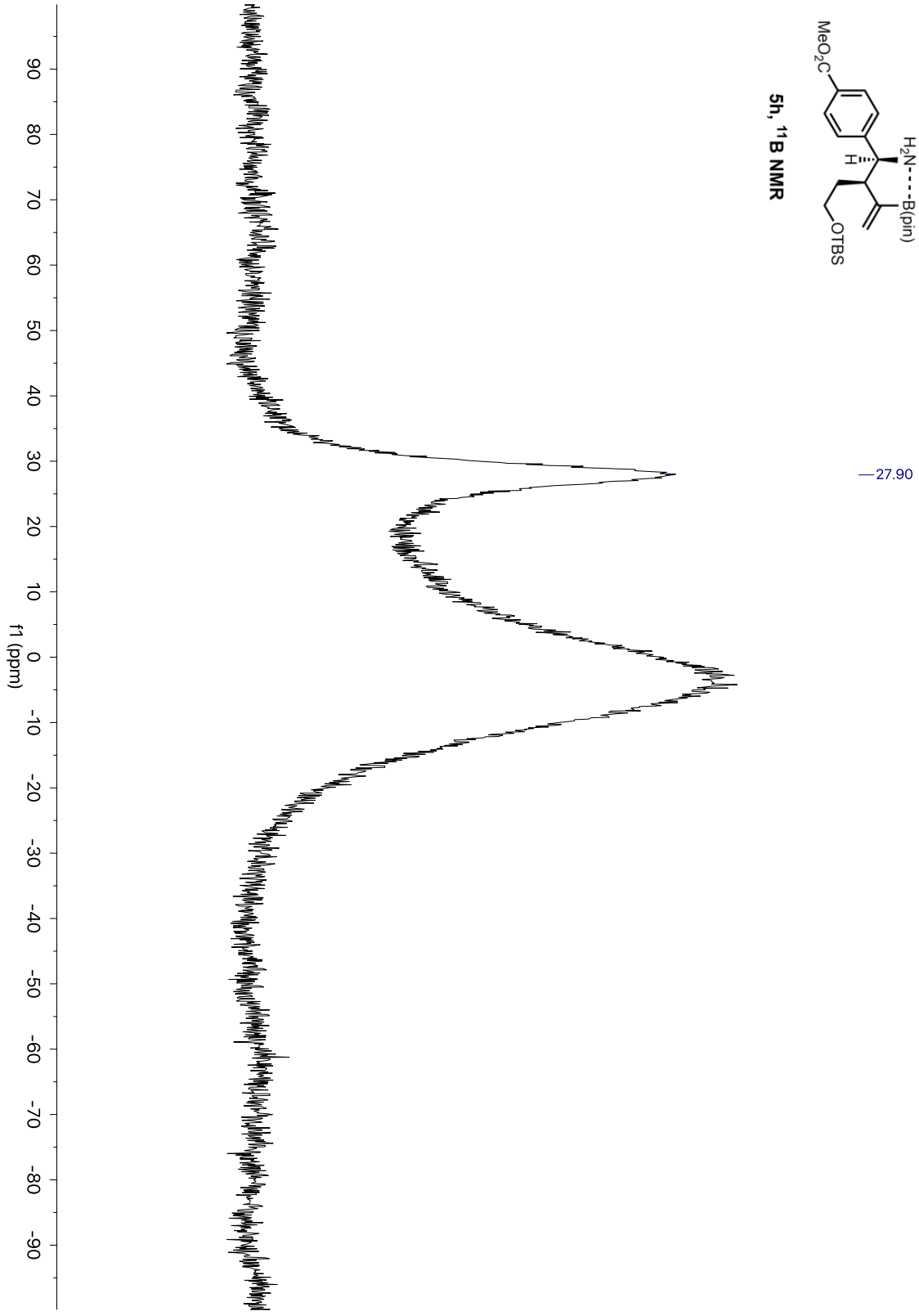
MeO2C
H2N---B(pin)
H
OTBS
5h, 11B NMR
27.90
f1 (ppm)
90
80
70
60
50
40
30
20
10
0
-10
-20
-30
-40
-50
-60
-70
-80
-90

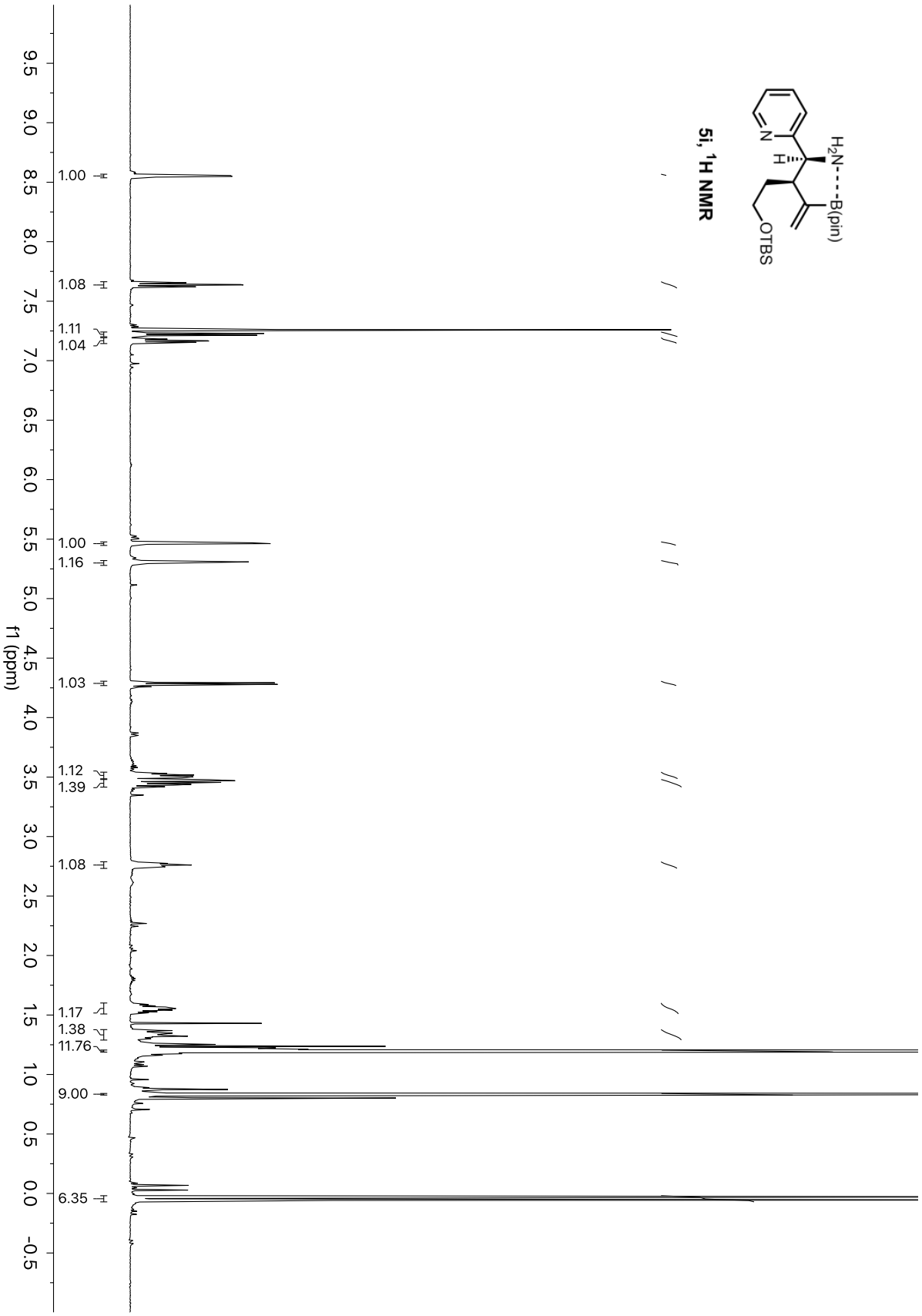
5i, $^1$H NMR
$H_2N$---B(pin)
OTBS
N
H
f1 (ppm)
1.00
1.08
1.11
1.04
1.00
1.16
1.03
1.12
1.39
1.08
1.17
1.38
11.76
9.00
6.35

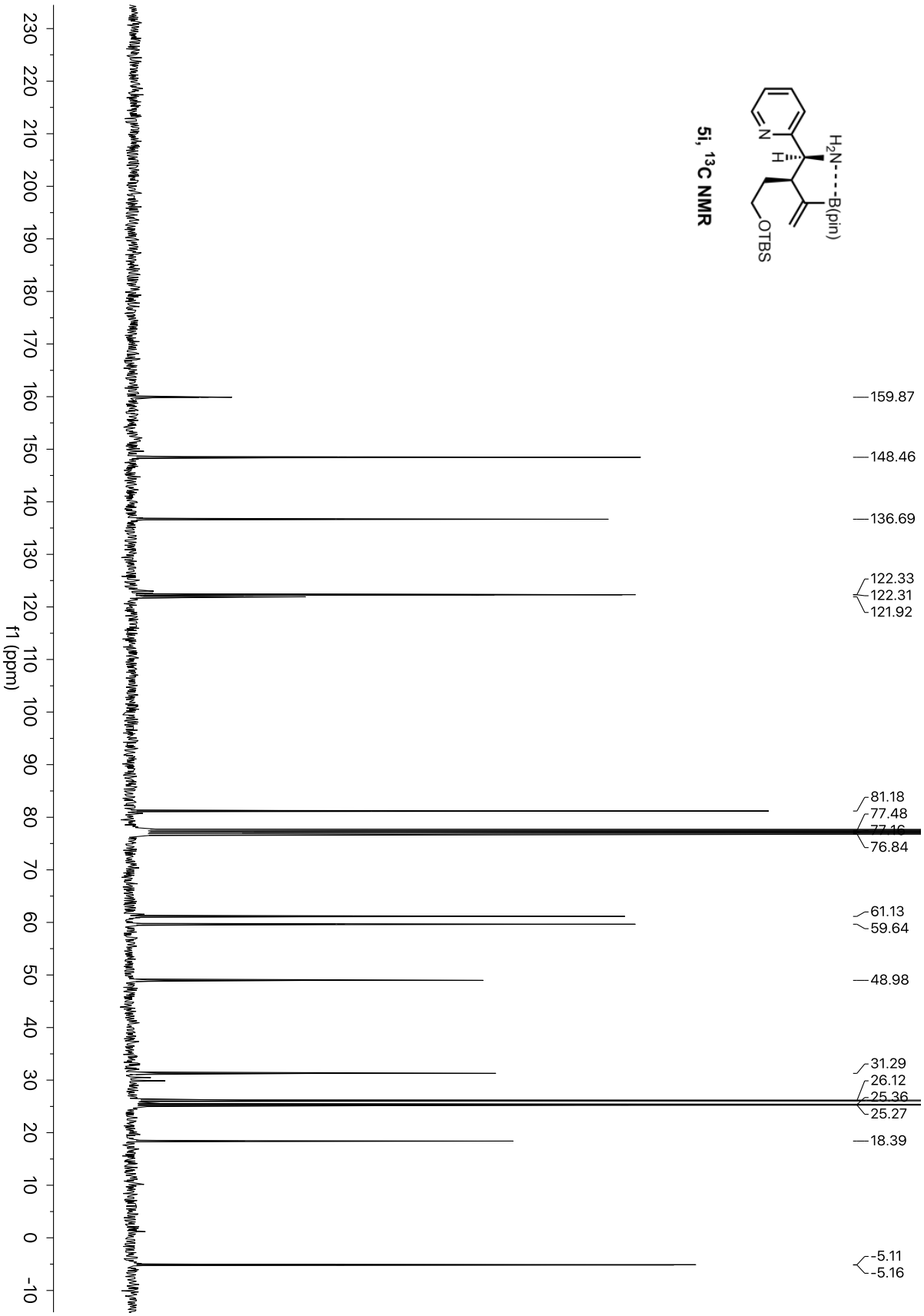
5i, $^{13}$C NMR
$H_2N$---B(pin)
OTBS
159.87
148.46
136.69
122.33
122.31
121.92
81.18
77.48
76.84
61.13
59.64
48.98
31.29
26.12
25.36
25.27
18.39
-5.11
-5.16
f1 (ppm)

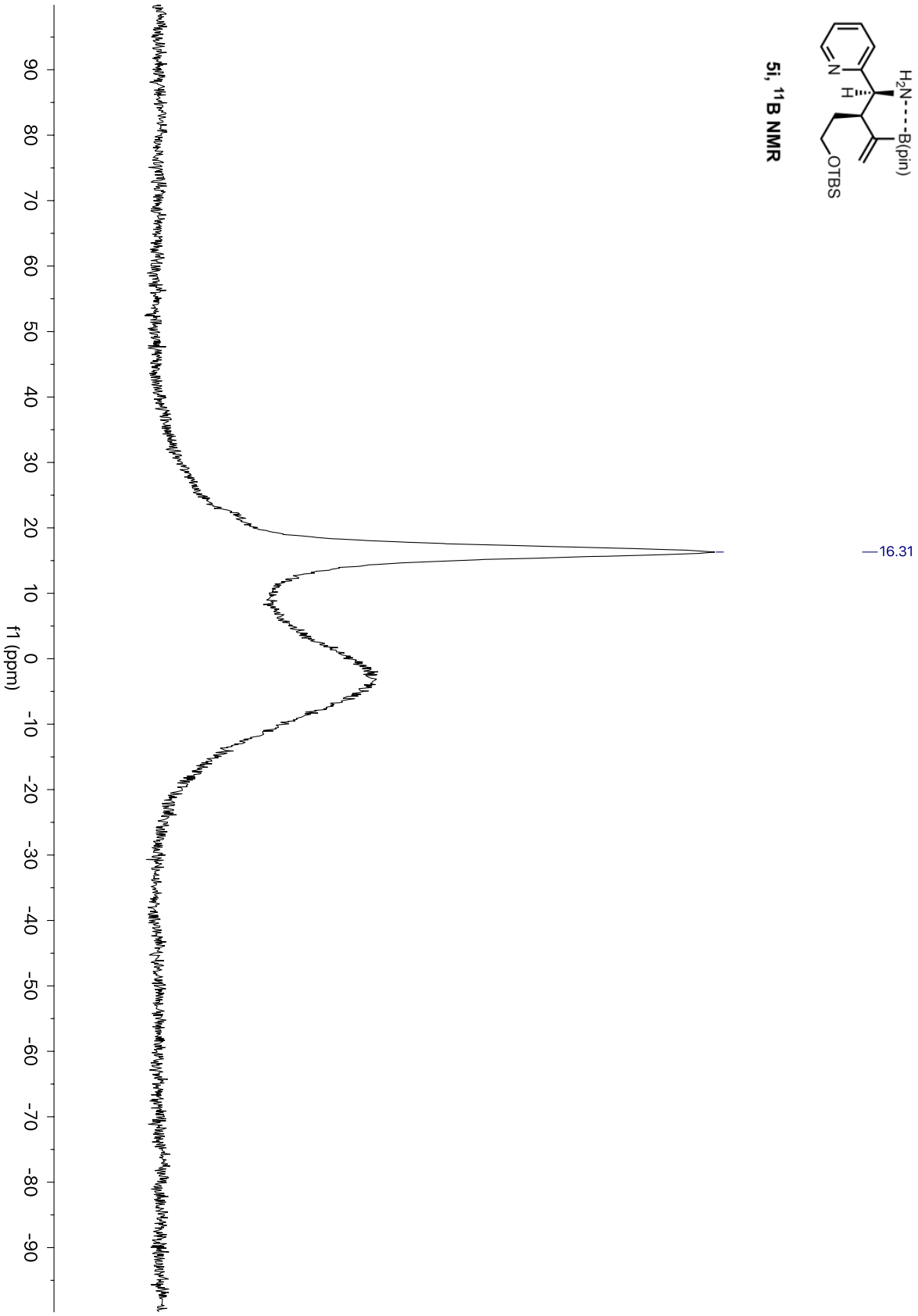
H2N---B(pin)
N
H
OTBS
5i, 11B NMR
16.31
90
80
70
60
50
40
30
20
10
0
-10
-20
-30
-40
-50
-60
-70
-80
-90
f1 (ppm)

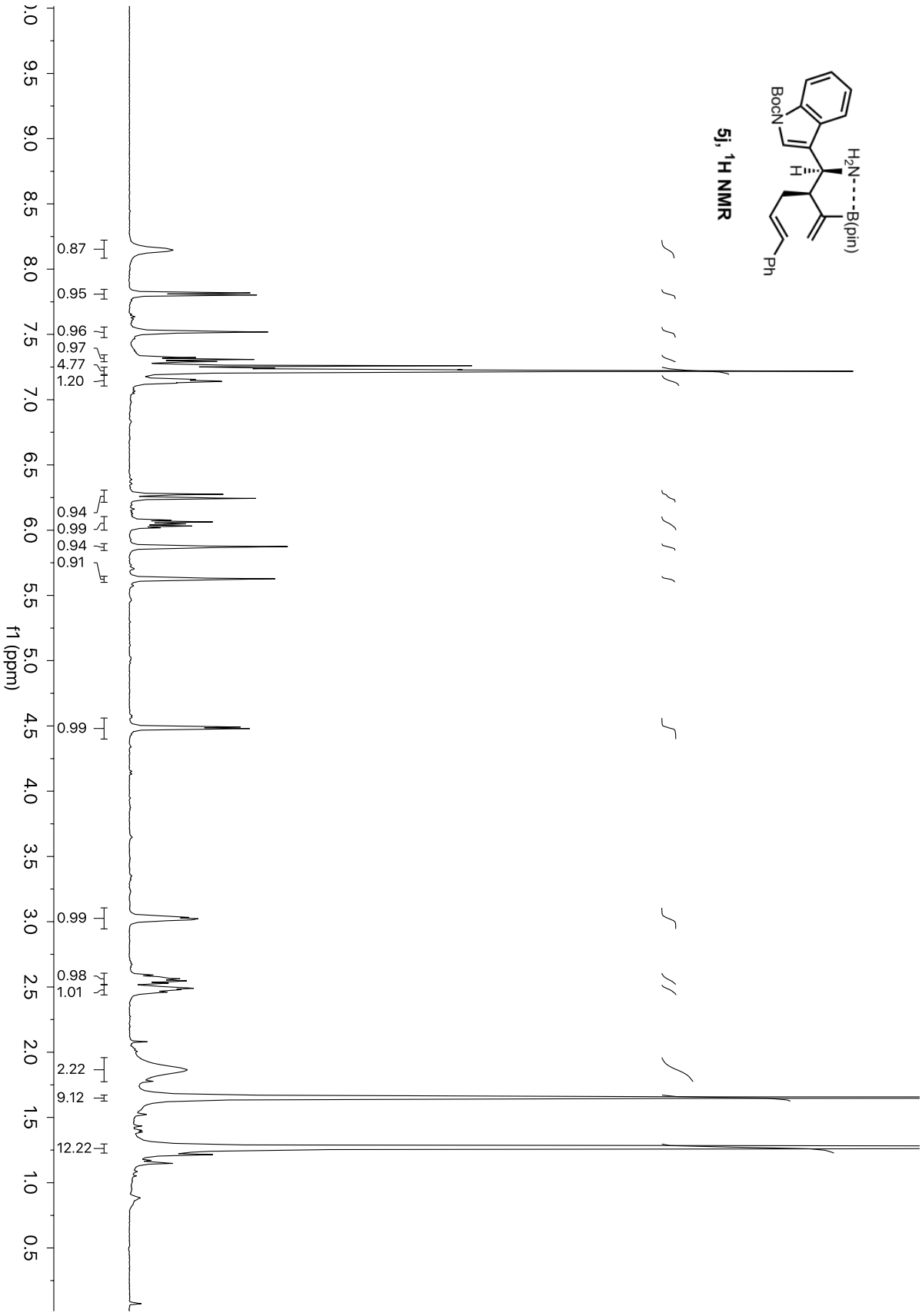
5j, $^1$H NMR
BocN
H
H$_2$N---B(pin)
Ph
f1 (ppm)
0.87
0.95
0.96
0.97
4.77
1.20
0.94
0.99
0.94
0.91
0.99
0.99
0.98
1.01
2.22
9.12
12.22

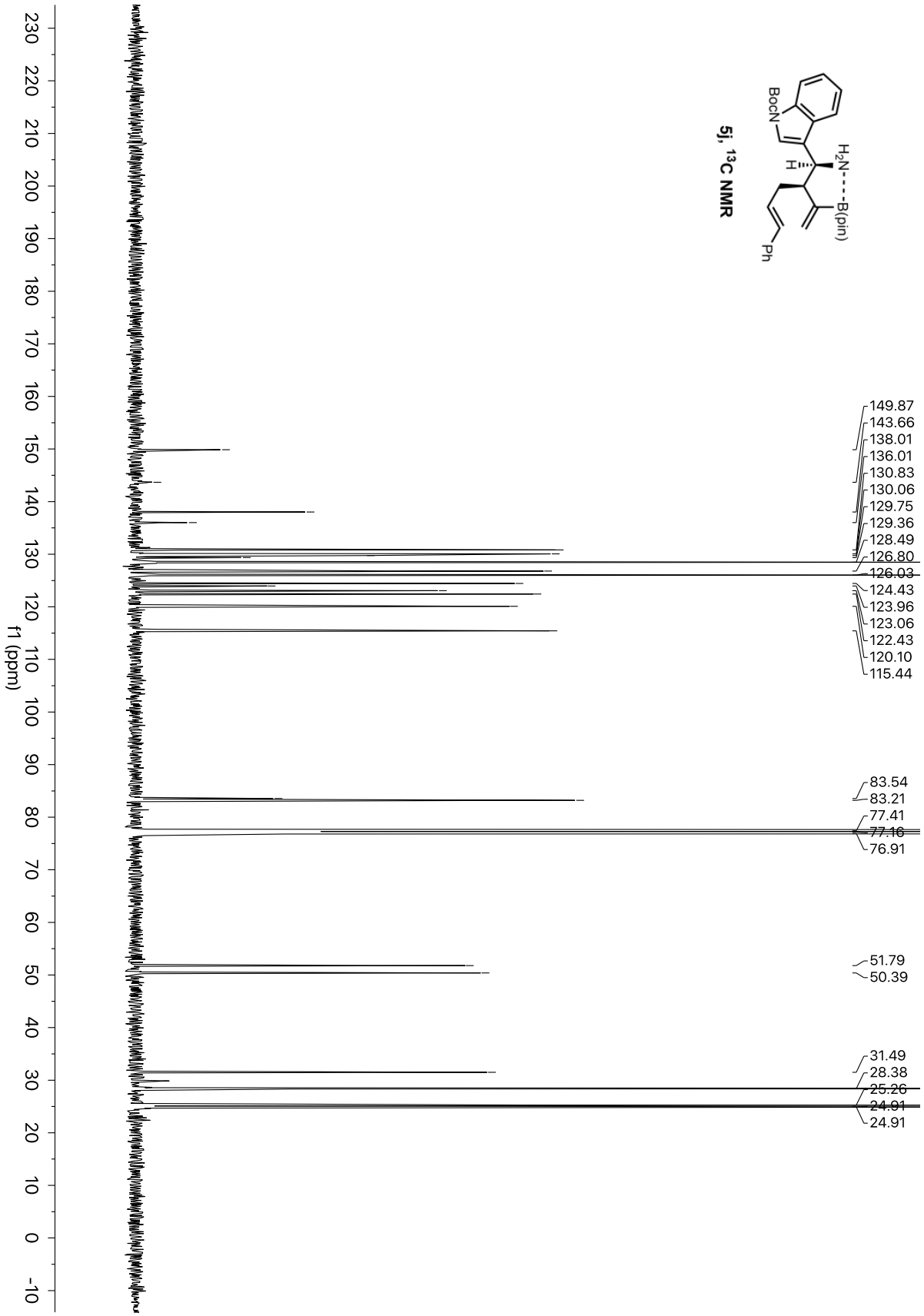
5j, $^{13}$C NMR
BocN
H
$H_2N$---B(pin)
Ph
149.87
143.66
138.01
136.01
130.83
130.06
129.75
129.36
128.49
126.80
126.03
124.43
123.96
123.06
122.43
120.10
115.44
83.54
83.21
77.41
77.16
76.91
51.79
50.39
31.49
28.38
25.26
24.91
24.91
f1 (ppm)
230 220 210 200 190 180 170 160 150 140 130 120 110 100 90 80 70 60 50 40 30 20 10 0 -10

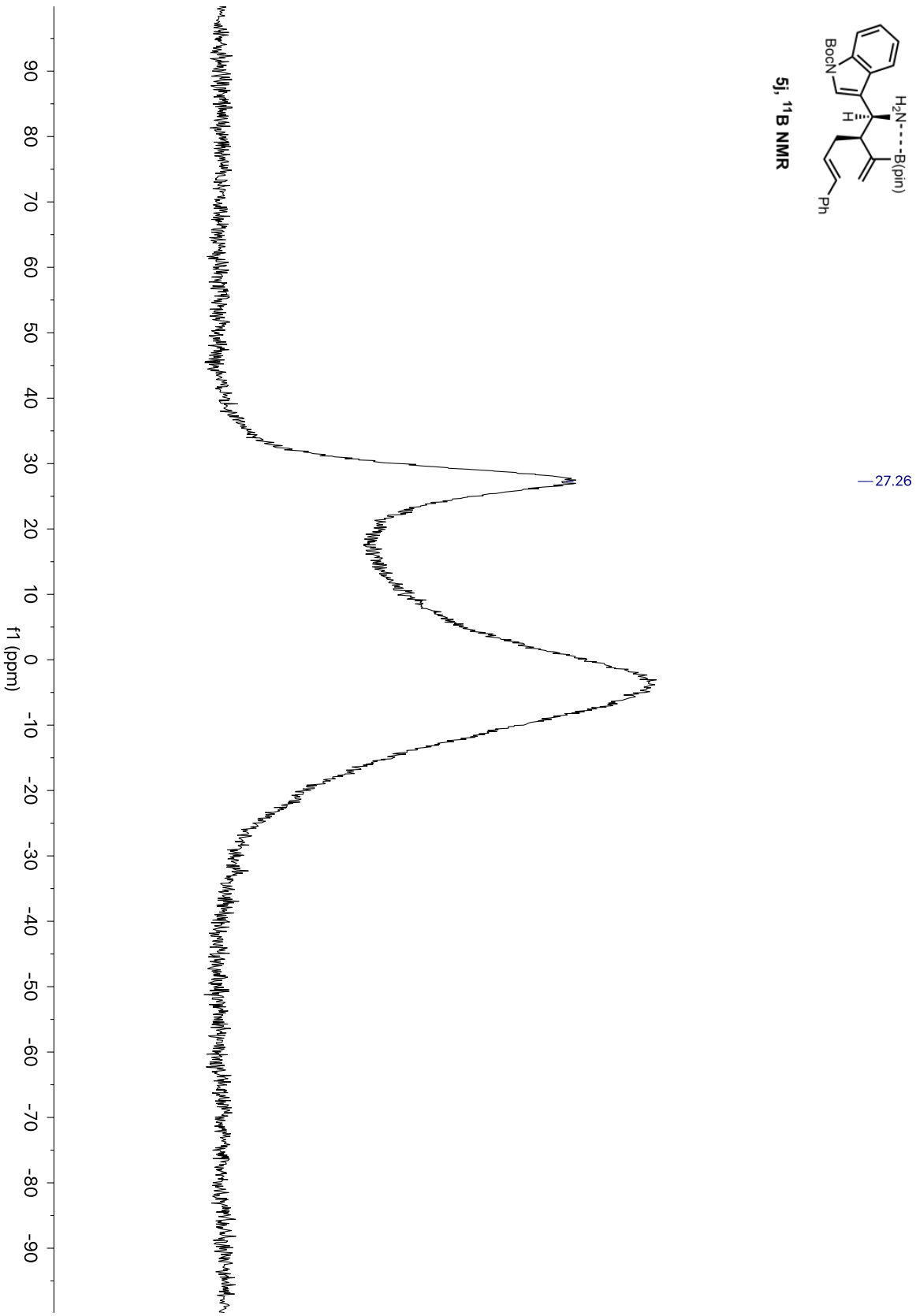
BocN
H
H2N----B(pin)
Ph
5j, 11B NMR
27.26
90
80
70
60
50
40
30
20
10
0
-10
-20
-30
-40
-50
-60
-70
-80
-90
f1 (ppm)

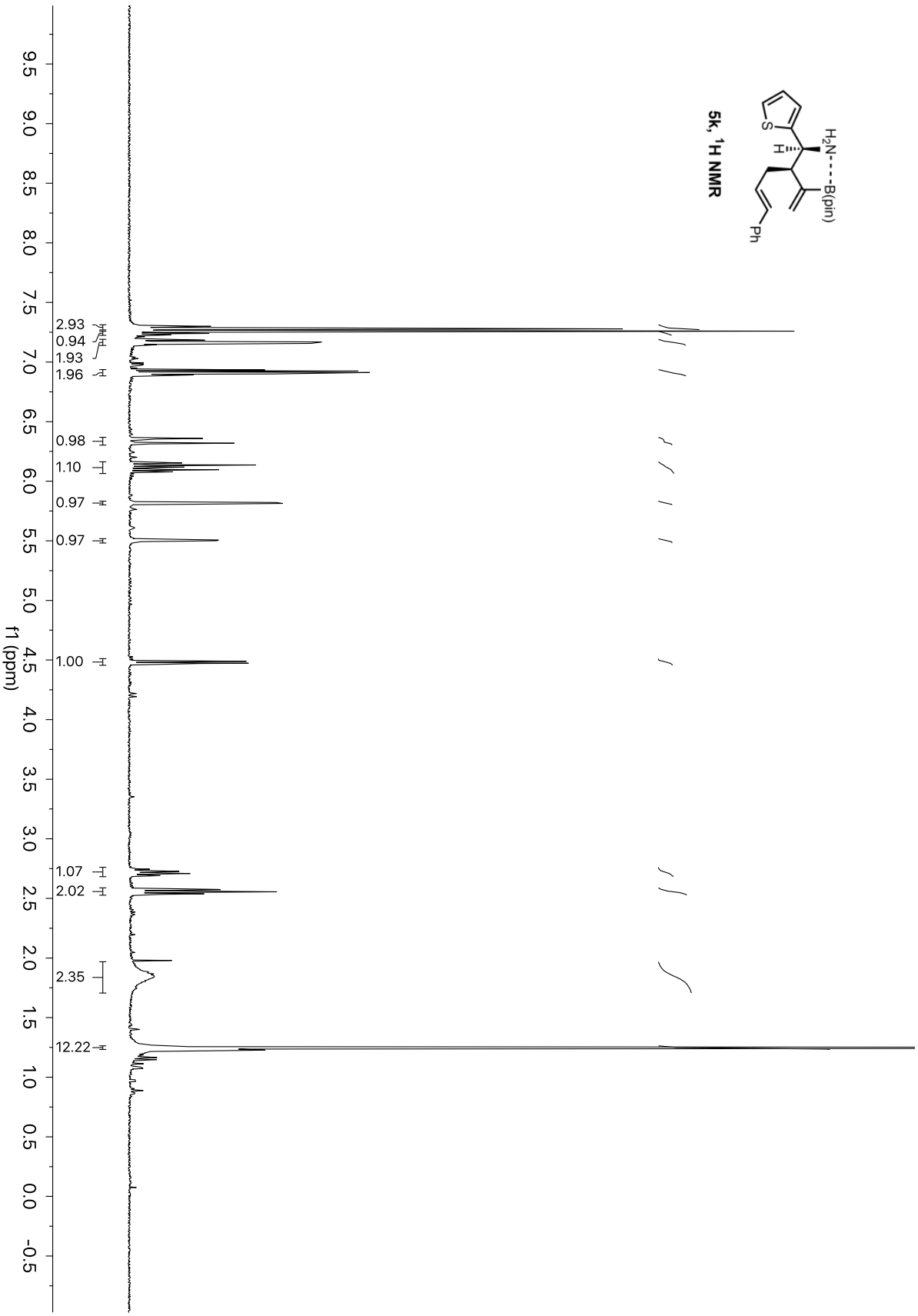
5k, 1H NMR
H2N---B(pin)
Ph
2.93
0.94
1.93
1.96
0.98
1.10
0.97
0.97
1.00
1.07
2.02
2.35
12.22
f1 (ppm)

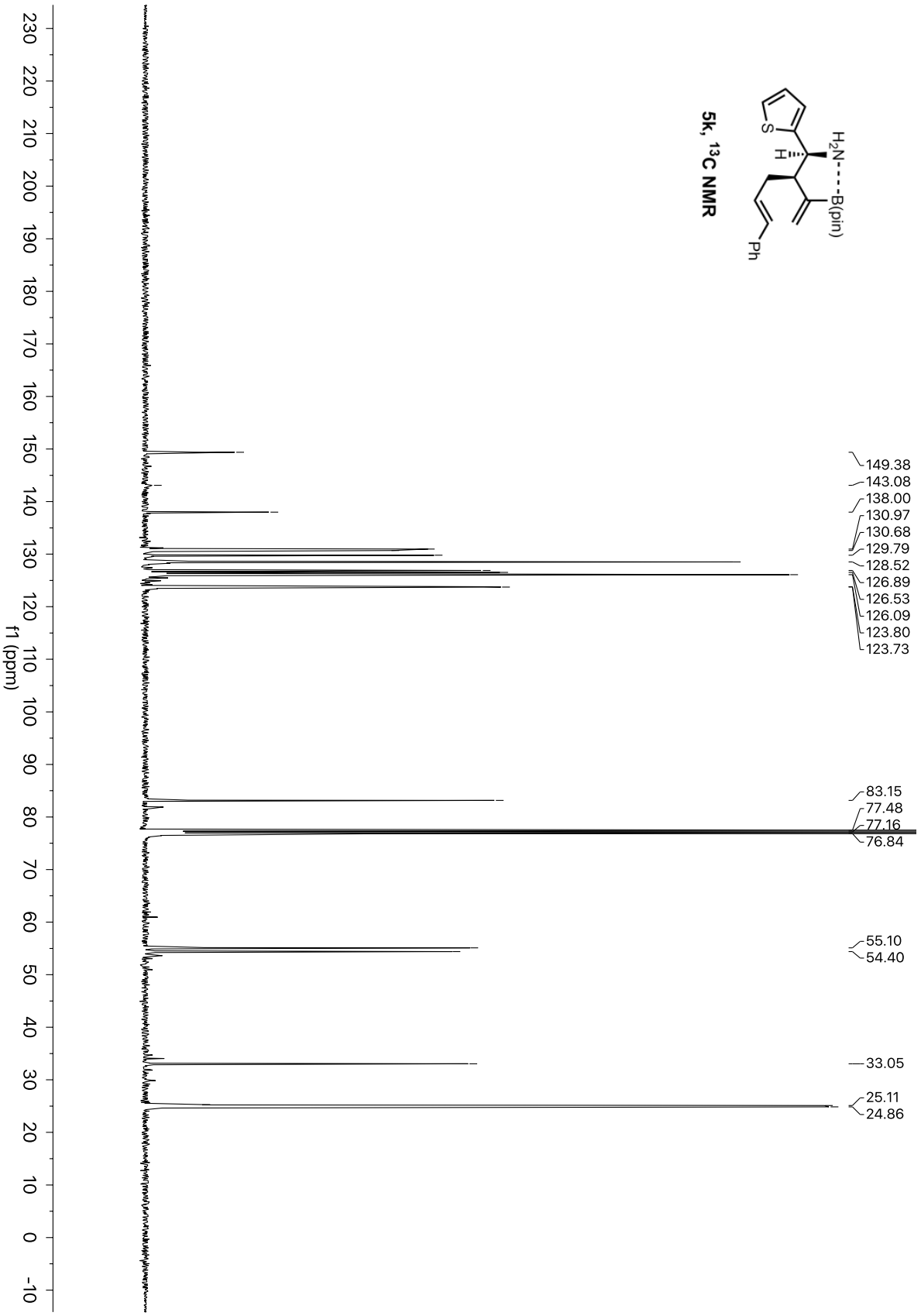
5k, $^{13}$C NMR
S
H
H2N---B(pin)
Ph
149.38
143.08
138.00
130.97
130.68
129.79
128.52
126.89
126.53
126.09
123.80
123.73
83.15
77.48
77.16
76.84
55.10
54.40
33.05
25.11
24.86
f1 (ppm)
230 220 210 200 190 180 170 160 150 140 130 120 110 100 90 80 70 60 50 40 30 20 10 0 -10

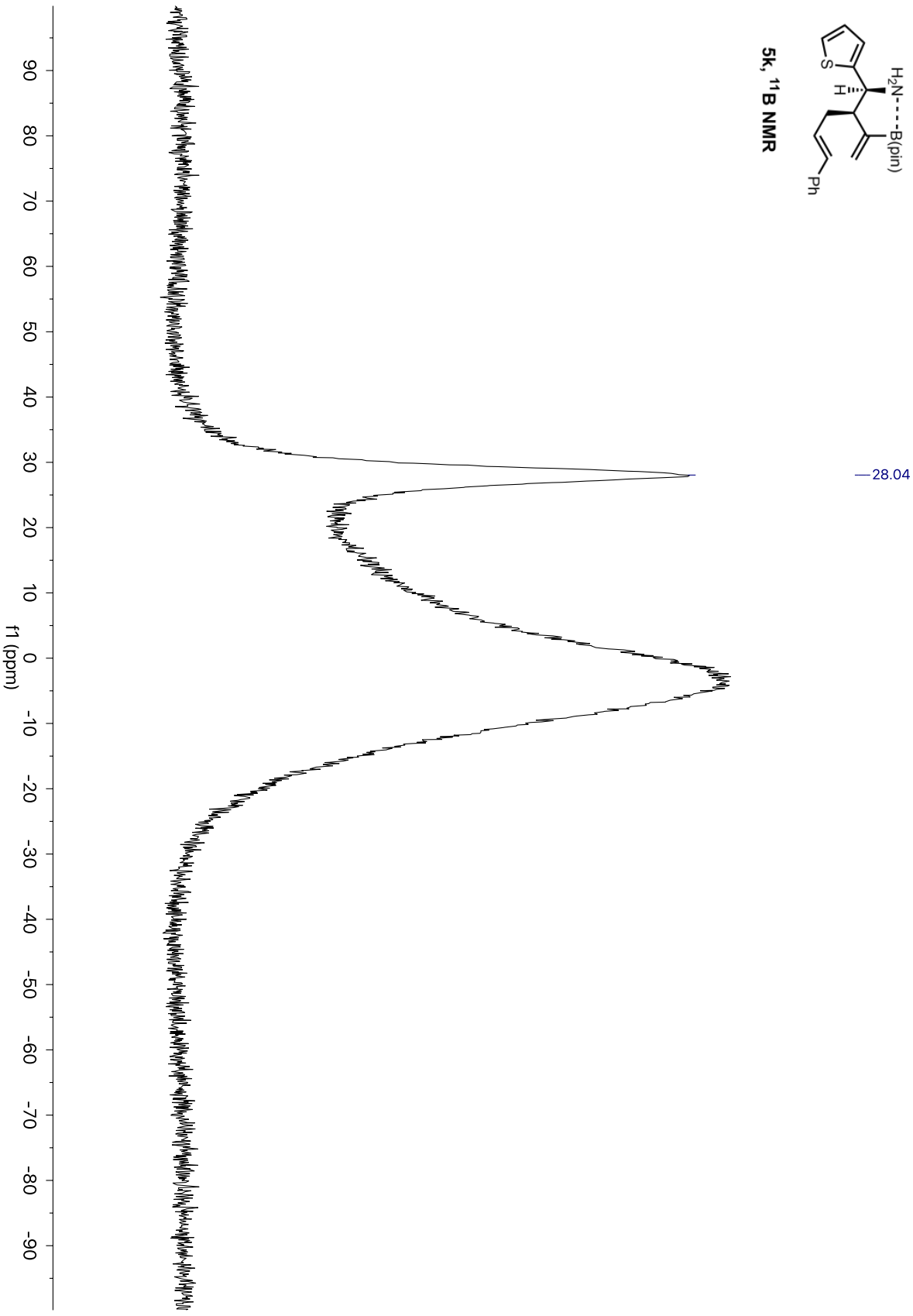
5k, $^{11}$B NMR
H2N---B(pin)
S
H
Ph
28.04
f1 (ppm)
90
80
70
60
50
40
30
20
10
0
-10
-20
-30
-40
-50
-60
-70
-80
-90

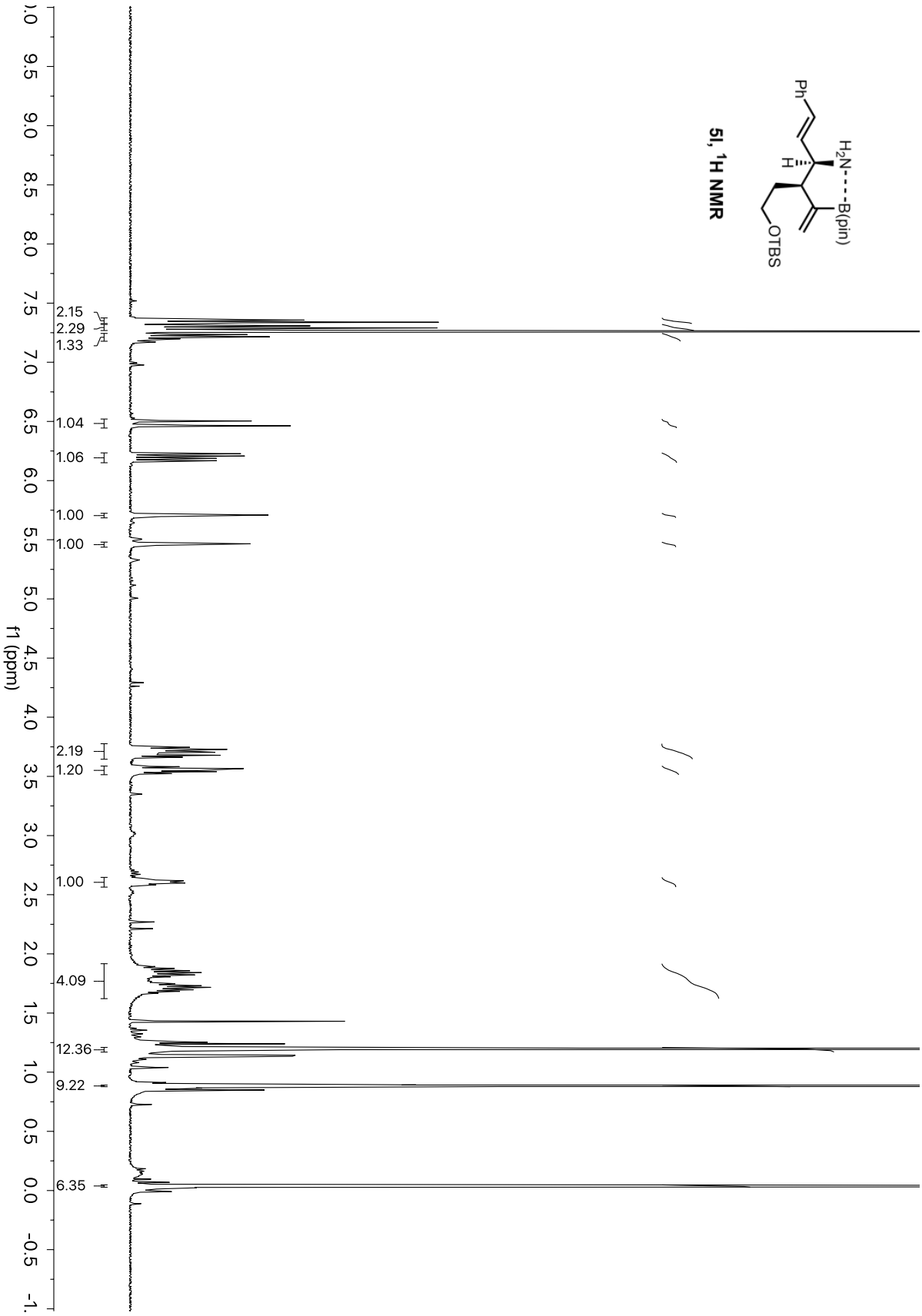
5l, $^1$H NMR
Ph
H
$H_2N$---B(pin)
OTBS
2.15
2.29
1.33
1.04
1.06
1.00
1.00
2.19
1.20
1.00
4.09
12.36
9.22
6.35
f1 (ppm)

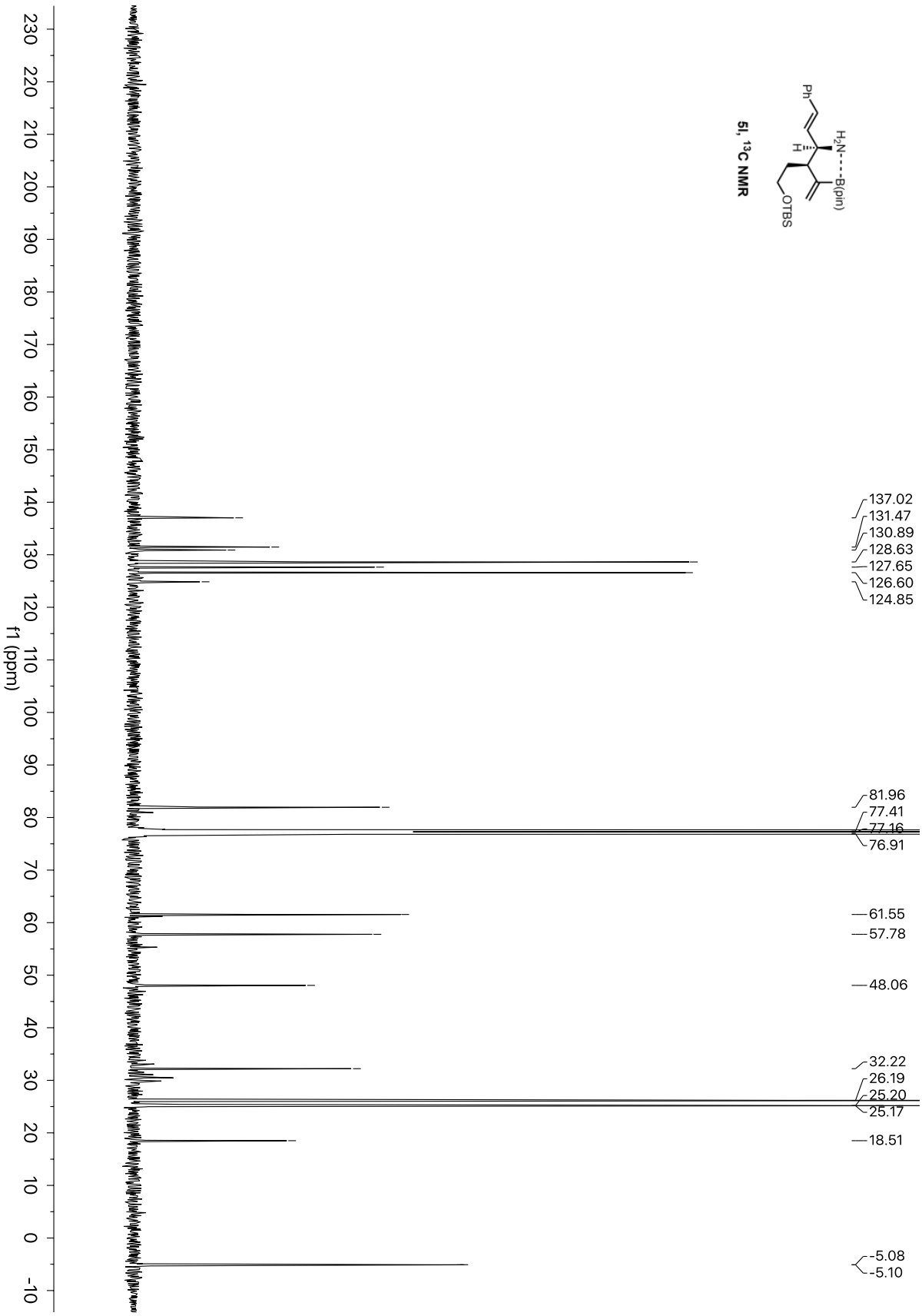
5l, 13C NMR
Ph
H2N---B(pin)
H
OTBS
137.02
131.47
130.89
128.63
127.65
126.60
124.85
81.96
77.41
77.16
76.91
61.55
57.78
48.06
32.22
26.19
25.20
25.17
18.51
-5.08
-5.10
f1 (ppm)

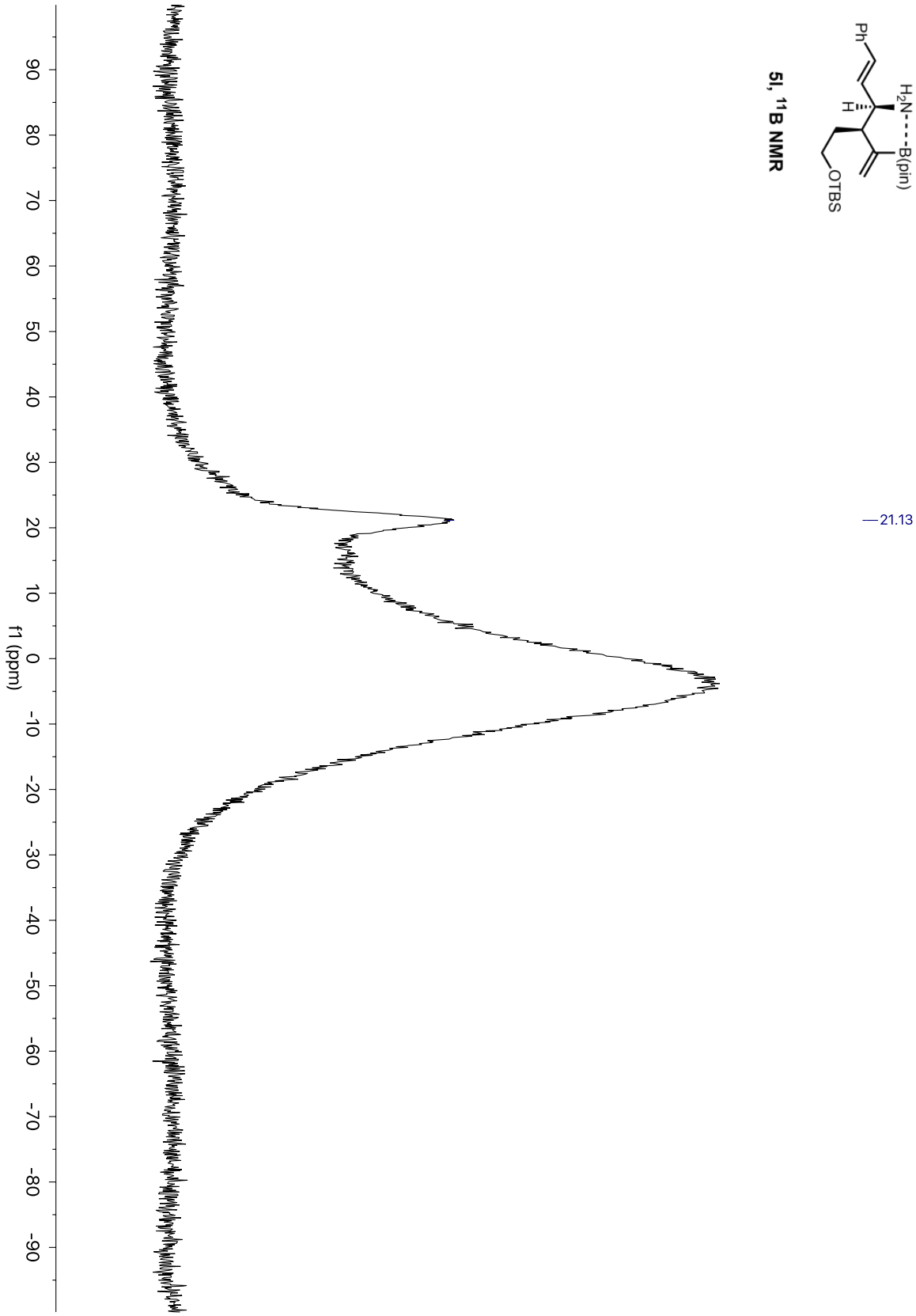
Ph
H
H2N---B(pin)
OTBS
5l, 11B NMR
21.13
f1 (ppm)
90
80
70
60
50
40
30
20
10
0
-10
-20
-30
-40
-50
-60
-70
-80
-90

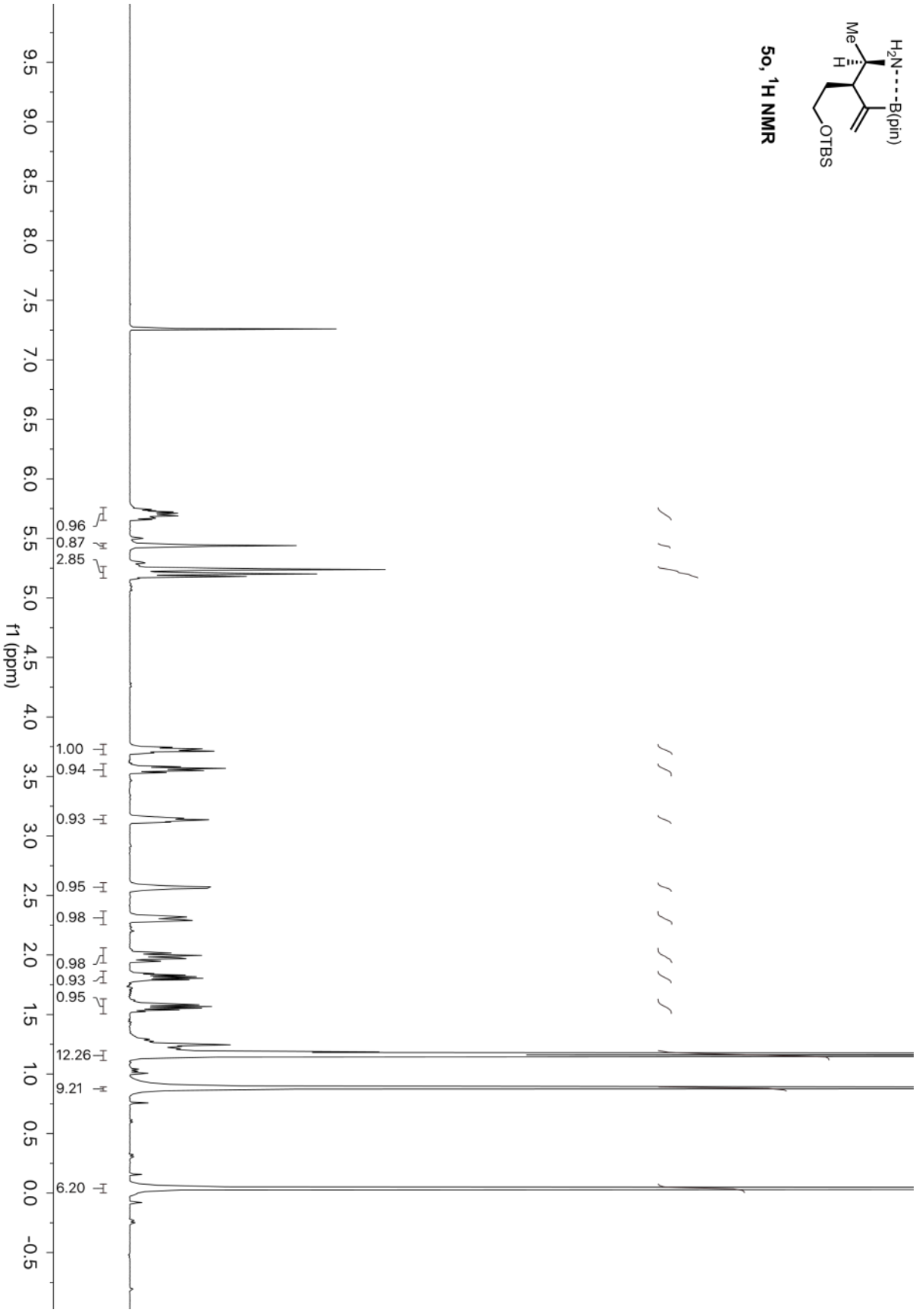
5o, $^1$H NMR
H2N---B(pin)
Me
H
OTBS
f1 (ppm)
0.96
0.87
2.85
1.00
0.94
0.93
0.95
0.98
0.98
0.93
0.95
12.26
9.21
6.20

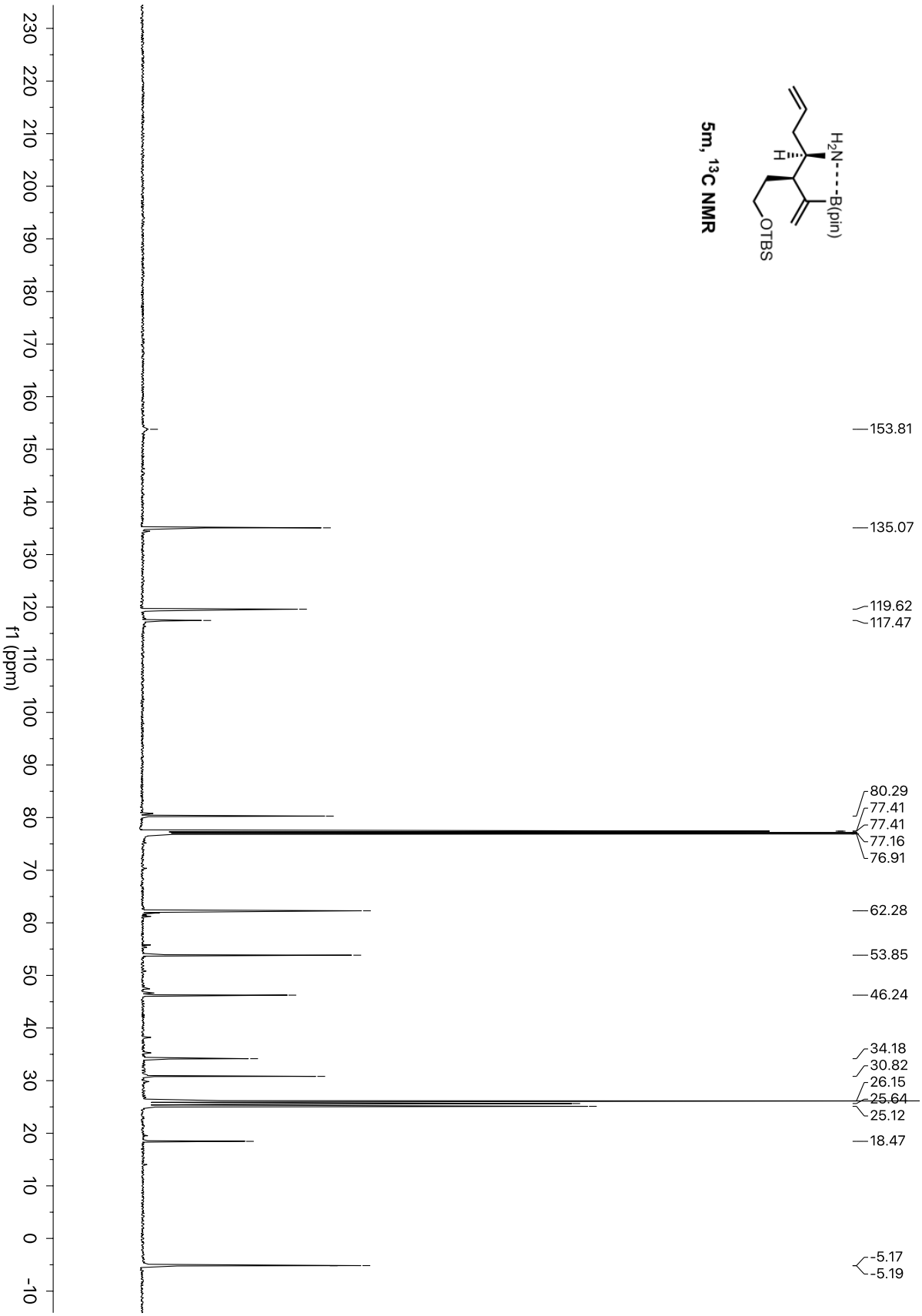
5m, $^{13}$C NMR
$H_2N$---B(pin)
H
OTBS
f1 (ppm)
230
220
210
200
190
180
170
160
150
140
130
120
110
100
90
80
70
60
50
40
30
20
10
0
-10
153.81
135.07
119.62
117.47
80.29
77.41
77.41
77.16
76.91
62.28
53.85
46.24
34.18
30.82
26.15
25.64
25.12
18.47
-5.17
-5.19

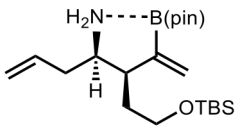


**5m, $^{11}$B NMR**

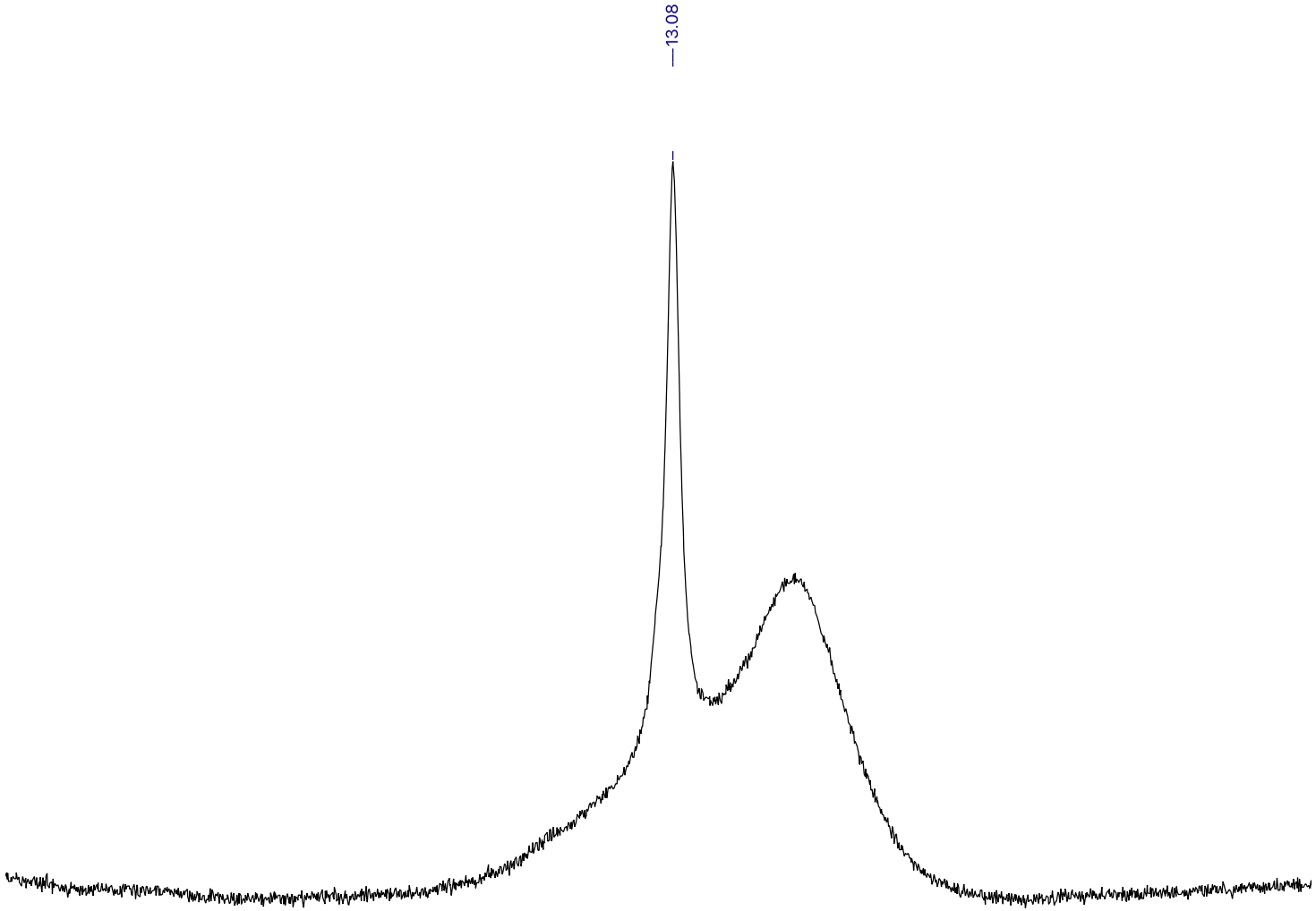

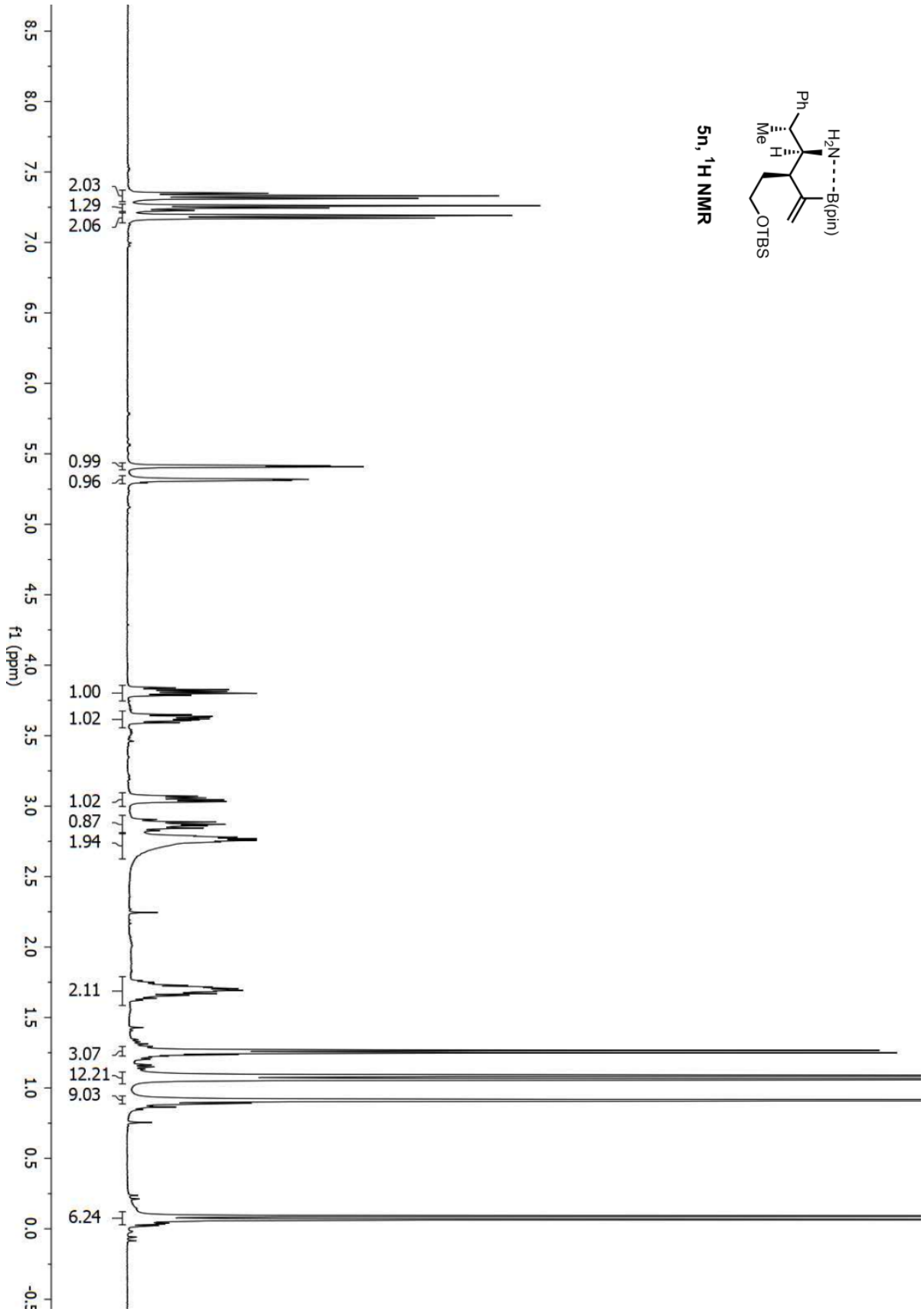
5n, $^1$H NMR
Ph
Me
H
H2N---B(pin)
OTBS
f1 (ppm)
2.03
1.29
2.06
0.99
0.96
1.00
1.02
1.02
0.87
1.94
2.11
3.07
12.21
9.03
6.24

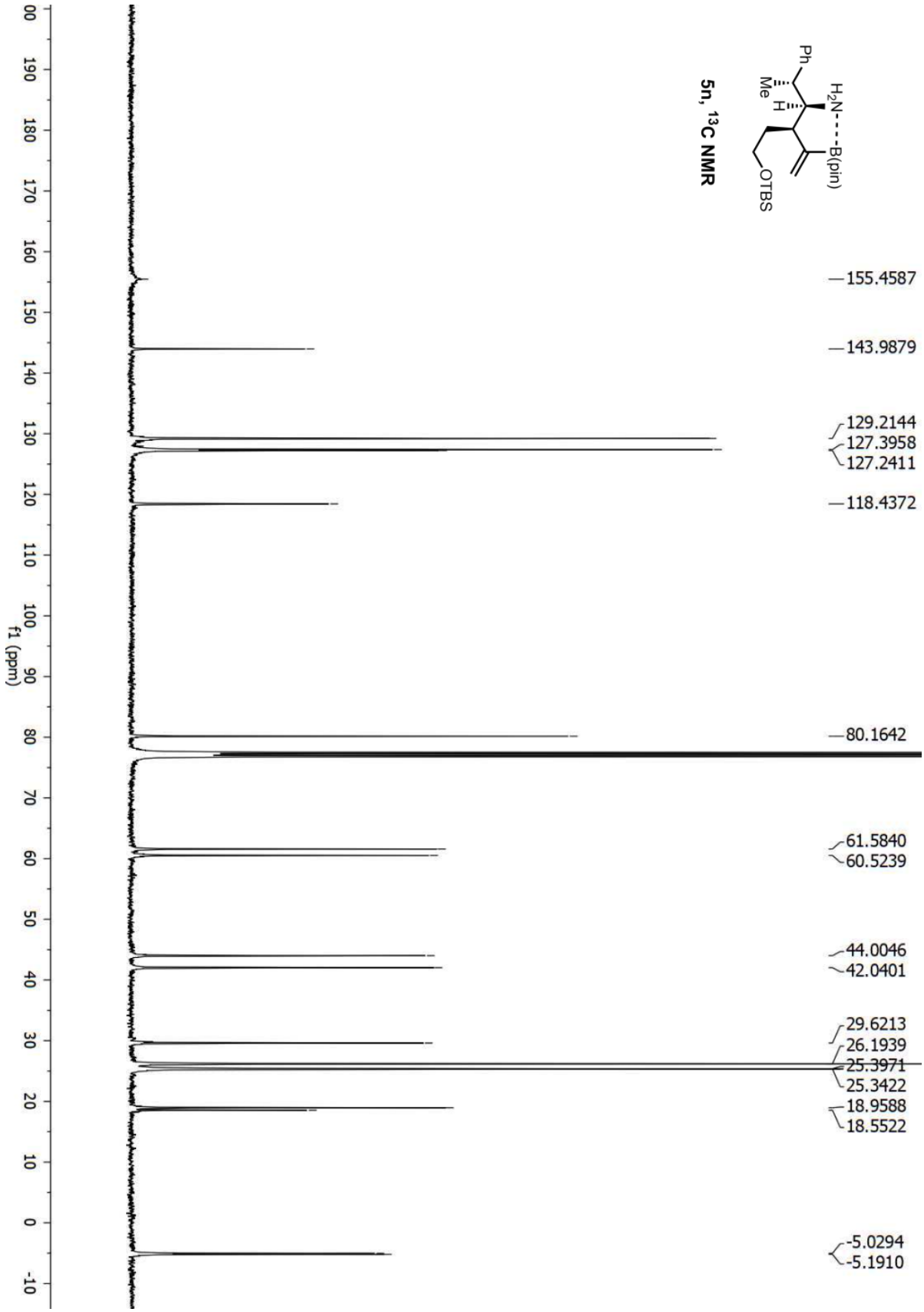
5n, $^{13}$C NMR
Ph
Me
H
$H_2N$---B(pin)
OTBS
155.4587
143.9879
129.2144
127.3958
127.2411
118.4372
80.1642
61.5840
60.5239
44.0046
42.0401
29.6213
26.1939
25.3971
25.3422
18.9588
18.5522
-5.0294
-5.1910
f1 (ppm)

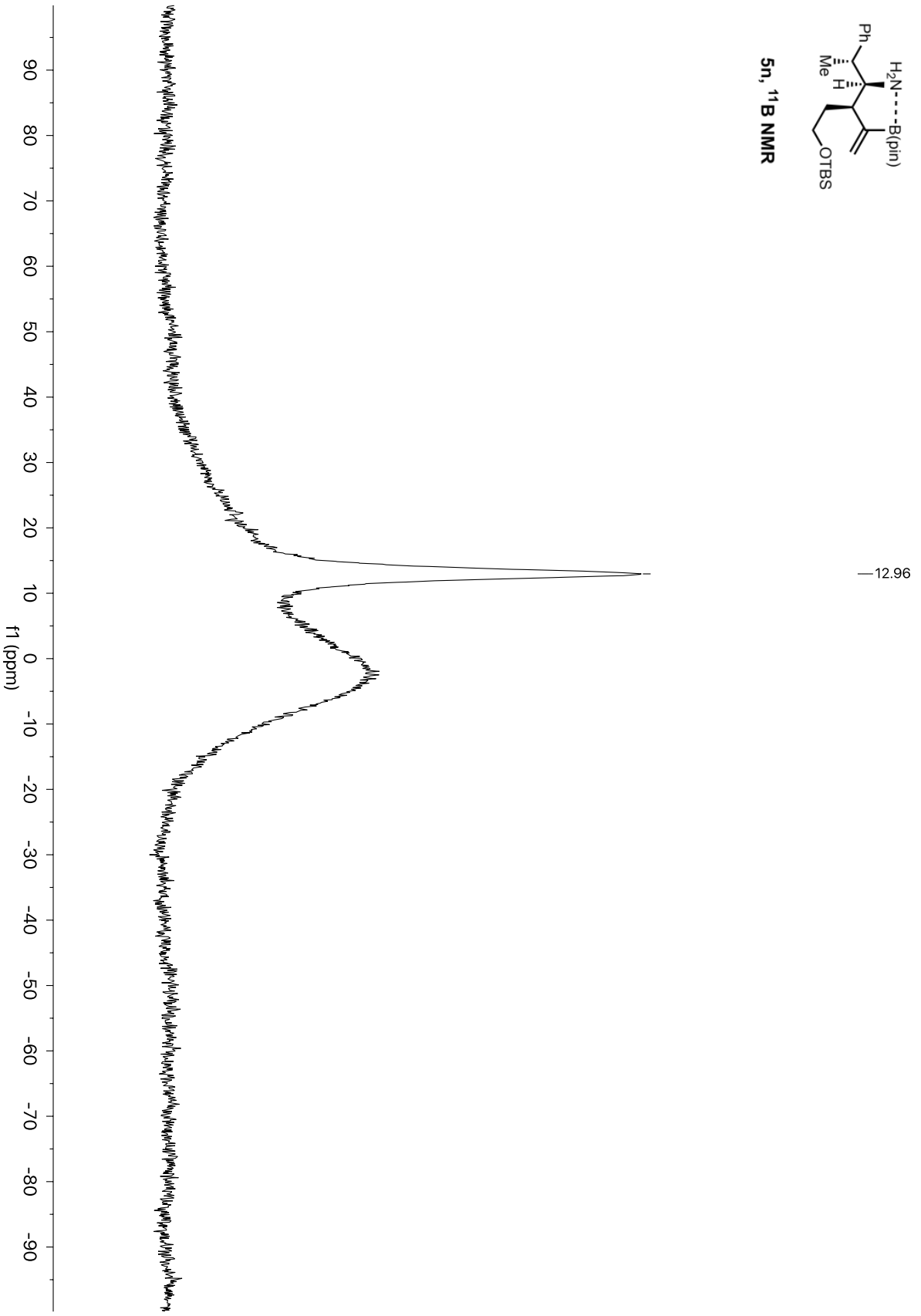
Ph
Me
H
H2N---B(pin)
OTBS
5n, 11B NMR
12.96
90
80
70
60
50
40
30
20
10
0
-10
-20
-30
-40
-50
-60
-70
-80
-90
f1 (ppm)

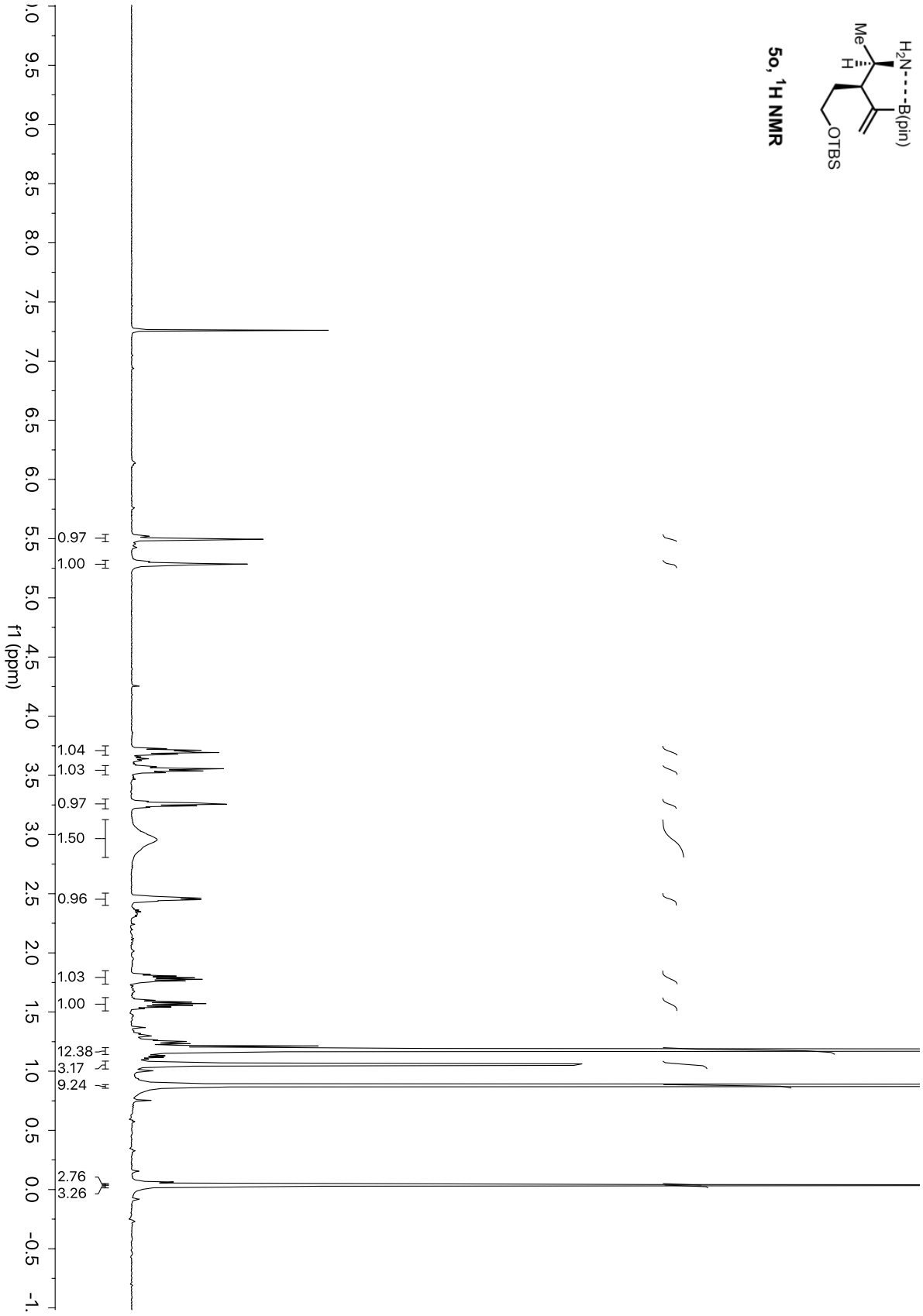
H2N---B(pin)
Me
H
OTBS
5o, 1H NMR
f1 (ppm)
0.97
1.00
1.04
1.03
0.97
1.50
0.96
1.03
1.00
12.38
3.17
9.24
2.76
3.26

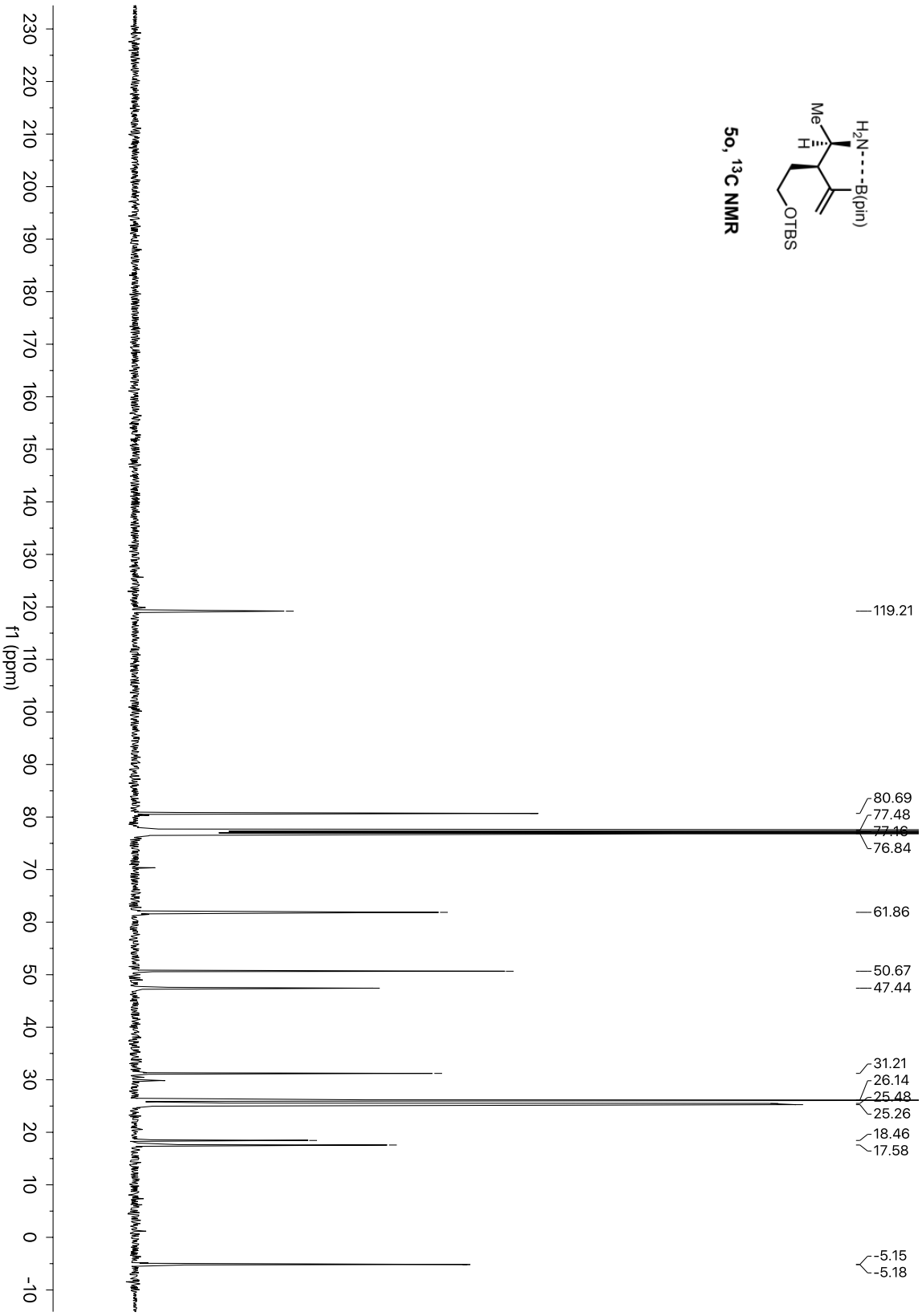
5o, 13C NMR
Me
H
H2N---B(pin)
OTBS
119.21
80.69
77.48
77.16
76.84
61.86
50.67
47.44
31.21
26.14
25.48
25.26
18.46
17.58
-5.15
-5.18
f1 (ppm)

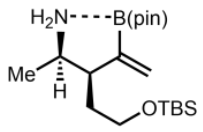
H2N----B(pin)
Me
H
OTBS

**5o, $^{11}$B NMR**


15.27
90
80
70
60
50
40
30
20
10
0
-10
-20
-30
-40
-50
-60
-70
-80
-90
f1 (ppm)

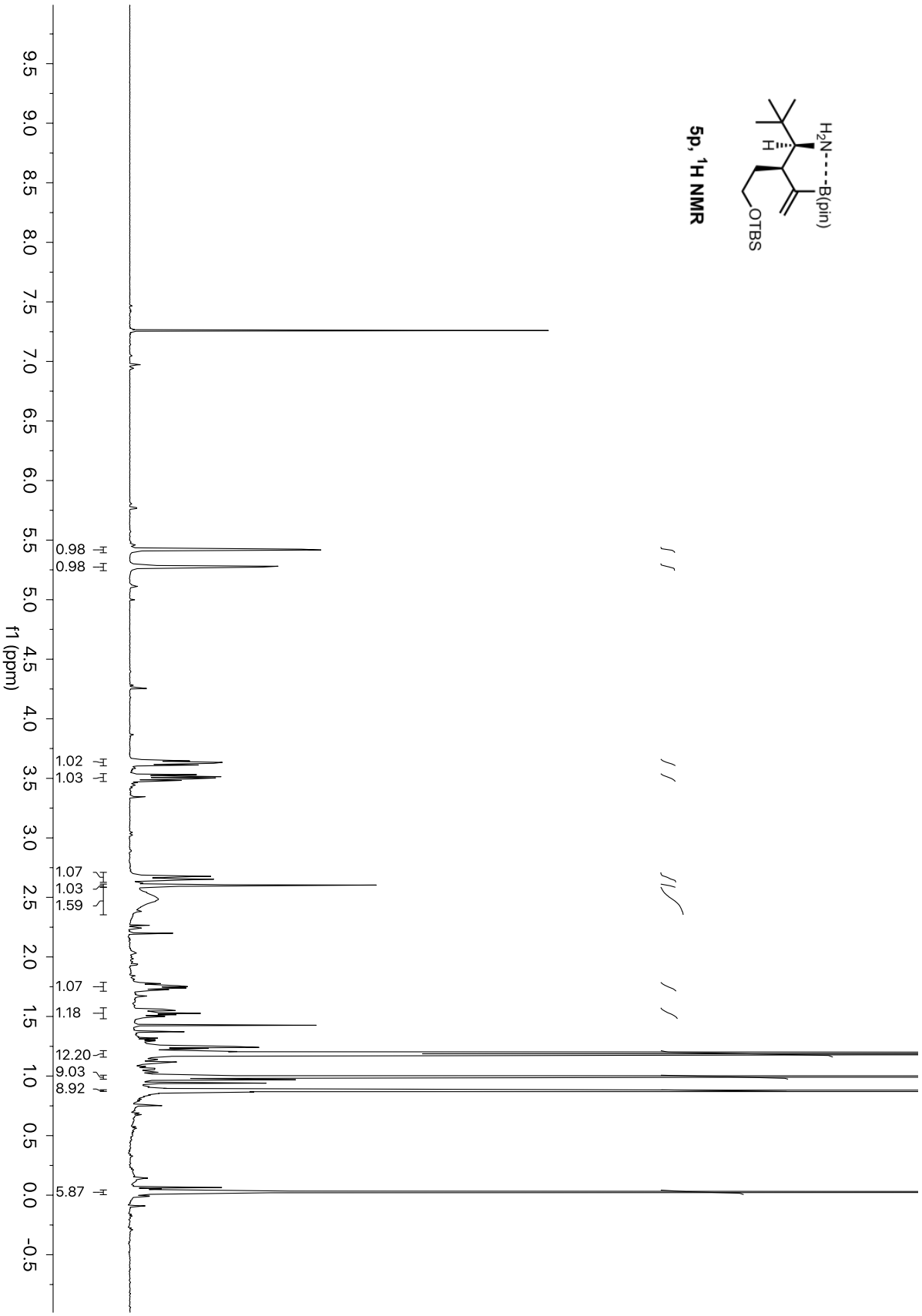
5p, $^1$H NMR
$H_2N$---B(pin)
H
OTBS
f1 (ppm)
9.5
9.0
8.5
8.0
7.5
7.0
6.5
6.0
5.5
5.0
4.5
4.0
3.5
3.0
2.5
2.0
1.5
1.0
0.5
0.0
-0.5
0.98
0.98
1.02
1.03
1.07
1.03
1.59
1.07
1.18
12.20
9.03
8.92
5.87

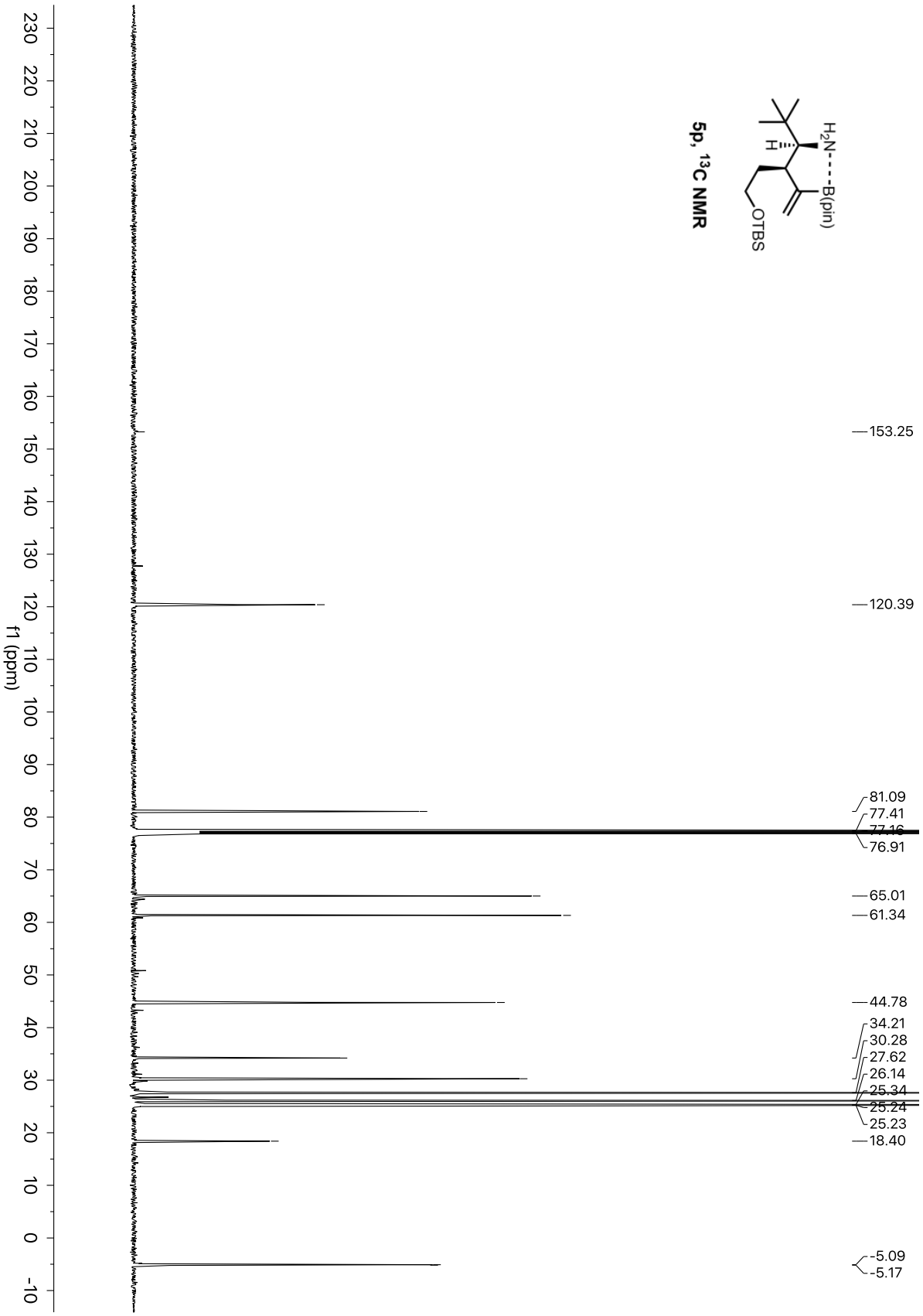
5p, $^{13}$C NMR
H$_2$N---B(pin)
H
OTBS
153.25
120.39
81.09
77.41
77.16
76.91
65.01
61.34
44.78
34.21
30.28
27.62
26.14
25.34
25.24
25.23
18.40
-5.09
-5.17
f1 (ppm)
230 220 210 200 190 180 170 160 150 140 130 120 110 100 90 80 70 60 50 40 30 20 10 0 -10

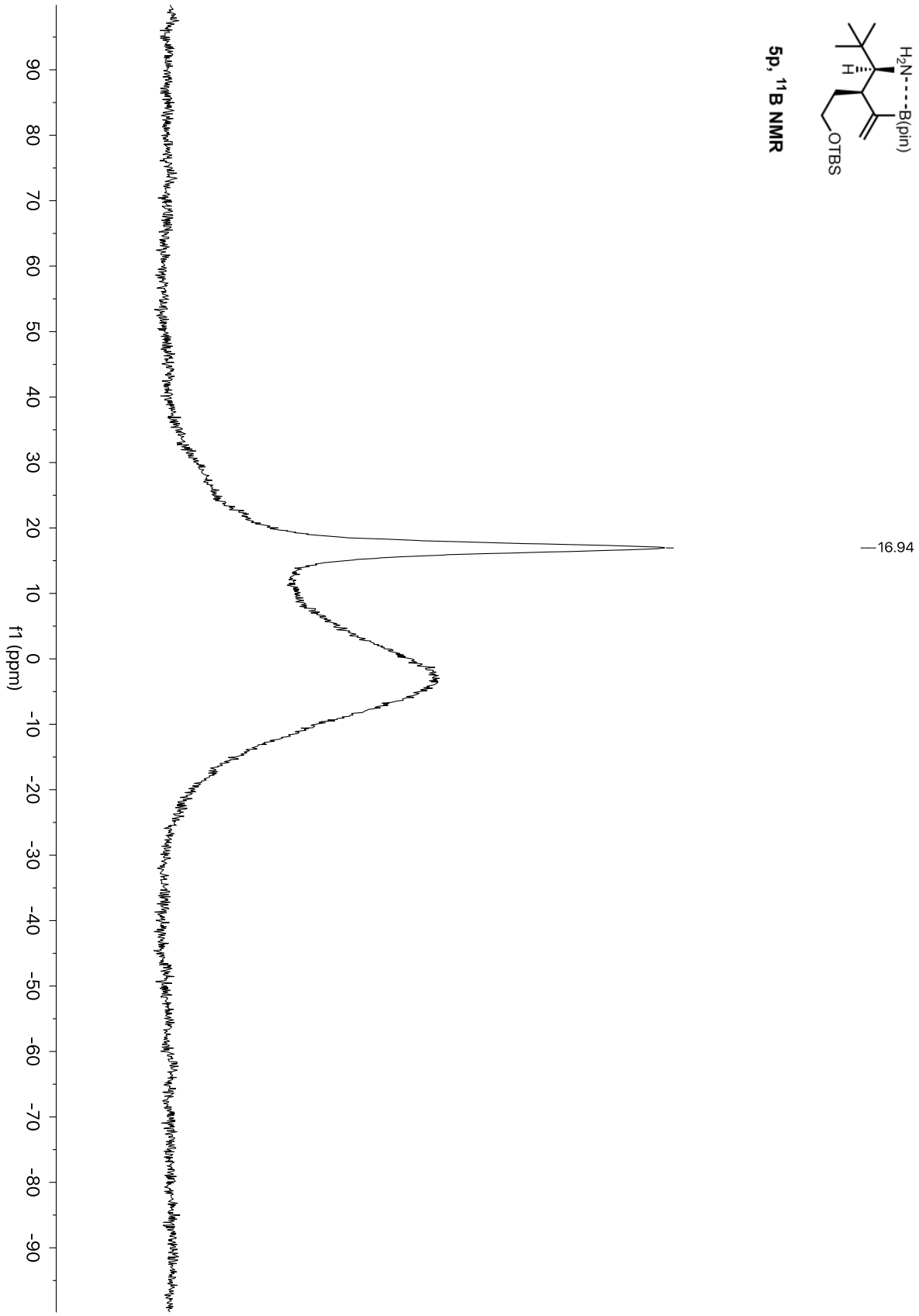
H2N---B(pin)
H
OTBS
16.94
90
80
70
60
50
40
30
20
10
0
-10
-20
-30
-40
-50
-60
-70
-80
-90
f1 (ppm)

**5p, $^{11}$B NMR**

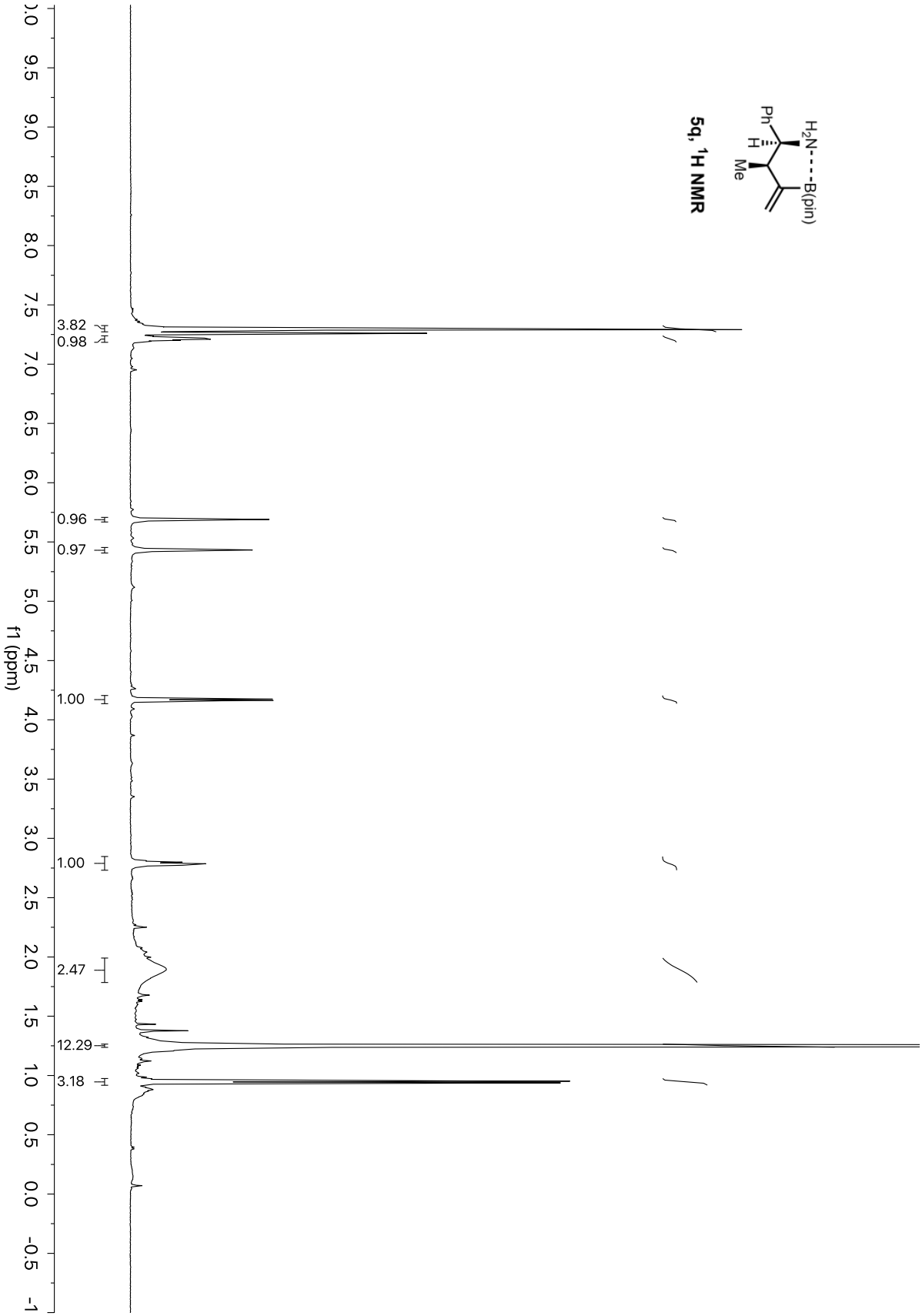
5q, $^1$H NMR
Ph
H
Me
$H_2N$----B(pin)
3.82
0.98
0.96
0.97
1.00
1.00
2.47
12.29
3.18
f1 (ppm)

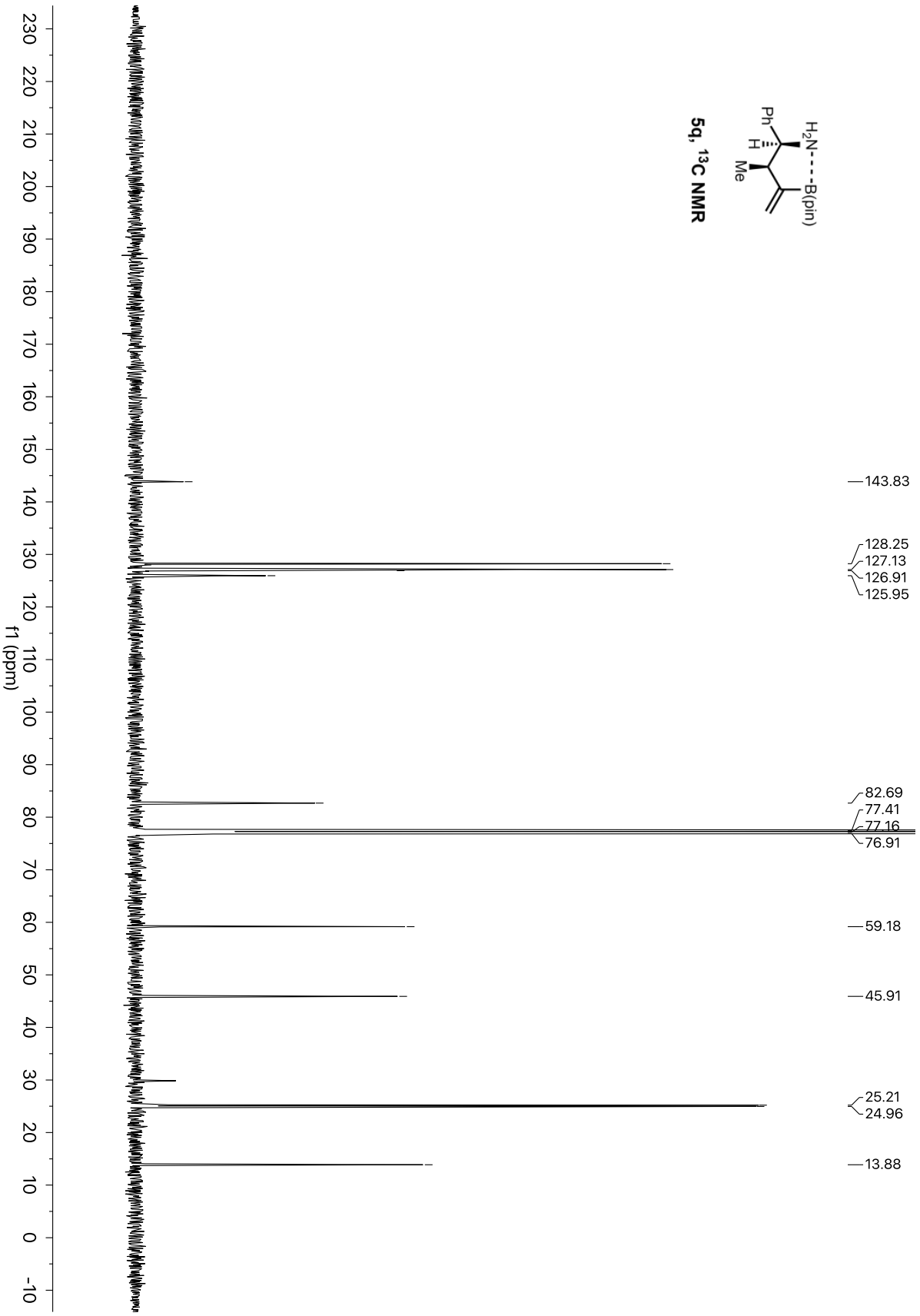
5q, 13C NMR
Ph
H
Me
H2N---B(pin)
143.83
128.25
127.13
126.91
125.95
82.69
77.41
77.16
76.91
59.18
45.91
25.21
24.96
13.88
f1 (ppm)

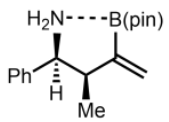
H2N----B(pin)
Ph
H
Me

**5q, $^{11}$B NMR**


25.41
90
80
70
60
50
40
30
20
10
0
-10
-20
-30
-40
-50
-60
-70
-80
-90
f1 (ppm)

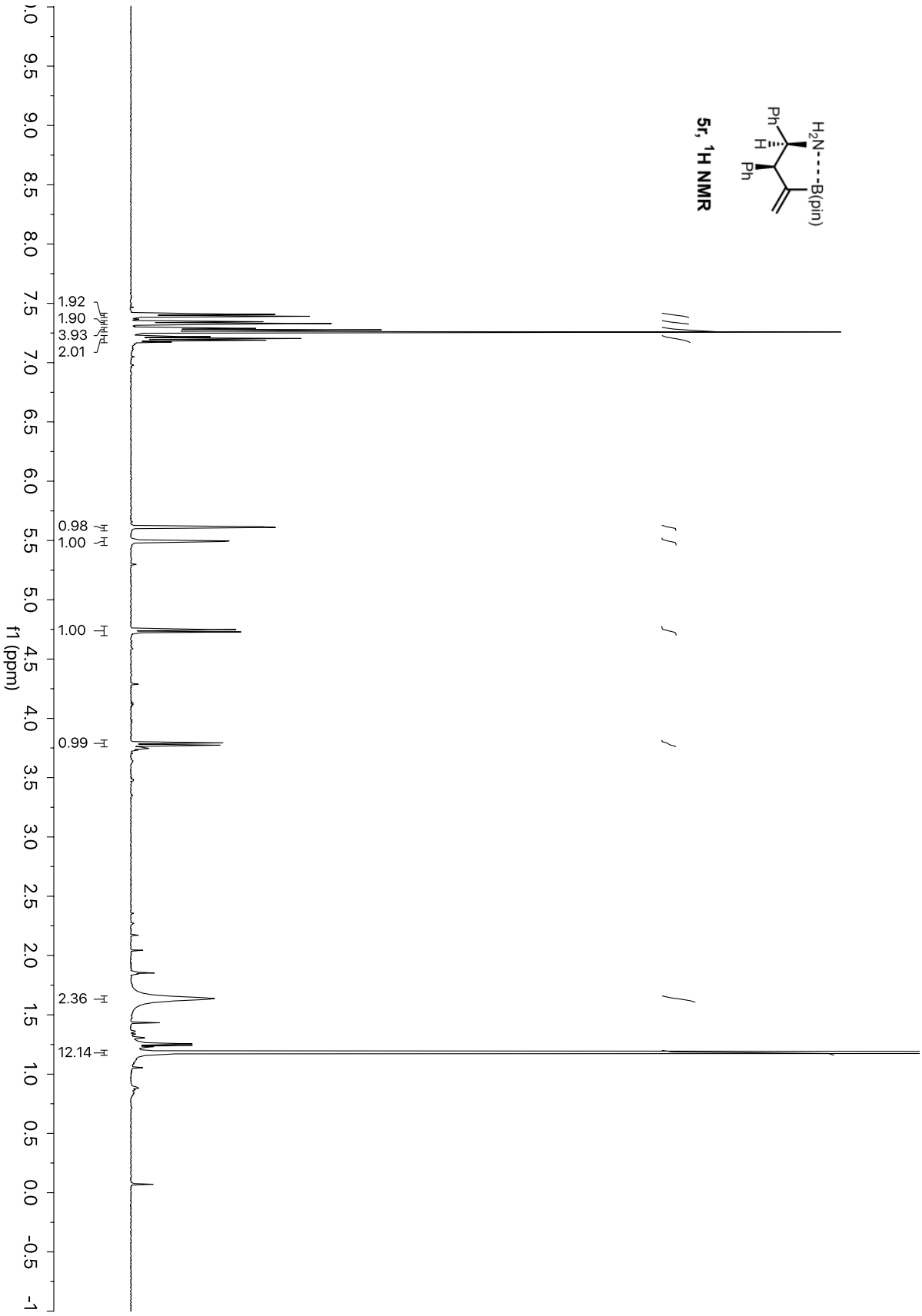
5r, $^1$H NMR
Ph
H
Ph
H$_2$N---B(pin)
1.92
1.90
3.93
2.01
0.98
1.00
1.00
0.99
2.36
12.14
f1 (ppm)

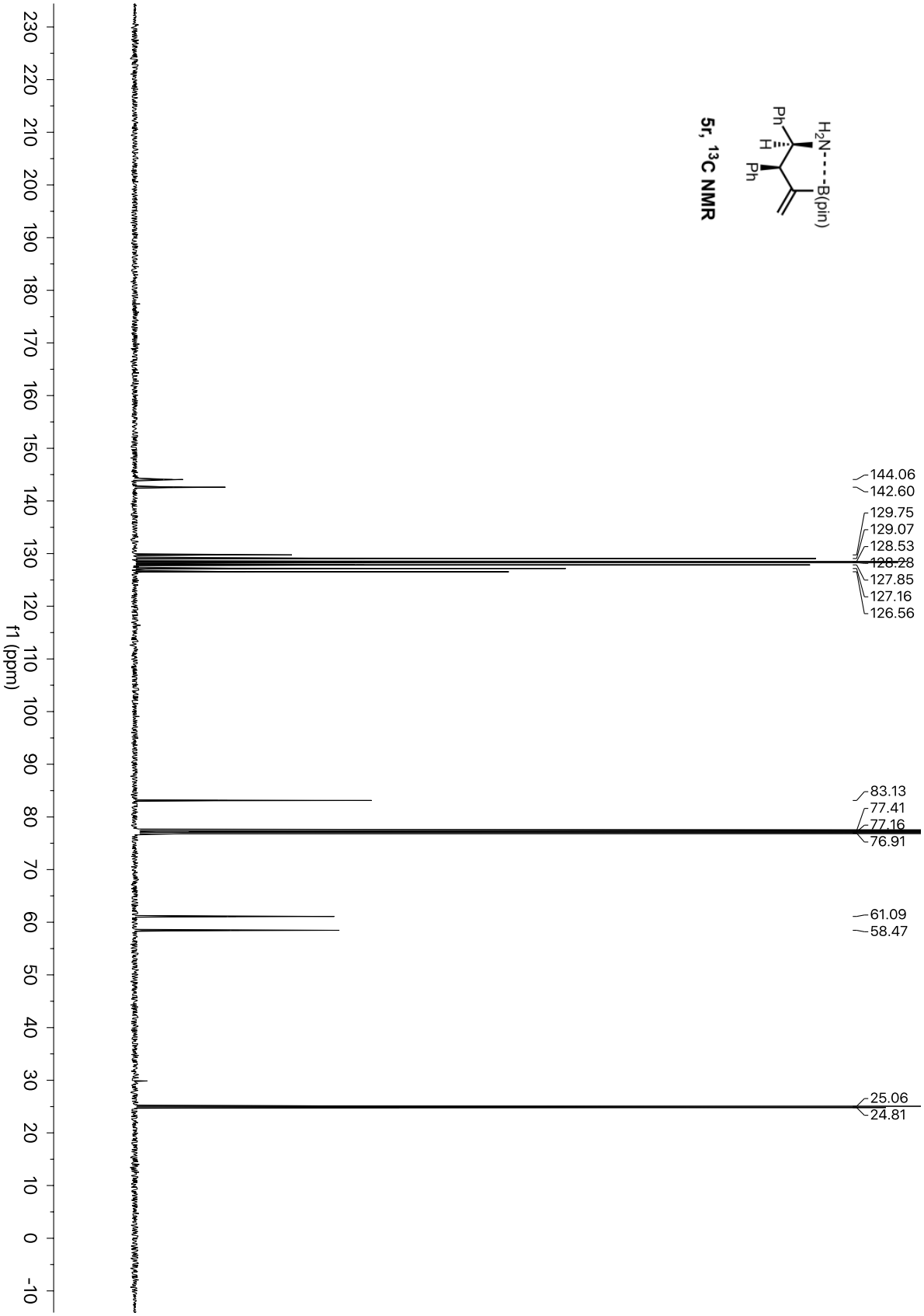
5r, 13C NMR
Ph
H
Ph
H2N---B(pin)
144.06
142.60
129.75
129.07
128.53
128.28
127.85
127.16
126.56
83.13
77.41
77.16
76.91
61.09
58.47
25.06
24.81
f1 (ppm)
230 220 210 200 190 180 170 160 150 140 130 120 110 100 90 80 70 60 50 40 30 20 10 0 -10

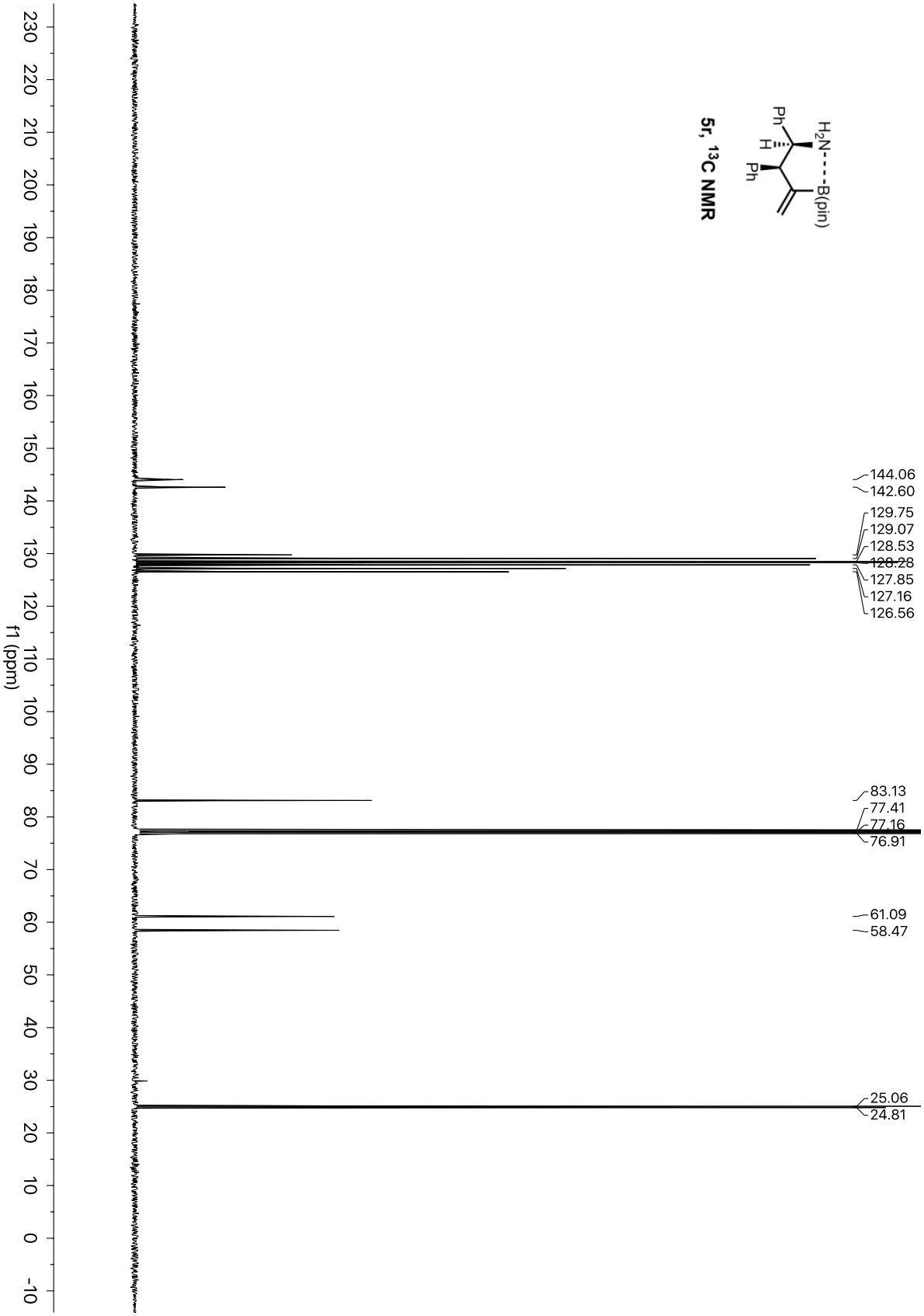
5r, 13C NMR
Ph
H
Ph
H2N---B(pin)
144.06
142.60
129.75
129.07
128.53
128.28
127.85
127.16
126.56
83.13
77.41
77.16
76.91
61.09
58.47
25.06
24.81
f1 (ppm)

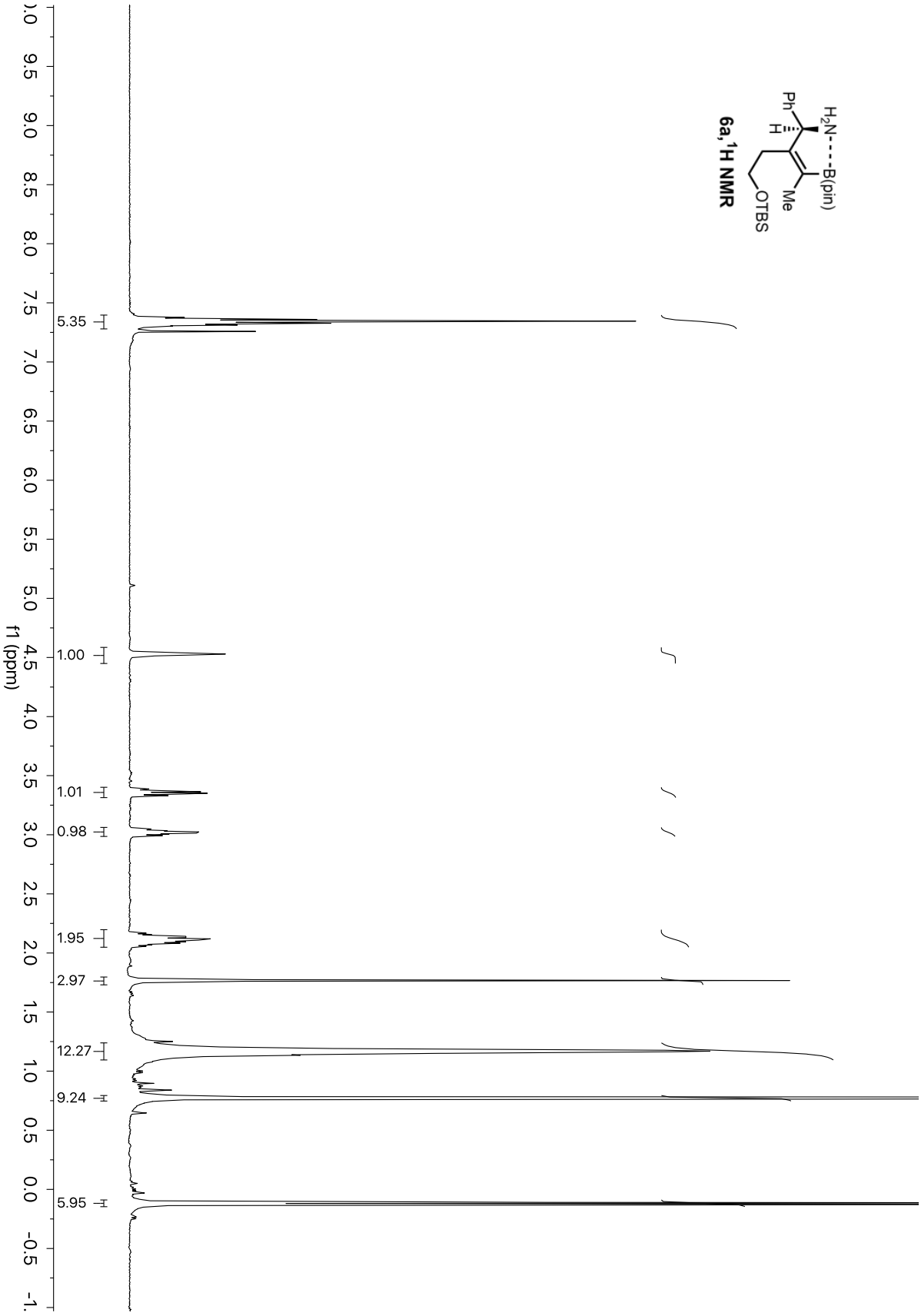
6a, $^1$H NMR
$H_2N$---B(pin)
Ph
H
Me
OTBS
5.35
1.00
1.01
0.98
1.95
2.97
12.27
9.24
5.95
f1 (ppm)

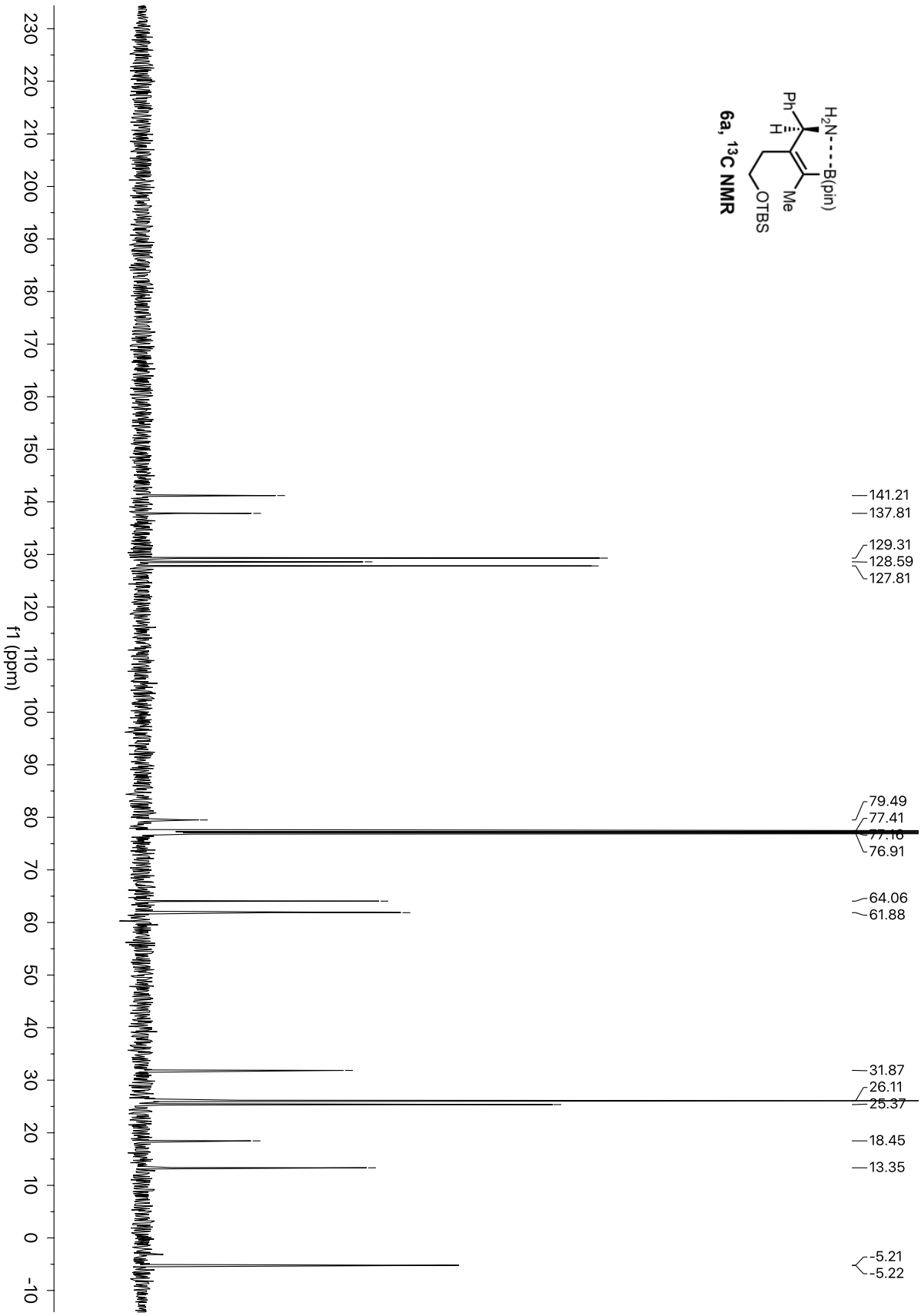
6a, 13C NMR
H2N---B(pin)
Ph
H
Me
OTBS
141.21
137.81
129.31
128.59
127.81
79.49
77.41
77.16
76.91
64.06
61.88
31.87
26.11
25.37
18.45
13.35
-5.21
-5.22
f1 (ppm)

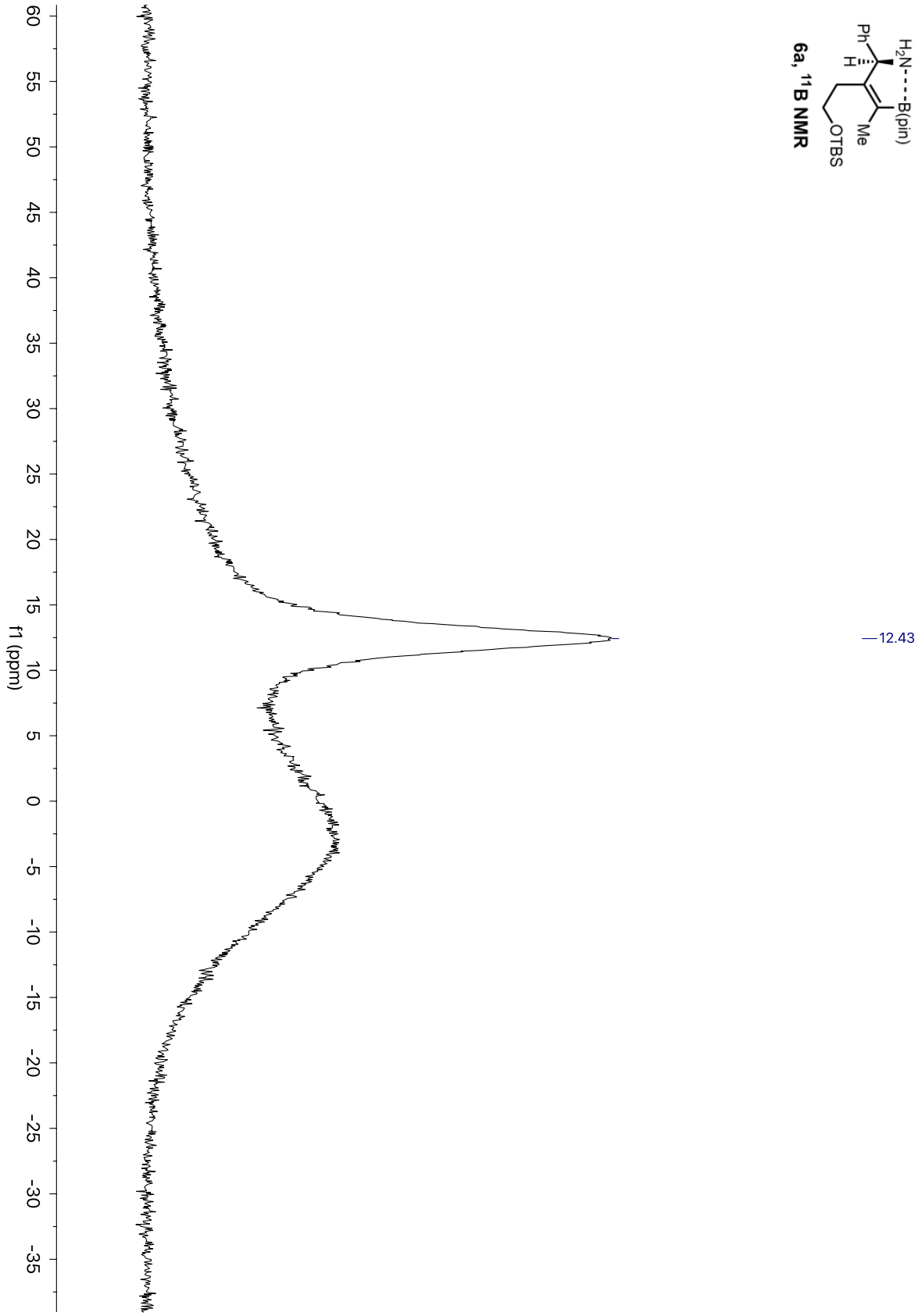
H2N---B(pin)
Ph
H
Me
OTBS
6a, 11B NMR
12.43
60
55
50
45
40
35
30
25
20
15
10
5
0
-5
-10
-15
-20
-25
-30
-35
f1 (ppm)

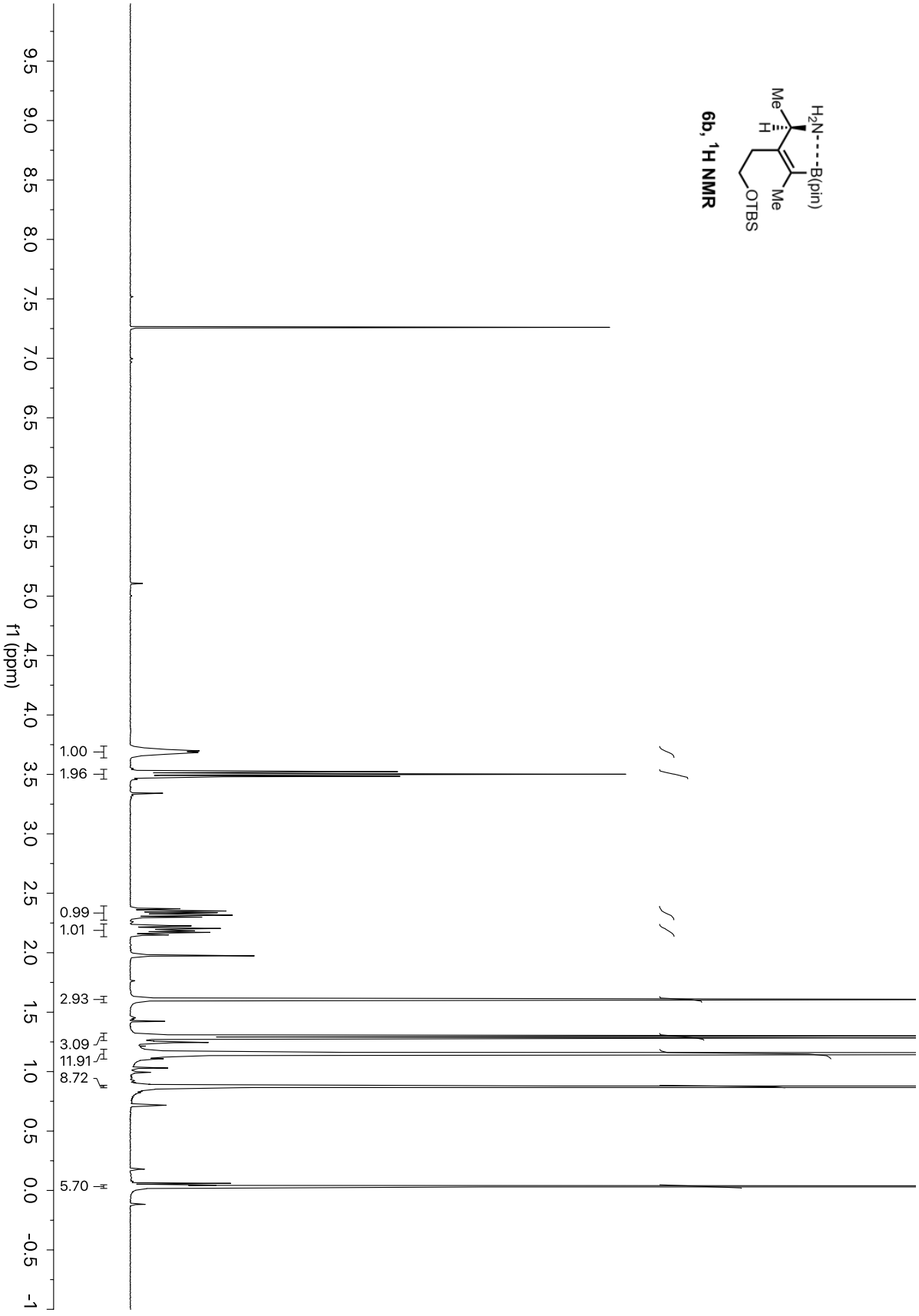
6b, $^1$H NMR
$H_2N$---B(pin)
Me
H
Me
OTBS
f1 (ppm)
9.5
9.0
8.5
8.0
7.5
7.0
6.5
6.0
5.5
5.0
4.5
4.0
3.5
3.0
2.5
2.0
1.5
1.0
0.5
0.0
-0.5
-1
1.00
1.96
0.99
1.01
2.93
3.09
11.91
8.72
5.70

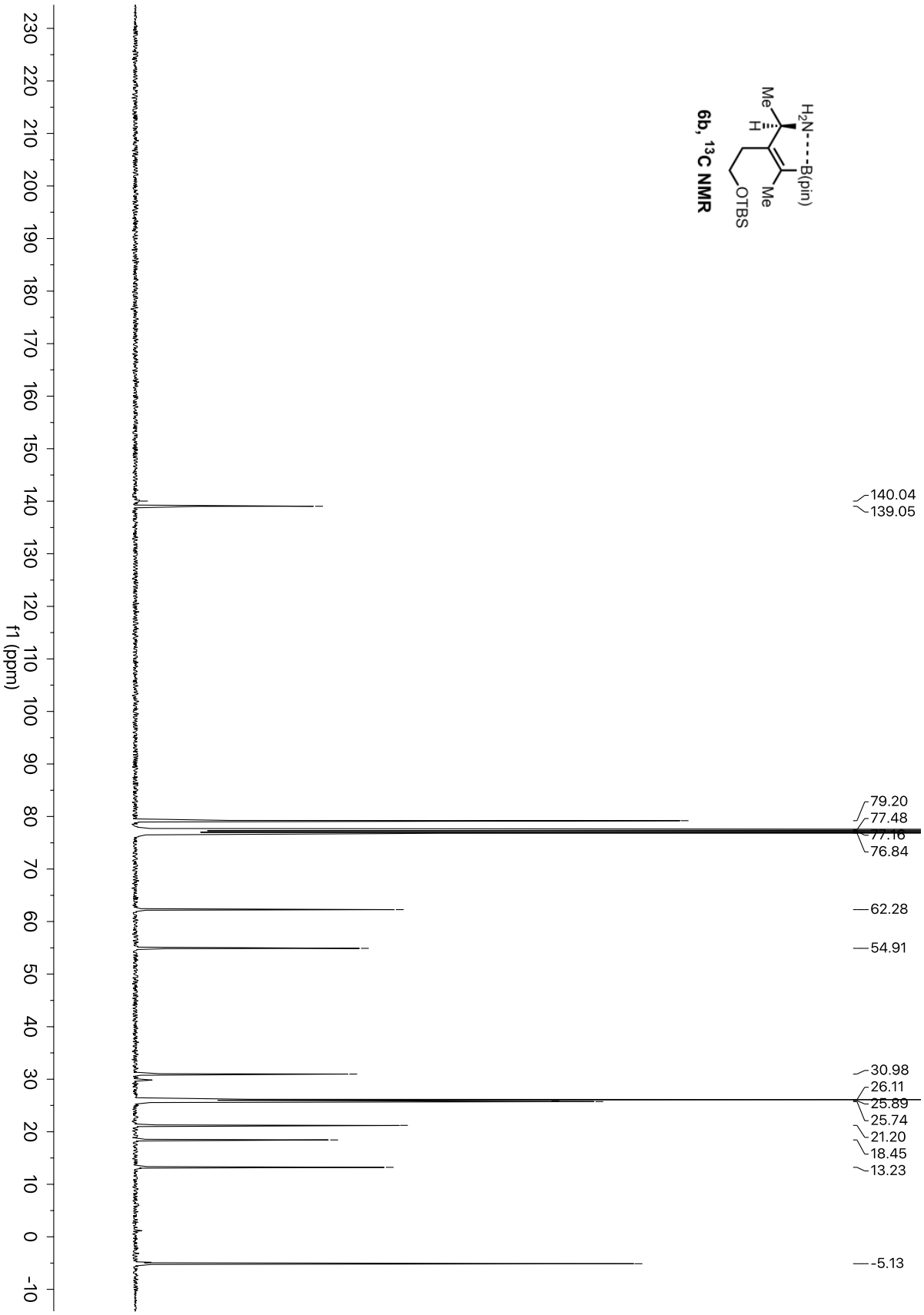
6b, 13C NMR
H2N---B(pin)
Me
H
Me
OTBS
f1 (ppm)
230
220
210
200
190
180
170
160
150
140
130
120
110
100
90
80
70
60
50
40
30
20
10
0
-10
140.04
139.05
79.20
77.48
77.16
76.84
62.28
54.91
30.98
26.11
25.89
25.74
21.20
18.45
13.23
-5.13

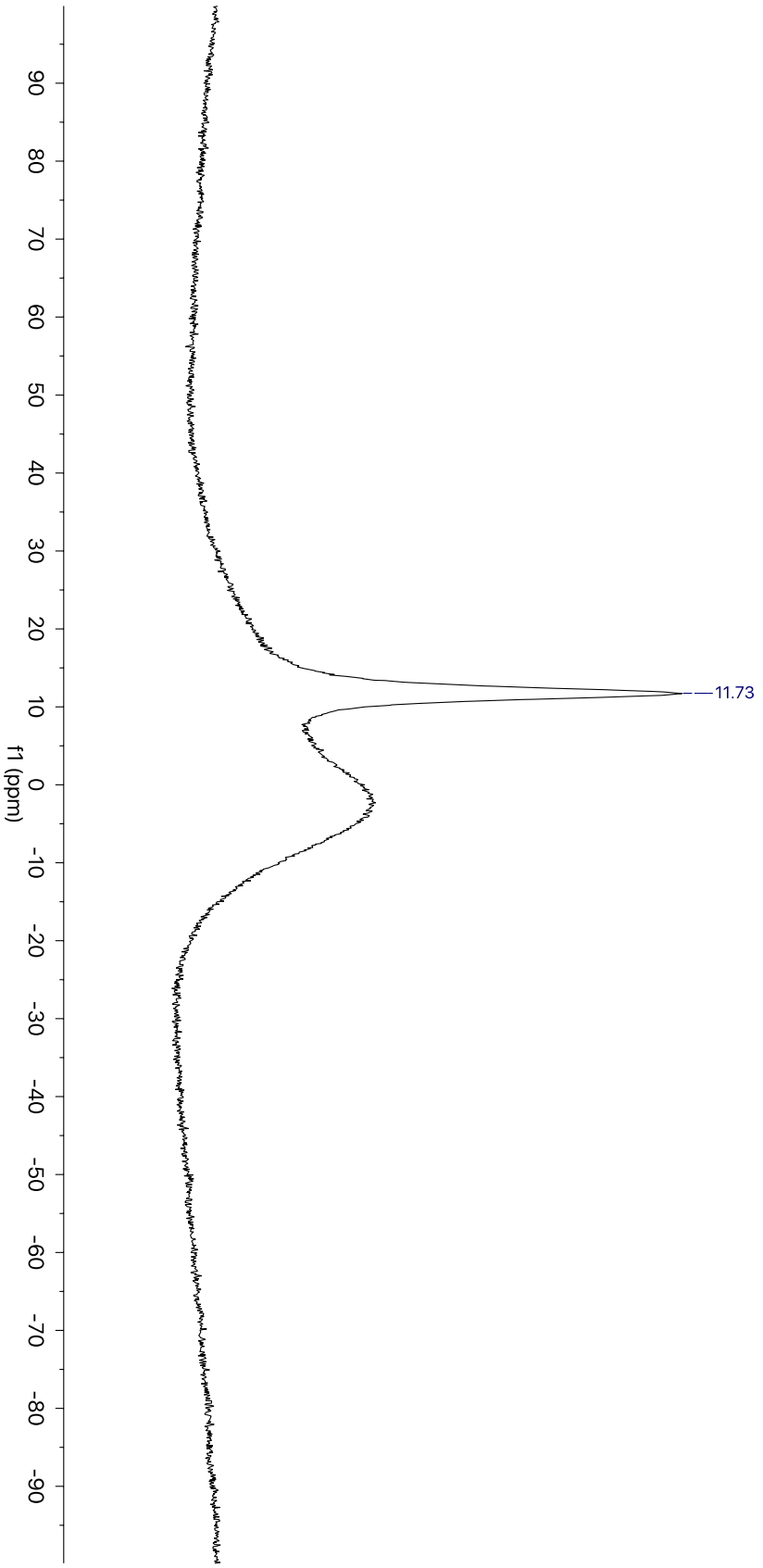
H2N---B(pin)
Me
H
Me
OTBS
6b, 13C NMR
11.73
90
80
70
60
50
40
30
20
10
0
-10
-20
-30
-40
-50
-60
-70
-80
-90
f1 (ppm)

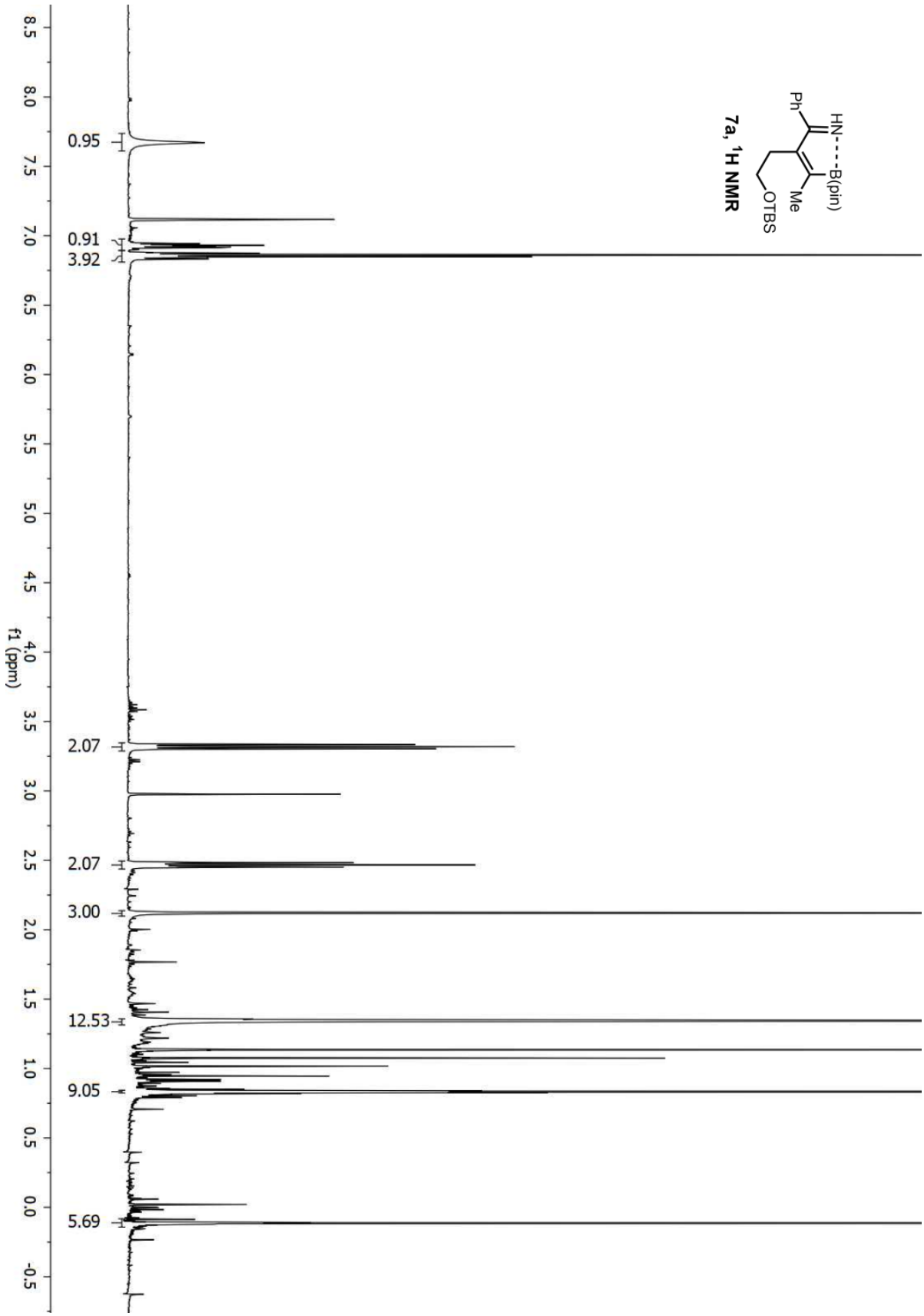
7a, $^1$H NMR
Ph
HN---B(pin)
Me
OTBS
0.95
0.91
3.92
2.07
2.07
3.00
12.53
9.05
5.69
f1 (ppm)

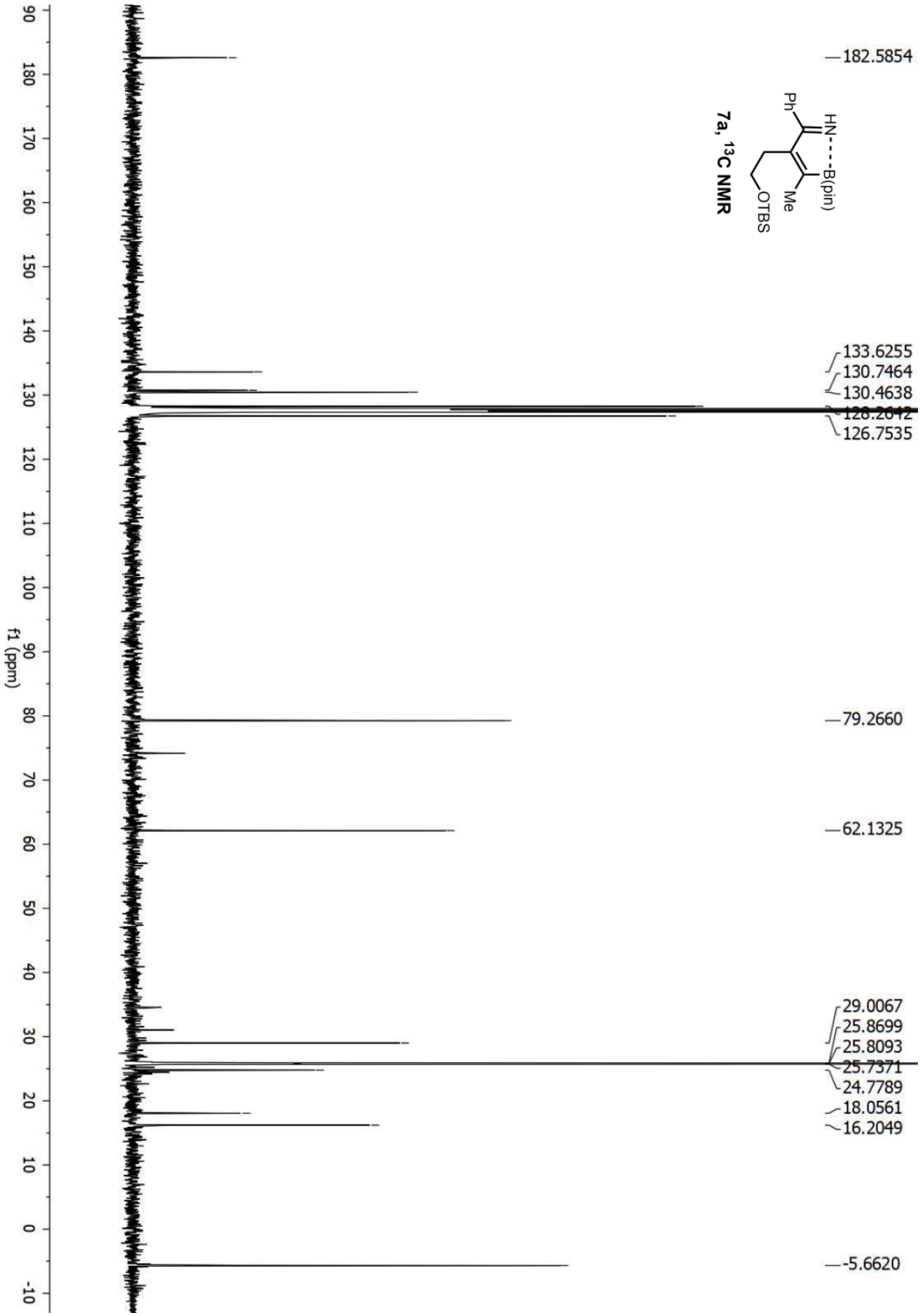
7a, 13C NMR
Ph
HN---B(pin)
Me
OTBS
182.5854
133.6255
130.7464
130.4638
128.2642
126.7535
79.2660
62.1325
29.0067
25.8699
25.8093
25.7371
24.7789
18.0561
16.2049
-5.6620
f1 (ppm)

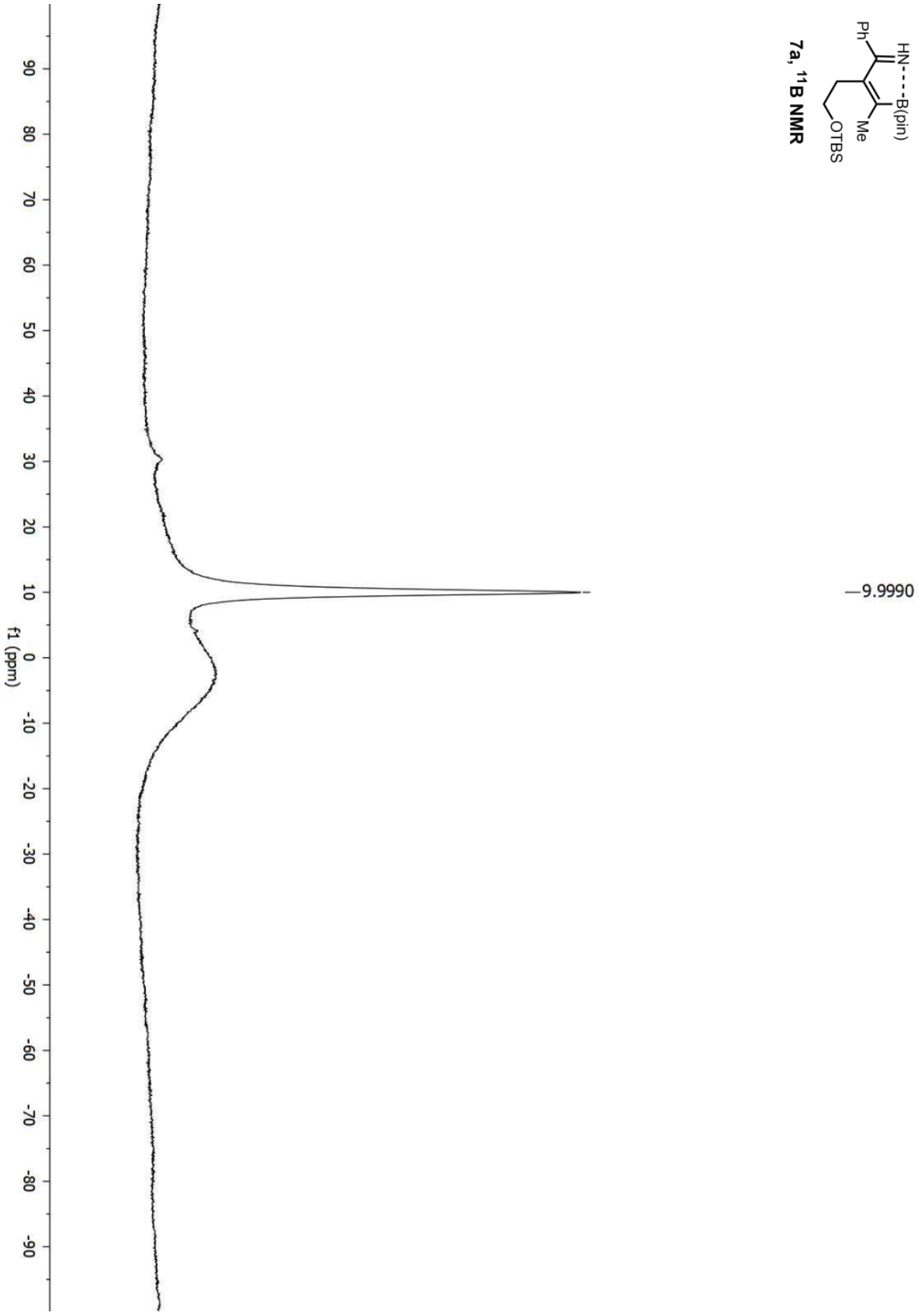
HN---B(pin)
Ph
Me
OTBS
7a, $^{11}$B NMR
9.9990
f1 (ppm)
90
80
70
60
50
40
30
20
10
0
-10
-20
-30
-40
-50
-60
-70
-80
-90

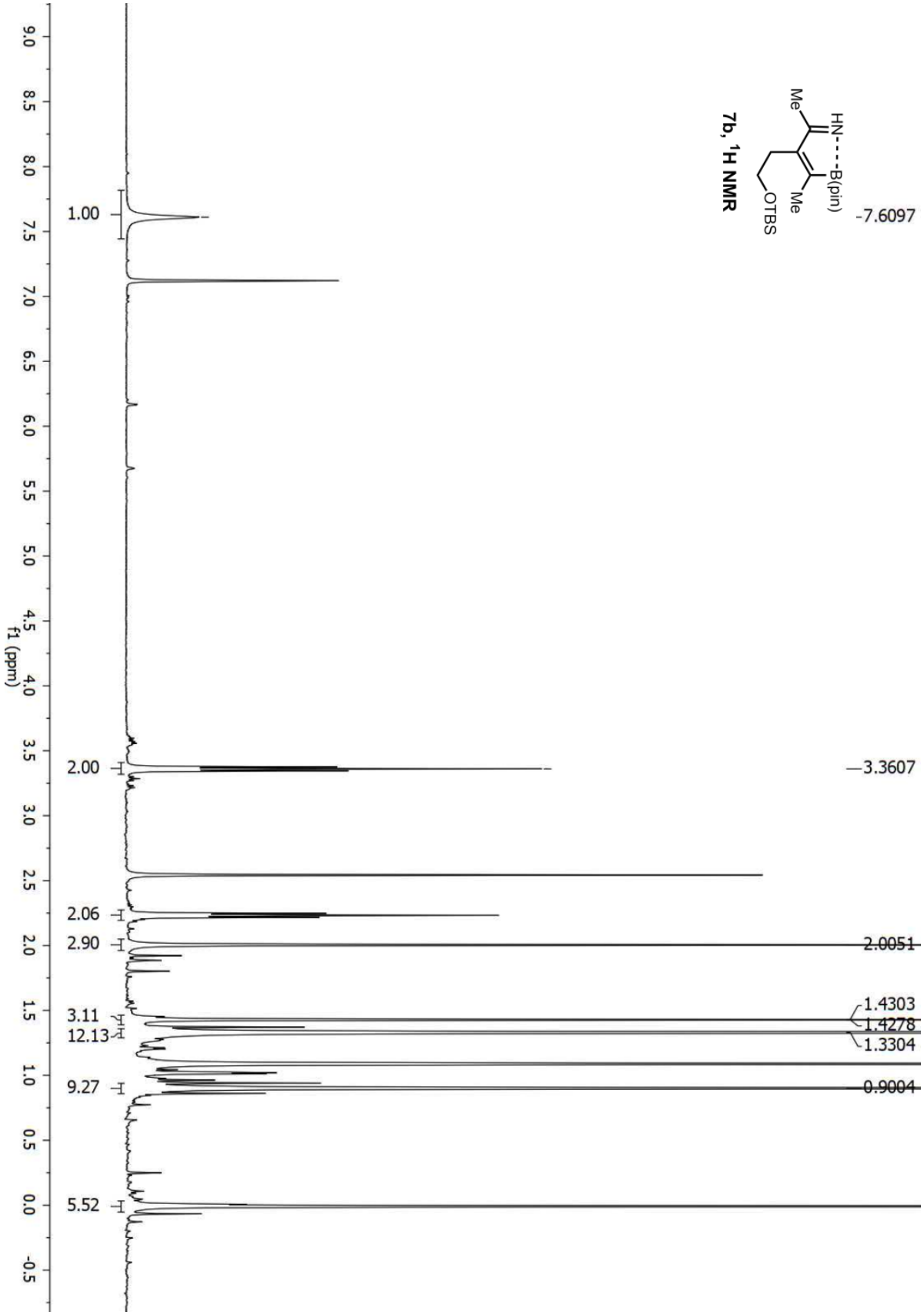
7b, $^1$H NMR
Me
HN---B(pin)
Me
OTBS
f1 (ppm)
1.00
2.00
2.06
2.90
3.11
12.13
9.27
5.52
-7.6097
3.3607
2.0051
1.4303
1.4278
1.3304
0.9004

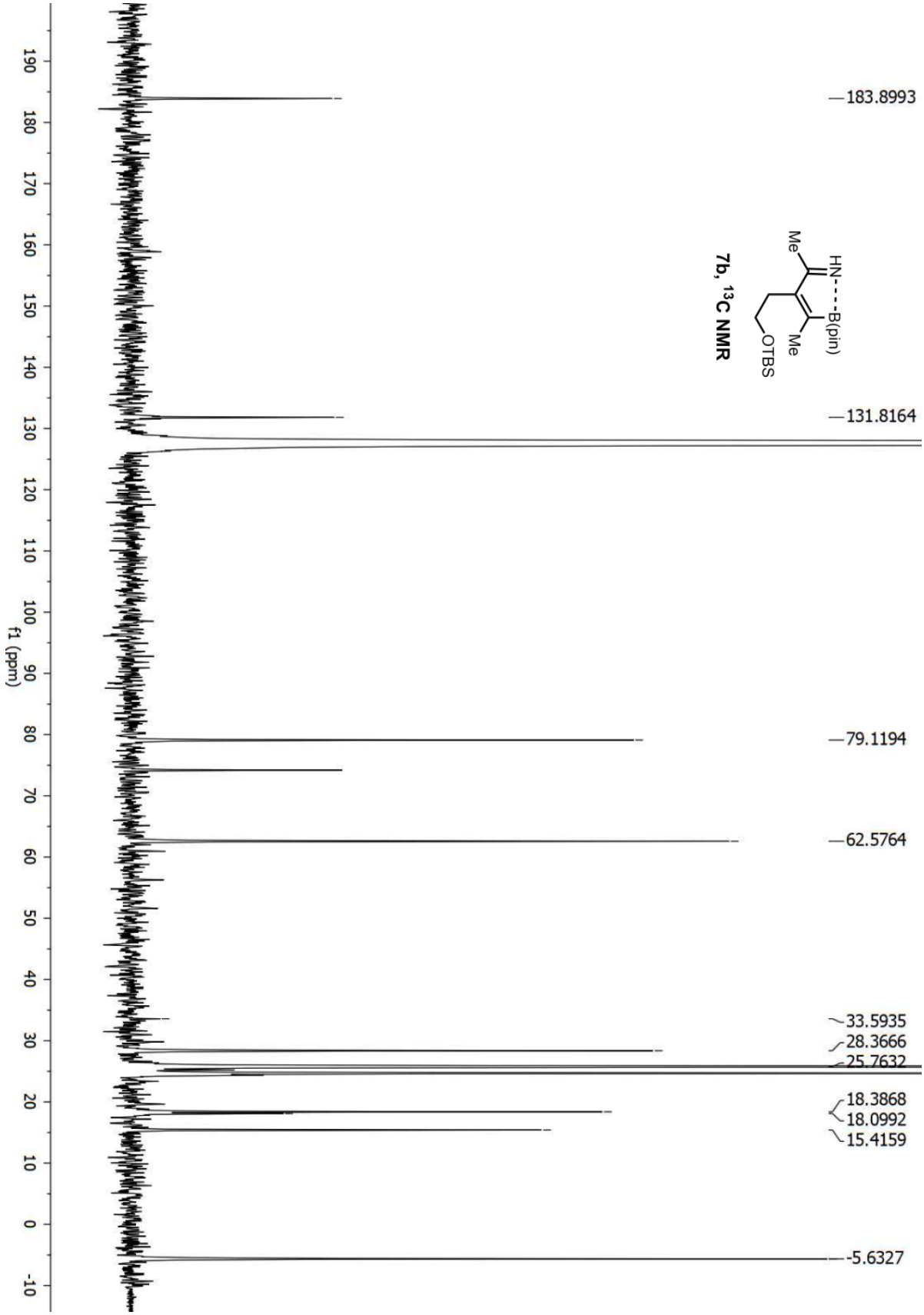
183.8993
131.8164
79.1194
62.5764
33.5935
28.3666
25.7632
18.3868
18.0992
15.4159
-5.6327
f1 (ppm)
7b, 13C NMR
Me
HN---B(pin)
Me
OTBS

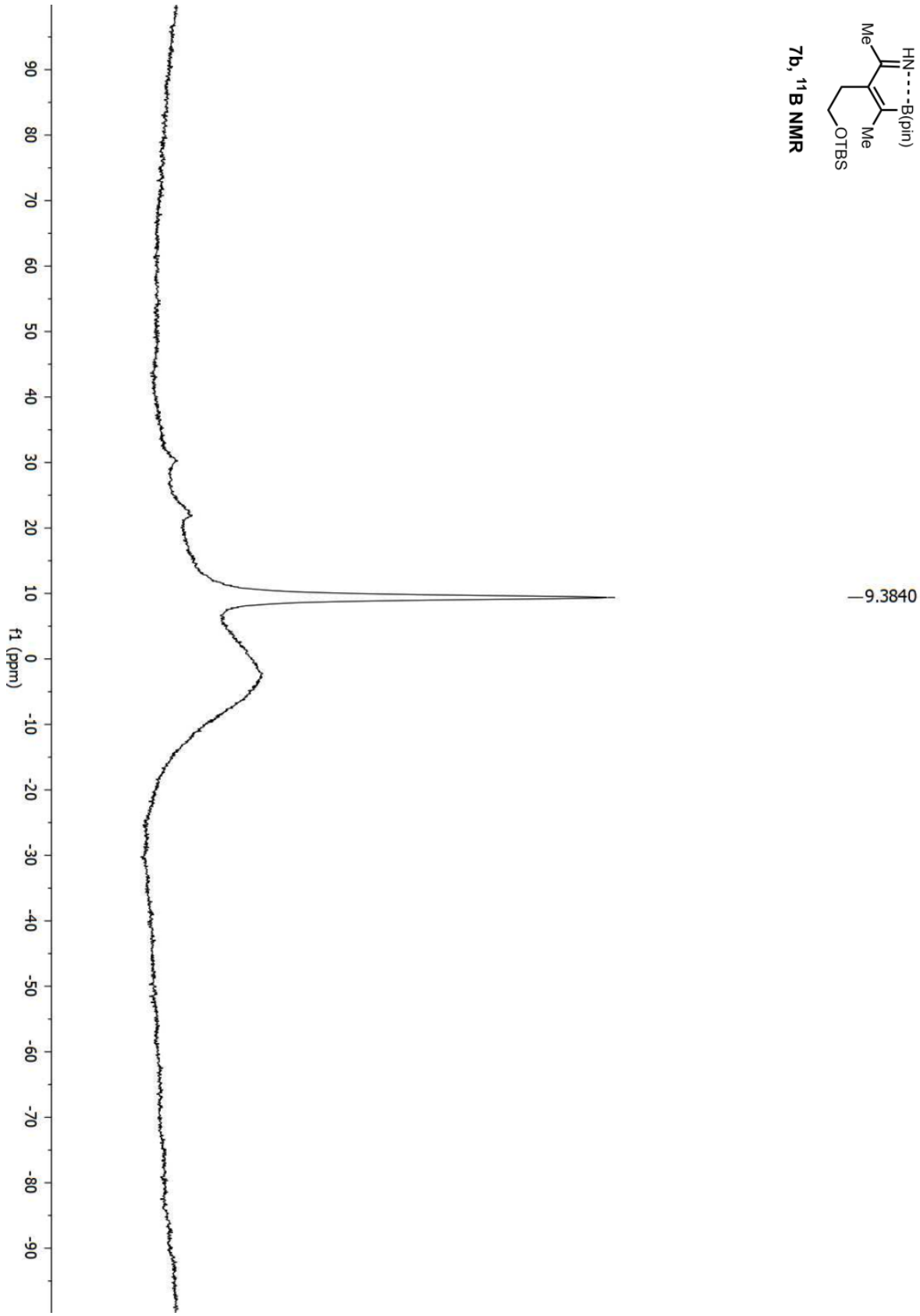
Me
HN---B(pin)
Me
OTBS
7b, $^{11}$B NMR
—9.3840
f1 (ppm)
90
80
70
60
50
40
30
20
10
0
-10
-20
-30
-40
-50
-60
-70
-80
-90

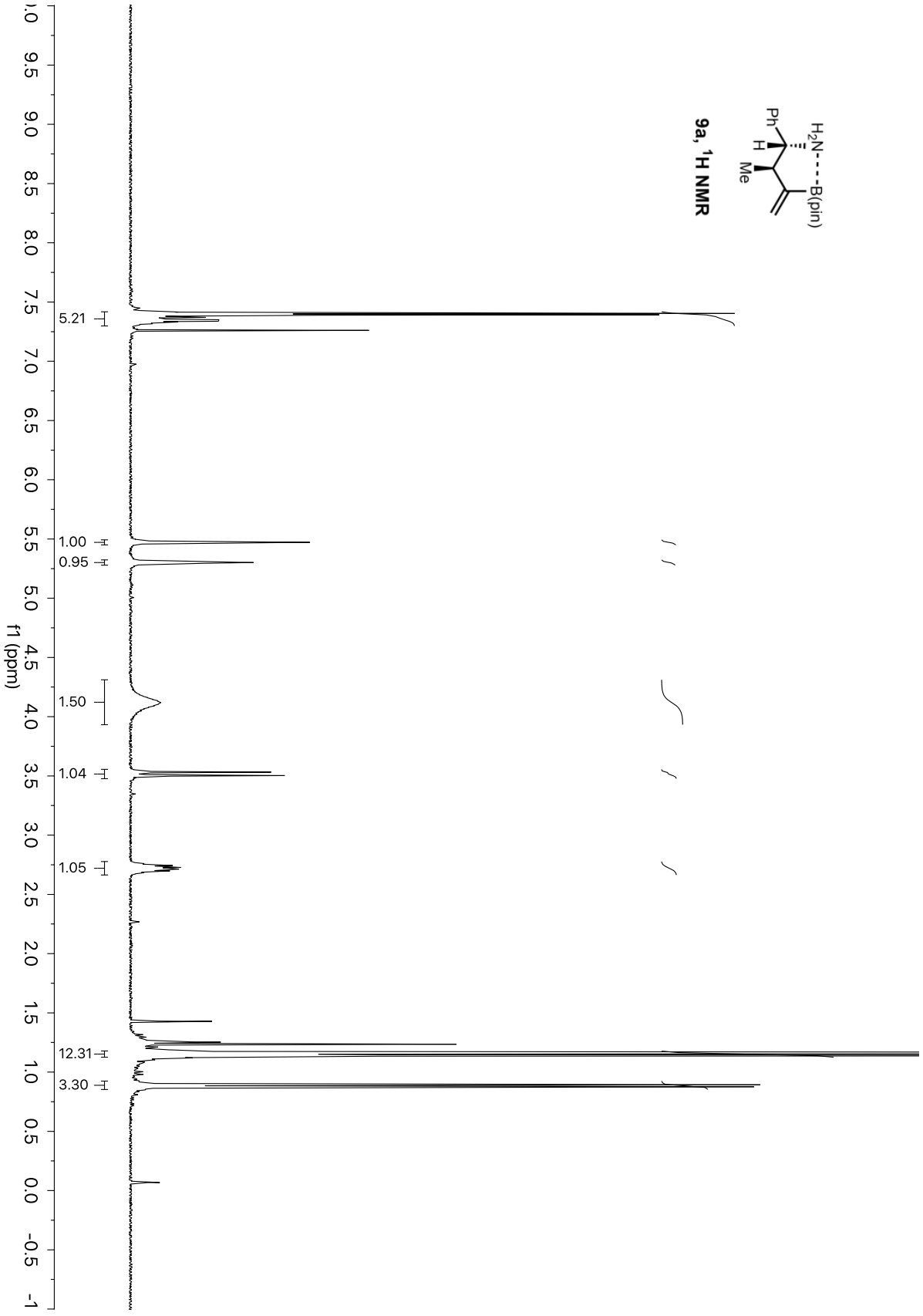
9a, 1H NMR
H2N---B(pin)
Ph
H
Me
5.21
1.00
0.95
1.50
1.04
1.05
12.31
3.30
f1 (ppm)

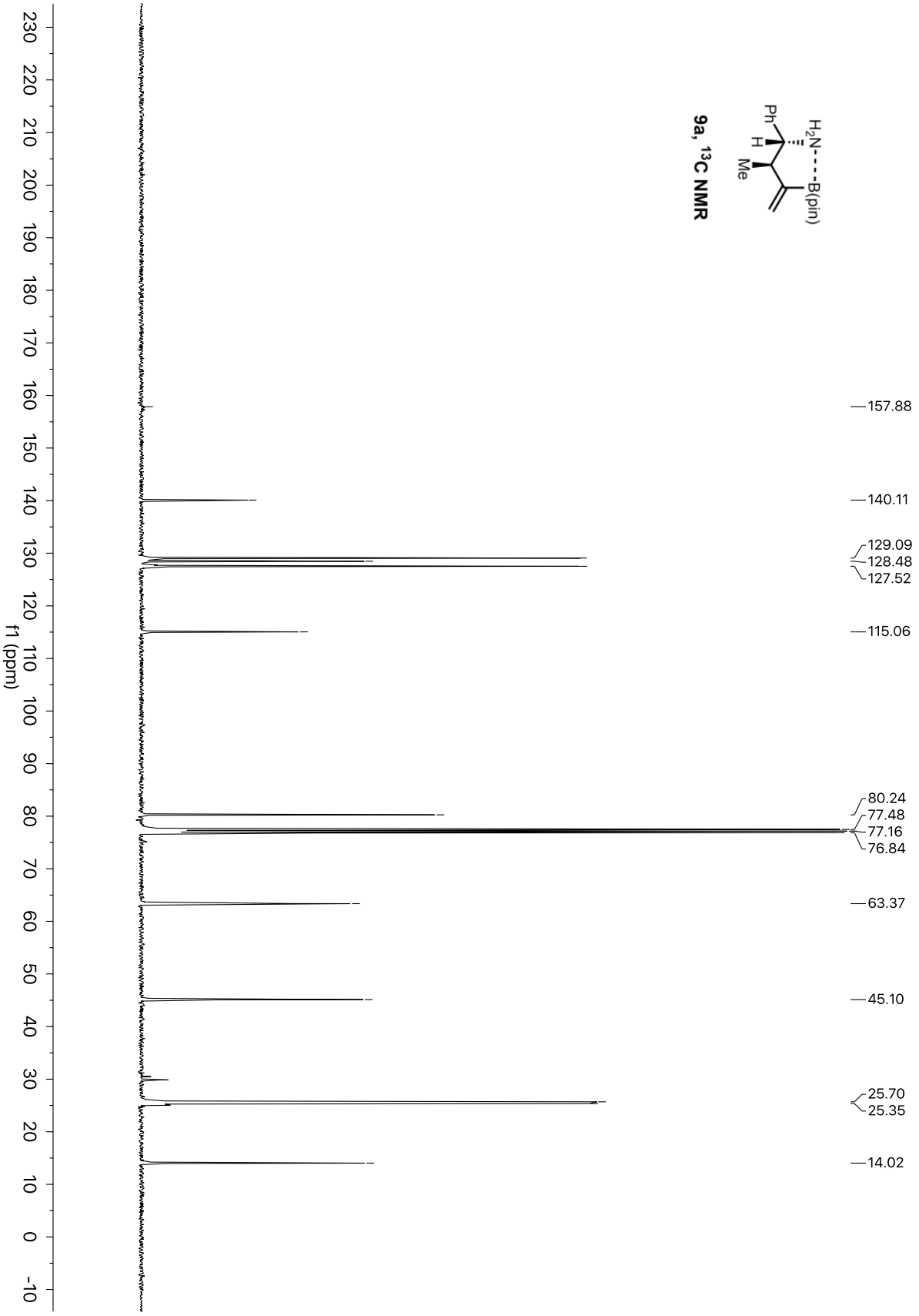
9a, 13C NMR
Ph
H
Me
H2N---B(pin)
157.88
140.11
129.09
128.48
127.52
115.06
80.24
77.48
77.16
76.84
63.37
45.10
25.70
25.35
14.02
f1 (ppm)

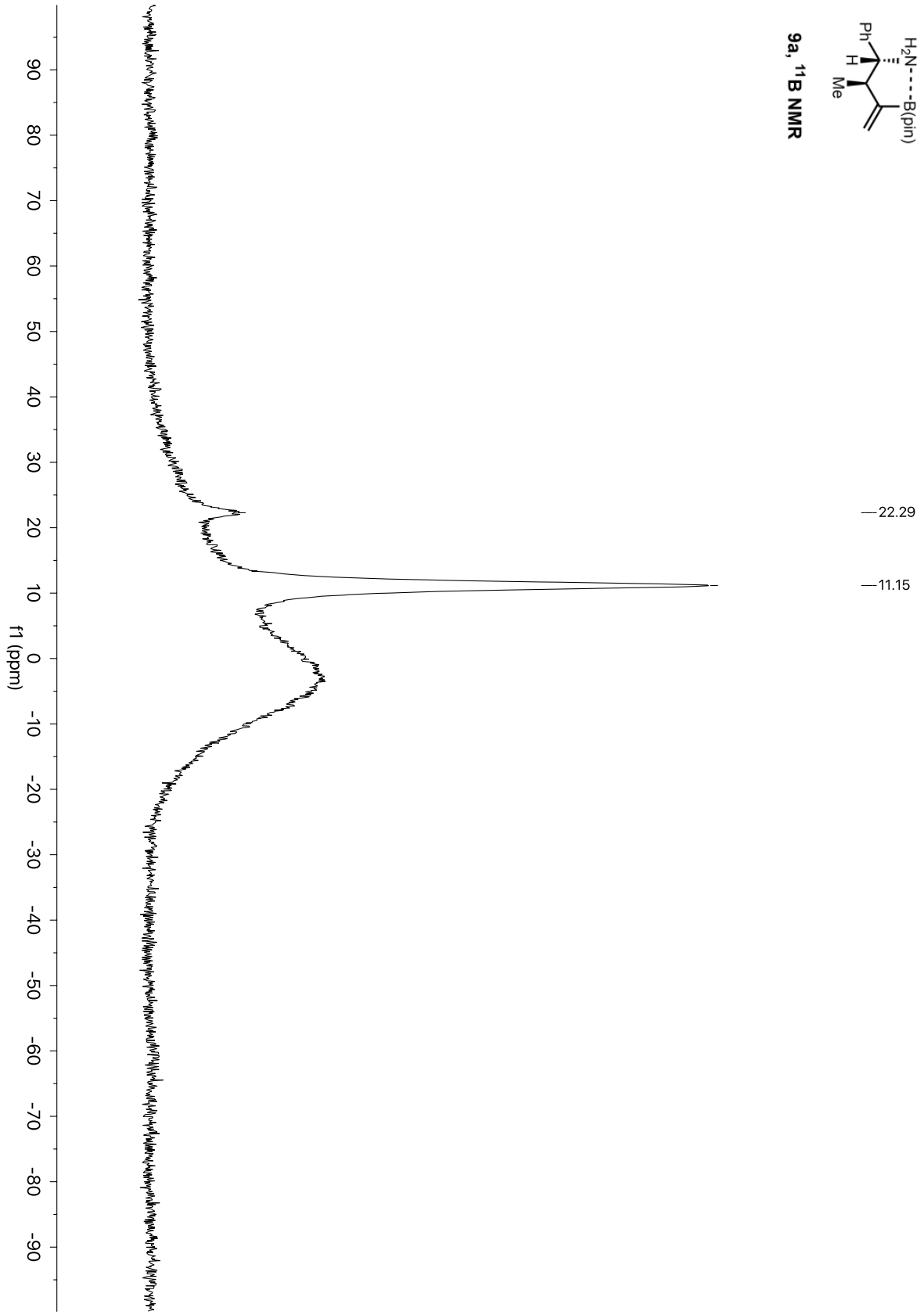
H2N---B(pin)
Ph
H
Me
9a, 11B NMR
22.29
11.15
f1 (ppm)
90
80
70
60
50
40
30
20
10
0
-10
-20
-30
-40
-50
-60
-70
-80
-90

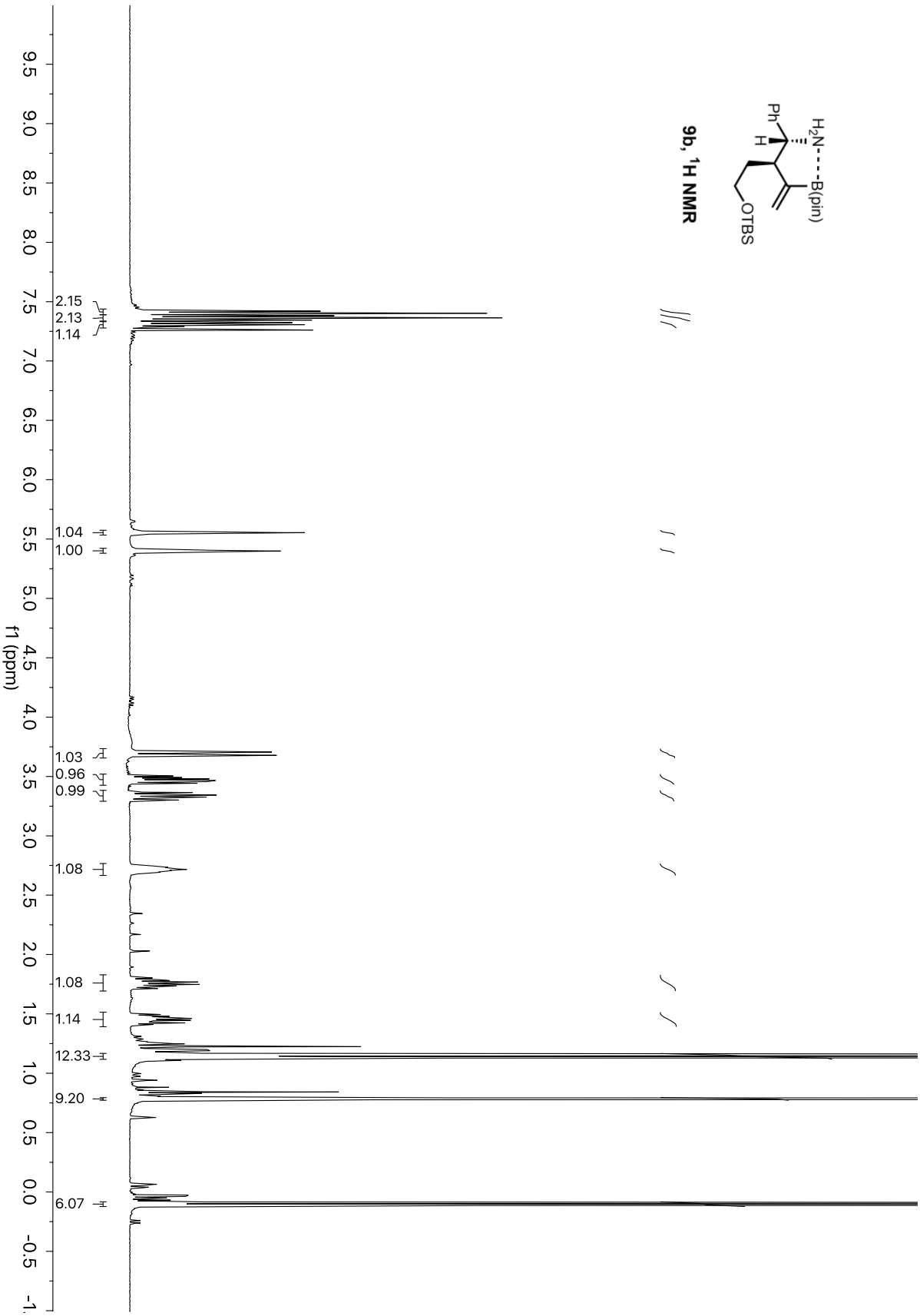
9b, $^1$H NMR
$H_2N$---B(pin)
Ph
H
OTBS
2.15
2.13
1.14
1.04
1.00
1.03
0.96
0.99
1.08
1.08
1.14
12.33
9.20
6.07
f1 (ppm)

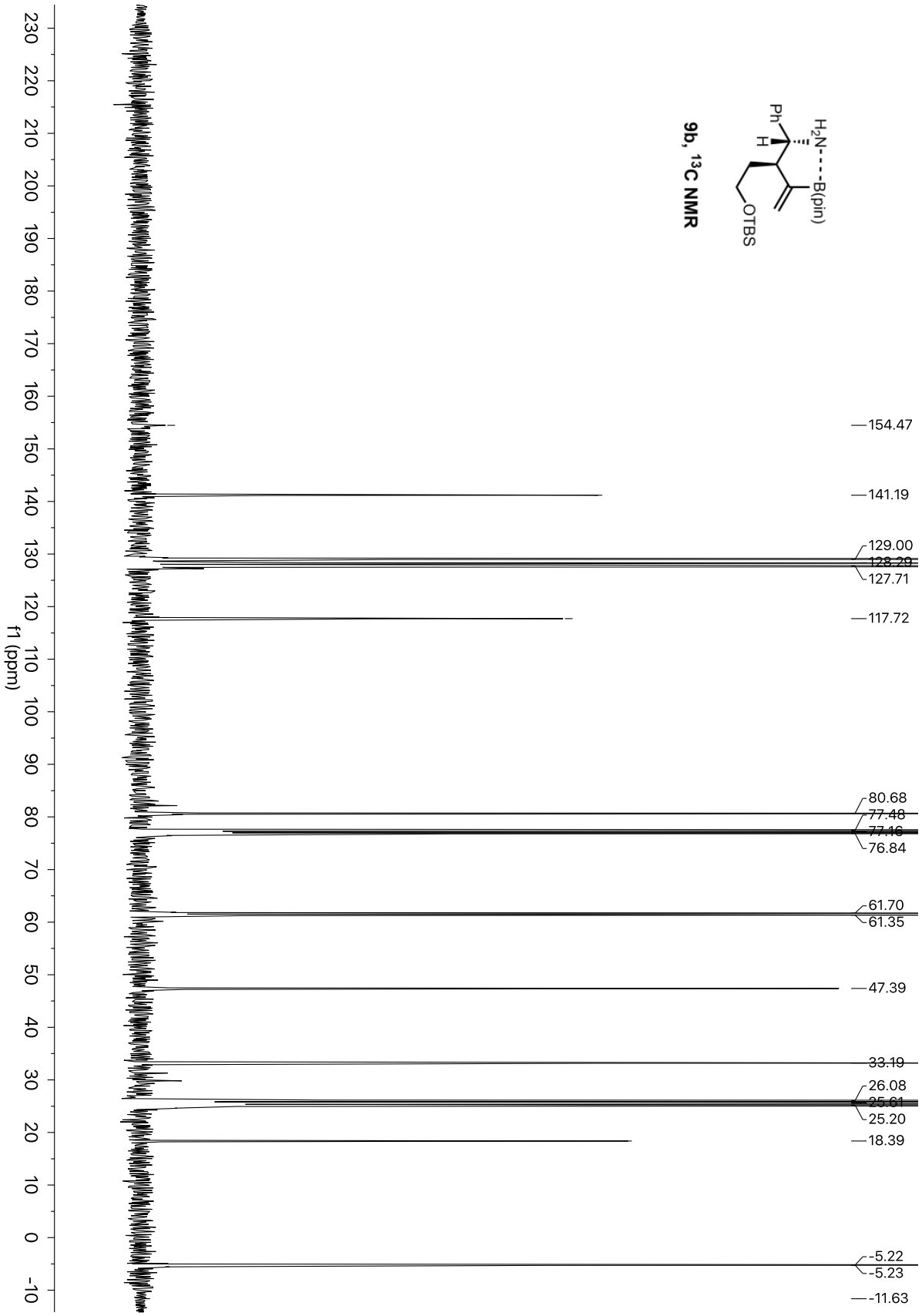
9b, $^{13}$C NMR
Ph
H
$H_2N$---B(pin)
OTBS
f1 (ppm)
230 220 210 200 190 180 170 160 150 140 130 120 110 100 90 80 70 60 50 40 30 20 10 0 -10
154.47
141.19
129.00
128.29
127.71
117.72
80.68
77.48
77.16
76.84
61.70
61.35
47.39
33.19
26.08
25.61
25.20
18.39
-5.22
-5.23
-11.63

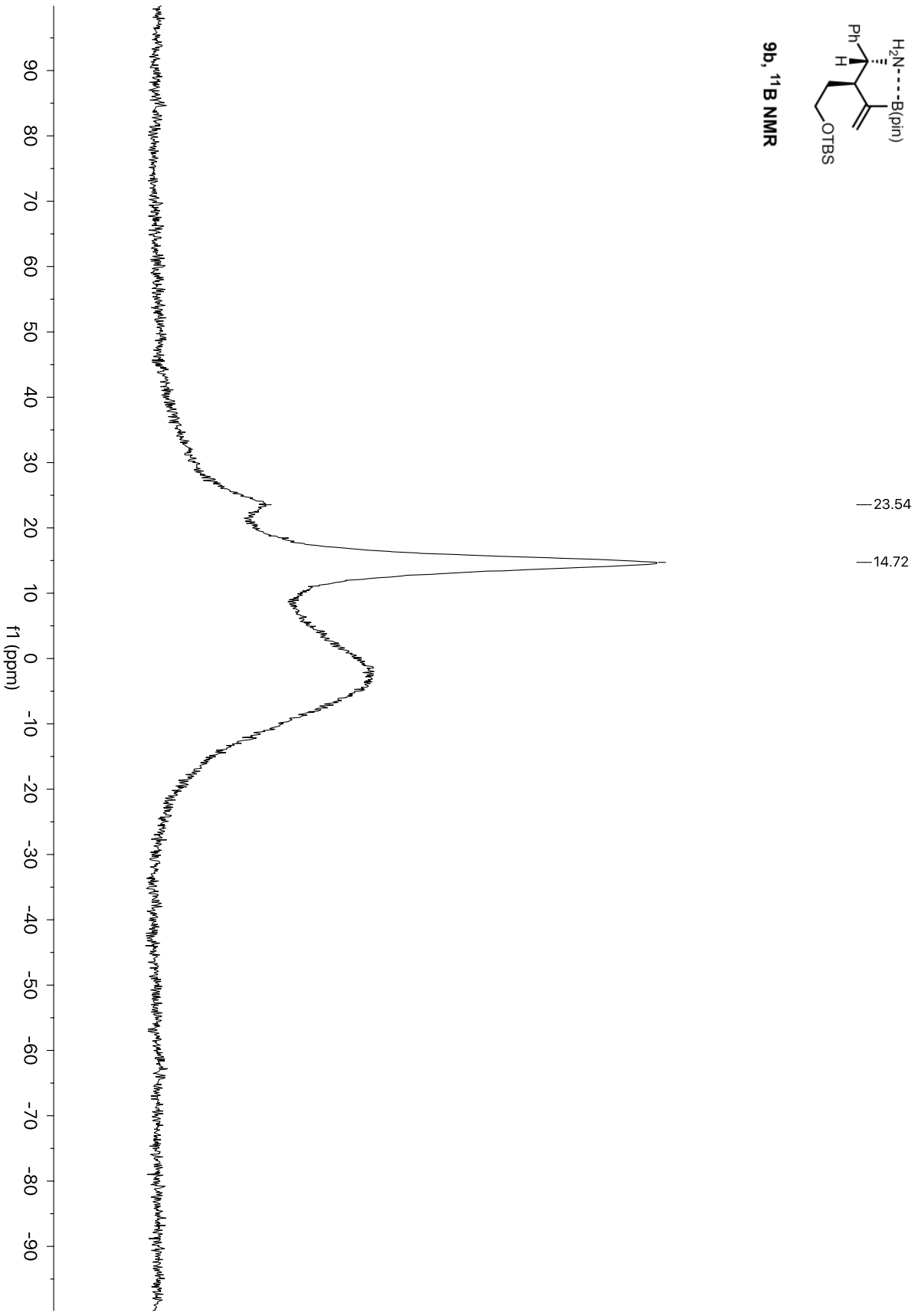
H2N---B(pin)
Ph
H
OTBS
9b, 11B NMR
23.54
14.72
f1 (ppm)
90
80
70
60
50
40
30
20
10
0
-10
-20
-30
-40
-50
-60
-70
-80
-90

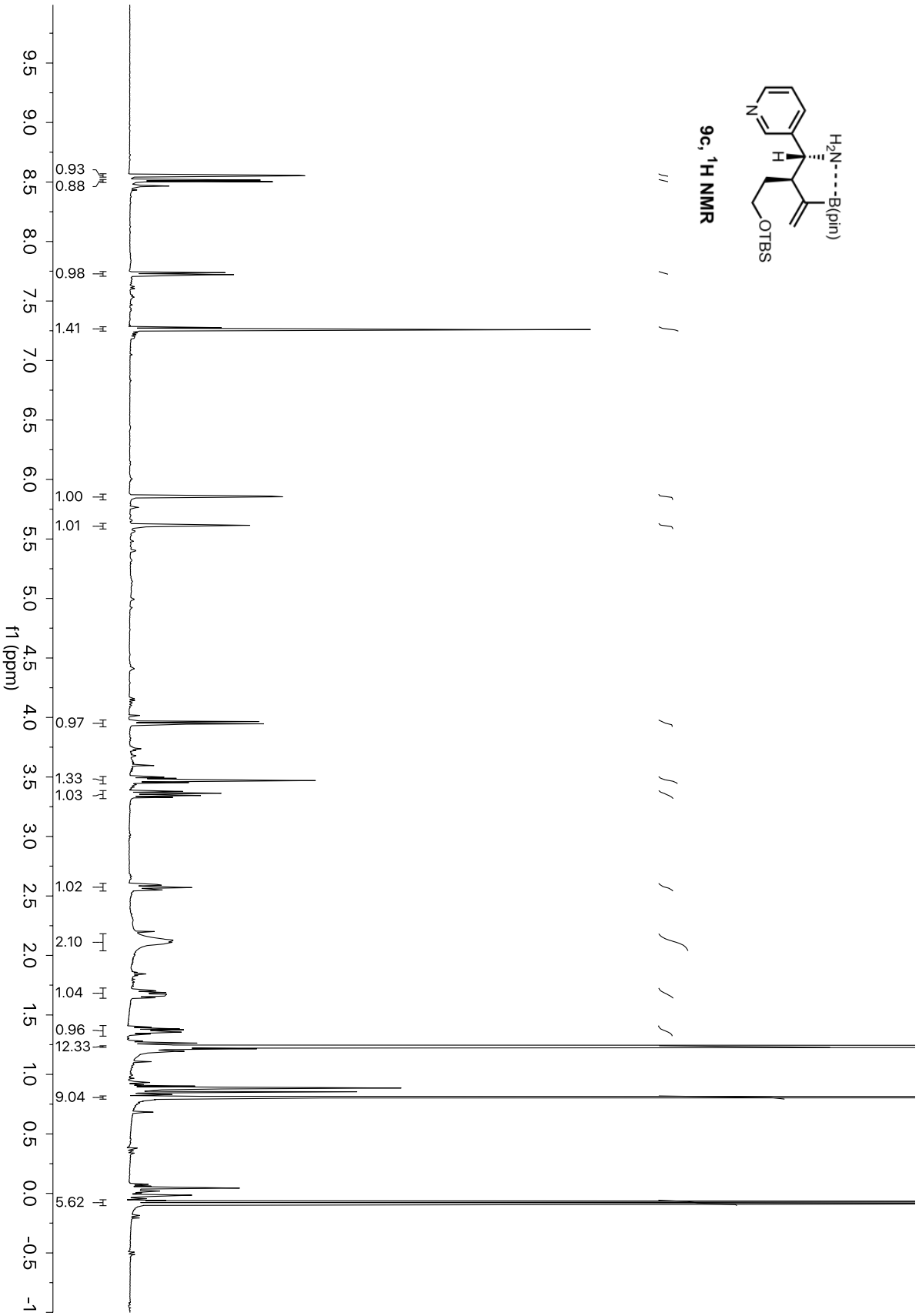
9c, 1H NMR
H2N---B(pin)
H
N
OTBS
f1 (ppm)
0.93
0.88
0.98
1.41
1.00
1.01
0.97
1.33
1.03
1.02
2.10
1.04
0.96
12.33
9.04
5.62

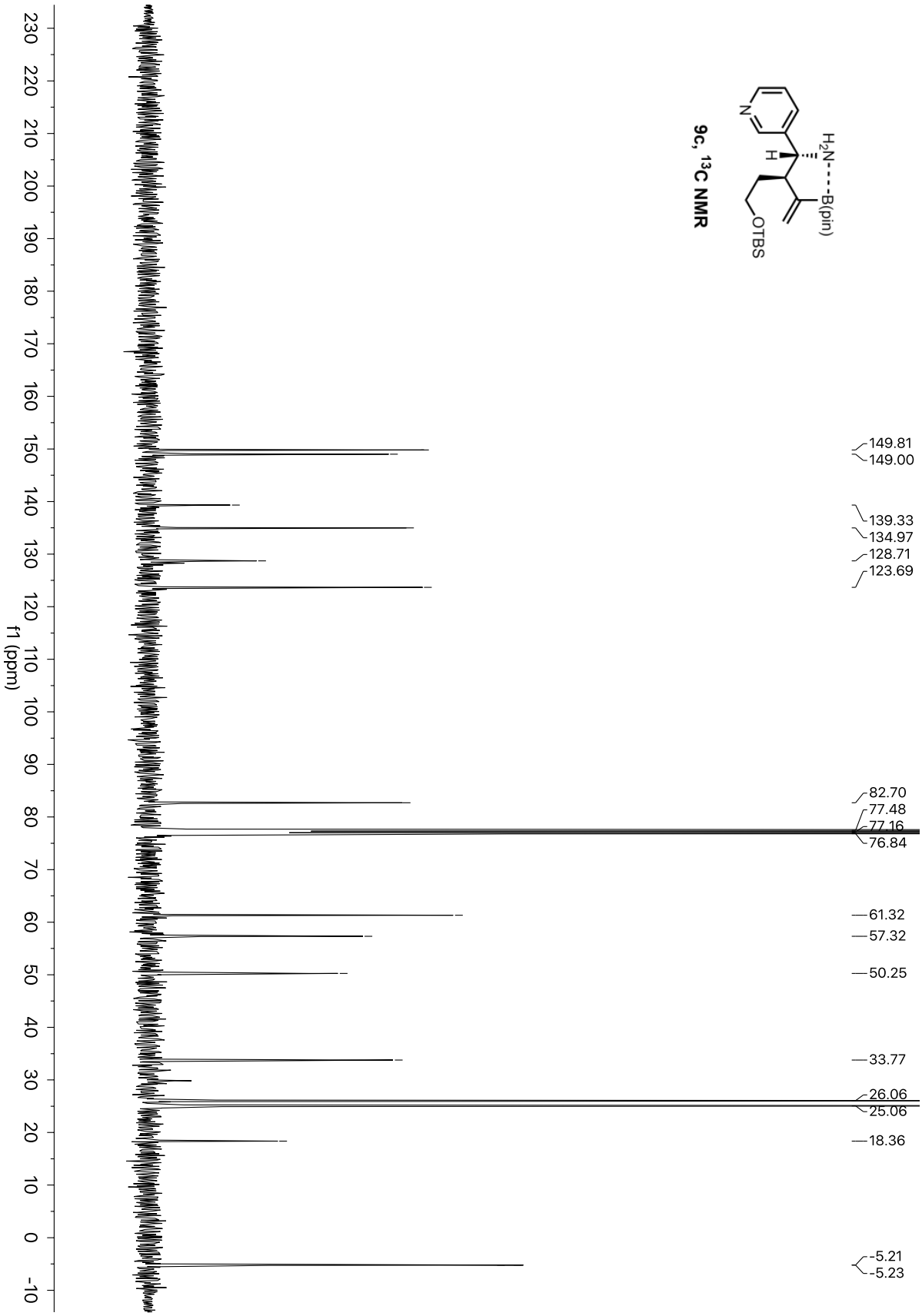
9c, 13C NMR
N
H
H2N---B(pin)
OTBS
149.81
149.00
139.33
134.97
128.71
123.69
82.70
77.48
77.16
76.84
61.32
57.32
50.25
33.77
26.06
25.06
18.36
-5.21
-5.23
f1 (ppm)

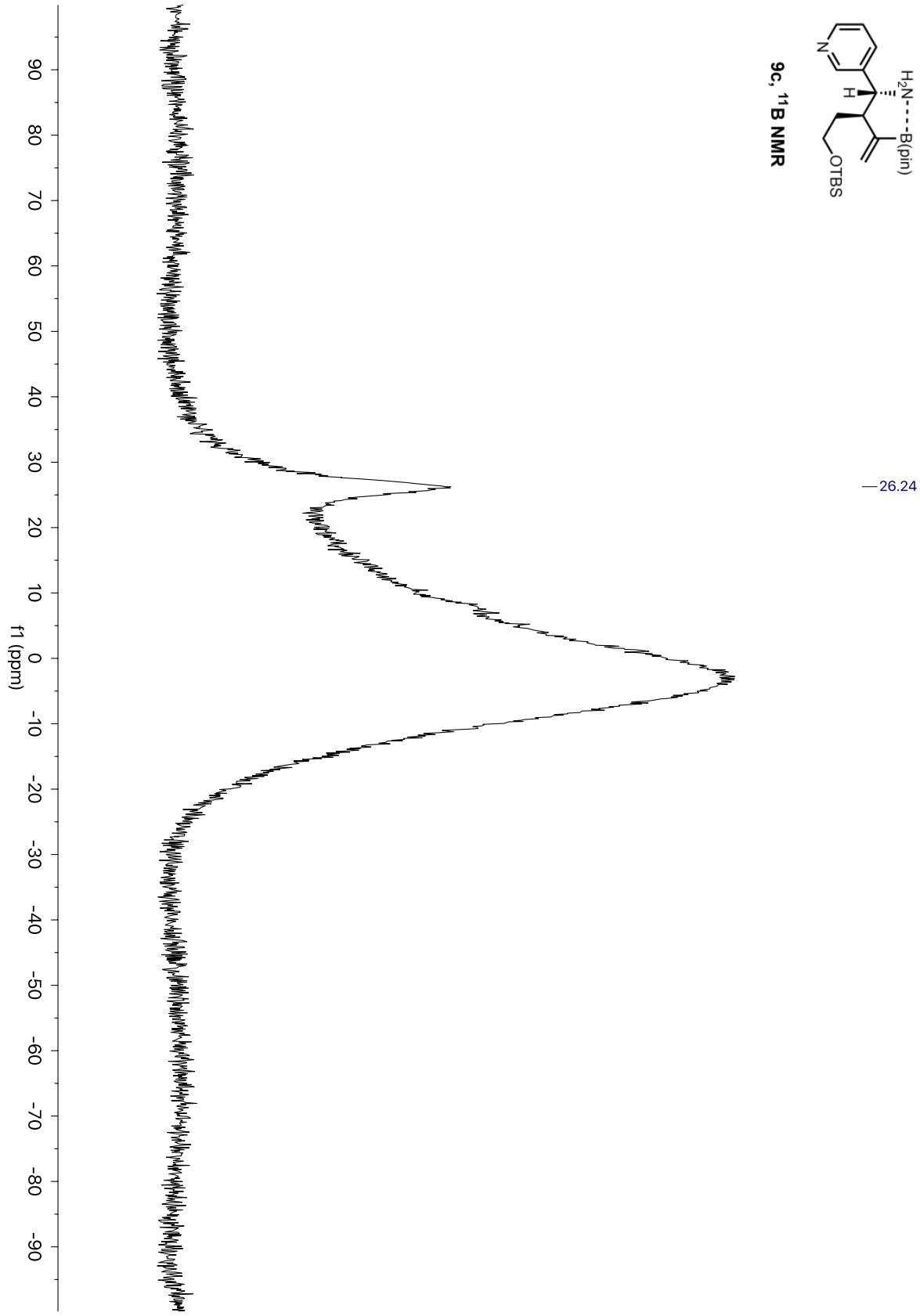
H2N---B(pin)
H
N
OTBS
9c, 11B NMR
26.24
f1 (ppm)
90
80
70
60
50
40
30
20
10
0
-10
-20
-30
-40
-50
-60
-70
-80
-90

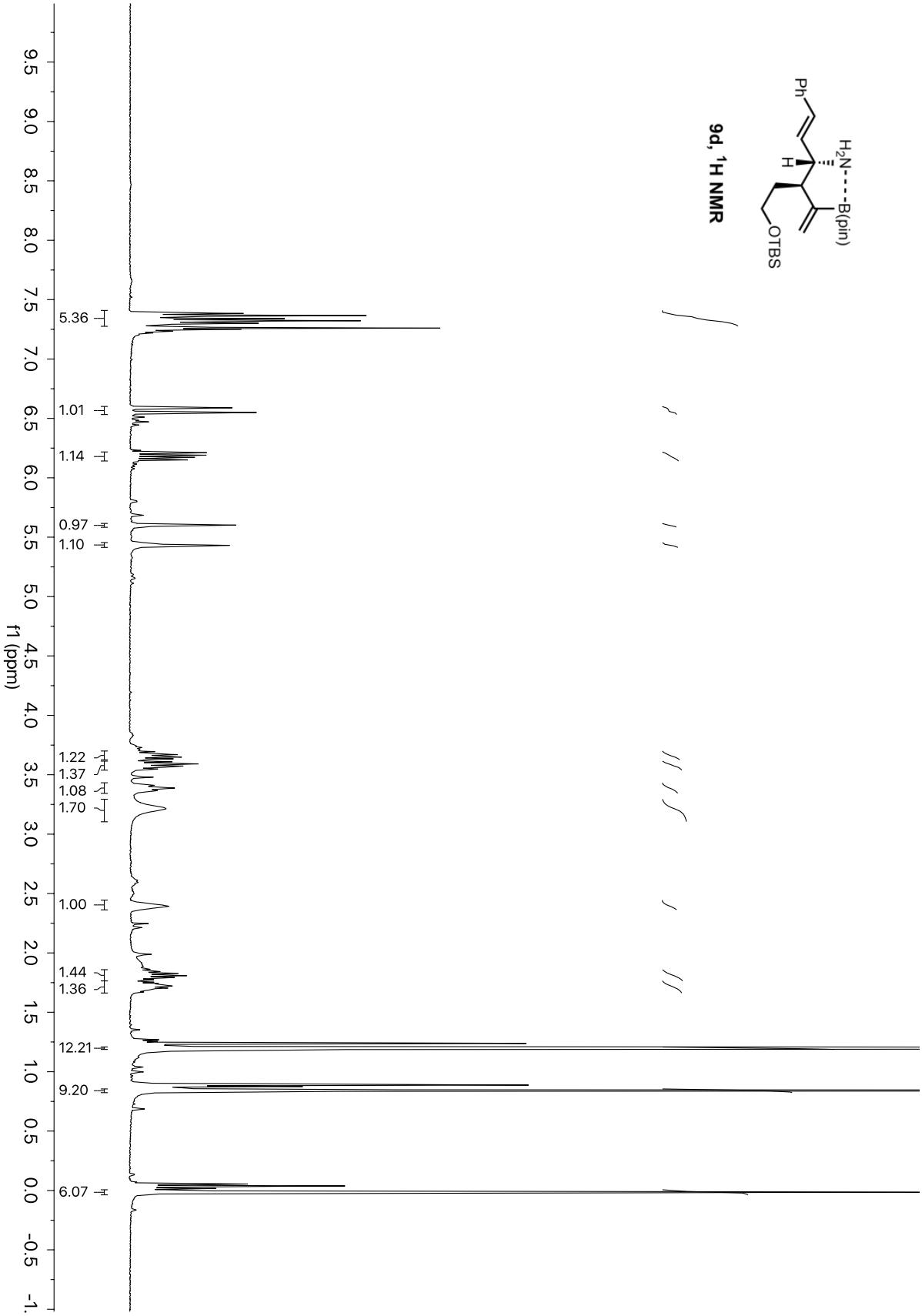
9d, 1H NMR
Ph
H
H2N---B(pin)
OTBS
f1 (ppm)
5.36
1.01
1.14
0.97
1.10
1.22
1.37
1.08
1.70
1.00
1.44
1.36
12.21
9.20
6.07

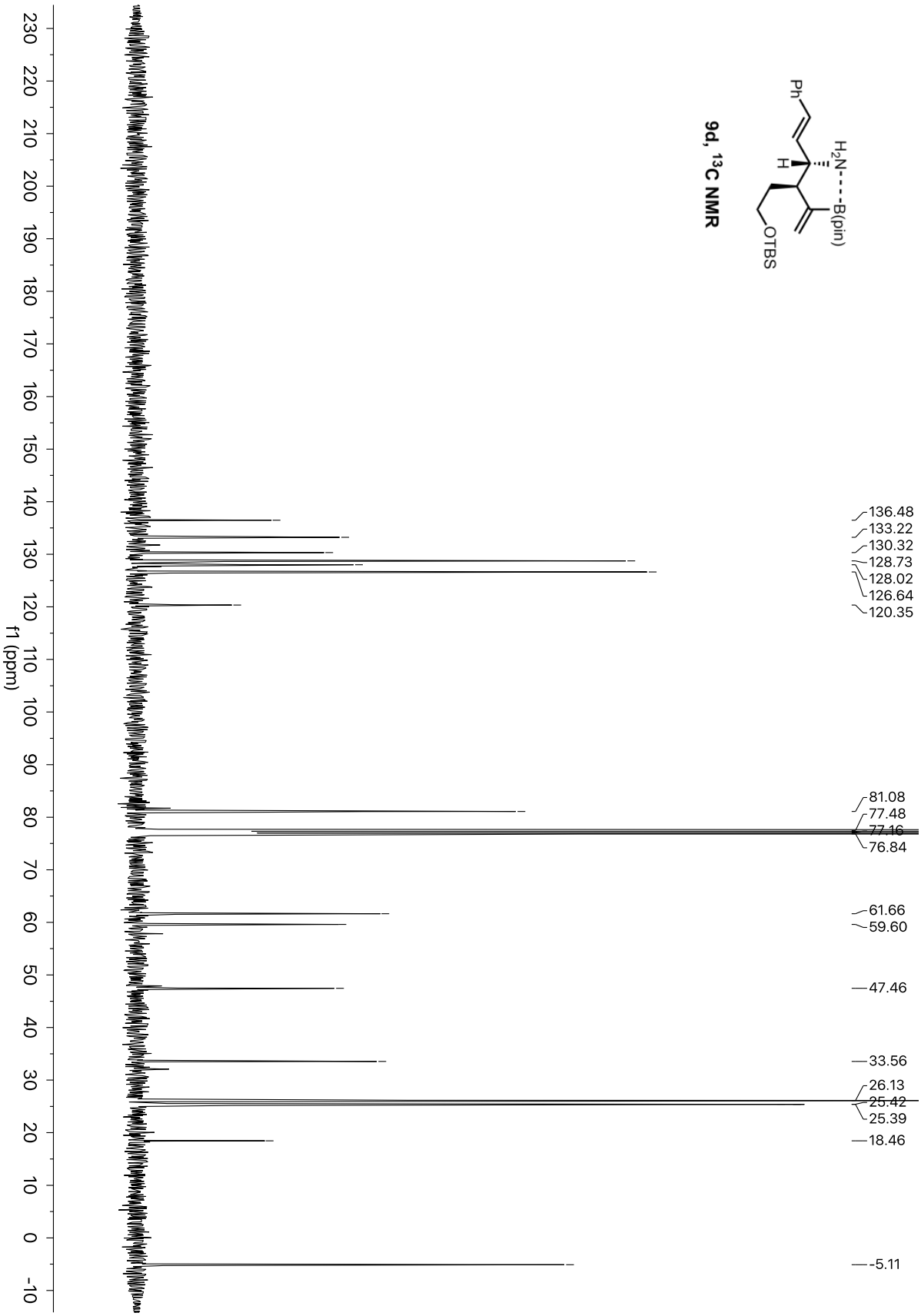
9d, $^{13}$C NMR
Ph
H
$H_2N$---B(pin)
OTBS
136.48
133.22
130.32
128.73
128.02
126.64
120.35
81.08
77.48
77.16
76.84
61.66
59.60
47.46
33.56
26.13
25.42
25.39
18.46
-5.11
f1 (ppm)

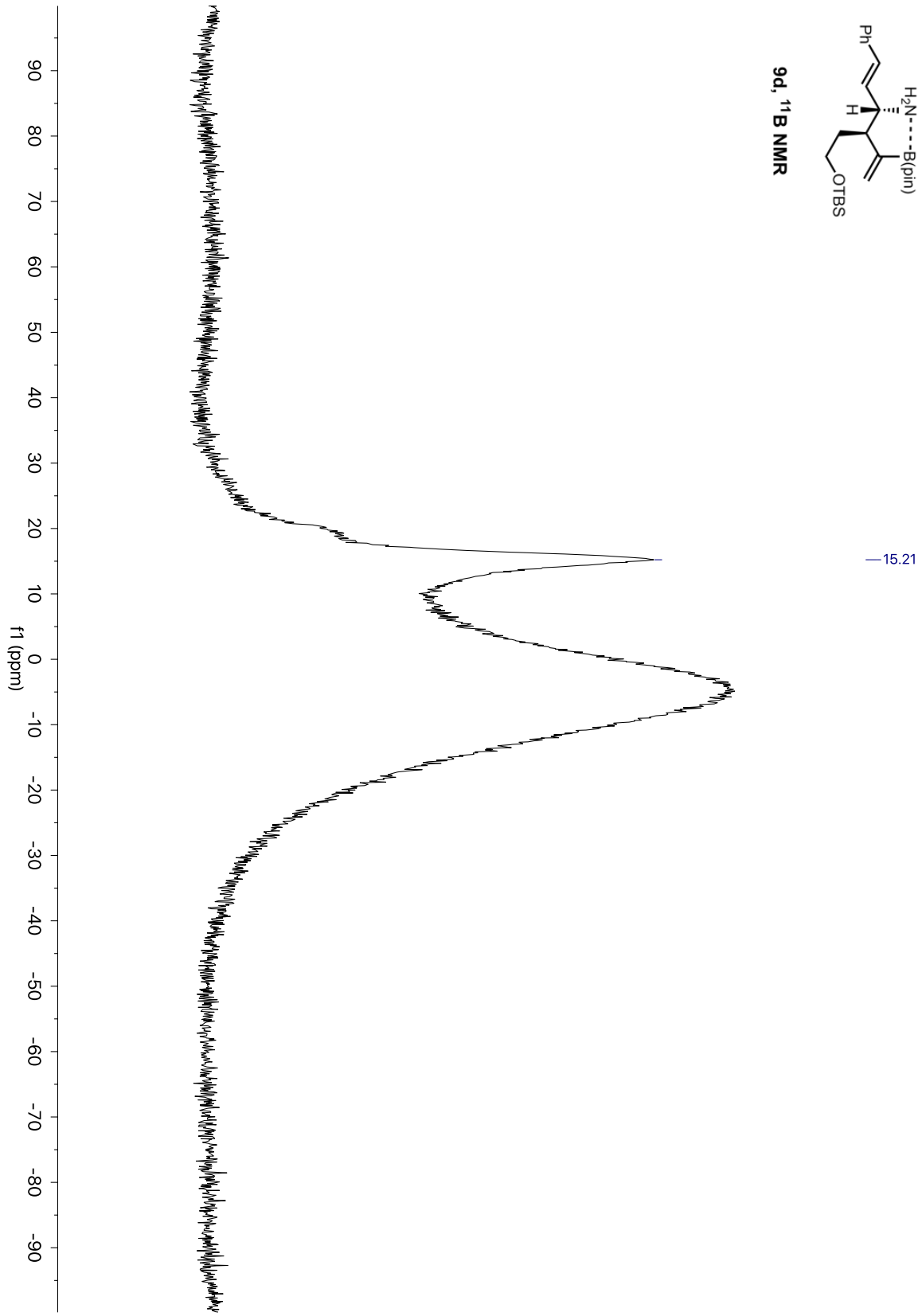
Ph
H
H2N---B(pin)
OTBS
9d, 11B NMR
15.21
f1 (ppm)
90
80
70
60
50
40
30
20
10
0
-10
-20
-30
-40
-50
-60
-70
-80
-90

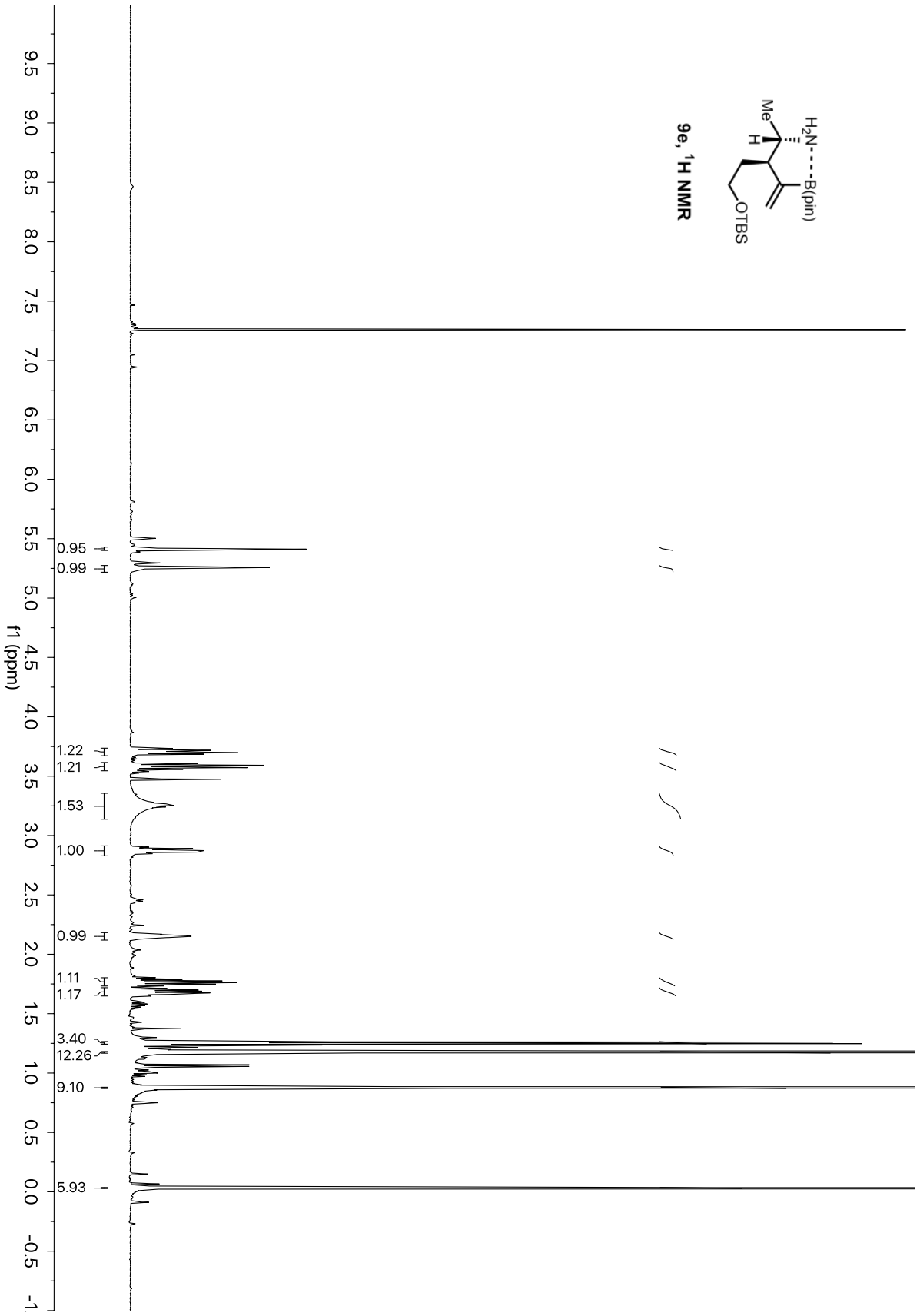
9e, $^1$H NMR
H2N---B(pin)
Me
H
OTBS
f1 (ppm)
0.95
0.99
1.22
1.21
1.53
1.00
0.99
1.11
1.17
3.40
12.26
9.10
5.93

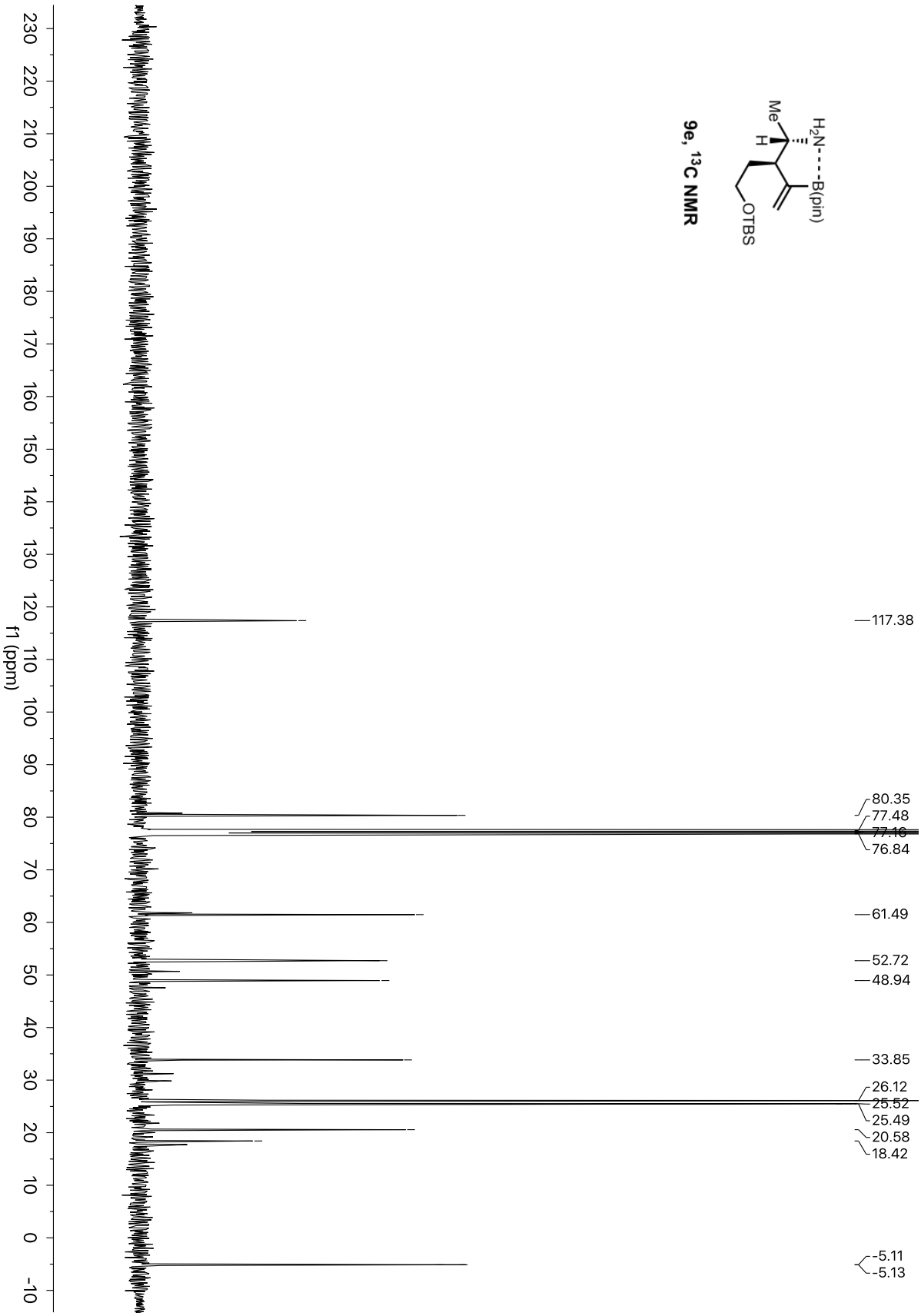
9e, $^{13}$C NMR
Me
H
$H_2N$---B(pin)
OTBS
f1 (ppm)
230
220
210
200
190
180
170
160
150
140
130
120
110
100
90
80
70
60
50
40
30
20
10
0
-10
117.38
80.35
77.48
77.16
76.84
61.49
52.72
48.94
33.85
26.12
25.52
25.49
20.58
18.42
-5.11
-5.13

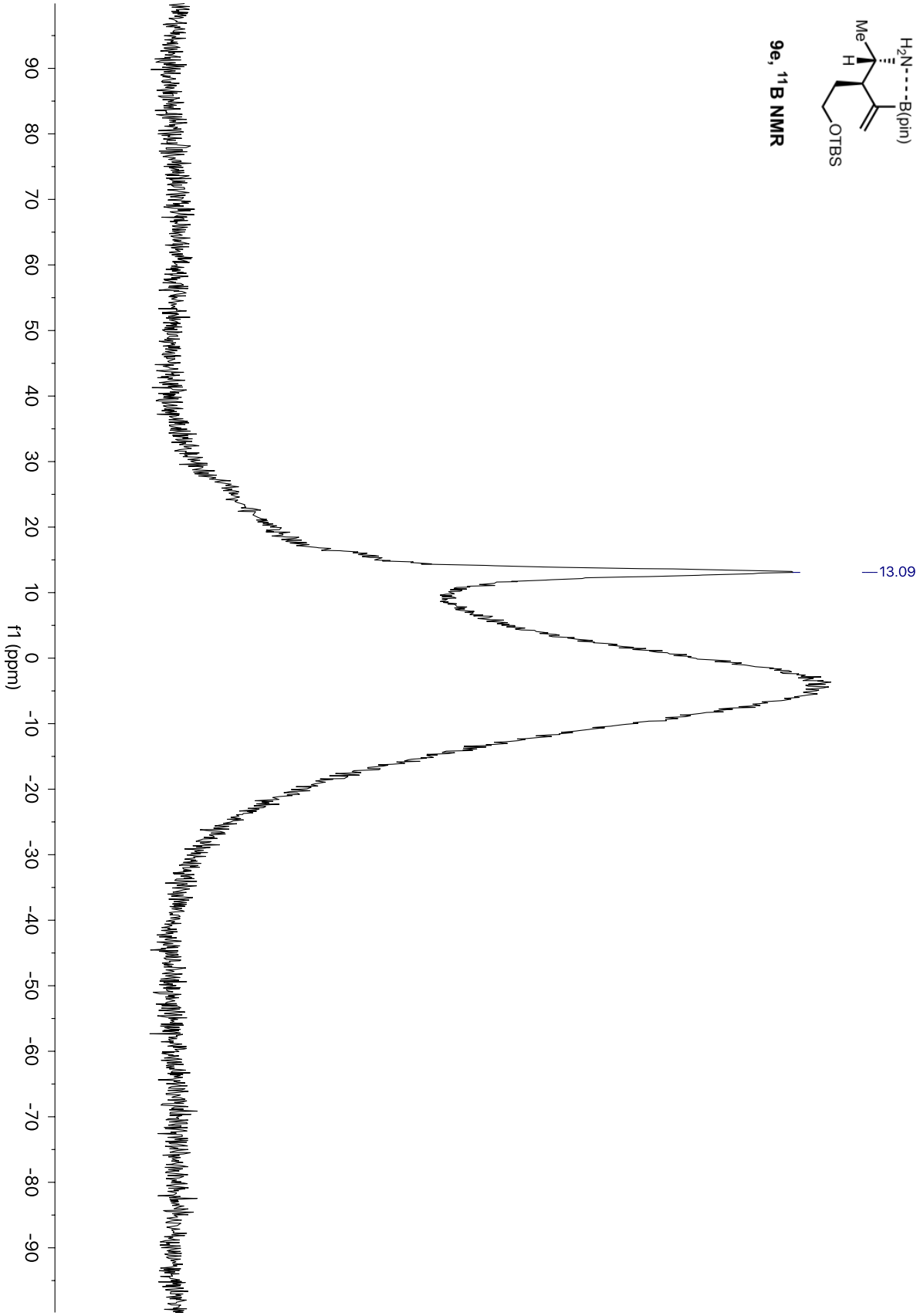
9e, 11B NMR
H2N---B(pin)
Me
H
OTBS
13.09
f1 (ppm)
90
80
70
60
50
40
30
20
10
0
-10
-20
-30
-40
-50
-60
-70
-80
-90

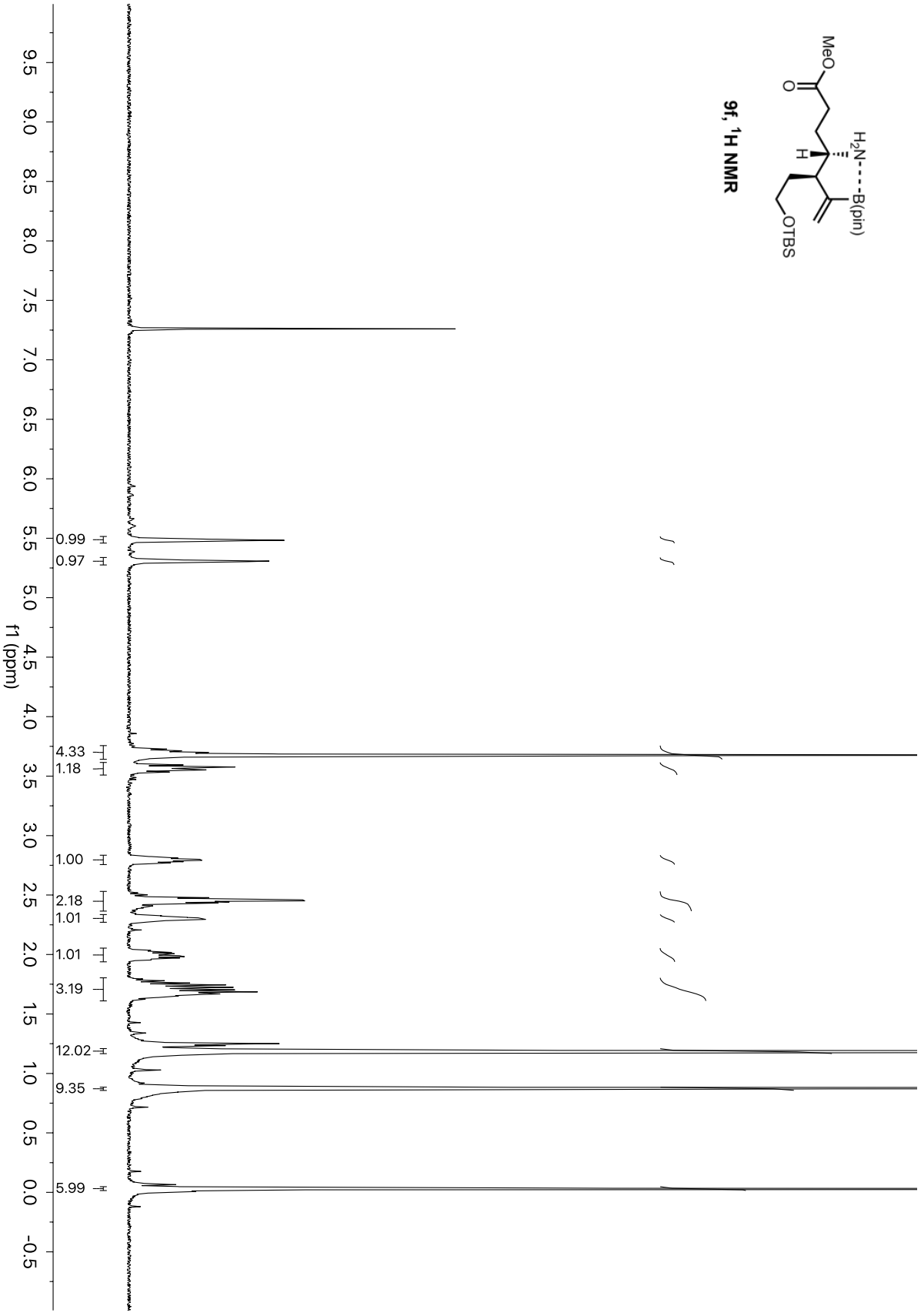
9f, $^1$H NMR
MeO
O
H
$H_2N$---B(pin)
OTBS
f1 (ppm)
9.5
9.0
8.5
8.0
7.5
7.0
6.5
6.0
5.5
5.0
4.5
4.0
3.5
3.0
2.5
2.0
1.5
1.0
0.5
0.0
-0.5
0.99
0.97
4.33
1.18
1.00
2.18
1.01
1.01
3.19
12.02
9.35
5.99

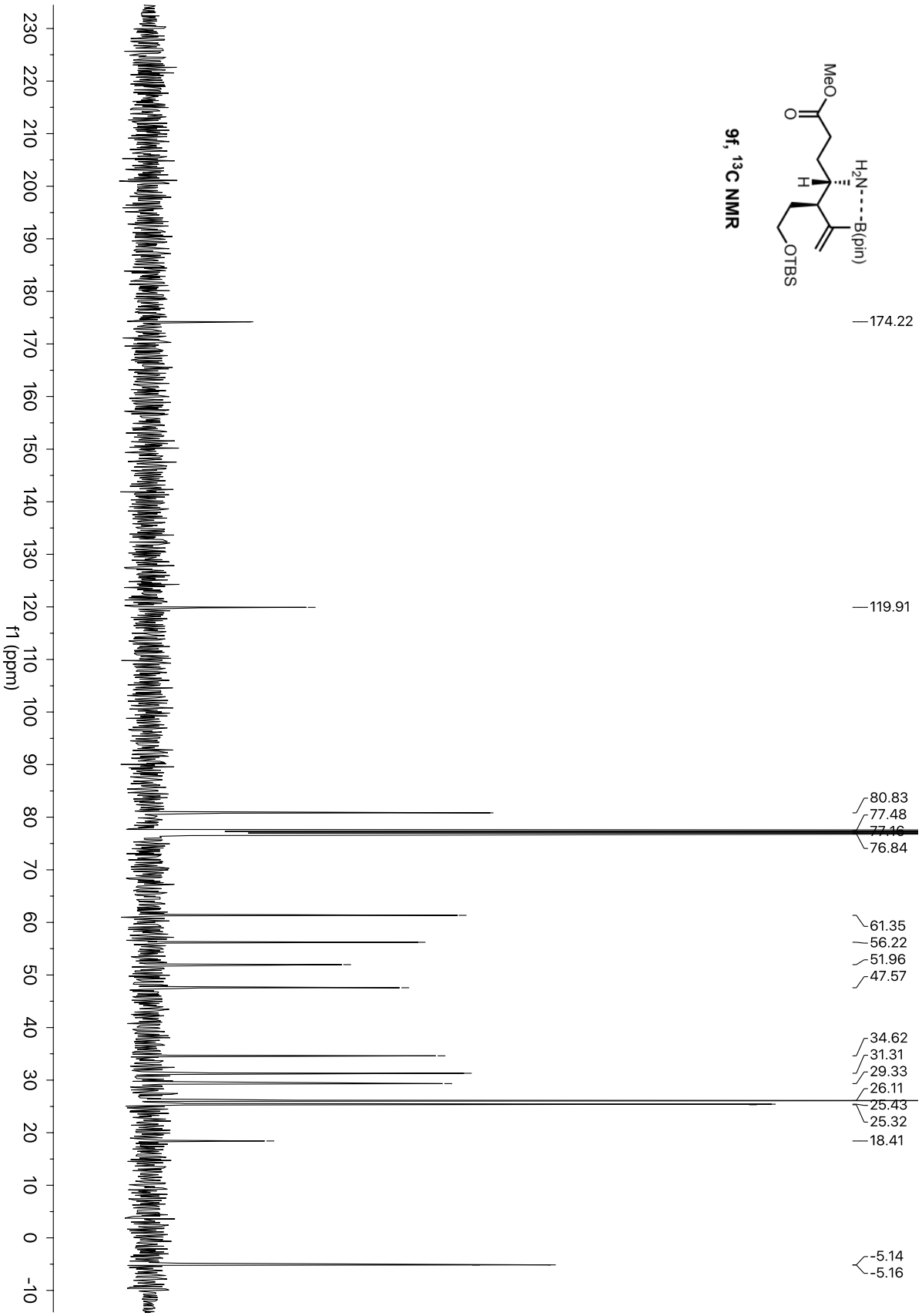
9f, $^{13}$C NMR
MeO
O
H
$H_2N$---B(pin)
OTBS
174.22
119.91
80.83
77.48
77.16
76.84
61.35
56.22
51.96
47.57
34.62
31.31
29.33
26.11
25.43
25.32
18.41
-5.14
-5.16
f1 (ppm)

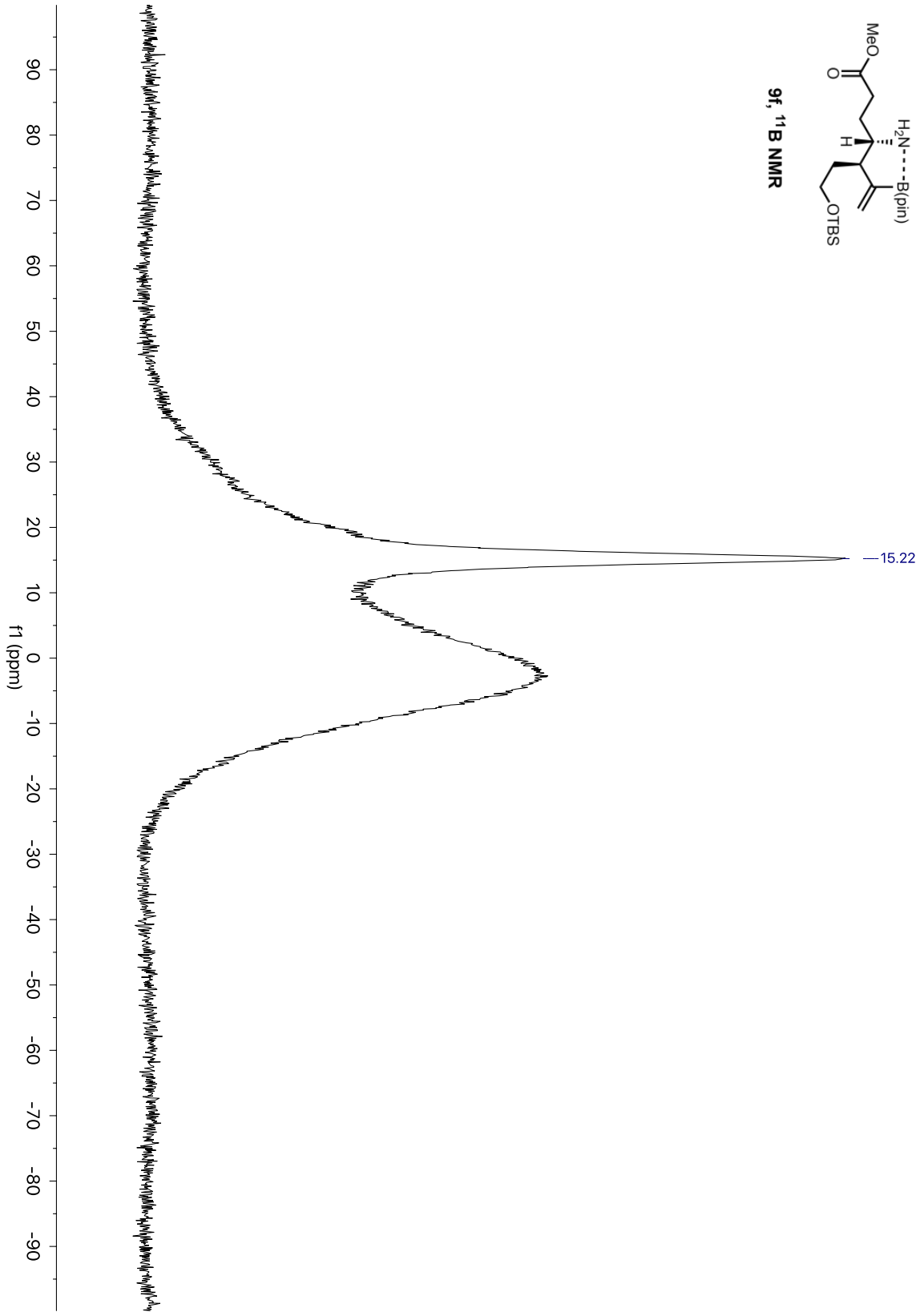
MeO
O
H
H2N---B(pin)
OTBS
9f, 11B NMR
15.22
f1 (ppm)
90
80
70
60
50
40
30
20
10
0
-10
-20
-30
-40
-50
-60
-70
-80
-90

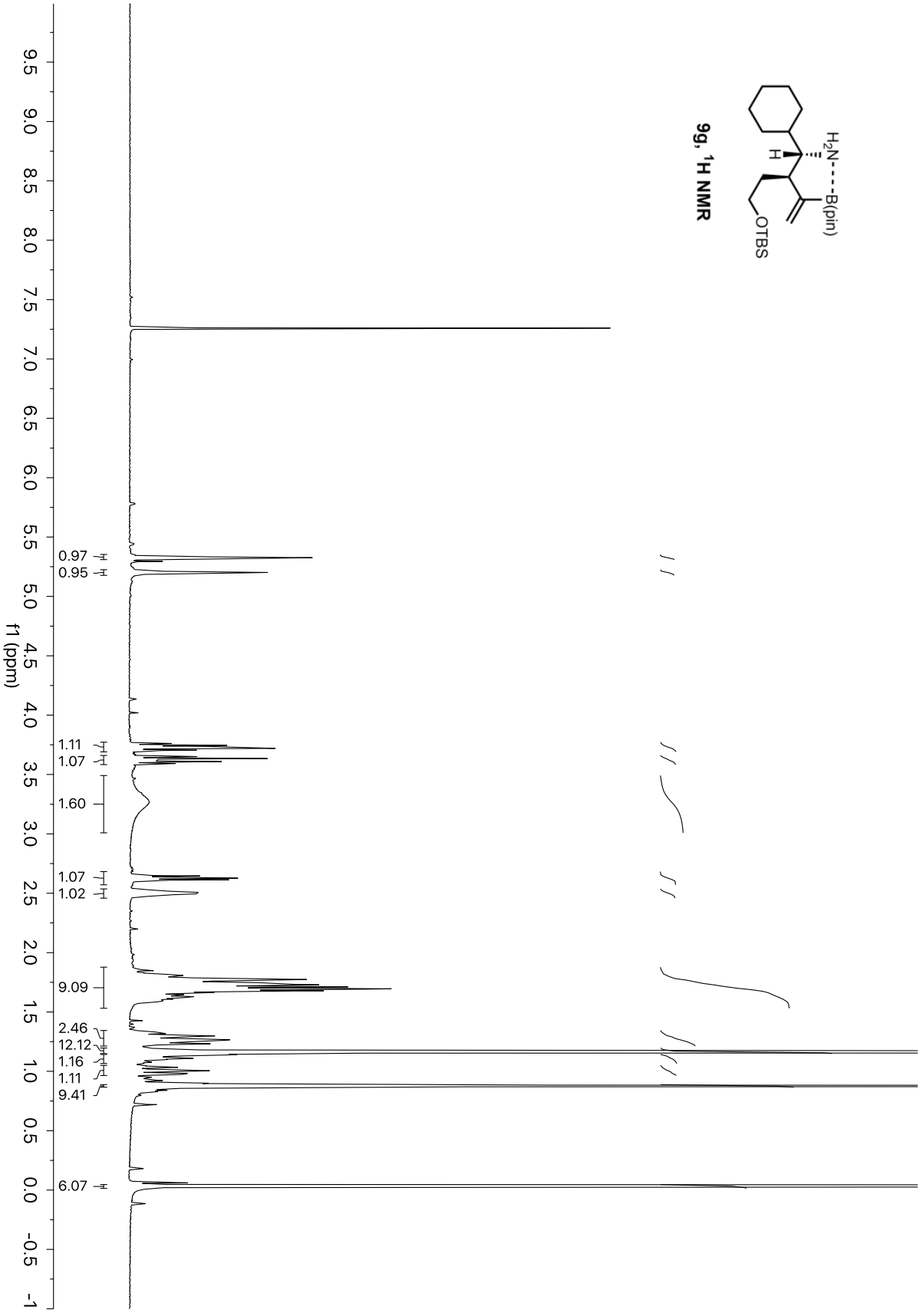
9g, 1H NMR
H2N---B(pin)
H
OTBS
f1 (ppm)
0.97
0.95
1.11
1.07
1.60
1.07
1.02
9.09
2.46
12.12
1.16
1.11
9.41
6.07

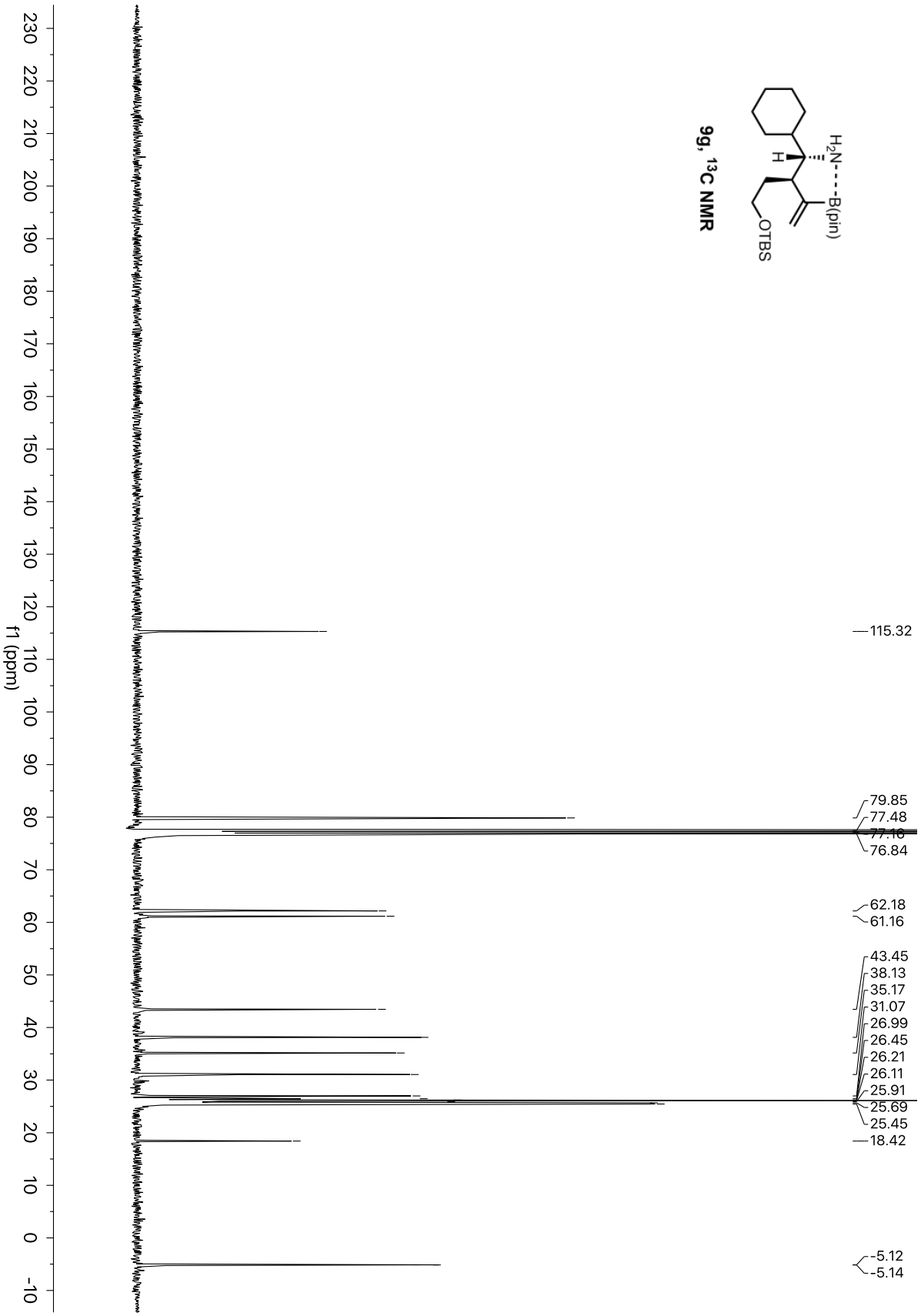
9g, 13C NMR
H2N---B(pin)
H
OTBS
f1 (ppm)
230
220
210
200
190
180
170
160
150
140
130
120
110
100
90
80
70
60
50
40
30
20
10
0
-10
115.32
79.85
77.48
77.16
76.84
62.18
61.16
43.45
38.13
35.17
31.07
26.99
26.45
26.21
26.11
25.91
25.69
25.45
18.42
-5.12
-5.14

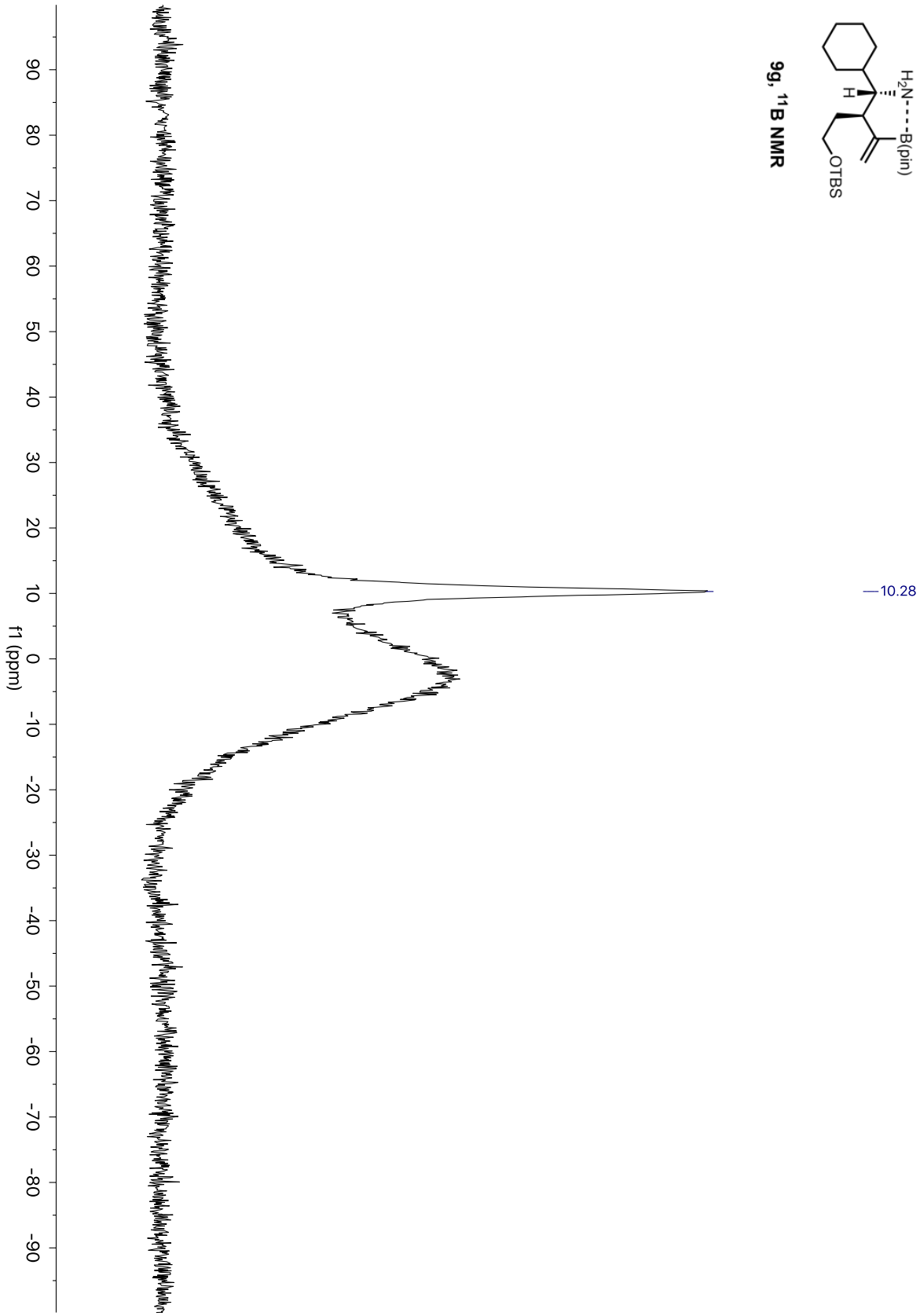
H2N---B(pin)
H
OTBS
9g, 11B NMR
10.28
f1 (ppm)
90
80
70
60
50
40
30
20
10
0
-10
-20
-30
-40
-50
-60
-70
-80
-90

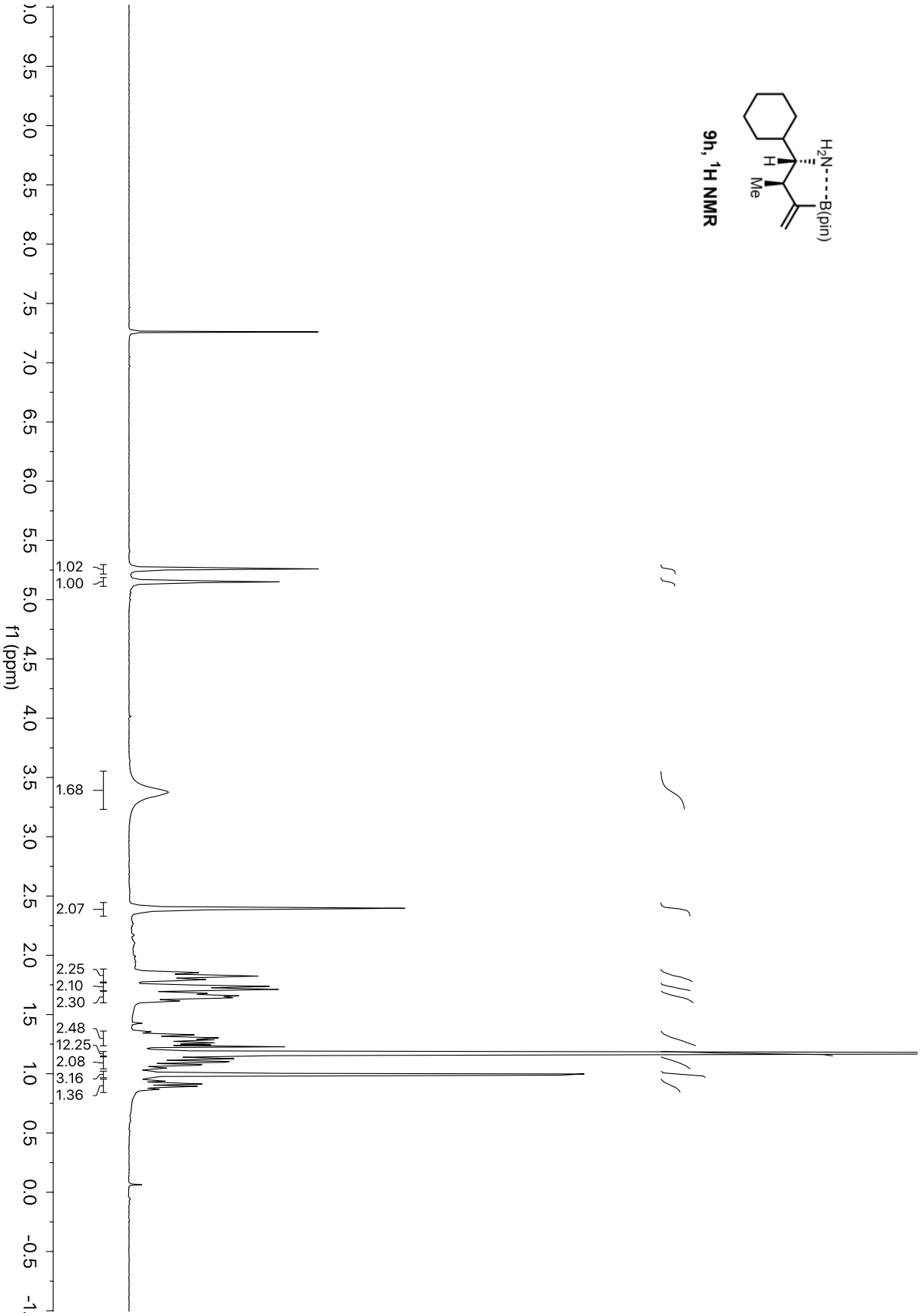
9h, 1H NMR
H2N---B(pin)
H
Me
f1 (ppm)
1.02
1.00
1.68
2.07
2.25
2.10
2.30
2.48
12.25
2.08
3.16
1.36

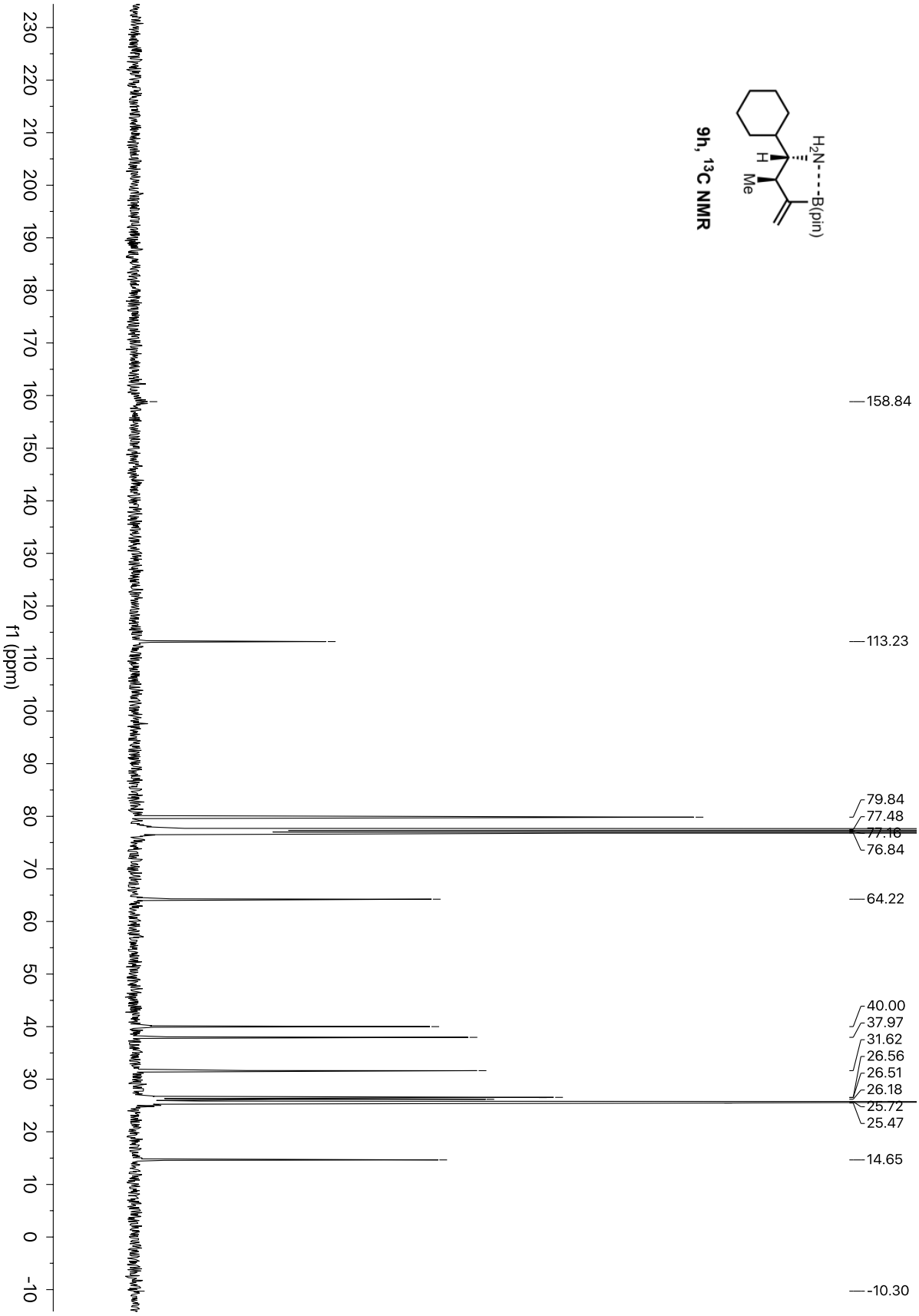
9h, $^{13}$C NMR
$H_2N$---B(pin)
H
Me
158.84
113.23
79.84
77.48
77.16
76.84
64.22
40.00
37.97
31.62
26.56
26.51
26.18
25.72
25.47
14.65
-10.30
f1 (ppm)

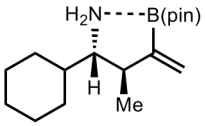


**9h, $^{11}$B NMR**

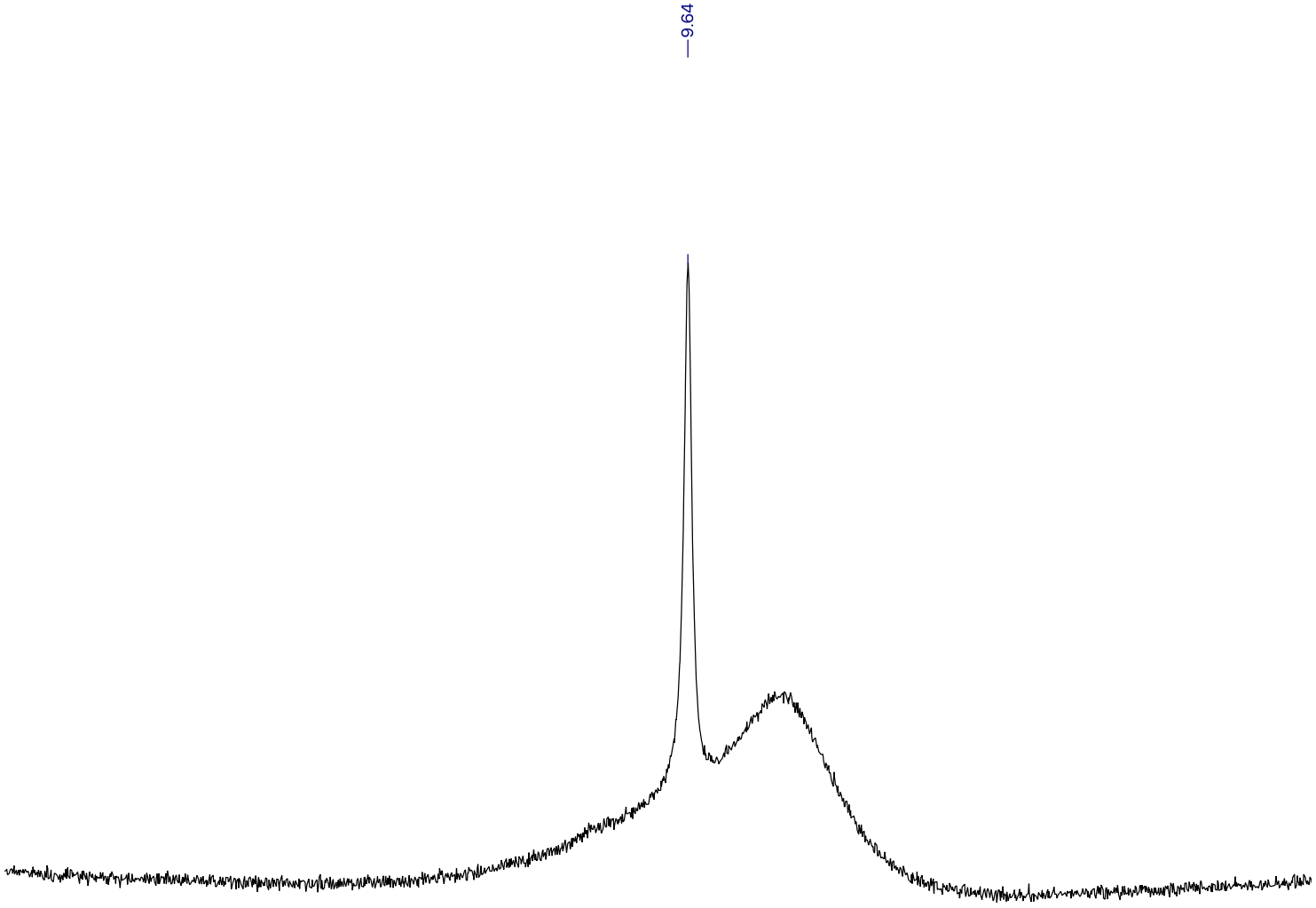

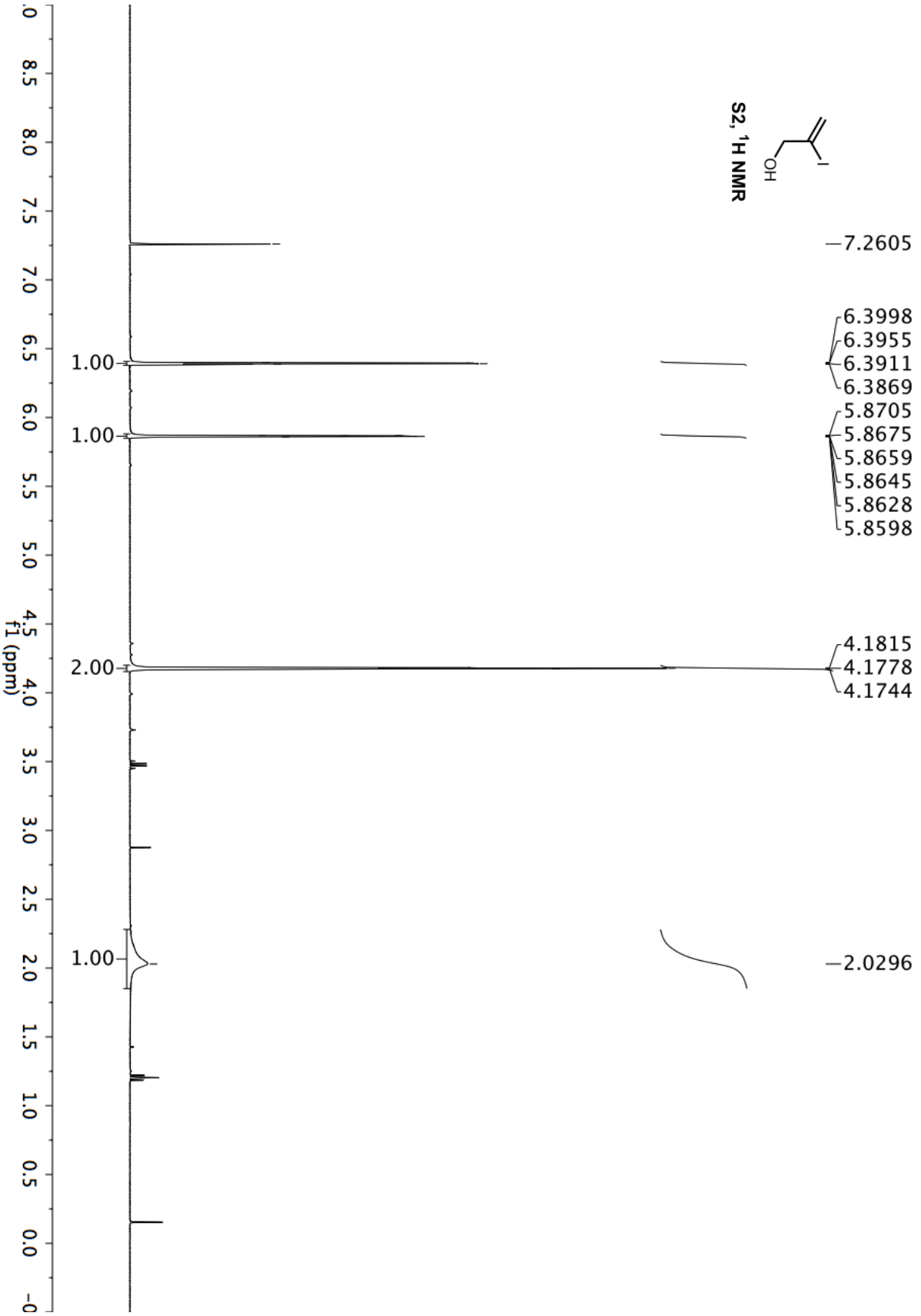
S2, $^1$H NMR
OH
I
7.2605
6.3998
6.3955
6.3911
6.3869
5.8705
5.8675
5.8659
5.8645
5.8628
5.8598
4.1815
4.1778
4.1744
2.0296
1.00
1.00
2.00
1.00
f1 (ppm)

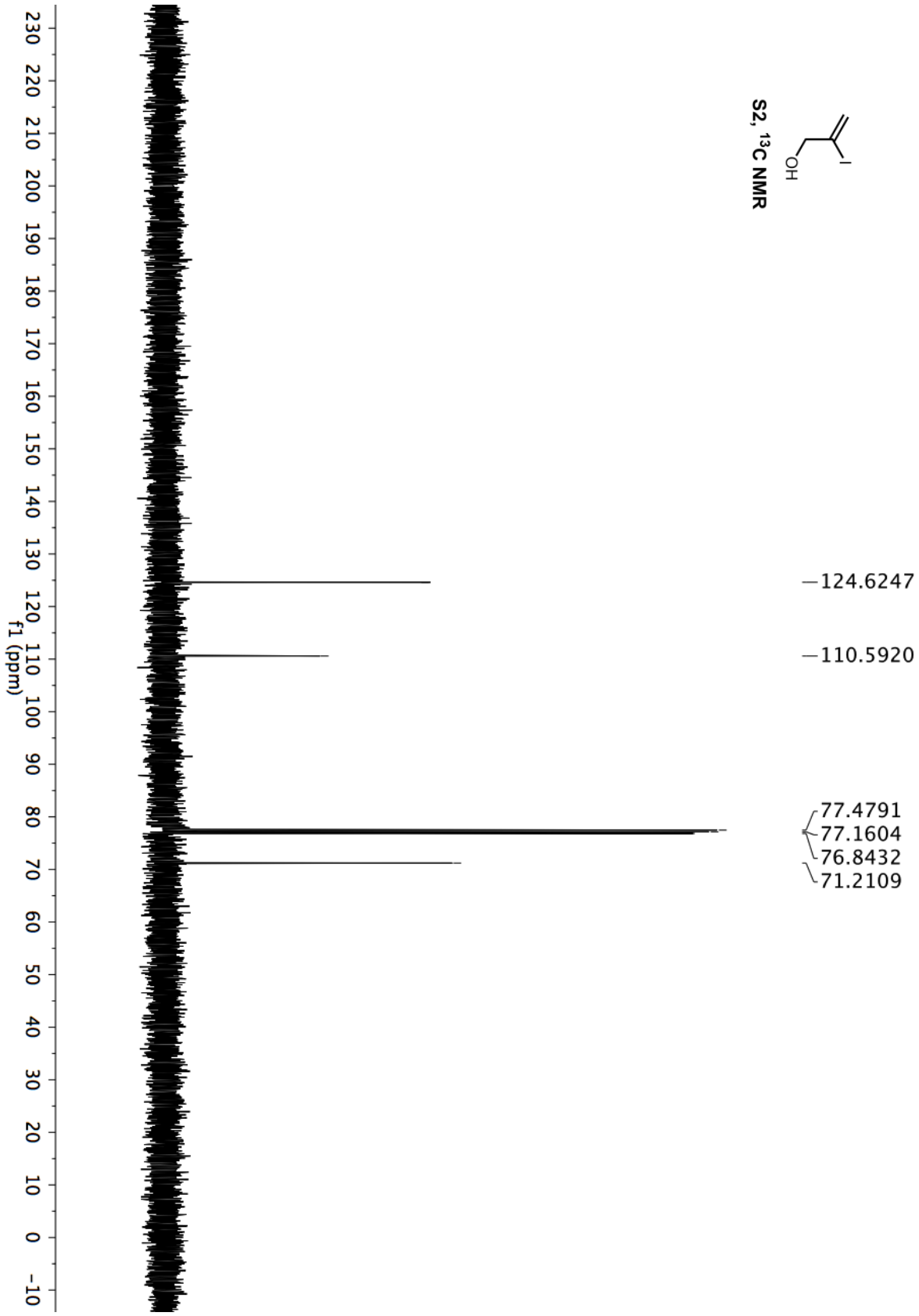
S2, $^{13}$C NMR
OH
I
124.6247
110.5920
77.4791
77.1604
76.8432
71.2109
f1 (ppm)
230 220 210 200 190 180 170 160 150 140 130 120 110 100 90 80 70 60 50 40 30 20 10 0 -10

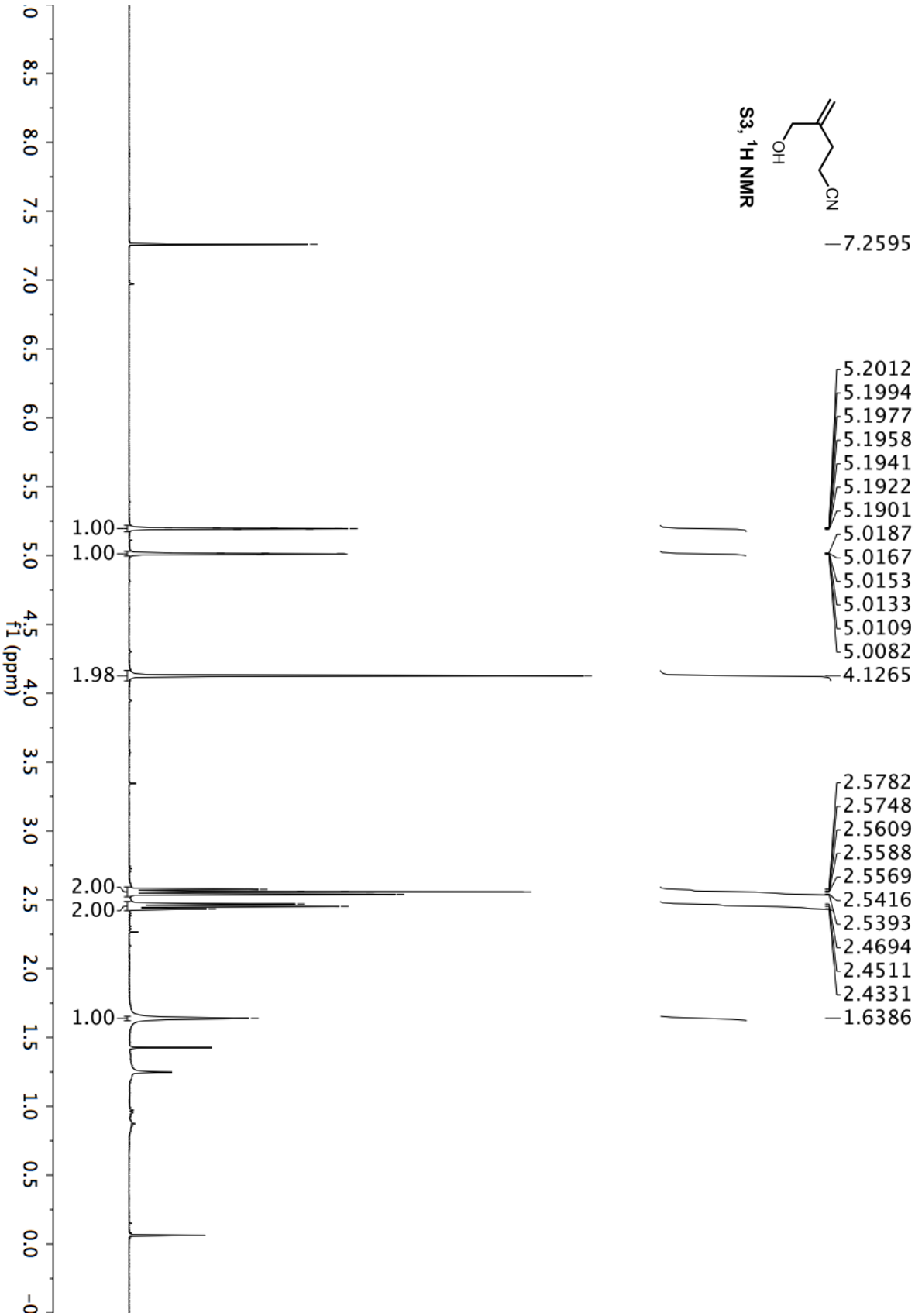
S3, $^1$H NMR
OH
CN
7.2595
5.2012
5.1994
5.1977
5.1958
5.1941
5.1922
5.1901
5.0187
5.0167
5.0153
5.0133
5.0109
5.0082
4.1265
2.5782
2.5748
2.5609
2.5588
2.5569
2.5416
2.5393
2.4694
2.4511
2.4331
1.6386
1.00
1.00
1.98
2.00
2.00
1.00
f1 (ppm)

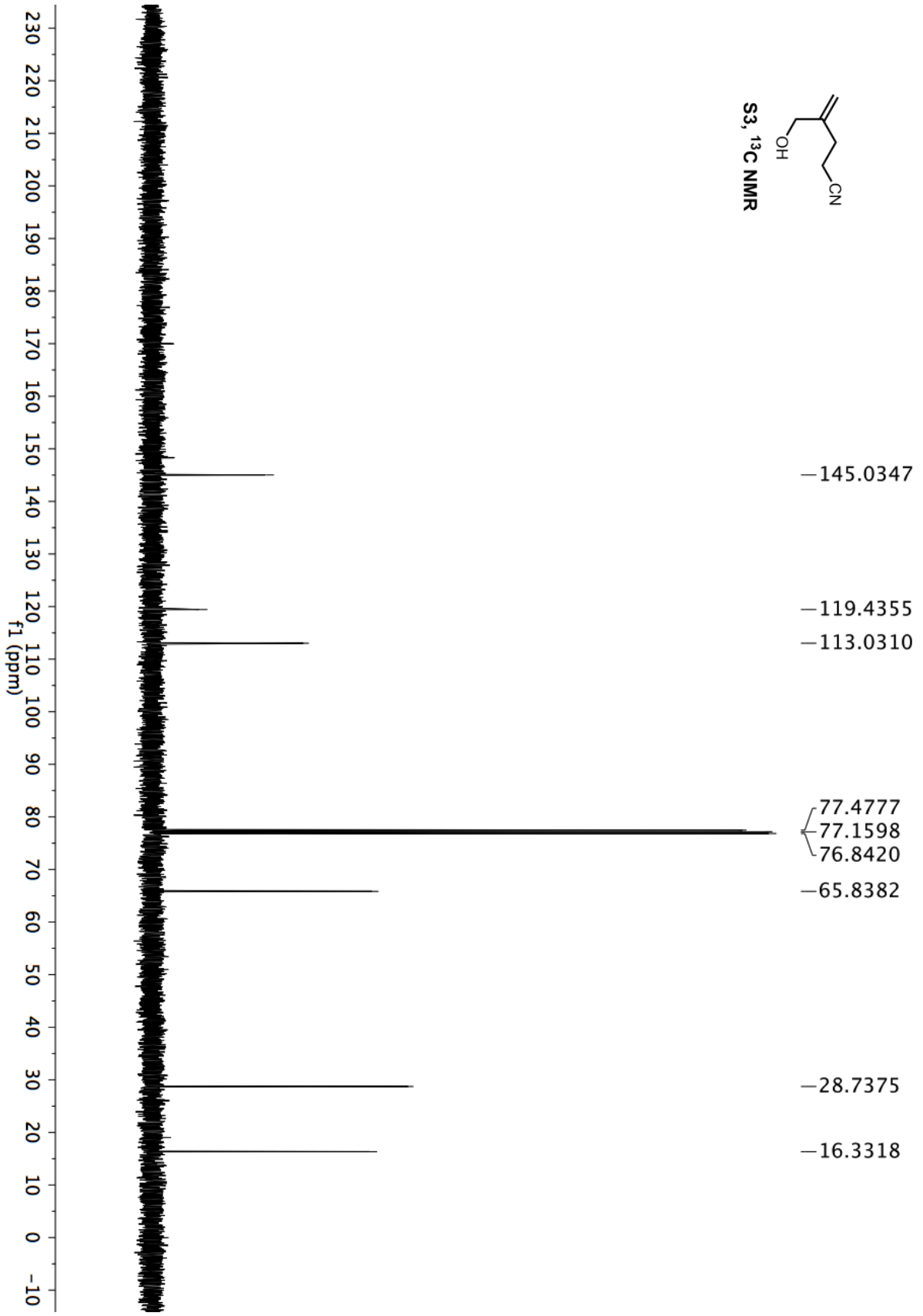
S3, $^{13}$C NMR
OH
CN
145.0347
119.4355
113.0310
77.4777
77.1598
76.8420
65.8382
28.7375
16.3318
f1 (ppm)

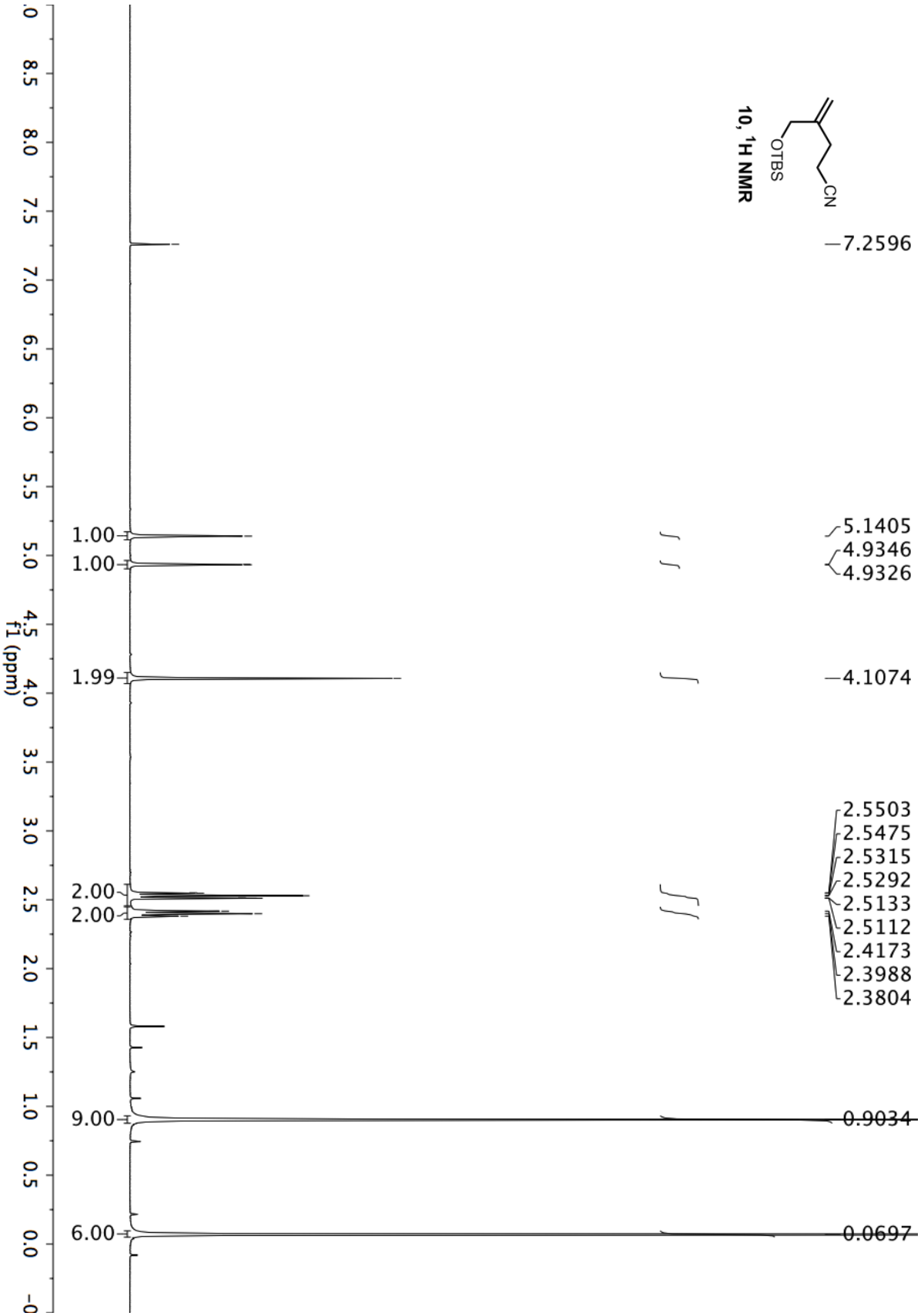
10, $^1$H NMR
OTBS
CN
7.2596
5.1405
4.9346
4.9326
4.1074
2.5503
2.5475
2.5315
2.5292
2.5133
2.5112
2.4173
2.3988
2.3804
0.9034
0.0697
1.00
1.00
1.99
2.00
2.00
9.00
6.00
f1 (ppm)

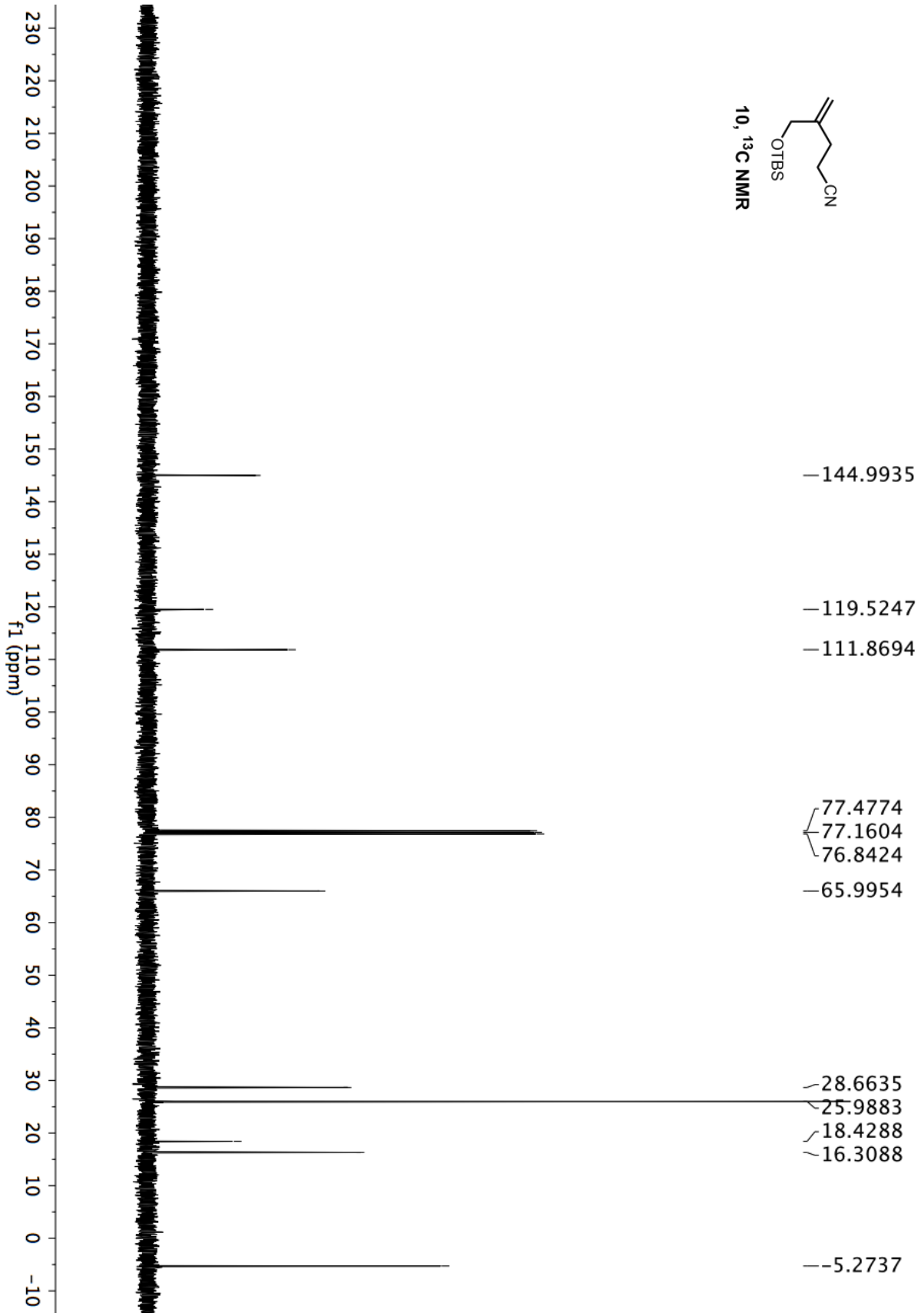
10, $^{13}$C NMR
OTBS
CN
144.9935
119.5247
111.8694
77.4774
77.1604
76.8424
65.9954
28.6635
25.9883
18.4288
16.3088
-5.2737
f1 (ppm)

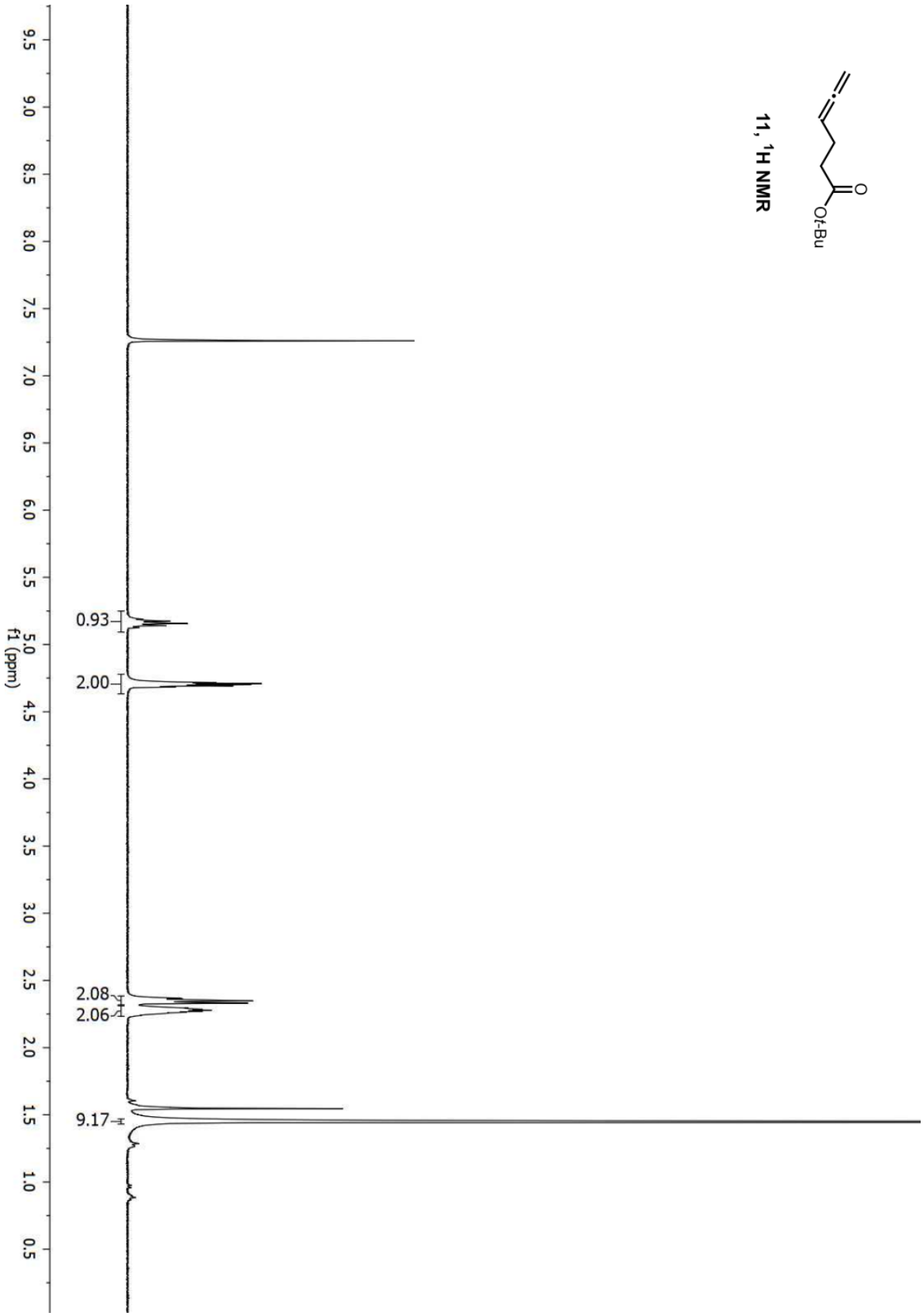
11, $^1$H NMR
Ot-Bu
O
f1 (ppm)
0.93
2.00
2.08
2.06
9.17

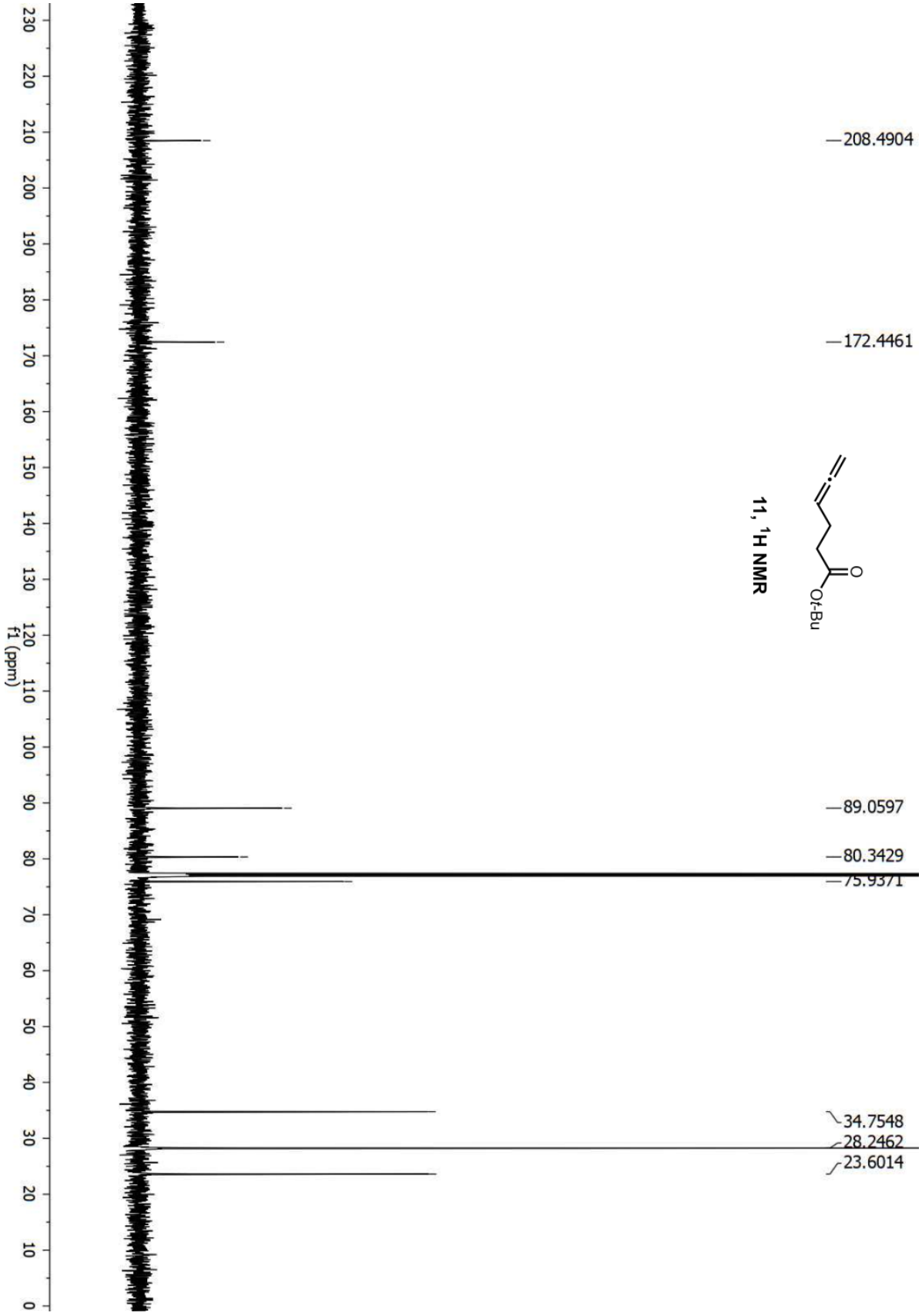
208.4904
172.4461
89.0597
80.3429
75.9371
34.7548
28.2462
23.6014
11, $^1$H NMR
Ot-Bu
O
f1 (ppm)

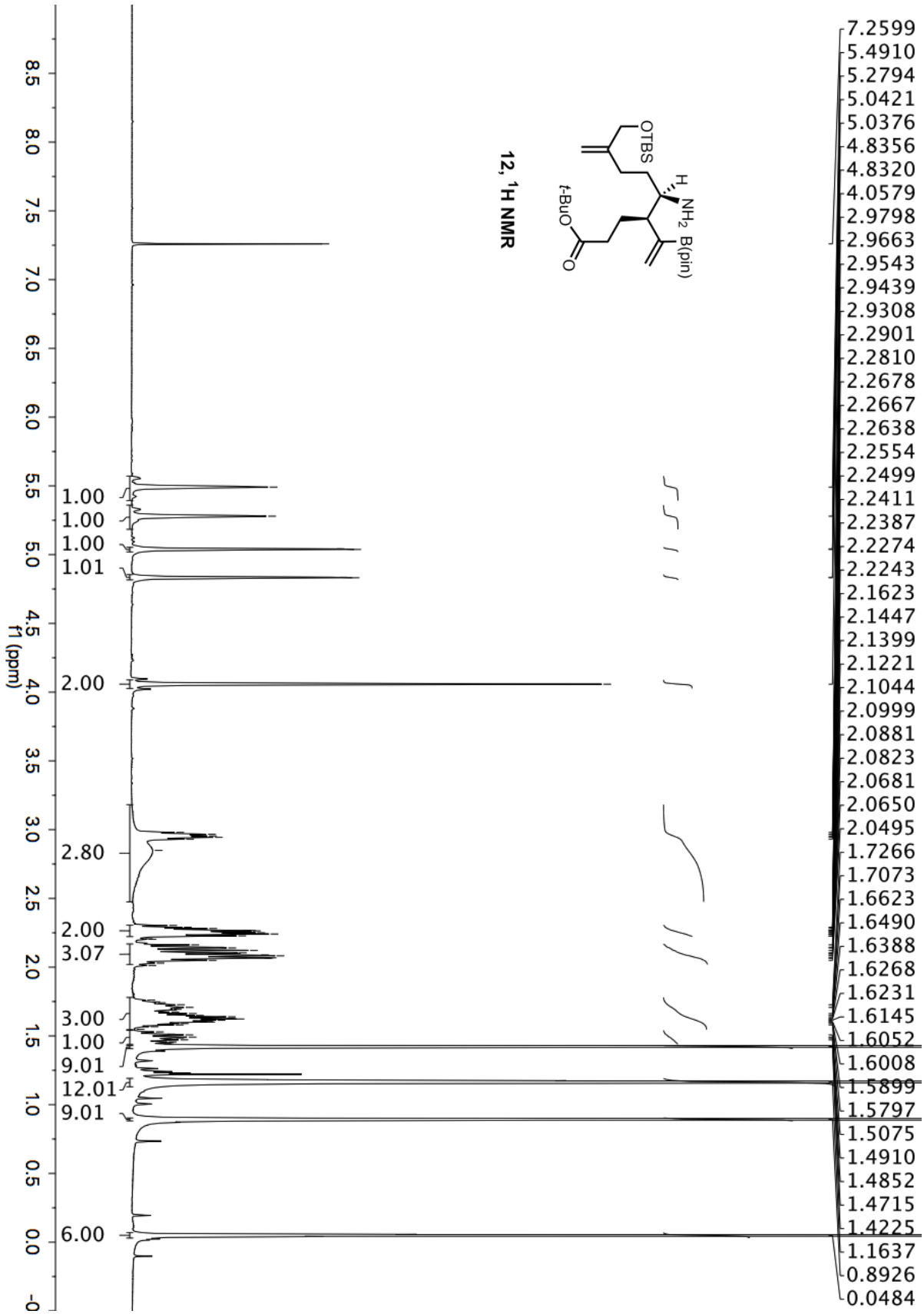
12, $^1$H NMR
OTBS
t-BuO
O
H
NH2
B(pin)
f1 (ppm)
1.00
1.00
1.00
1.01
2.00
2.80
2.00
3.07
3.00
1.00
9.01
12.01
9.01
6.00
7.2599
5.4910
5.2794
5.0421
5.0376
4.8356
4.8320
4.0579
2.9798
2.9663
2.9543
2.9439
2.9308
2.2901
2.2810
2.2678
2.2667
2.2638
2.2554
2.2499
2.2411
2.2387
2.2274
2.2243
2.1623
2.1447
2.1399
2.1221
2.1044
2.0999
2.0881
2.0823
2.0681
2.0650
2.0495
1.7266
1.7073
1.6623
1.6490
1.6388
1.6268
1.6231
1.6145
1.6052
1.6008
1.5899
1.5797
1.5075
1.4910
1.4852
1.4715
1.4225
1.1637
0.8926
0.0484

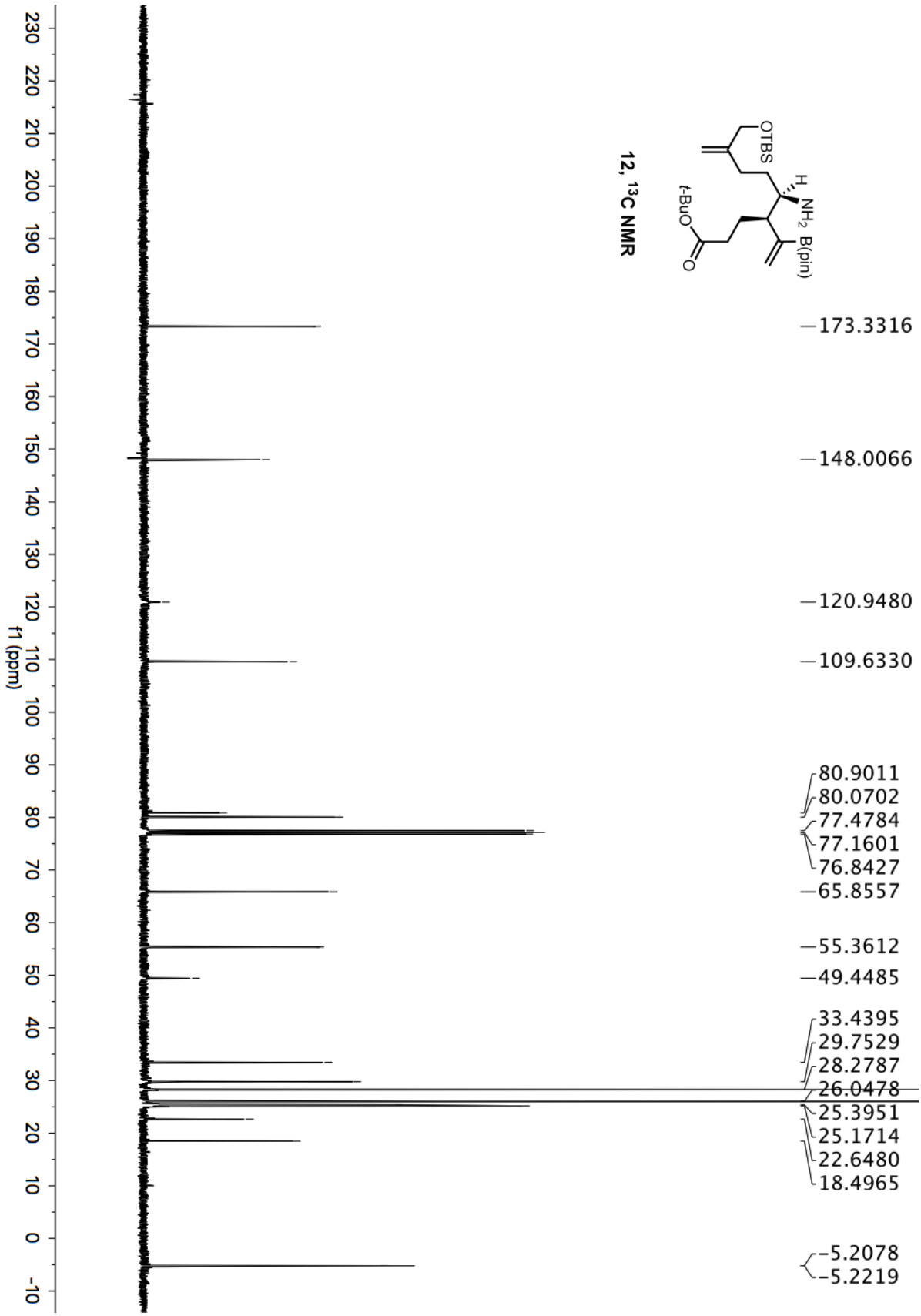
12, $^{13}$C NMR
OTBS
H
NH$_2$
B(pin)
t-BuO
O
f1 (ppm)
230
220
210
200
190
180
170
160
150
140
130
120
110
100
90
80
70
60
50
40
30
20
10
0
-10
173.3316
148.0066
120.9480
109.6330
80.9011
80.0702
77.4784
77.1601
76.8427
65.8557
55.3612
49.4485
33.4395
29.7529
28.2787
26.0478
25.3951
25.1714
22.6480
18.4965
-5.2078
-5.2219

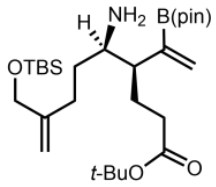
H
NH2
B(pin)
OTBS
t-BuO
O

**12, $^{11}$B NMR**


22.00
16.02
38 36 34 32 30 28 26 24 22 20 18 16 14 12 10 8 6 4 2 0 -2 -4 -6 -8 -10 -12 -14 -16 -18 -20 -22 -24 -26
f1 (ppm)

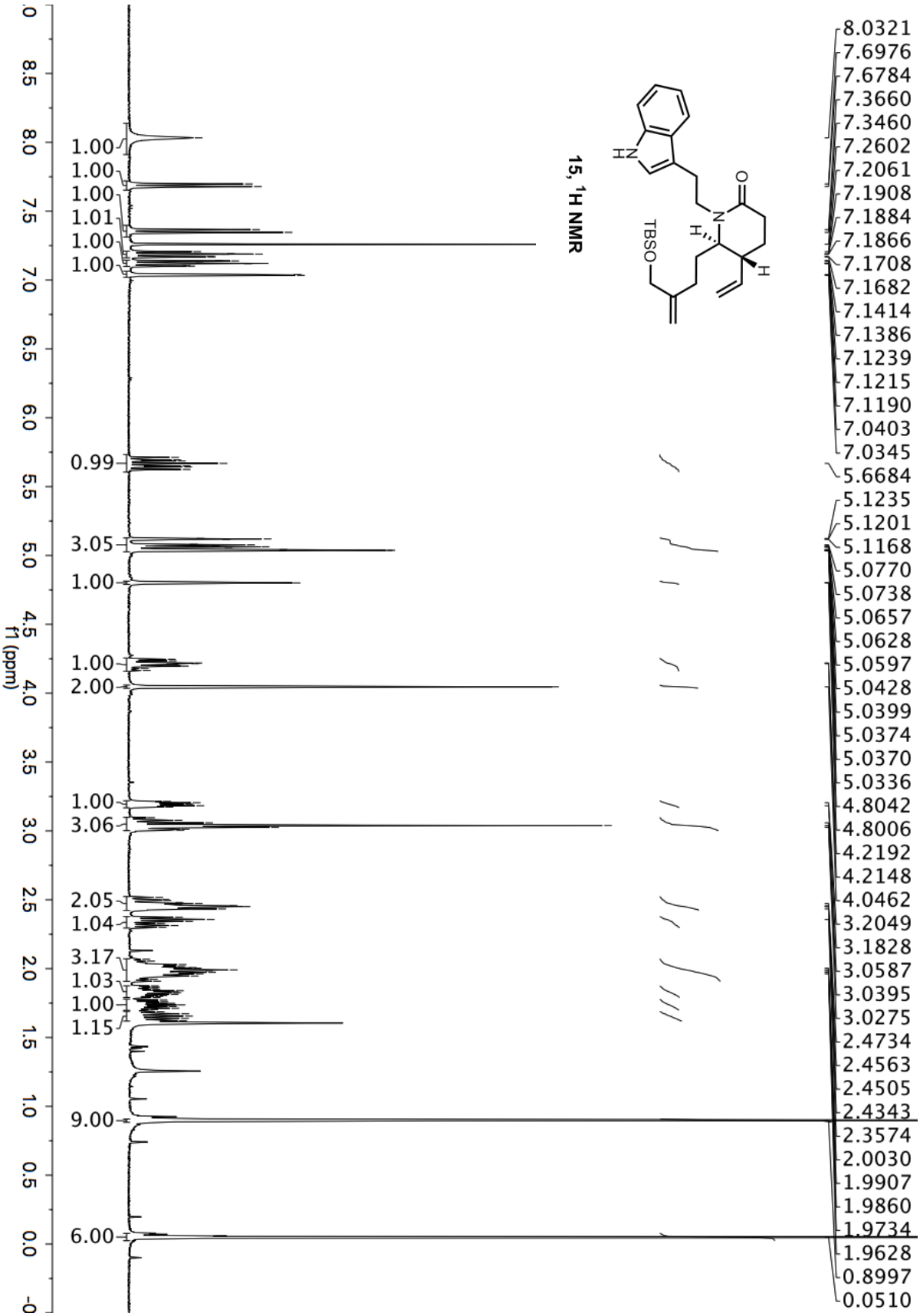
15, $^1$H NMR
f1 (ppm)
1.00
1.00
1.00
1.01
1.00
1.00
0.99
3.05
1.00
1.00
2.00
1.00
3.06
2.05
1.04
3.17
1.03
1.00
1.15
9.00
6.00
8.0321
7.6976
7.6784
7.3660
7.3460
7.2602
7.2061
7.1908
7.1884
7.1866
7.1708
7.1682
7.1414
7.1386
7.1239
7.1215
7.1190
7.0403
7.0345
5.6684
5.1235
5.1201
5.1168
5.0770
5.0738
5.0657
5.0628
5.0597
5.0428
5.0399
5.0374
5.0370
5.0336
4.8042
4.8006
4.2192
4.2148
4.0462
3.2049
3.1828
3.0587
3.0395
3.0275
2.4734
2.4563
2.4505
2.4343
2.3574
2.0030
1.9907
1.9860
1.9734
1.9628
0.8997
0.0510

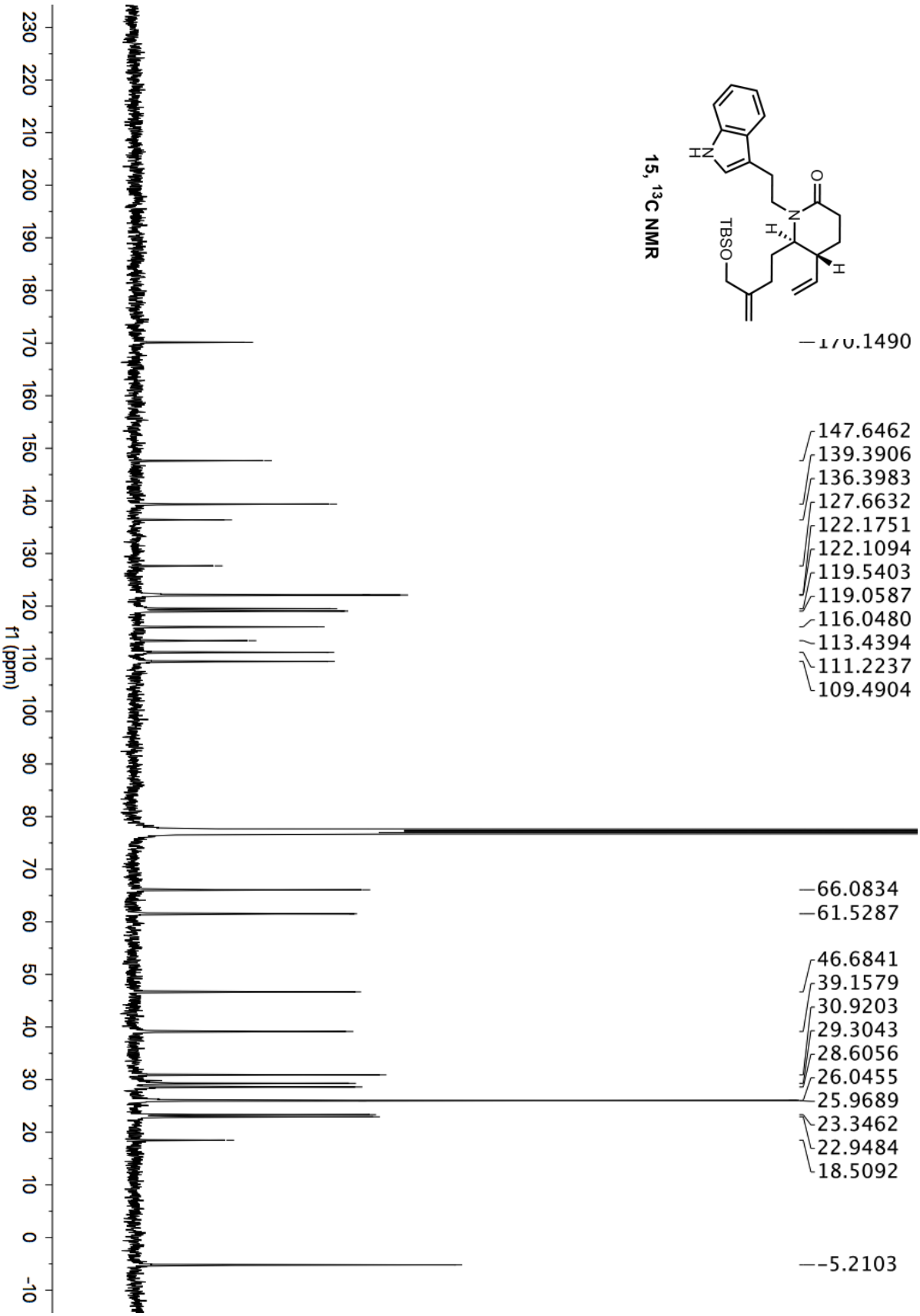
15, $^{13}$C NMR
TBSO
170.1490
147.6462
139.3906
136.3983
127.6632
122.1751
122.1094
119.5403
119.0587
116.0480
113.4394
111.2237
109.4904
66.0834
61.5287
46.6841
39.1579
30.9203
29.3043
28.6056
26.0455
25.9689
23.3462
22.9484
18.5092
-5.2103
f1 (ppm)

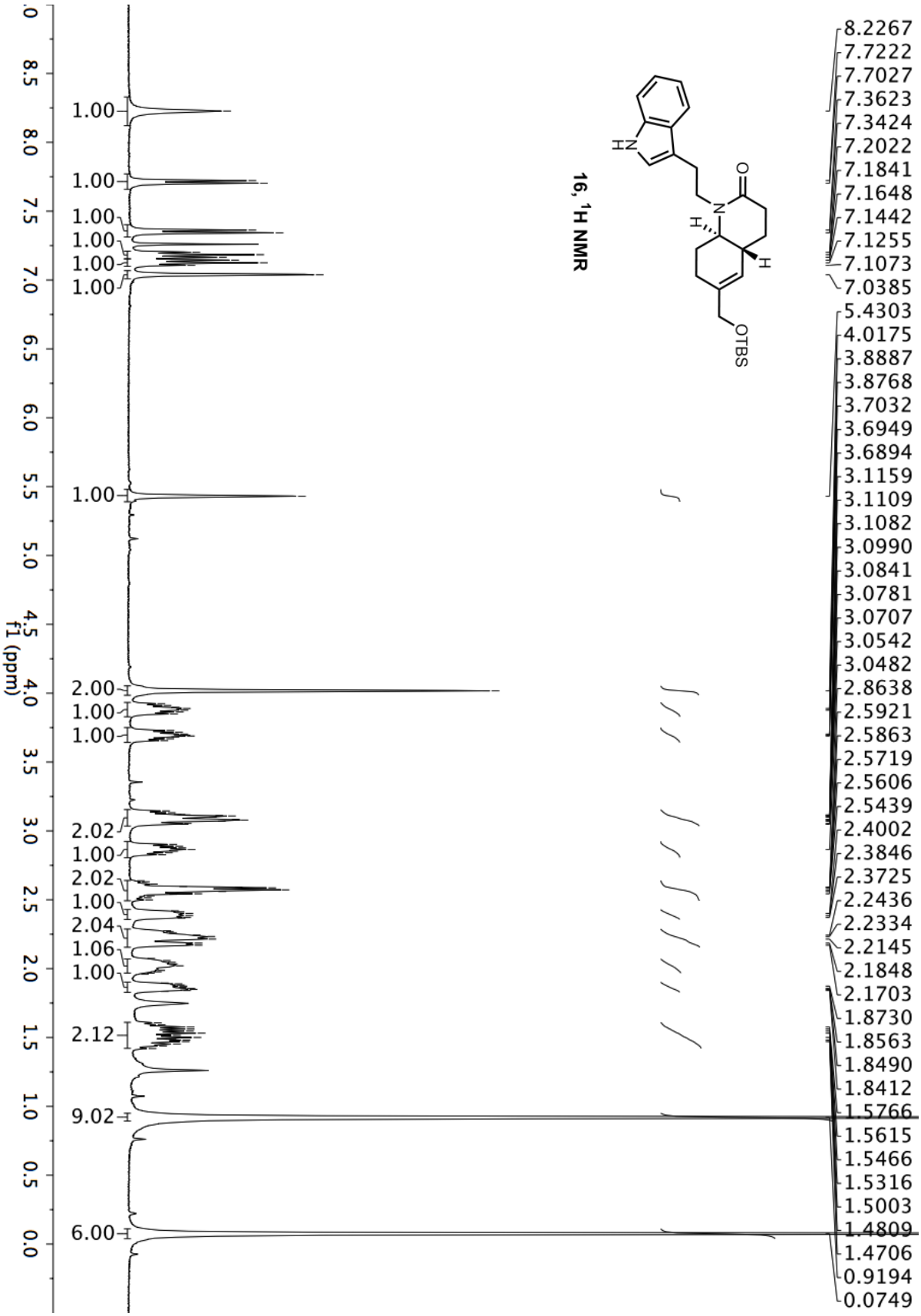
16, $^1$H NMR
f1 (ppm)
1.00
1.00
1.00
1.00
1.00
1.00
1.00
2.00
1.00
1.00
2.02
1.00
2.02
1.00
2.04
1.06
1.00
2.12
9.02
6.00
8.2267
7.7222
7.7027
7.3623
7.3424
7.2022
7.1841
7.1648
7.1442
7.1255
7.1073
7.0385
5.4303
4.0175
3.8887
3.8768
3.7032
3.6949
3.6894
3.1159
3.1109
3.1082
3.0990
3.0841
3.0781
3.0707
3.0542
3.0482
2.8638
2.5921
2.5863
2.5719
2.5606
2.5439
2.4002
2.3846
2.3725
2.2436
2.2334
2.2145
2.1848
2.1703
1.8730
1.8563
1.8490
1.8412
1.5766
1.5615
1.5466
1.5316
1.5003
1.4809
1.4706
0.9194
0.0749
OTBS

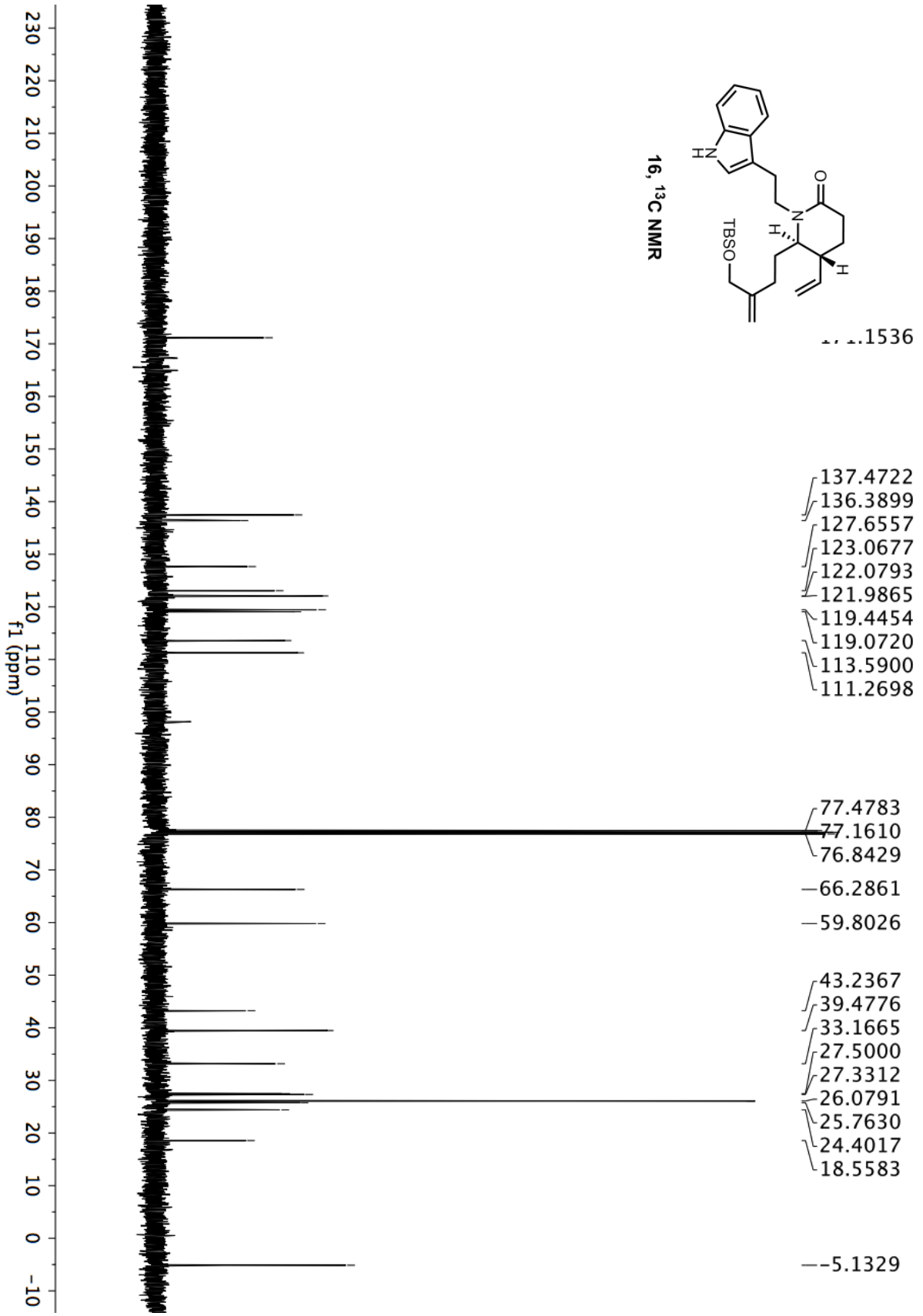
16, 13C NMR
TBSO
1.1536
137.4722
136.3899
127.6557
123.0677
122.0793
121.9865
119.4454
119.0720
113.5900
111.2698
77.4783
77.1610
76.8429
66.2861
59.8026
43.2367
39.4776
33.1665
27.5000
27.3312
26.0791
25.7630
24.4017
18.5583
-5.1329
f1 (ppm)

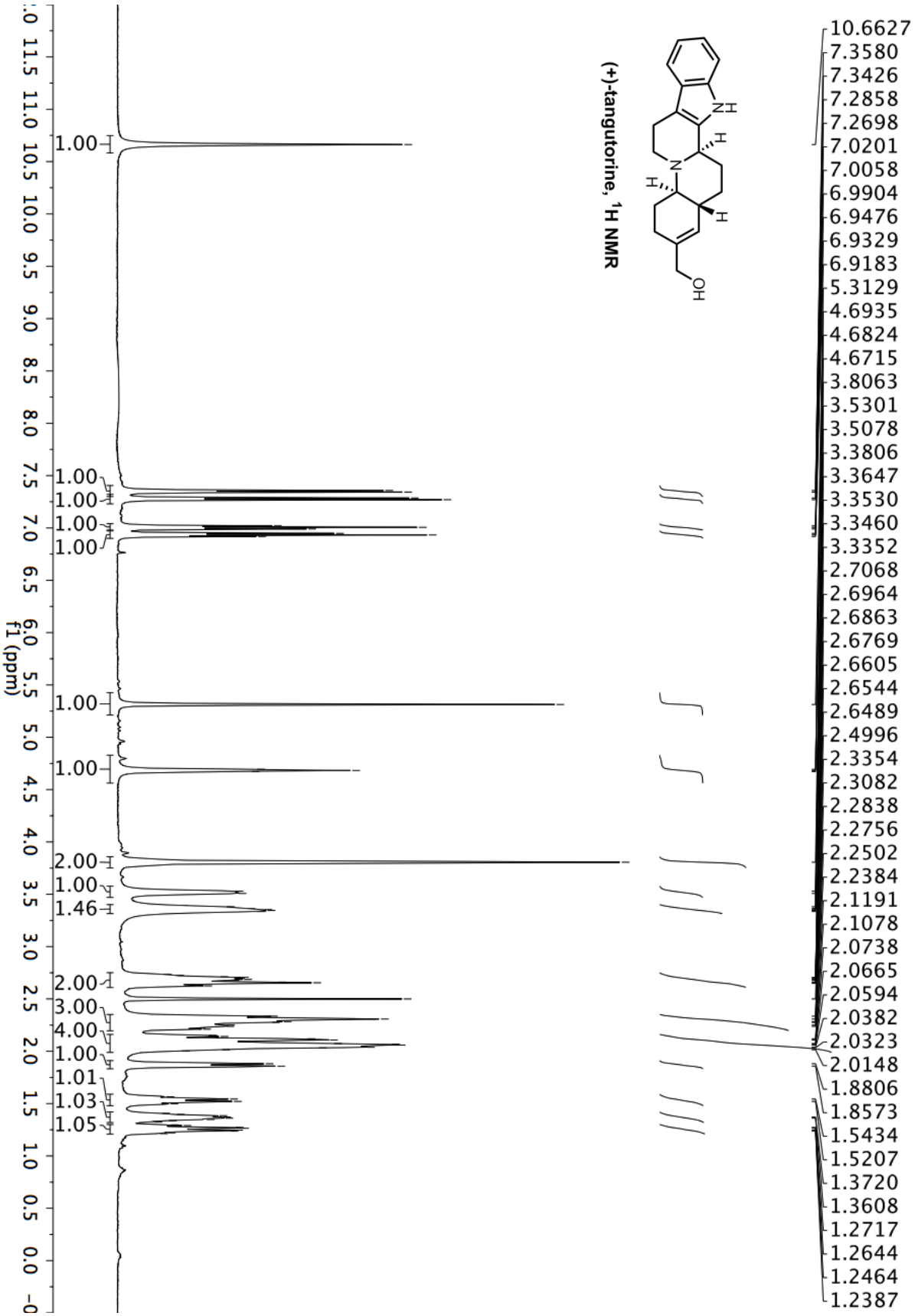
(+)-tangutorine, $^1$H NMR
f1 (ppm)
1.00
1.00
1.00
1.00
1.00
1.00
2.00
1.00
1.46
2.00
3.00
4.00
1.00
1.01
1.03
1.05
10.6627
7.3580
7.3426
7.2858
7.2698
7.0201
7.0058
6.9904
6.9476
6.9329
6.9183
5.3129
4.6935
4.6824
4.6715
3.8063
3.5301
3.5078
3.3806
3.3647
3.3530
3.3460
3.3352
2.7068
2.6964
2.6863
2.6769
2.6605
2.6544
2.6489
2.4996
2.3354
2.3082
2.2838
2.2756
2.2502
2.2384
2.1191
2.1078
2.0738
2.0665
2.0594
2.0382
2.0323
2.0148
1.8806
1.8573
1.5434
1.5207
1.3720
1.3608
1.2717
1.2644
1.2464
1.2387

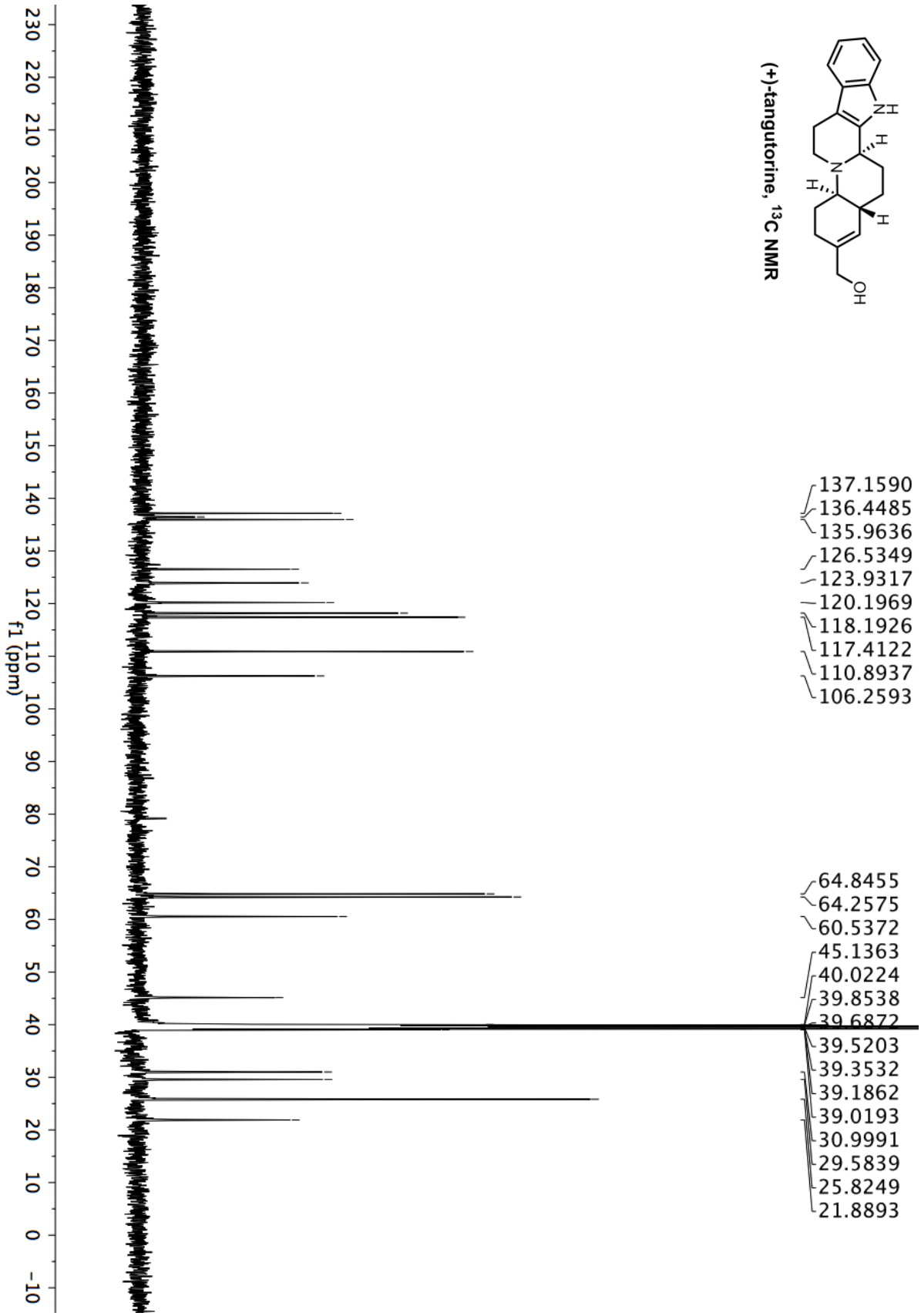
(+)-tangutorine, $^{13}$C NMR
137.1590
136.4485
135.9636
126.5349
123.9317
120.1969
118.1926
117.4122
110.8937
106.2593
64.8455
64.2575
60.5372
45.1363
40.0224
39.8538
39.6872
39.5203
39.3532
39.1862
39.0193
30.9991
29.5839
25.8249
21.8893
f1 (ppm)

# 14 References


42. D. S. Laitar, P. Müller, J. P. Sadighi, *J. Am. Chem. Soc.* **127**, 17196–17197 (2005).
43. N. P. Mankad, D. S. Laitar, J. P. Sadighi, *Orgamometallics* **23**, 3369–3371 (2004).
44. P. Crabbé, H. Fillion, D. André, J. L. Luche, *J. Chem. Soc. Chem. Commun.* 859–860 (1979).
45. F. Meng, K. P. McGrath, A. H. Hoveyda, *Nature* **513**, 367–374 (2014).
46. B. Jung, A. H. Hoveyda, *J. Am. Chem. Soc.* **134**, 1490–1493 (2012).
47. F. Meng, H. Jang, B. Jung, A. H. Hoveyda, *Angew. Chem. Int. Ed.* **52**, 5046–5051 (2013).
48. F. Meng, K. P. McGrath, A. H. Hoveyda, *Nature* **513**, 367–374 (2014).
49. T. H. Lemmen, *et al. Inorg. Chem.* **29**, 3680–3685 (1990).
50. T. Tsuda, T. Hashimoto, T. Saegusa, *J. Am. Chem. Soc.* **94**, 658–659 (1972).
51. T. Tsuda, T. Yazawa, K. Watanabe, T. Fujii, T. Saegusa, *J. Org. Chem.* **46**, 192–194 (1981).
52. M. Stollenz, F. Meyer, *Organometallics.* **31**, 7708–7727 (2012).
53. J. Lee, S. Radomkit, S. Torker, J. del Pozo, A. H. Hoveyda *Nat. Chem.* **10**, 99–108 (2018).
54. S. J. Ferrara, J. W. Burton, *Chem. Eur. J.* **22**, 11597–11600 (2016).
55. K. Miura, D. Itoh, T. Hondo, A. Hosomi, *Tetrahedron Lett.* **35**, 9605–9608 (1994).
56. Z.-L. Zang, *et al. Org. Lett.* **18**, 5014–5017 (2016).
57. P. R. Werkhoven, *et al. Org. Biomol. Chem.* **14**, 701–710 (2016).
58. A. Younai, B.-S. Zeng, H. Y. Meltzer, K. A. Scheidt, *Angew. Chem. Int. Ed.* **54**, 6900–6904 (2015).
59. C. J. Cramer, D. G. Truhlar, *Phys. Chem. Chem. Phys.* **11**, 10757–10816 (2009).
60. R. Peverati, D. G. Truhlar, *Phil. Trans. R. Soc. A* **372**, 20120476 (2014).
61. N. Mardirossian, M. Head-Gordon, *J. Chem. Theory Comput.* **12**, 4303–4325 (2016).
62. N. Mardirossian, M. Head-Gordon, *J. Chem. Phys.* **144**, 214110 (2016).
63. B. Brauer, M. K. Kesharwani, S. Kozuch, J. M. Martin, *Phys. Chem. Chem. Phys.* **18**, 20905–20925 (2016).
64. T. Weymuth, E. P. A. Couzijn, P. Chen, M. Reiher, *J. Chem. Theory Comput.* **10**, 3092–3103 (2014).
65. W. Zhang, D. G. Truhlar, M. Tang, *J. Chem. Theory Comput.* **9**, 3965–3977 (2013).
66. H. S. Yu, X. He, S. L. Li, D. G. Truhlar, *Chem. Sci.* **7**, 5032–5051 (2016).
67. M. Steinmetz, S. Grimme, *ChemistryOpen* **2**, 115–124 (2013).
68. L. Goerigk, H. Kruse, S. Grimme, *ChemPhysChem* **12**, 3421–3433 (2011).
69. M. J. Frisch, *et al. Gaussian 09, Revision D.01,* Gaussian, Inc., Wallingford CT, 2009.
70. Y. Zhao, D. G. Truhlar, *Acc. Chem. Res.* **41**, 157–167 (2008).
71. F. Weigend, R. Ahlrichs, *Phys. Chem. Chem. Phys.* **7**, 3297–3305 (2005).
72. F. Weigend, *Phys. Chem. Chem. Phys.* **8**, 1057–1065 (2006).
73. A. V. Marenich, C. J. Cramer, D. G. Truhlar, *J. Phys. Chem. B* **113**, 6378–6396 (2009).
74. M. Page, J. W. Jr. McIver, *J. Chem. Phys.* **88**, 922–935 (1988).
75. M. Page, M.; C., Jr. Doubleday Jr., J. W. Jr. McIver, *J. Chem. Phys.* **93**, 5634–5642 (1990).
76. S. Torker, D. Merki, P. Chen, *J. Am. Chem. Soc.* **130**, 4808–4814 (2008).
77. Y. Minenkov, G. Occhipinti, A. Singstad, V. R. Jensen, *Dalton Trans.* **41**, 5526–5541 (2012).
78. Y. Minenkov, G. Occhipinti, V. R. Jensen, *Organometallics* **32**, 2099–2111 (2011).
79. R. K. M. Khan, S. Torker, A. H. Hoveyda, *J. Am. Chem. Soc.* **136**, 14337–14340 (2014).
80. S. Torker, M. J. Koh, R. K. M. Khan, A. H. Hoveyda, *Organometallics* **35**, 543–562 (2016).

81. M. S. Mikus, S. Torker, A. H. Hoveyda, *Angew. Chem. Int. Ed.* **55**, 4997–5002 (2016).
82. C. Xu, Z. Liu, S. Torker, X. Shen, D. Xu, A. H. Hoveyda, *J. Am. Chem. Soc.* **139**, 15640–15643 (2017).
83. Y. Zhou, Y. Shi, S. Torker, A. H. Hoveyda, *J. Am. Chem. Soc.* **140**, 16842–16854 (2018).
84. J. Lee, S. Radomkit, S. Torker, J. del Pozo, A. H. Hoveyda, *Nat. Chem.* **10**, 99–108 (2018).
85. Y. Huang, J. del Pozo, S. Torker, A. H. Hoveyda, *J. Am. Chem. Soc.* **140**, 2643–2655 (2018).
86. J.-D. Chai, M. Head-Gordon, *Phys. Chem. Chem. Phys.* **10**, 6615–6620 (2008).
87. D. L. Lichtenberger, J. A. Gladysz, *Organometallics* **33**, 835–835 (2014).
88. J. P. Wagner, P. R. Schreiner, *Angew. Chem. Int. Ed.* **54**, 12274–12296 (2015).
89. L. Chen, P. Ren, B. P. Carrow, *J. Am. Chem. Soc.* **138**, 6392–6395 (2016).
90. L. Albers, S. Rathjen, J. Baumgartner, C. Marschner, T. Müller, *J. Am. Chem. Soc.* **138**, 6886–6892 (2016).